ANALYSIS OF CELL SIGNALLING IN DYSTROPHIN-DEFICIENT MYOBLASTS

by

MUHAMMAD DA'IN BIN YAZID

A thesis submitted to the

University of Birmingham

for the degree of

DOCTOR OF PHILOSOPHY

School of Biosciences

College of Life and Environmental Sciences

The University of Birmingham

January 2017

Abstract

An absence of dystrophin in muscle has a massive impact throughout muscle development, and Duchene Muscular Dystrophy (DMD) is one of the consequences. The disruption of the dystrophin-glycoprotein complex (DGC) is caused by a mutation in the DMD gene, which affects muscle integrity, resulting in progressive muscle degeneration and weakness. In this study, dfd13 (dystrophin-deficient) and C2C12 (non-dystrophic) myoblasts were cultured in low mitogen conditions for 10 days to induce differentiation; however, dfd13 myoblasts did not achieve terminal differentiation. It has been suggested that Pax7 may play a major role during myogenesis, therefore its expression pattern and transport protein were examined for any impairments. It was established that Pax7 localises in the cytoplasm of dystrophin-deficient myoblasts and high expression is retained during differentiation. Co-localisation analysis of Pax7 with subcellular markers indicated that Pax7 is synthesised during the proliferative state. Pax7 was shown to possess a nuclear location signal and KPNA2 was suggested as escort protein for Pax7 translocation into the nucleus. The PTEN-PI3K/Akt signalling pathway was investigated and protein synthesis regulation and FoxO3 were found to be impaired. Autophagy related genes were found to be highly expressed; however, LC3 lipidation and autophagy flux showed a reduction upon differentiation, indicating defective autophagy. The contribution of PTEN overexpression was assessed in relation to endoplasmic reticulum (ER) stress and activation of the unfolding protein response (UPR). It was established that a reduction in ER stress and changes to UPR activation lead to apoptosis. Finally, minidystrophin-transfection of both types of myoblasts was utilised to examine the effect, especially in dystrophin-deficient myoblasts. Minidystrophin improved protein synthesis activation and increased autophagy (increased LC3 lipidation), suggesting that minidystrophin ameliorates dystrophic events (at the level of autophagosome formation. To conclude, destabilisation of the plasma membrane owing to a dystrophin mutation causes cell signalling alterations which minidystrophin restoration can partly improve.

This thesis is dedicated to my beloved wife Nurul'Ain binti Jasmani,

my daughter Auni Zulaikha binti Muhammad Da'in and

my son Nukman Nazim bin Muhammad Da'in

Acknowledgments

First of all, I would like to show my gratitude to both my supervisors, Dr. Neil Hotchin and Dr. Janet Smith, who have given me a golden opportunity and good guidance during my Ph.D. studies; the completion of this thesis gives me much pleasure. Special thanks are due to Dr. Chen Hung-Chih for his useful advice and suggestions. I also would like to expand my gratitude to Professor John Heath, Dr. Melissa Grant, Dr. Debbie Cunningham, Dr. Mike Tomlinson, Dr. Trushar Patel, Adil Rashid, Maihafizah Mohd Zahari, Shabana Begum and all those on the fifth and eighth floors who have been directly or indirectly involved in my study. I would like to thank to Majlis Amanah Rakyat (MARA) and Universiti Kebangsaan Malaysia (UKM) for their financial support for my study and family stipend.

Finally, I would like to give special thanks to my family: my father Mr. Yazid bin Bodot and mother Mrs. Roha binti Amir, my father-in-law Mr. Jasmani bin Lajis and mother-in-law Mrs. Zaimaf binti Mohd Ariff for their emotional support. Finally, I would like to express my appreciation for my beloved wife Nurul'Ain binti Jasmani and my two children, Auni Zulaikha binti Muhammad Da'in and Nukman Nazim bin Muhammad Da'in, for their sacrifices and support in the moments when I needed help to become calm again.

Thank you.

Table of Contents

List of Figures

List of Tables

List of Abbreviations

bHLH	Basic Helix-Loop-Helix
BMD	Becker Muscular Dystrophy
BSA	Bovine Serum Albumin
DGC	Dystrophin-Associated Glycoprotein Complex
dH20	Distilled Water
DM	Differentiation Medium
DMD	Duchenne Muscular Dystrophy
DNA	Deoxyribonucleic Acid
EDTA	Ethylenediaminetetra Acetic Acid
ER	Endoplasmic Reticulum
FGF	Fibroblast Growth Factor
F-MyHC	Fast Myosin Heavy Chain
GM	Growth Medium
GRMD	Golden Retriever Muscular Dystrophy
HD	Homeodomain
IGF	Insulin-Like Growth Factor
IGF-1R	Type 1 Igf Receptor
IGF-2R	Type 2 Igf Receptor
IR	Insulin Receptor
kDa	kilo-Dalton
LGMD	Limb-Girdle Muscular Dystrophy
MD	Muscular Dystrophy
Mdx mdx	X-linked muscular dystrophy (mouse)
MRF	Myogenic Regulatory Factor
MSTN	Myostatin
MyHC	Myosin Heavy Chain
NaCl	sodium chloride
NE	nuclear envelope
NES	Nuclear Export Signal
NLS	Nuclear localisation signal

NPC	Nuclear Pore Complex
OP	Octapeptide
PAGE	Polyacrylamide Gel Electrophoresis
PBS	Phosphate-Buffered Saline
PBST	Phosphate Buffer Saline Containing Tween20
PD	Paired Domain
PFA	Paraformaldehyde
RNA	ribonucleic acid rpm revolutions per
rpm	Revolutions Per Minute
TBS	Tris-Buffered Saline
TGF	Transforming Growth-Factor
UPR	Unfolded Protein Response

Chapter 1 - Introduction

Muscular dystrophy (MD) has been observed to begin early in the embryonic stage. It has been shown that the attrition of Pax7-positive cells and a substantial reduction in Pax7 expression occurred at the E15.5 and E17.5 stages in *mdx* embryos, the mouse model of Duchenne Muscular Dystrophy (DMD) (Merrick et al. 2009). Pax7-positive cell fragments also have been found in dystrophic muscle, suggesting that cells were undergoing apoptosis. These findings suggest that Pax7 play ~~as a~~ major role during myogenesis in the embryonic stage. At the postnatal stage, myoblasts have been reported to undergo extensive cell proliferation (hyper-proliferation) and increased apoptosis in *mdx* mice (Merrick et al. 2009) and in DMD patients (Sandri et al. 1998). Pax7 also has been reported play a role in satellite cells during the postnatal stage (Oustanina, Hause, and Braun 2004) but is indispensable during the adult stage (Sambasivan et al. 2011).

In this study, dfd13 myoblasts have been used as the main subject by comparing it with the established C2C12 myoblast cell line. The dfd13 myoblast is derived from a 5-week-old *mdx* mouse, which ~~is~~ has dystrophin-deficient myoblasts (Smith and Schofield 1994; Smith and Schofield 1997). In the *mdx* mouse the period of myopathy has been reported to begin after the three weeks of proliferative post-natal growth ends (Duddy et al. 2015). Therefore, dfd13 myoblasts were isolated from a 5-week-old *mdx* mouse and expanded via the micro-explant culture technique (Merrick et al. 2009). In addition, progressive muscle degeneration has been reported to begin at this stage. Therefore, the aim of the project was to investigate/characterise these dystrophin-deficient myoblasts in terms of Pax7 expression patterns and levels of ~~the~~ associated

proteins. Intrinsic protein signalling, i.e. the PI3K/Akt pathway that leads to autophagy modulation, as well as phospholipase C (PLC) and endoplasmic reticulum (ER) stress during differentiation is also investigated. Finally, minidystrophin restoration is carried out in order to determine whether it could improve the impairment in dystrophin-deficient myoblasts.

1.1 Muscular Dystrophy

1.1.1 Types of Muscular Dystrophy

It has been reported that more than 70,000 people in the UK are affected by MD, and approximately 1 in 5,000 boys are born with Duchenne muscular dystrophy (DMD) (Muscular Dystrophy Campaign website). DMD is inherited muscle diseases caused by deletion, duplication or a point mutation of the DMD gene (dystrophin) which is located on the human X chromosome (Hoffman, Brown, and Kunkel 1987). These diseases are characterised by progressive skeletal muscle weakness, defects in muscle proteins, and the death of muscle tissue (Meryon 1852). A person suffering from the disease will gradually lose the ability to perform daily routine activities, starting as early as after birth to 2 years old, and by around the ages of ten years old they will need a wheelchair for movement, with death occurring in their early 30s, mostly due to cardiomyopathy together with respiratory failure (Walton and Nattrass 1954; Eagle et al. 2002; Passamano et al. 2012). The life expectancy for each individual who has MD depends on the degree of weakened muscles in the heart.

Types of MD are classified according to the age onset, muscles affected, as well as rate of progression. According to the National Institute of Child Health and Human Development (NICHD), there are more than 30 forms of MD which have been classified into nine primary types (Table 1.1), and Figure 1.1 illustrates the classification of MD

according to the muscles affected. However, there remains no treatment to cure MD, either drugs based or reverse genetic mutations. Currently, drug therapy, i.e. corticosteroids, is used to slow muscle degeneration, while physical therapy, speech therapy and orthopaedic appliances are used to support MD patients in their daily lives (Angelini and Peterle 2012).

Table 1.1: Primary types of muscular dystrophy
Source: University of Rochester Medical Center website https://www.urmc.rochester.edu/encyclopedia/content.aspx?ContentTypeID=85&ContentID=P00792

Type	Age at onset	Symptoms, rate of progression, and life expectancy
Becker	Adolescence to early adulthood	Symptoms are almost identical to Duchenne, but less severe; progresses more slowly than Duchenne; survival into middle age.
Congenital	Birth	Symptoms include general muscle weakness and possible joint deformities; disease progresses slowly; shortened life span.
Duchenne	2 to 6 years	Symptoms include general muscle weakness and wasting; affects pelvis, upper arms, and upper legs; eventually involves all voluntary muscles; survival beyond 20s is rare.
Distal	40 to 60 years	Symptoms include weakness and wasting of muscles of the hands, forearms, and lower legs; progression is slow; rarely leads to total incapacity.
Emery-Dreifuss	Childhood to early teens	Symptoms include weakness and wasting of shoulder, upper arm, and shin muscles; joint deformities are common; progression is slow; sudden death may occur from cardiac problems.
Facioscapulohumeral	Childhood to early adults	Symptoms include facial muscle weakness and weakness with some wasting of shoulders and upper arms; progression is slow with periods of rapid deterioration; life span may be many decades after onset.
Limb-Girdle	Late childhood to middle age	Symptoms include weakness and wasting, affecting shoulder girdle and pelvic girdle first; progression is slow; death is usually due to cardiopulmonary complications.
Myotonic	20 to 40 years	Symptoms include weakness of all muscle groups accompanied by delayed relaxation of muscles after contraction; affects face, feet, hands, and neck first; progression is slow, sometimes spanning 50 to 60 years.

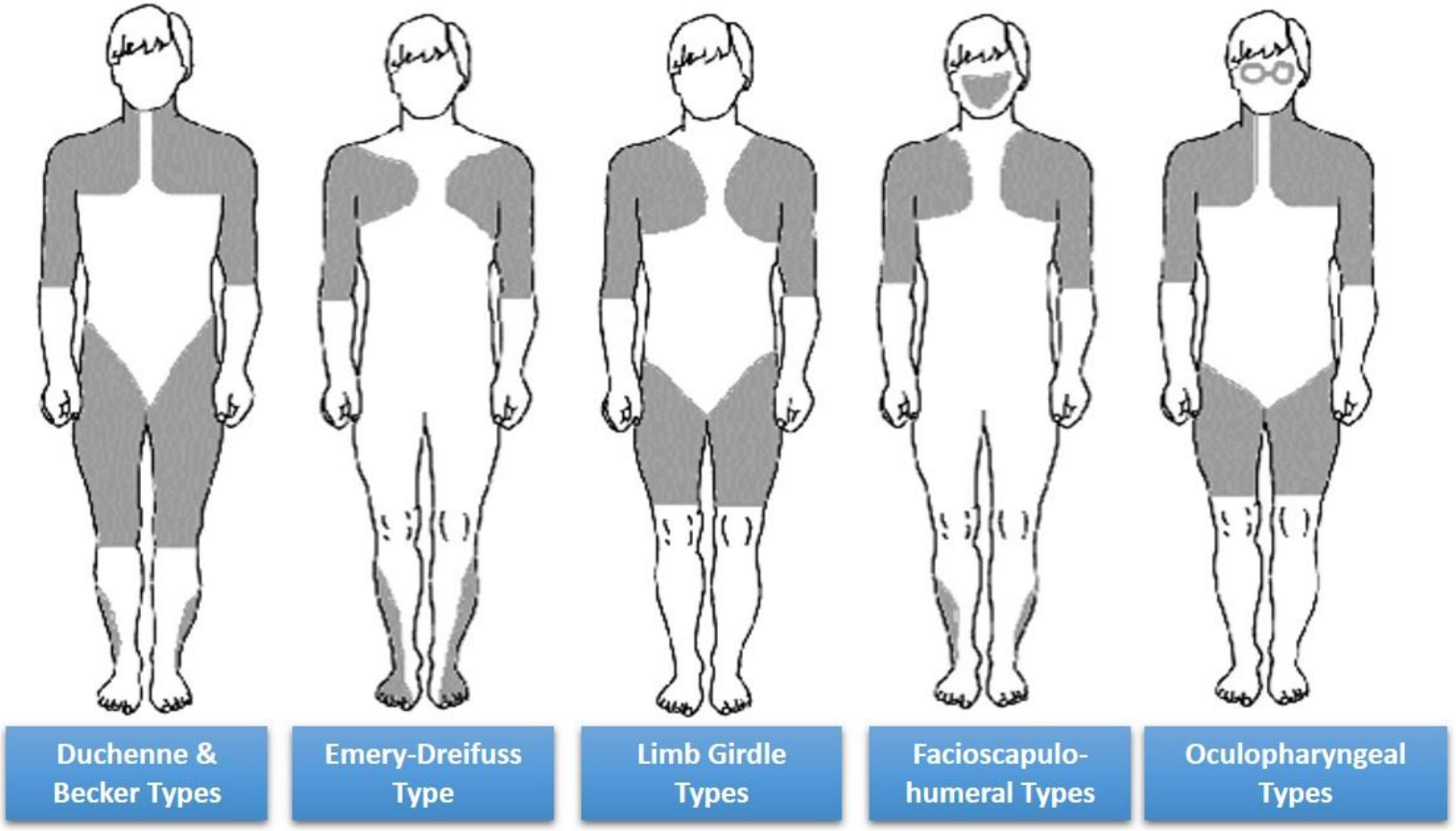

Figure 1.1: Different types of muscular dystrophy with defects in different muscles

Image from http://patient.info/health/muscular-dystrophies-an-overview

1.1.2 Duchene Muscular Dystrophy

DMD is the most well-known and the severest form of MD, and is caused by a mutation in the DMD gene which encodes the protein dystrophin (Hoffman, Brown, and Kunkel 1987; Nowak and Davies 2004). DMD can be diagnosed using several tests, including that for creatine phosphokinase (CK), which can be detected through high levels in the blood as it leaks out from damaged muscle. A DNA test also can be performed to examine whether the specific mutation present is a deletion, duplication or point mutation of the *dmd* gene (Muscular Dystrophy Association website). As DMD is an inherited disease, it is essential that family members who are potential carriers can access genetic counselling.

Dystrophin plays an important role in providing stability to the cell membrane, and connects the extracellular matrix and cytoskeleton components via the sarcolemma membrane (D. J. Blake et al. 2002). Dystrophin is associated with other protein partners, such as β-dystroglycan and sarcoglycan, which together form the dystrophin-associated glycoprotein complex (DGC) which is embedded in the sarcolemma membrane. Sarcospan, dystrobrevin and syntrophins are located in the cytoplasm, while α-dystroglycan as well as laminin 2 are present in an extracellular matrix (Figure 1.2A) (Ervasti and Campbell 1991; D. J. Blake et al. 2002). Based on its complex and important connections, the absence of dystrophin causes membrane instability (Figure 1.2B). The characterisation of this impairment is much worse in humans compared to the animal model, the *mdx* mouse; however, its reproducibility and applicability provides vital evidence and is the best available model for pre-clinical scientific research. Other models have also been developed for the mutations present in other types of MD (Figure 1.3). These animal models aid in the understanding of the

molecular basis of MD and are expected to enable the development of effective treatments.

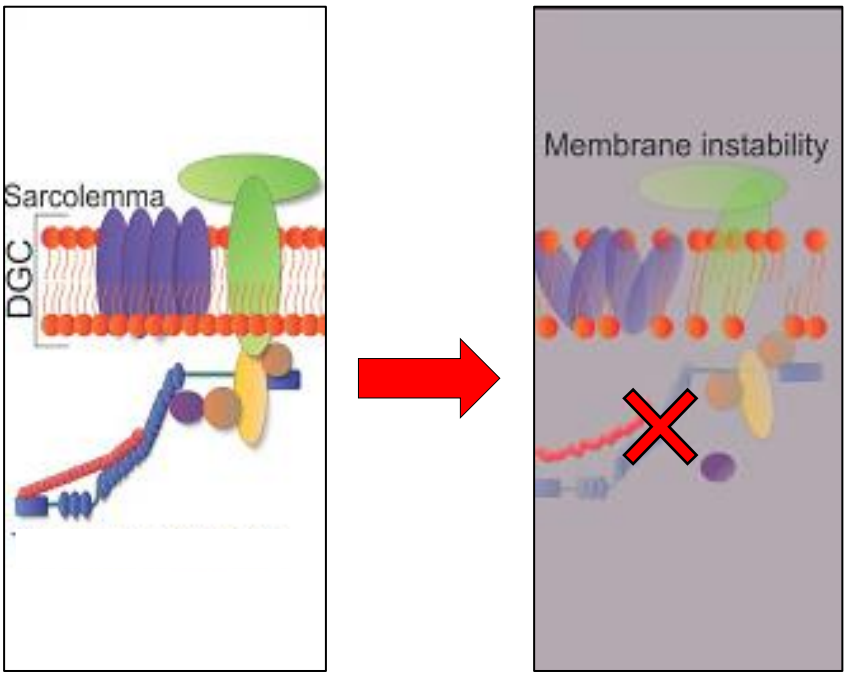

Figure 1.2: Absence of dystrophin causes membrane instability in the sarcolemma membrane
Schematic of the normal structure of the dystrophin-associated glycoprotein complex (DGC) and absence of dystrophin showing membrane instability within the sarcolemma membrane. (Modified from (Fiorillo et al. 2015))

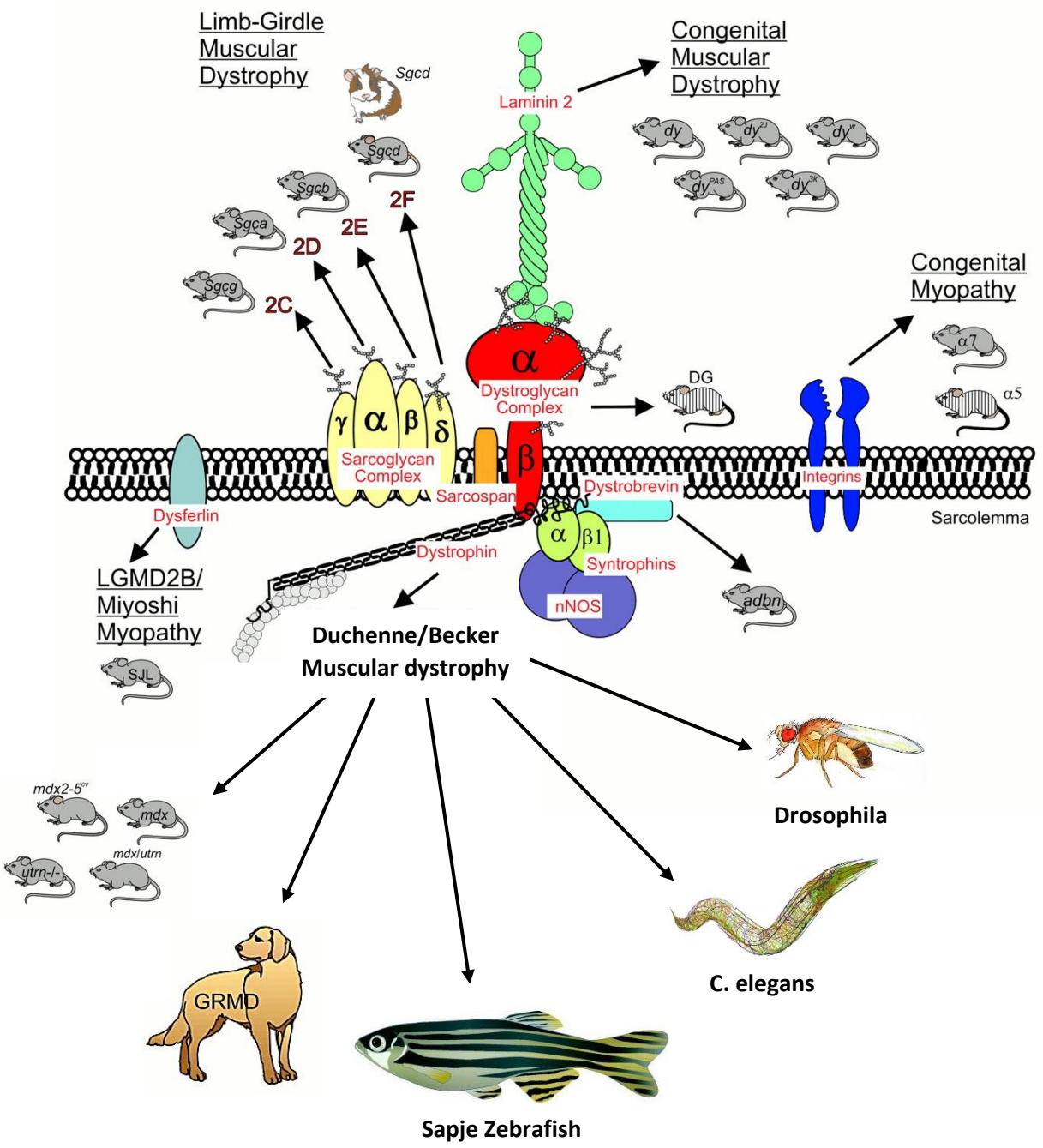

Figure 1.3: Animal models of the mutations in different types of muscular dystrophy
Two animals model for Duchenne/Becker MD have been developed; Golden Retriever MD (GRMD) and mouse models (including *mdx, mdx/utrn, utrn*$^{-/-}$, *mdx2-5*^{cv}). Swiss Jim Lambert (SJL) mice is a model for Lim-Girdle muscular dystrophy-2B (LGMD2B), while sarcoglycan-gamma/alpha/beta/delta (Sgd-g/a/b/d) are mouse models for LGMD2B/2C/2D/2E/2F, respectively. *dy* mice are a model for congenital muscular dystrophy (CMD), *α7* and *α5* mice are a model for congenital myopathy, and *Adbn* mice are a model for dystrobrevin deficiency. (modified from (Allamand and Campbell 2000; McGreevy et al. 2015)).

1.2 Myogenesis

Myogenesis is the process of muscle tissue development throughout life, and predominantly occurs during embryonic stages with muscle regeneration taking place during adult stages. There are three different types of myoblasts, embryonic myoblasts, foetal myoblasts and satellite cells, which are involved in myogenesis and the transitions between these myoblasts are thought to overlap (Messina and Cossu 2009). Myogenesis is thought to have two myogenic waves with a distinct muscle fibre morphology being formed during the gestational period. There are four key factors which play an important role in differentiating progenitor myoblasts into the myofibres Myf5, MyoD, myogenin, and Mrf4.

1.2.1 Embryonic Myogenesis

In chick embryos the somite develops from the ventral region of the mesoderm, where it generally gives rise to major axial structures, i.e. cartilage cells (vertebrae and ribs), all skeletal muscles (including limbs) and also the dermis. The dermomyotome is formed from cells located in the dorsal and lateral regions of the somite, and consists of the myotome and dermatome which give rise to all trunk muscle cells and dermis, respectively. The dermomyotome also gives rise to muscle cells that migrate into the limb bud (Figure 1.4) (Wolpert et al. 2002). Initially, delamination of the cells from the edges of the dermomyotome causes the formation of the epithelial dermomyotome and skeletal muscle of the myotome. At this stage, Pax3 is highly expressed in migrating hypaxial cells and dermomyotome cells where is mediates the transcription of c-Met. The survival and proliferation of myoblasts is regulated by c-Met prior to migration and during secondary myogenesis (Wolpert et al. 2002).

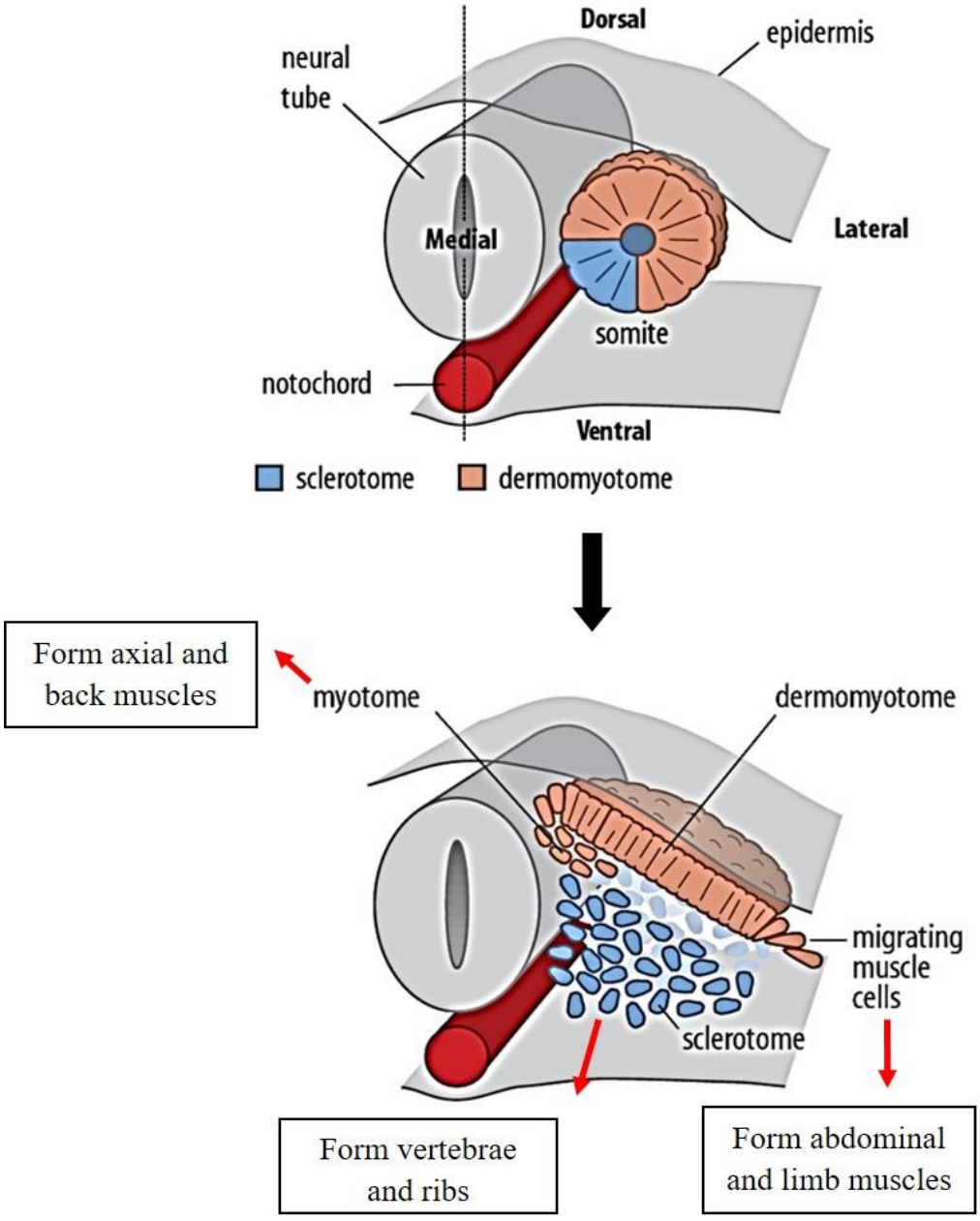

Figure 1.4: Fate map of the somite within the chick embryo
The sclerotome (forms cartilage) and dermomyotome arise from the somite. The myotome, part of the dermomyotome, gives rise to muscle cells. During day four embryogenesis, cells from the medial region of the somite will form the axial and back muscles, whereas cells from the lateral region migrate to give rise to abdominal and limb muscles.
(Modified from Wolpert et al., 2002).

During embryogenesis, skeletal muscles are derived from the paraxial mesoderm of the somite. Early myogenesis, also known as primary myogenesis, begins at E8.5 to E10.5 and is composed of myocytes. The fusion of myocytes to form multinucleate muscle

fibre cells between E10.5 and E12.0 establishes the basic muscle pattern. At this stage, the key factors for muscle differentiation, i.e. MyoD and myogenin, begin to be expressed, together with myosin heavy chain (MyHC). Pax7 expression commences during E11.5, and it begins to take over the role of Pax3, which is down-regulated after E13.5+ (Figure 1.5).

1.2.2 Foetal Myogenesis

The second wave of myogenesis, also known as foetal myogenesis, begins at E13.5. At this stage, the bulk of the newly formed muscle has a longer and thinner shape formed around the primary fibres (Cossu et al. 1996). These fibres are the result of the fusion of foetal myoblasts with each other or fusion with primary fibres. At the end of this stage, E17.5, a basal lamina is formed with satellite cells residing between the fibres and sarcolemmal membrane. These satellite cells have been morphologically identified as mononucleated cells which are responsible for postnatal growth and muscle regeneration in adults (Messina and Cossu 2009).

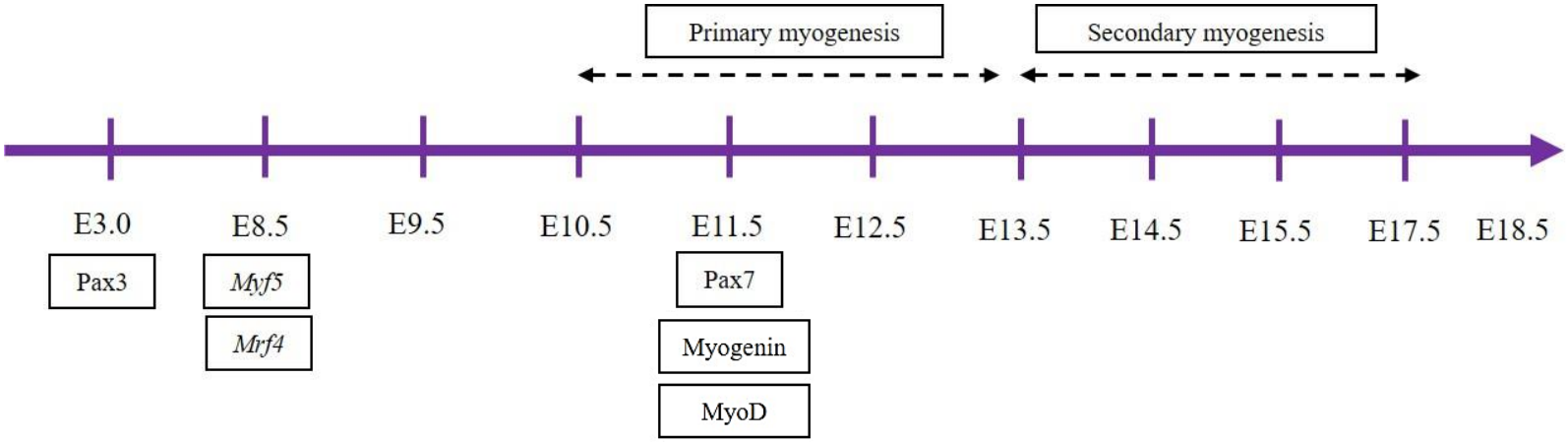

Figure 1.5: Timeline of the initiation of genes involved in the regulation of myogenesis

1.2.3 Adult Myogenesis and Muscle Regeneration

The third wave of myogenesis occurs at the postnatal stage, immediately after birth until the third or fourth week. At this stage, satellite cells, play an important role in maintaining muscle, for instance, during muscle injuries. A previous study showed that Pax7 and Pax3 are indispensable in adults (Sambasivan et al. 2011). Satellite cells will remain in a quiescent state until the signal for muscle generation is received and the satellite cell is activated ready to commit to differentiation. Once the signal is received, satellite cells undergone a series of activation steps involving specific protein expression, subsequently achieving terminal differentiation (Figure 1.6).

1.2.4 Satellite Cells

Satellite cells also known as skeletal muscle stem cells are localised between the sarcolemma and basement membrane of myofibres (Hawke and Garry 2001). ISatellit cells have the ability to differentiate into myotube to provide additional muscle fibres (Siegel, Kuhlmann, and Cornelison 2011) and to self-renew to maintain the stem cells pool (Zammit et al. 2004). The satellite cells are the main source of new myonuclei for growing myofibers which is a cellular unit of adult skeletal muscle. Previous study has proved that Satellite cells can repair damaged muscle tissue in acute injury (Lepper, Partridge, and Fan 2011). The performance of this stem cell pool within each myofiber is a critical factor for maintaining myofiber integrity throughout life. Myofibres are sustained by hundreds of post mitotic myonuclei and are efficiently repaired and regenerated in damaged tissues (Zammit and Beauchamp 2001). Satellite cells have been reported to express the paired box transcription factor family member Pax7. This factor plays a critical role in the specification of satellite cells in skeletal muscle (Kuang et al. 2006). The inactivation of *Pax7* results in severe depletion of these muscle stem

cells, thus trigger the development of muscle cells process (Lepper, Partridge, and Fan 2011). 2011).

1.3 Paired-type Homeobox Transcription Factors

1.3.1 Pax protein

Pax proteins are the key factors in the development of tissues and organs during embryogenesis. These proteins are characterised by the presence of a paired domain (PD), which specifically binds to DNA sequences where it acts as a transcription repressor or activator, and is generally located in the N-terminal part. *Pax* genes may also have an octapeptide (OP) motif and a homeobox DNA-binding domain (homeodomain; HD). *Pax* genes can be categorised into four subfamilies according to their structural characteristics Table 1.2). Within these subfamilies there is some overlap in expression during the development of tissues or organs in determining the choice of cell fate (Buckingham and Relaix 2007).

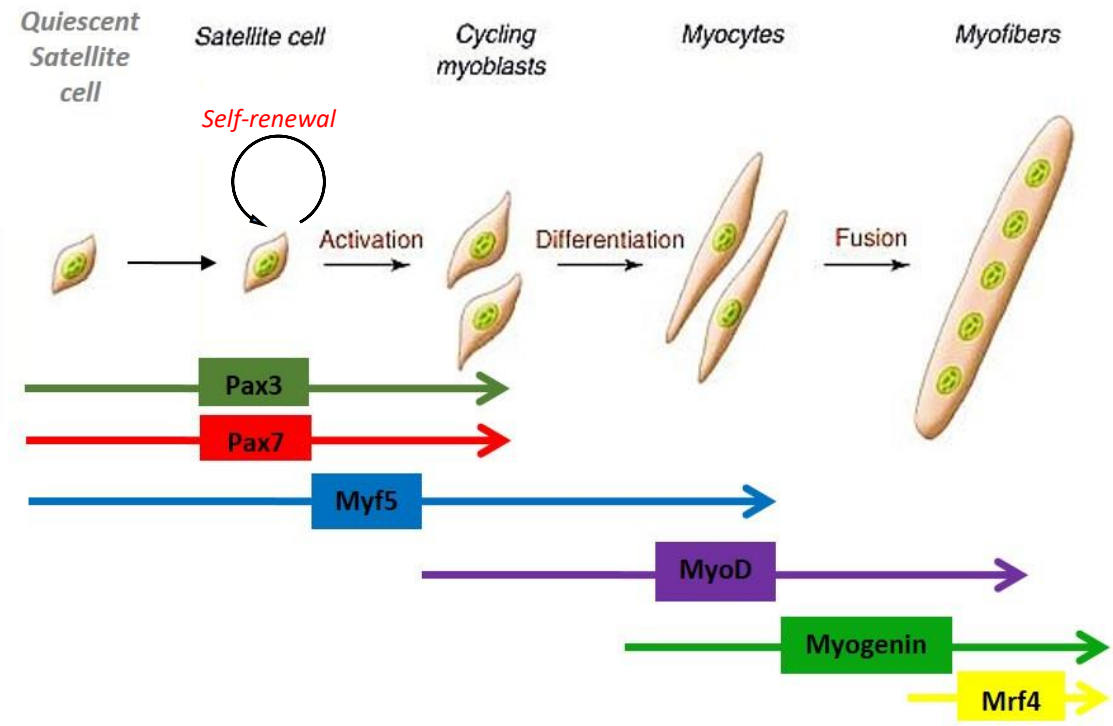

Figure 1.6: Sequence of myogenic regulatory expression within satellite cells
Quiescent and activated satellite cells express Pax3 and Pax7, which then start to differentiate into myocytes initiated by Myf5. Myogenic differentiation factors, i.e. MyoD, myogenin and Mrf4, are then expressed during the differentiation process.

Table 1.2: *Pax* genes and the four subfamilies
Pax genes are classified into four subfamilies based on their structural characteristics. (Buckingham and Relaix 2007).

***Pax* gene**	**Structural Characteristics**	**Expression in developing tissues/organs**	**Examples of human diseases associated with *pax* mutations**
Pax3	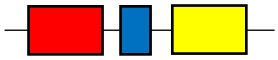	Central nervous system, craniofacial tissue, trunk neural crest, somites/skeletal muscle	Waardenburg syndrome, rhabdomyosarcoma,
Pax7		Central nervous system, craniofacial tissue, somites/skeletal muscle	Melanoma, neuroblastoma, rhabdomyosarcoma,
Pax4	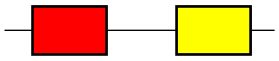	Pancreas, gut	Diabetes
Pax6		Central nervous system, pancreas, gut, nose, eye	Aniridia, cataracts, G1 tumors
Pax2	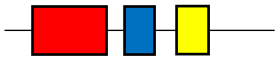	Central nervous system, kidney, ears	Kidney disease, e.g., Colomba syndrome, renal carcinomas
Pax8		Central nervous system, kidney, thyroid	Congenital hypothyroidism, thyroid follicular carcinomas
Pax5		Central nervous system, B-lymphocytes	Lymphomas
Pax1	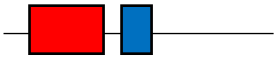	Skeleton, thymus, oarathyroid	Vertebral malformations, e.g., Klippell-Feil syndrome
Pax9		Skeleton, Thymus, craniofacial tissue, teeth	Oligodentia

Key: red box – Paired Domain, Blue box - Octapeptide and yellow box – Homeodomain1/2/3.

1.3.2 Pax3 and Pax7

Pax3 and Pax7 have been widely studied due to their role in myogenesis and as a marker of the origin of myogenic progenitor cells during the embryonic and foetal stages (Relaix et al. 2006; Lagha et al. 2008). During muscle development and muscle

regeneration in the postnatal and adult stages, respectively, Pax3 and Pax7 are known to be essential for satellite cells to play their important role (Buckingham and Relaix 2007; Relaix et al. 2006), while in embryos, these proteins play a role as a regulator of the myogenic programme. Both Pax3 and Pax7 have been shown to coordinate MyoD expression in adult skeletal muscle during chronic skeletal muscle overload, suggesting that both are involved in muscle development and regeneration (Hyatt et al. 2008).

Pax3 is initially expressed in all cells that form somites, specifically the dermomyotome, from as early as day 3 of embryogenesis in mouse and chick. It is modulated by a member of the TGF beta superfamily, BMP-4, and Wnt family proteins, to become muscle precursors (Wolpert et al. 2002). A Pax3-deficient embryo cannot survive due to multiple defects in the neural tube, myogenesis and morphogenesis. The hypaxial muscle development by Myf5 is Pax3 dependent, but the regulation of the entry of cells into the myogenic programme is Pax3 independent (Bajard et al. 2006). In the embryo, Pax3 is known to be expressed in both quiescent and activated cells of adult mice at different frequencies in different muscles; it is abundantly present in the diaphragm (Relaix et al. 2006). A study by Zhou et al. (2008) showed that a *pax3* heterozygous mutation causes a semi-dominant phenotype, which means that different levels/dosages of Pax3 expression are required in each different muscle in the mouse and human (Zhou et al. 2008).

Pax7 is expressed specifically during the development of the nervous and muscular system. A study by Merrick et al. (2009) showed that Pax7 can be detected as early as E11.5 in wild-type embryos and its level increases throughout the gestational period (Merrick et al. 2009). It plays a role in the regulation of muscle precursor cell proliferation by recruiting the histone-3-lysine-4 methyltransferase (H3K4 HMT)

complex via Pax3/7BP and the Wdr5 adaptor. This complex then target genes, i.e. *Cdc20* and *Id3*, which are involved in cell-division cycle activation and the transcription inhibition process, respectively (Diao et al. 2012). The down-regulation of pax7 protein levels in an embryo correlates with an increased level of apoptosis in myoblasts isolated from *mdx* and *cav3*$^{-/-}$ mice (Merrick et al. 2009).

The diversion function of Pax3 and Pax7 was shown by Relaix et al. (2004), when Pax3 was replaced by Pax7 in gene targeting, and the migration of muscle progenitor cells (pax3^{+} cells) showed a negative substitution indicating that pax7 is unable to replace pax3 function in the embryo (Relaix et al. 2004). Constitutive expression of both *pax* genes in both satellite cells and C2C12 cells showed an increased proliferation rate but a decrease in size (Collins et al. 2009). In the absence of Pax3 and Pax7 skeletal muscle differentiation still can occur, as Myf5 can activate myogenin directly (Relaix et al. 2006). Pax3 has previously been found to be sufficient for the establishment of muscle development in a *pax7*$^{-/-}$ mice as pax3^{+} cells were found in the interstitial space of adult skeletal muscle at pax7^{+} cells population location, that is essential for growth and regeneration (Kuang et al. 2006).

Further observations have shown the attrition of a Pax7-positive cell population in *mdx* and *cav3*$^{-/-}$ embryos until late in gestation. Pax7-positive cells fragments were found in dystrophic muscle (E15.5: *cav3*$^{-/-}$ and *mdx*; E17.5: *mdx*) and was much more severe in *mdx/cav3*$^{+/-}$, suggesting that these cells may undergo apoptosis (Merrick et al. 2009). From the results, the severity of the double mutant showed that dystrophin and cav-3 play an important role for the survival of Pax7-positive cells during myogenesis. However, *in vitro* analysis of apoptosis in dystrophin-deficient myoblasts is lacking,

which would demonstrate the frequency of apoptosis, as well as the significance of the event.

Further study on caveolins showed that the over-expression of caveolin-3 (Cav-3) caused the up- and down-regulation of Pax7 protein levels in dystrophin-deficient myoblasts and WT myoblasts, respectively, whilst the over-expression of caveolin-1 (Cav-1) resulted in the down-regulation of Pax7 protein level in both cell lines. Furthermore, a knockdown of *cav-3* leads to the up-regulation of Pax7 protein levels in both dystrophin-deficient myoblasts and WT myoblasts, whilst a knockdown of cav-1 resulted in the up-regulation of Pax7 only in dystrophin-deficient myoblasts. Therefore, it has been suggested that Pax7 regulation is affected by the ratio of Cav-1/Cav-3 in myoblasts and that the homeostasis of Pax7/Cav-1/Cav-3 has been disturbed in dystrophin-deficient myoblasts. It has also been suggested that reduced protein levels of Pax7 in *mdx* mice may be attributable to the up-regulation of IGF-2 protein levels mediated through Cav-1 and Cav-3, as IGF-2 is associated with Pax7 and was found to be expressed at high levels at E17.5 in *mdx* embryos (Hung-chih 2013).

1.3.3 Post-Translational Modification of Pax7

Generally, translated proteins change their confirmational structure in order to carry out specific functions within a cell. One such modification within a cell is phosphorylation, which can either activate or deactivate an enzyme via the action of kinases at specific phosphorylation sites. Amino acids where phosphorylation can occur are serine (S), threonine (T), tyrosine (Y), histidine (H) and aspartate (D), with serine being the most common site followed by threonine. The structural characteristics of Pax7 are illustrated in Figure 1.7.

Pax3 has been demonstrated to be phosphorylated at ser205 in the region of surrounding the octapeptide domain in proliferating mouse primary myoblasts by casein kinase two alpha 1 (CK2A1) (Miller, Dietz, and Hollenbach 2008). Further study has also shown that GSK3β phosphorylates Pax3 at ser201 and -209, and that all three sites demonstrate a changing pattern in early myogenic differentiation. However, the phosphorylation pattern is different for Pax3-FOXO1 in the alveolar rhabdomyosarcoma (ARMS) cell line, suggesting that an alteration in phosphorylation sites may contribute to protein fusion (Dietz et al. 2011). To date, there have been no studies on Pax7 phosphorylation sites or on the Pax7-FOXO1 fusion protein.

Transcriptional misregulation in cancer of both Pax3 and Pax7 has been reported in alveolar rhabdomyosarcoma (ARMS). This is a soft tissue malignancy which mostly occurs in children aged 1 to 5 years old but less commonly in teens. This sarcoma possesses a fusion protein consisting of Pax3 or Pax7 with FOXO1, result in the formation of cytoplasmic pax-FOXO1 (fusion protein), a transcriptional activator which alters transcriptional activity in the nucleus. Chromosomal aberrations occur involving the translocations t(2;13) (q35;q14) and t(1;13) (p36;q14), which have been identified in about 75-80% of ARMS cells (Bridge et al. 2010).

Recently, it has been reported that Pax7 is regulated/modified by SUMOylation. Pax7 interacts with the SUMO conjugating enzyme known as UBC9, which SUMOylates Pax7 at lysine85 (K85) within the DNA binding domain (Luan et al. 2013). SUMOylated-Pax7 is essential during neural crest development, C2C12 myogenic differentiation, and transcriptional transactivation. In adult satellite cells, the arginine methyltransferase Carm1, specifically methylates an arginine present in the N-terminus of Pax7, and thus is recruited to the WDR5-ASH2L-MLL2 complex for up-

regulating Pax7 target genes (Kawabe et al. 2012). Pax3/7 have also been shown to interact with other proteins involved in chromatin binding, including HIRA, DAXX and PAX3/7BP (Figure 1.8) (Buckingham and Relaix 2015). This binding is important for the up-regulation of Pax7 target genes, such as *Id3* and *Cdc20*. Id3 is a helix-loop-helix (HLH) protein that can also bind with other HLH proteins as a heterodimer. The lack of a basic DNA-binding domain inhibits other HLH proteins from binding to DNA, thus acting as a transcription inhibitor. Binding of Pax7 to the *Id3* promoter is also thought to up-regulate and increase its expression during differentiation. Cdc20 is a regulatory protein that interacts with other proteins during cell division and is highly expressed in proliferating cells. It is responsible for mediating the association of the anaphase protein complex with the mitotic spindle checkpoint protein, MAD1L1 (Kim et al. 2011).

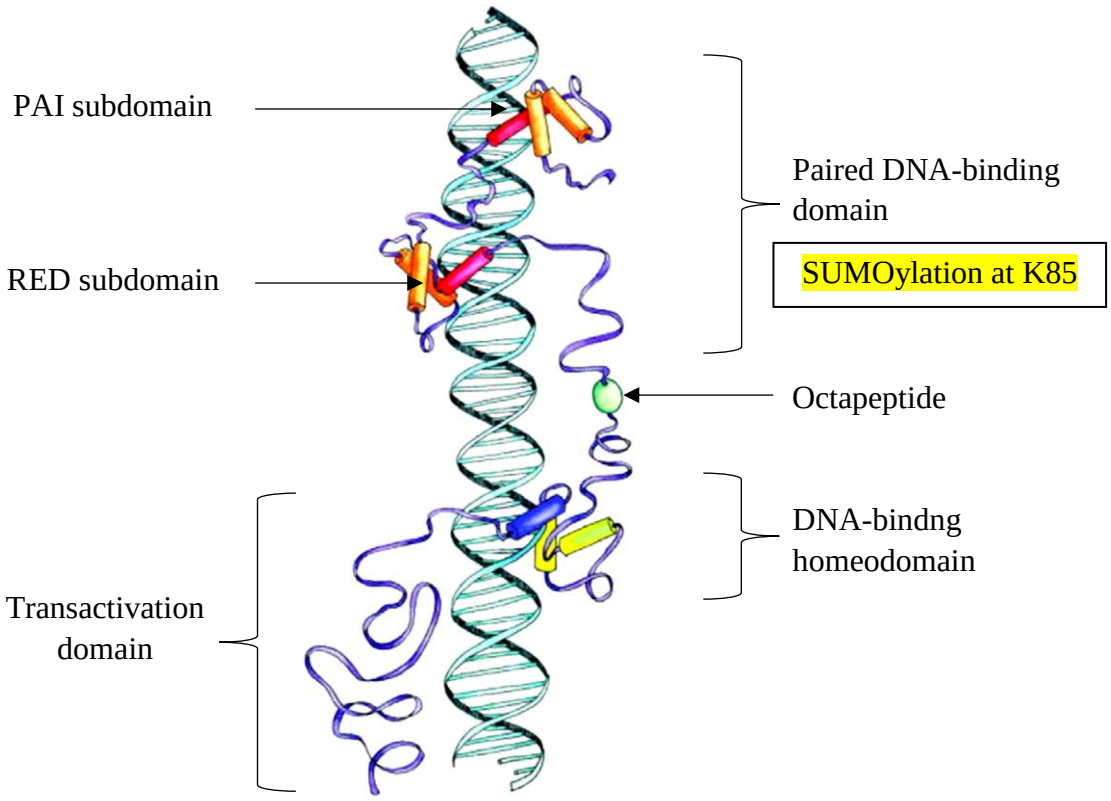

Figure 1.7: Structural characteristics of Pax7
Pax-7 contains a transactivation domain and a DNA-binding domain (also known as a paired domain (PD)). The DNA-binding domain consists of PAI and RED subdomains, which are composed of a three helix-turn-helix motif. There is also an additional DNA-binding homeodomain and octapeptide region.
(modified from (J. A. Blake and Ziman 2014)

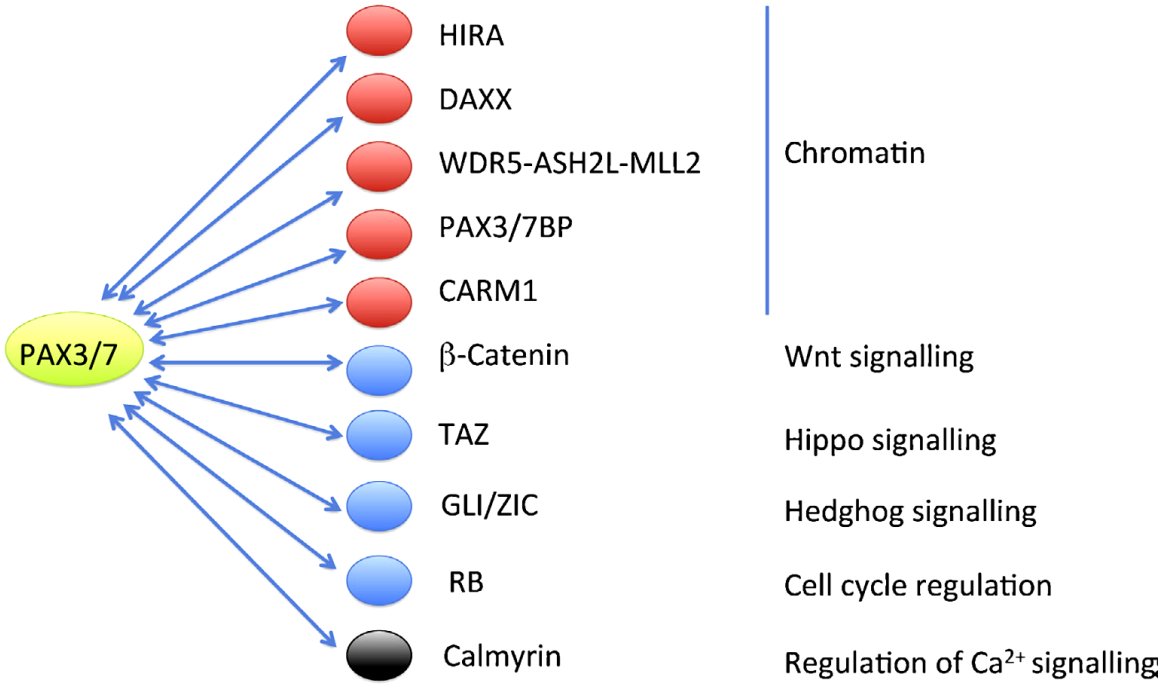

Figure 1.8: Pax3/7 interactions with other proteins
Pax3/7 interacts with proteins that are involved in chromatin binding and regulate the activation of specific genes. It also interacts with B-catenin, TAZ, GLI, RB and Calmyrin, where it is involved in Wnt, Hippo, Hedghog signalling, cell cycle regulation and Ca^{2+} signalling, respectively.
(reviewed in Buckingham and Relaix, 2015)

1.4 Nuclear-Cytoplasmic Machinery

Different from prokaryotic cells, the nucleus and cytoplasm are separated by a double lipid bilayer nuclear envelope (NE) in eukaryotic cells. The nuclear pore complex (NPC), in the NE, tightly mediates the bidirectional traffic of molecules, including proteins, nucleic acids and small molecules, via aqueous channel either passively or actively (Kau, Way, and Silver 2004; Wente and Rout 2010). The nuclear-cytoplasmic machinery involves the NPC, cellular apoptosis susceptibility (CAS), RanGTP, karyopherins (also known as importins/exportins) as well as the specific proteins/RNA complex to be transported. Alterations to any of these factors can cause the failure of protein regulation within a cell, thus affecting the whole process, i.e. up-regulation or down-regulation of genes. For instance, in carcinoma cells the overexpression of CAS (a nuclear export receptor) causes a disruption to the nuclear import of p53 by karyopherin-α, resulting in the cytoplasmic mislocalisation of p53 (Schlamp et al. 1997). CAS overexpression leads to constitutive binding of karyopherin-α and RanGTP, thus depleting karyopherin-α stores for nuclear import (Kau, Way, and Silver 2004).

1.4.1 Nuclear-Cytoplasmic Transport Mechanism for Pax Proteins

The regulation of translated proteins in the cytoplasm is control by various signalling mechanisms, either for secretion or to remain within a cell. For those proteins that play a role as an activator, adaptor or gene regulator, specific transcription factors are need to already be present in the nucleus for the up-regulation, as well as down-regulation of genes, thus they need to be transported into the nucleus. As most of these proteins are larger than 40 kDa, protein adaptors (β-karyopherins) are needed to shuttle them through the nuclear membrane.

Transport receptors, also known as β-karyopherins (importins/exportins), only recognise proteins containing a nuclear localisation signal (NLS). This is a sequence highly enriched with the basic amino acids lysine (K), arginine (R) and histidine (H). It has been reported that phosphorylation of the NLS enhances the binding affinity of importin-α to become part of a complex (Nardozzi, Lott, and Cingolani 2010), which then binds to importin-β and is translocated into the nucleus via the NPC as the karyopherin-β has a binding affinity for nucleoporins within the NPC. This translocation process is also regulated by the gradient of RanGTP, which is asymmetrically distributed and predominantly found in the nucleus. Dissociation of the NLS-protein complex by RanGTP occurs within the nucleus, where the concentration of RanGTP is controlled by RanGEF which converts RanGDP to RanGTP. Importin-β is carried out of the nucleus by RanGTP, while importin-α needs a protein receptor (CAS) to form a complex with in order for RanGTP to be recycled back into the cytoplasm. This nuclear-cytoplasmic transport mechanism is summarised in Figure 1.9 (Kau, Way, and Silver 2004).

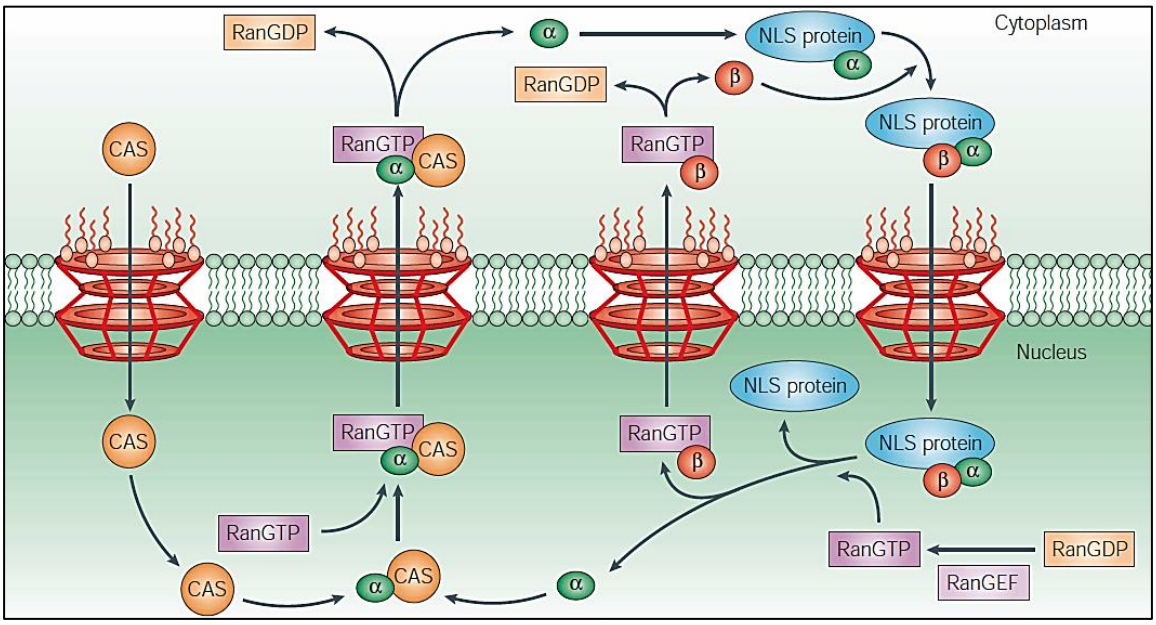

Figure 1.9: Nuclear-cytoplasmic transport of proteins
Karyopherin-α recognises proteins with a nuclear location sequence (NLS) and forms a complex with karyopherin-β before being translocated into the nucleus, where the complex is dissociated by RanGTP. Both karyopherin-β and karyopherin-α are recycled back to the cytoplasm with the aid of RanGTP and CAS, respectively.
(Kau, Way, and Silver 2004)

1.5 The PI3K/Akt Signalling Network in Skeletal Muscles

1.5.1 Regulation of PI3K/Akt in Skeletal Muscle

Skeletal muscle growth is regulated by a highly conserved signalling pathway known as insulin-like growth factor-1 (Igf-1) (Schiaffino and Mammucari 2011; Yu et al. 2015). Activation via the specific growth factor Igf-1 is through binding to the Igf-1 receptor (IGF-1R), a transmembrane protein that resides within the cell plasma membrane and the membrane of subcellular compartments. It has been classified as a class II receptor tyrosine kinase (RTK). Binding of Igf-1 to IGF-1R leads to the activation of protein tyrosine kinase and a series of phosphorylation events. Phosphorylated tyrosine kinase also triggers neighbouring kinases, subsequently generating docking sites for the insulin receptor substrate (IRS), which is also phosphorylated by IGF-1R. Phosphorylated IRS then activates phosphatidylinositol-4,5-biphosphate 3-kinase, also known phosphatidylinositide-3-kinase (PI3K), which is responsible for phosphoinositide-3,4,5-triphosphate (PIP_3) production through phosphorylation of the membrane lipid, phosphoinositide-4,5-biphosphate (PIP_2). PIP_3 acts as a docking site for phosphoinositide dependent kinase-1 (PDK1) and protein kinase B (Akt). Meanwhile, PDK1 is also responsible for Akt phosphorylation at Thr308, which is also phosphorylated at Ser473 by mTORC2 (Sarbassov et al. 2005). Activated Akt regulates various cell signalling activities, including proliferation, differentiation, protein synthesis, protein degradation and apoptosis (Figure 1.10) (Schiaffino and Mammucari 2011).

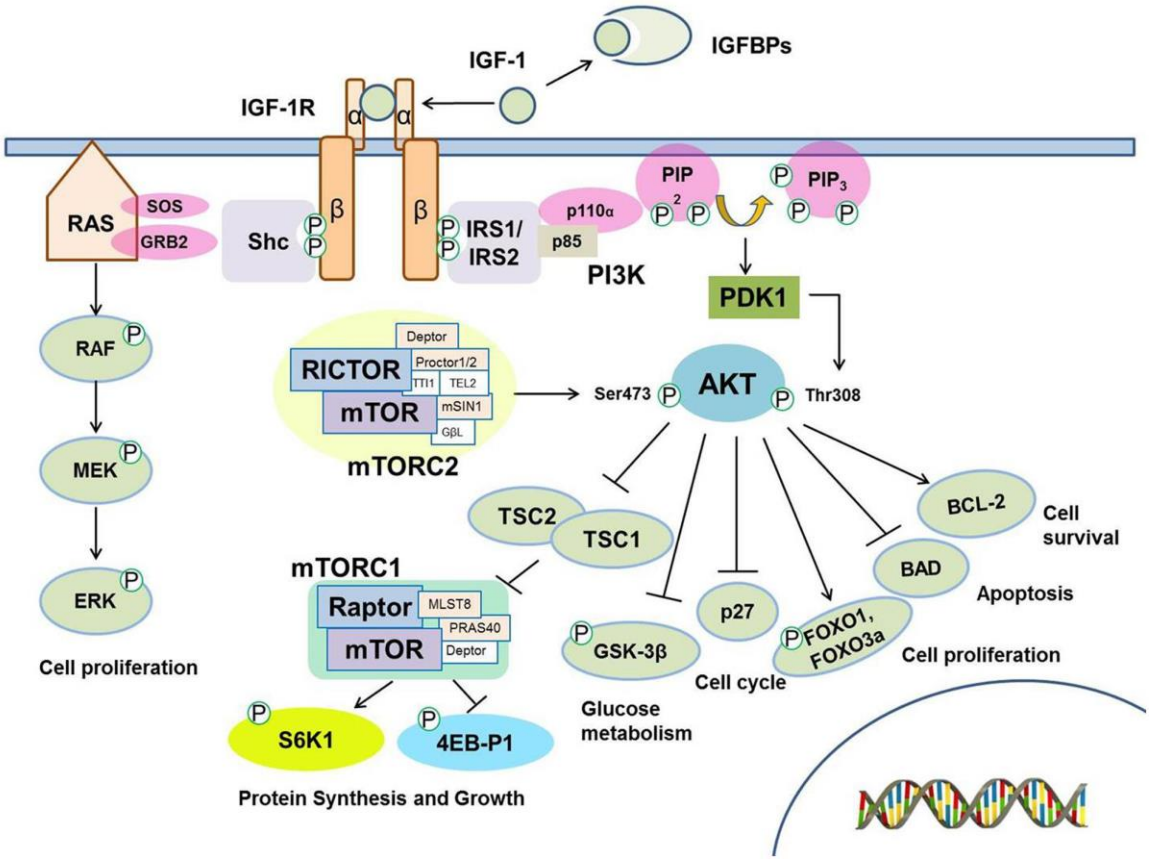

Figure 1.10: The insulin-like growth factor 1 (Igf-1) signalling pathway
The binding of Igf-1 protein to its receptor activates two distinct pathways: 1) PI3K/Akt and 2) Ras/Raf/MEK. The PI3K/Akt pathway results in various cell signalling activities, such as protein synthesis and growth, glucose metabolism, cell cycle, cell proliferation, apoptosis and cell survival. Meanwhile, Ras/Raf/MEK activates cell proliferation signalling.
(Modified from Jin-Jung and Suh, 2015)

1.5.2 Akt

Protein kinase B (PKB), also known as Akt, is a serine/threonine-specific protein kinase that widely regulates various cell signalling activities. It has three distinct isoforms, Akt1, Akt2 and Akt3, with each isoform playing a distinct role in cell regulation. Akt has three major domains, a regulatory domain (hydrophobic region), a catalytic kinase domain, and a pleckstrin homology domain (Du and Tsichlis 2005). Nascent Akt is phosphorylated by mTORC2 at Thr450 within the C-terminal region and this is important for the stability of AGC kinases (Liao and Hung 2010). Phosphorylated Akt is localised to the cytoplasmic compartment in its inactive form until another two

phosphorylation events take place; phosphorylation at Ser473 by mTORC2 and at Thr308 by PDK1. Both phosphorylations have been reported to be important for the full activation of Akt (Sarbassov et al. 2005) however, it remains debatable whether both phosphorylations are necessary in skeletal muscle development.

1.5.3 Mammalian Target of Rapamycin (mTOR) Complexes

mTOR is a protein that functions within multiprotein complexes. It was named after the anti-fungal rapamycin, which specifically targets mTOR and causes association disruption within mTOR complexes. mTOR is an important regulator of skeletal myogenesis and regulates various signalling mechanisms, particularly those involved in myoblast fusion and myotube formation (Shu and Houghton 2009). mTOR exists in two complexes, mTORC1 and mTORC2, and details for each complex are illustrated in Figure 1.11 (Tchevkina and Komelkov 2012).

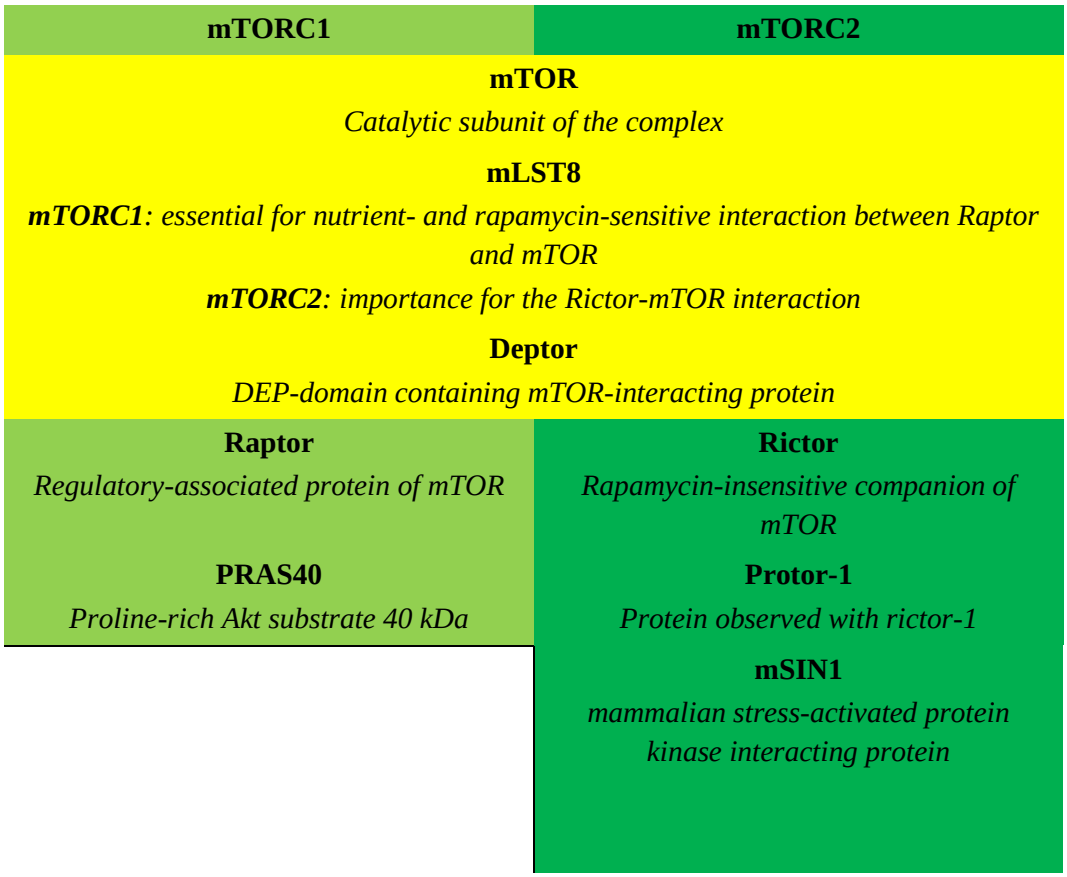

Figure 1.11: The mTORC complexes
mTOR exists in two complexes which contain three similar components, i.e. mTOR, mLST8 and Deptor (yellow). In addition, mTORC1 contains Raptor and PRAS40, while mTORC2 contains Rictor, Protor-1 and mSIN1.

1.5.4 PTEN (Phosphatase & Tensin Homologue Protein)

The phosphatase Tensin homologue deletion on chromosome 10, PTEN, is also known to be a tumour suppressor. PTEN is mainly found in the cytosol and nucleus (Bononi and Pinton 2015) and contains three domains, a phosphatase domain located at the N-terminal region, a C2 domain and a PDZ domain located at the C-terminal region. The phosphatase domain contains a motif for PIP2 binding, while the C2 domain is essential for membrane targeting. The C-terminal region contains multiple phosphorylation sites that regulate its stability, activity and recruitment to the membrane. PTEN acts as a negative regulator for PIP_3 by hydrolysing phosphates in position 3′ to form PIP_2 (Ono

et al. 2001). In its unphosphorylated form, PTEN assumes an open conformation which can activate its phosphatase domain for phosphate hydrolysation. Phosphorylation of PTEN at Ser380 assumes a closed conformation and represents the inactive form.

1.5.5 PI3K/Akt Regulation in Muscular Dystrophy

Many studies have been carried out concerning PI3K/Akt impairment in the *mdx* mouse as well as in DMD in humans. Activation of Akt has been found to be higher in the *mdx* mouse compared to non-dystrophic mouse (Dogra et al. 2006; Clara De Palma et al. 2014) and also in DMD patients (Peter and Crosbie 2006). As Akt plays a major role in cell signalling, its impairment leads to various defects in downstream protein signalling, including cell proliferation, differentiation, apoptosis, autophagy and protein synthesis perturbation.

Akt has also been reported to be highly activated and associated with α-integrin in the *mdx/utr*$^{-/-}$ mouse model (Boppart, Burkin, and Kaufman 2011). Boppart et al. (2011) demonstrated that α-integrin transgenic *mdx/utr*$^{-/-}$ mice (α7βX2-*mdx/utr-/-*) showed increased phosphorylation of Akt at Ser473, indicating that α-integrin expression is connected to Akt. The *mdx/utr*$^{-/-}$ mouse lacks both dystrophin and utrophin, and develops a severe pathology that closely resembles that seen in DMD (Boppart, Burkin, and Kaufman 2011).

Similarly, PTEN has been reported to contribute to the MD phenotype. A study by Feron et al. (2009) on the Golden Retriever muscular dystrophy (GRMD) dog demonstrated that PTEN was present at high levels, which led to a reduction of Akt1, glycogen synthase kinase-3β (GSK3β) and p70S6K, in addition, ERK1/2 displayed decreased phosphorylation levels in GRMD dog muscle. The GRMD dog is characterised by rapidly progressive clinical dysfunction, severe muscle weakness, and

displays a disease progression that is more similar to human DMD compared to the *mdx* mouse (Feron et al. 2009).

1.6 Autophagy in Skeletal Muscle

1.6.1 Mechanisms of Autophagosome Formation

Autophagy is the process of engulfment of cargo into the double lipid formation known as a autophagosome, which eventually fuses with a lysosome and is degraded (Glick, Barth, and Macleod 2010). Autophagic activity is rapidly increased in cells under stress conditions and nutrient deprivation in order to maintain cell homeostasis (Grumati and Bonaldo 2012).

Several autophagy related genes are known to be involved in the formation of autophagosomes. FoxO3 has been shown to induce multiple autophagy genes, including LC3B transcription within skeletal muscle (Mammucari et al. 2007). The light chain 3B (LC3B) isoform of LC3 plays a critical role in this event and undergoes post-translational modification. Next, LC3B-I is converted to lipidated-LC3B-II by the conjugation of membrane lipid phosphatidylethanoleamine (PE) involving the E1-like enzyme ubiquitin Atg7 (Autophagy related 7) and the E2-like enzyme Atg10. LC3B-II then binds to the isolation membrane and mediates membrane elongation until its edges fuse to create an autophagosome. The isolation membrane appears when a cell is placed under starvation conditions. Atg7 also conjugates Atg5 to Atg12 to become the Atg5-Atg12 complex, which then binds to the isolation membrane together with Atg16. This complex binding is necessary for autophagosome formation (Banduseela et al. 2013). A schematic of autophagosome formation is illustrated in Figure 1.12.

1.6.2 FoxO3

Forkhead Box O3 (FoxO3) is a transcription factor/activator and belongs to the O subclasses forkhead family (Webb and Brunet 2014). Its fork head DNA-binding domain recognises and binds to DNA sequences to promote gene activation. It has been reported that FoxO3 up-regulates autophagy related genes (Mammucari et al. 2007). FoxO3 is responsible for regulating two major pathways of muscle protein degradation: 1) the proteasomal-lysosomal, and 2) autophagic-lysosomal pathways (Schiaffino and Mammucari 2011).

1.6.3 LC3B

LC3B is a subunit of microtubule-associated proteins 1A/1B light chain 3B (MAP1LC3B). LC3B belongs to the LC3 family, which consists of three members, LC3A, LC3B and LC3C. LC3B is a structural protein found in the autophagosome membrane. Initially, LC3 is cleaved by Atg4 to produce active LC3B-I, which in turn is activated by Atg7 and becomes membrane-bound during autophagosome formation (Ichimura et al. 2000; Banduseela et al. 2013).

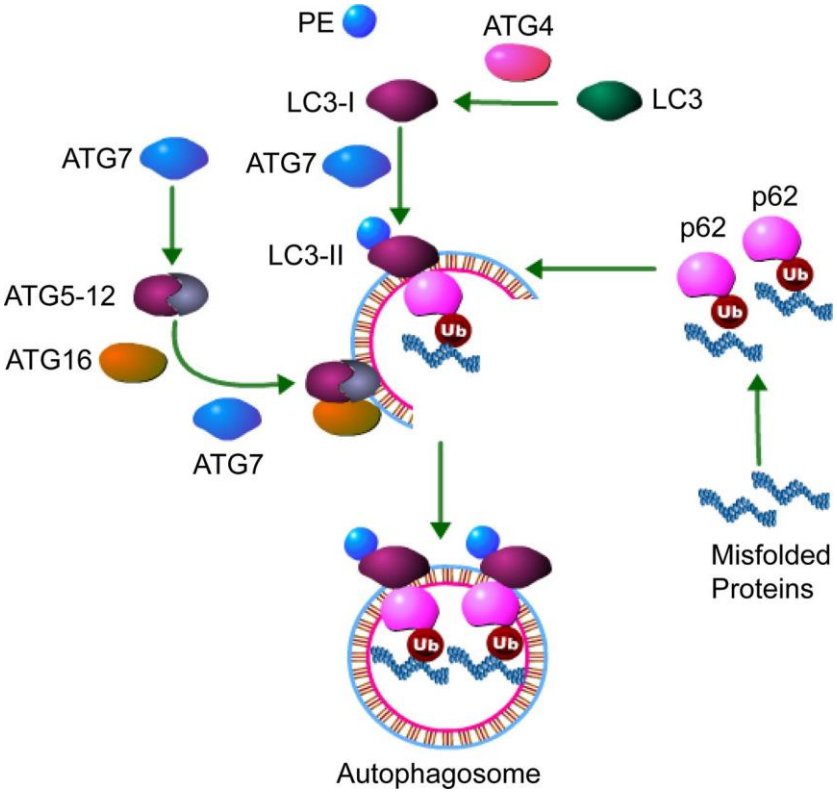

Figure 1.12: Schematic of autophagosome formation
After being translated, LC3B is cleaved by Atg4 to form LC3-I, which is conjugated to PE by Atg7 to become lipidated-LC3-II. LC3-II binds to the isolated membrane and subsequently forms an autophagosome
(Modified from Banduseela et al., 2013)

1.6.4 Autophagy in Models of Muscular Dystrophy

Generally, defective autophagy exhibits a dual response; at high levels it causes muscle atrophy, whilst at low levels it contributes to muscle degeneration. High levels of autophagy result in excessive protein degradation due to high levels of autophagy gene activation (Grumati and Bonaldo 2012). In this state activation of Akt inhibits the activation of autophagy related genes indirectly via mTOR and/or directly phosphorylates the FoxO3a transcription factor (Tchevkina and Komelkov 2012). This event leads to reduced muscle mass and muscle wasting. In contrast, low level autophagy is defined as low autophagy activity which causes an accumulation of dysfunction and unused organelles, i.e. mitochondria, as well as unfolded protein within skeletal muscle. This condition leads to an altered muscle structure with prominent

myonuclei centralisation and fusion abnormalities, which eventually weakens the muscle leading to the dystrophic phenotype (Masiero et al. 2009). Therefore, maintaining autophagy at the appropriate level is crucial within skeletal muscle.

Autophagy is defective in *mdx* mice (Neel, Lin, and Pessin 2013) and DMD humans (C De Palma et al. 2012). Restoration of beclin1 levels in *Col6a1*$^{-/-}$ animals and long-term exposure to a low-protein diet (Grumati et al. 2010; Clara De Palma et al. 2014) can reactivate autophagy and partly ameliorate the dystrophic features/phenotype. *Col6a1*$^{-/-}$ animals display an impairment of basal autophagy, which determines the persistence of dysfunctional organelles in muscle fibres leading to muscle degeneration (Grumati et al. 2010). Treatment with a long-term low-protein diet can reactivate autophagy by normalised Akt activation, thus increasing LC3B conversion and up-regulating autophagy related genes (Langenbach and Rando 2002; C De Palma et al. 2012).

1.7 Endoplasmic Reticulum Stress in Skeletal Muscles

1.7.1 Activation and Regulation of Endoplasmic Reticulum Stress

ER stress occurs when ER homeostasis is disturbed, i.e. there is an imbalance in calcium levels, as well as impaired protein modification in the ER lumen. As a result, the unfolded protein response (UPR) is triggered to alleviate the situation (Rayavarapu, Coley, and Nagaraju 2012; Vandewynckel et al. 2013). UPR activation involves the activation of three distinct ER membrane associated protein receptors: 1) PKR-like eukaryotic initiation factor 2α kinase (PERK); (2) inositol requiring enzyme-1 (IRE1); and (3) activating transcription-6 (ATF6) (Figure 1.13) (Pluquet, Pourtier, and Abbadie 2015).

ER stress causes the dissociation of the Ca^{2+} chaperon protein, BiP (binding immunoglobulin protein) from its conformational binding state on the receptors, thereby activating the receptors (Mekahli et al. 2011). Activated PERK phosphorylates eukaryotic initiation factor-2α (eIF2α) and blocks assembly of 80S ribosomes, thus protein synthesis is disturbed which causes cell cycle arrest. Phosphorylated-eIF2α, in some cases up-regulates activating transcription factor-4 (ATF4) expression to initiate CHOP regulation expression (Rao and Bredesen 2004).

Dissociation of BiP from IRE1 is one aspect of UPR activation, and activated IRE1 acts as a ribonuclease (RNase), which splices the mRNA of X-box-binding protein-1 (XBP1). Consequently, the translational frame is shifted and spliced-XBP1 encodes for ER chaperons and proteins implicated in ER-associated degradation (ERAD) (Rao and Bredesen 2004). Dissociation of BiP also causes the translocation of ATF6 to the Golgi, where it undergoes cleavage by serine protease site-1 (S1P) and metalloprotease site-2 protease (S2P) (Chen, Shen, and Prywes 2002; Nakanishi, Sudo, and Morishima 2005). This results in an active transcription factor being produced which is translocated to the nucleus and induces ER gene activation.

1.7.2 CHOP

CHOP, also known as growth arrest and DNA damage inducible protein 153 (GADD153), is a member of the C/EBP (CCAAT-enhancer binding protein) group of proteins which consists of C/EBPα, C/EBPβ, C/EBPγ, C/EBPδ, and C/EBPε; CHOP is the newest member of this group identified by Ron and Habrer (1992). CHOP is able to dimerise with other C/EBP members and act as a dominant-negative inhibitor (McCullough et al. 2001). Once dimerised, it impairs the C/EBP binding site thus inhibiting C/EBP expression.

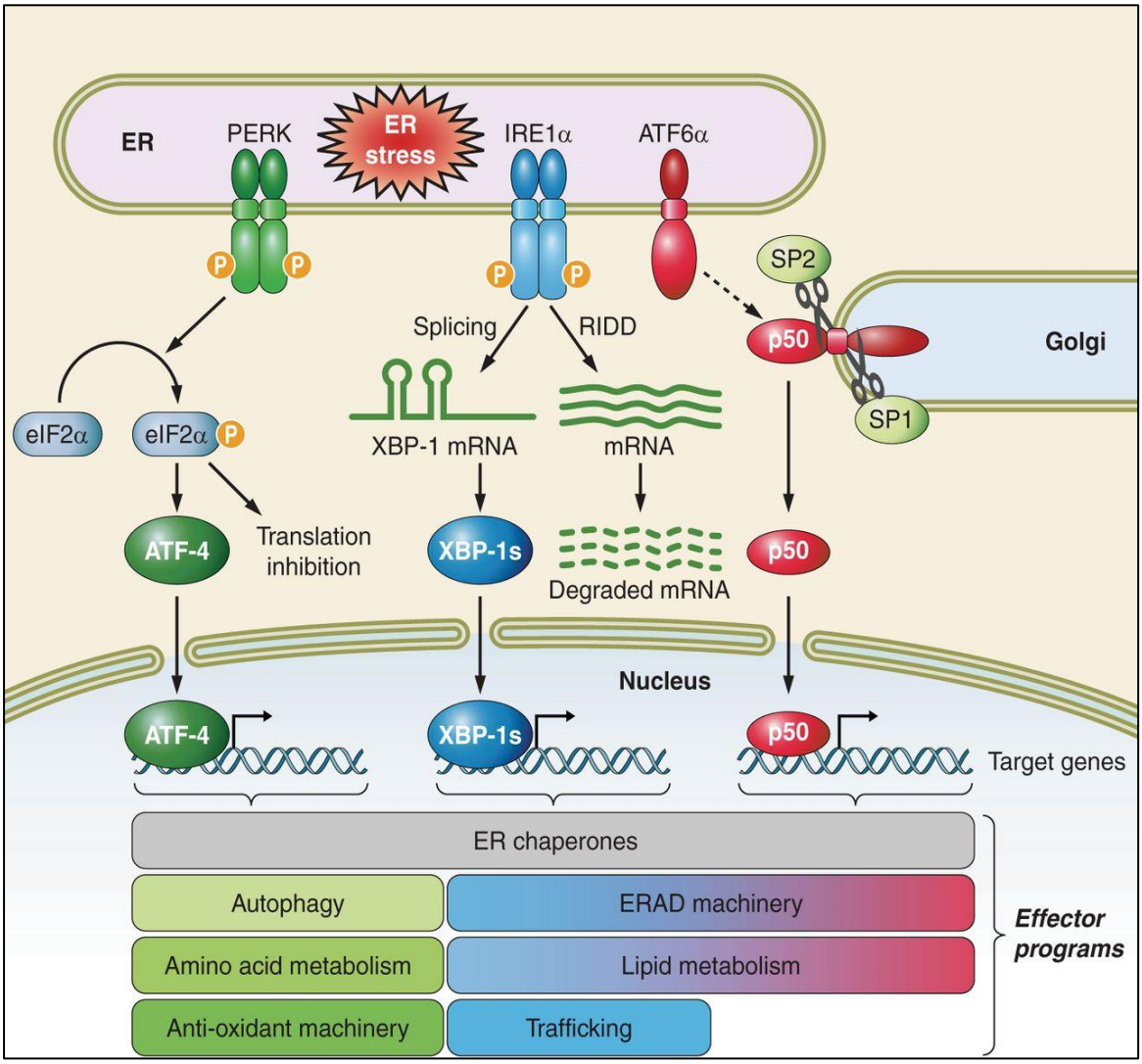

Figure 1.13: Schematic of the unfolded protein response activation
The UPR is activated via three ER transmembrane proteins: 1) PKR-like eukaryotic initiation factor 2α kinase (PERK), (2) inositol requiring enzyme-1 (IRE1); and (3) activating transcription-6 (ATF6). The activated protein receptors subsequently activate ER chaperons to alleviate the ER stress condition.
(Modified from (Pluquet, Pourtier, and Abbadie 2015))

1.8 Hypothesis

In this study, it is hypothesised that pax7 is misregulated and the restoration of minidystrophin to dystrophin-deficient myoblasts can repair/improve/mitigate the dynamics of the protein signalling pathway of PTEN-PI3K/Akt/mTOR, PLC and PKC, as well as alleviate ER stress.

1.9 Aim and Objectives

The goal of this project is to understand Pax7 expression patterns and the underlying protein signalling pathway in dystrophin-deficient myoblasts and to establish whether minidystrophin can fully or partly improve this condition. To achieve this goal, several objectives need to be completed and are listed below:

1. ***Determine Pax7 expression patterns and its transport protein in dystrophin-deficient myoblasts***

It has been reported that the Pax7 expression level is decreased in *mdx* embryos upon gestation (Merrick et al. 2009). However, no study has described the levels *in vitro,* specifically in dystrophin-deficient myoblasts. The first objective is to determine Pax7 expression patterns sub-cellularly in dystrophin-deficient myoblasts. This was achieved via immunofluorescence labelling, as well as immunoblotting. *In silico* analysis, immunoprecipitation and co-immunoprecipitation technique s are used to examine candidates for Pax7 transport, generally known as karyopherins that are responsible for facilitating the transport of Pax7 within the nucleocytoplasmic machinery.

2. ***Investigate the PTEN-PI3K/Akt/mTOR signalling pathway and autophagy modulation in dystrophin-deficient myoblasts during differentiation***

PI3K/Akt/mTOR is a conserved pathway that is activated via the IGF-IR by Igf-1. It has previously been reported that Igf-1 is responsible for myoblast differentiation and that Igf2 triggers myoblast differentiation which controlled by mTOR at the transcriptional level (Erbay et al. 2003). The second objective is therefore to investigate PTEN-PI3K expression in the control of the Akt/mTOR signalling pathway and autophagy modulation in dystrophin-deficient myoblasts. This is achieved by using immunoblotting methods to determine protein expression levels and immunofluorescence for protein localisation. Flow cytometry is used for autophagy flux analysis.

3. ***Investigate the relationship between PTEN elevation and ER stress events in dystrophin-deficient myoblasts during differentiation***

A previous study showed that ER stress occurs during myoblast differentiation and consequently the UPR is activated. During ER stress unfolded and misfolded proteins accumulate in the ER lumen. In the short term, the UPR inhibits protein synthesis but in the longer term it leads to adaptive changes, such as an increase in ER protein folding chaperones. If this is not sufficient to alleviate the stress, apoptosis will occur. Therefore the third objective is to investigate the effects of PTEN overexpression in differentiating dystrophin-deficient myoblasts on PLC and PKC regulation which subsequently affects ER stress and UPR activation. Immunoblotting is used to determine protein expression levels during differentiating stages.

4. ***Examination of the effects of minidystrophin restoration in dystrophin-deficient myoblasts during differentiation***

The absence of dystrophin within a myoblast causes impairments in myoblast differentiation. As full-length dystrophin is very large, minidystrophin restoration will be used to test whether it can improve protein signalling and subsequently improve the

effectiveness of myoblast differentiation. Therefore, the fourth objective is to examine the effects of minidystrophin restoration within dystrophin-deficient myoblasts. PI3K/Akt/mTOR, as well as PLC, PKC and UPR activation, are examined via immunoblotting techniques.

Chapter 2 - Materials and Methods

2.1 Tissue Culture Techniques

Sterile techniques were applied throughout whilst handling all cell lines, culture media and cell culture reagents within the tissue culture room. This room was kept in a clean condition to avoid any contamination.

2.1.1 Cell Lines

The C2C12 myoblast cell line was used in this study, and was established from an adult mouse myoblast C2 cell line derived from the thigh muscle of a 2-month-old mice. The dfd13 cell line was derived from a 5 week-old *mdx* mouse (Smith and Schofield 1994; Smith and Schofield 1997). Mouse embryonic fibroblast (MEF) cells were a gift from Adil Rashid, University of Birmingham, and were used as a control for the phosphorylation of Akt at threonine-308.

2.1.2 Thawing Cell Lines

Before taking a vial containing cells out from the liquid nitrogen tank, the growth medium (GM) was pre-warmed in a water bath at 37°C, and approximately 5 mL of growth medium was added to a new falcon tube. The vial was taken out and quickly thawed in a 37°C water bath until three-quarters melted, before transferring the cells to the falcon tube and subjecting them to centrifugation for 3 minutes at 1200 rpm. The supernatant was discarded and the pelleted cells re-suspended in 5 mL growth medium before repeating the centrifugation step. The supernatant was again discarded and the cells re-suspended in 5 mL growth medium and transferred to a T25 flask with a filter cap before being incubated in a 37°C incubator supplied with 5% CO_2 overnight. The cells were monitored and observed daily under a microscope and sub-cultured when

they reached 70% to 80% confluence, as greater than 80% confluency will cause cells to differentiate.

2.1.3 Sub-culture of Cell Lines

After 2 or 3 days of culture, or when ~70% to 80% confluence was reached, cells were sub-cultured into a new flask using the 1:10 ratio. The spent medium was removed and the cells rinsed twice with phosphate buffered saline (PBS). Approximately 1 mL of trypsin-EDTA was added and the cells were incubated in a 37°C incubator supplied with 5% CO_2 for 3 minutes to allow the cells to detach. The flask was then knocked gently and observed under a microscope to check whether the cells had fully detached from the surface. Approximately 1 mL of growth medium was added to stop the trypsin-EDTA reaction and the cells were then split using the 1:10 ratio into new flasks or frozen down for stocks.

2.1.4 Freezing Down Cell Lines

After trypsinisation the cells were collected by centrifugation at 1200 rpm for 3 minutes, and the supernatant discarded and the pelleted cells resuspend in 5 mL growth medium. The centrifugation step was then repeated, the supernatant replaced with freezing medium (growth medium + 10% DMSO), and the cells aliquoted into labelled vials. The vials were stored in a -80°C freezer overnight prior to transfer into a liquid nitrogen tank the following day.

2.2 Determination of the Cell Number

A haemocytometer was used to determine the number of cells. After trypsinisation, approximately 10 µL of the cell suspension was removed and pipetted slowly onto the haemocytometer with cover glass on it (Figure 2.1). Both counting chambers were filled

with cells and placed under an inverted microscope in order to visualise the cells within the large square (grids) of the haemocytometer (Figure 2.1). The cells were counted and the total cell number was calculated according to the formula:

$$\text{Cell count (cell/mL)} = \frac{\text{Average cell number counted}}{\text{4 squares}} \times 10^4 \times \text{Dilution factor}$$

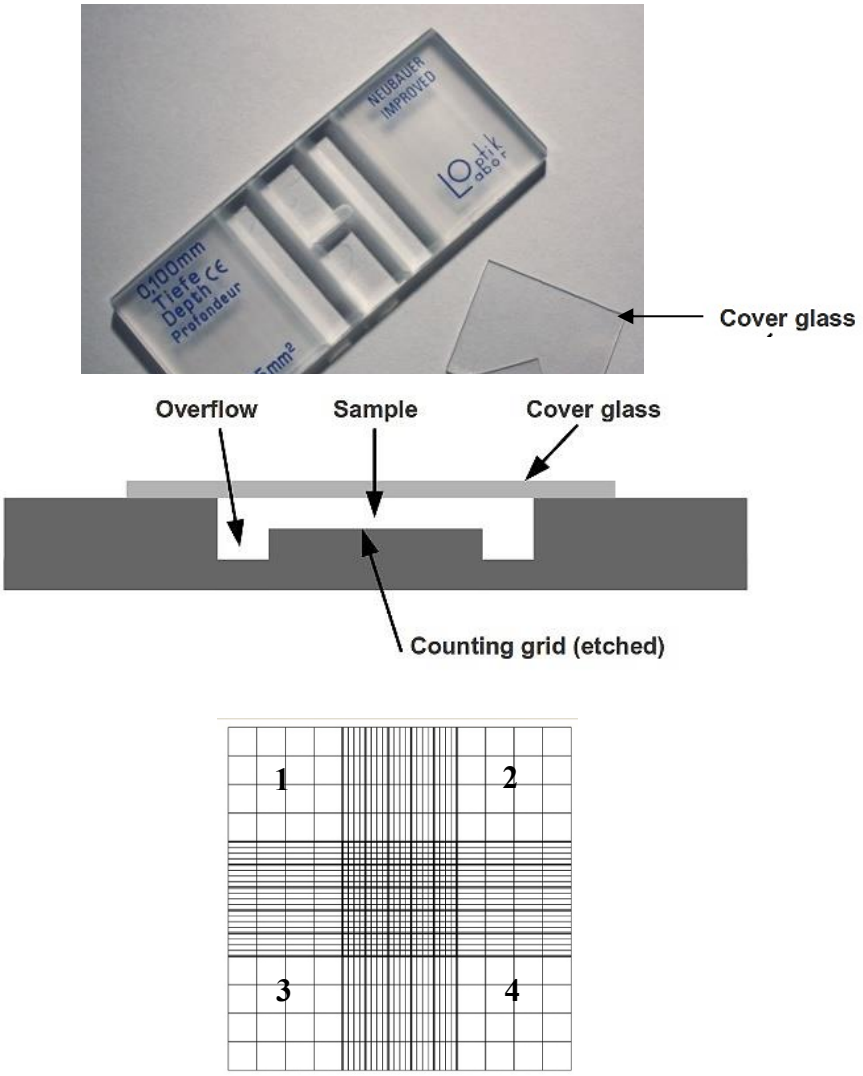

Figure 2.1: Haemocytometer for counting the cell number
Cells were pipetted between the slide and cover slip prior to counting the number of cells on the numbered grids.

2.3 Production of Pax7-FLAG and Mini-Dystrophin$^{\Delta H2\text{-}R19}$ Myoblasts

2.3.1 Bacterial Culture for Plasmid Amplification

Bacterial stocks containing recombinant plasmid and control plasmid (obtained from Dr. Chen Hung-Chih) were removed from a -80°C freezer and thawed on ice. Approximately 200 µL of bacterial stock was added to 250 mL of Luria-Bertani (LB) medium containing 100 µg/mL ampicillin (Sigma Aldrich, UK) and incubated with vigorous shaking at 37°C in incubator shaker (INNOVA™ 433, New Brunswick Scientific) for ~18 hours. The cultures were then transferred into universal tubes and subjected to centrifugation (Avanti™ 30 centrifuge, Beckman Coulter, UK) at 4°C for 10 minutes before proceeding with the plasmid purification.

2.3.2 Plasmid Purification using the PureYield™ Plasmid MaxiPrep System

Recombinant plasmids were purified using the commercial kit PureYield™ Plasmid MaxiPrep System (Promega, UK), and the purification was performed according to the manufacturer's protocol. The cultures were pelleted by centrifugation at 6000 rpm (Avanti 30 centrifuge, Beckman Coulter, UK) at 4°C for 10 minutes and cells lysed using the cell lysis solution before subjecting to centrifugation at 6000 rpm at 4°C for 30 minutes. The pellets were discarded and the supernatant transferred to a new tube for the plasmid purification step. A special binding column attached to a vacuum manifold was used to obtain plasmid DNA. To the column bound-plasmid, endotoxin removal solution was added to eliminate endotoxin contamination before washing and eluting the plasmid DNA in nuclease-free water. The yield was determined via optical density (OD) readings.

2.3.3 Introduction of the Pax7-FLAG Plasmid into Myoblasts via the K2® Transfection System

K2 transfection system is based on powerful cationic lipids. It is also containing multiplier which decreased cells' ability to detect nucleic acids thus reduced defense modus activation (immune system activation). Approximately 9.0 x 10^5 myoblasts were added to a 6 well-plate and cultured until 90% to 100% confluence was reached. When the cell growth coverage area is at its strongest them this allows the uptake of plasmid DNA into the nucleus through the break up and rebuilding of the core membrane during cell division. Approximately 2.4 µg of plasmid DNA was introduced into both C2C12 and dfd13 myoblasts.

2.3.4 Introduction of the Minidystrophin-eGFP Plasmid into Myoblasts using Lipofectamine® LTX and PLUS™ Reagents

Transfection of minidystrophin-eGFP myoblasts was undertaken by Dr. Chen Hung-Chih during his doctoral research under the supervision of Dr. Janet Smith (Hung-chih 2013). A schematic of minidystrophin-eGFP is illustrated in Figure 2.2. Selection of the transfectants was performed by myself. Approximately 3 x 10^5 myoblasts were plated in a 24-well plate and cultured until they reached 80-100% confluence. About 1.5 µg of plasmid DNA was diluted in 100 µL of SFM and 1.5 µL of PLUS™, and the mixture mixed and incubated at room temperature for 5 minutes. Lipofectamine® LTX was then added and incubated for 20 minutes at room temperature. Cells were washed with SFM during the DNA-liposome complex formation and after 20 minutes of incubation the DNA-liposome complex was dropped onto the cells and incubated for at least 16 hours at 37°C. The medium was replaced with fresh medium and cultured for 24 hours before selection.

2.3.5 Transfectant Selection and Verification

All the cells were selected for stable plasmid expression of minidystrophin-eGFP. The cells were selected by culture in growth medium containing 800 µg/mL of geniticin (G418; Invitrogen, UK). The medium was changed every two days until the colonies derived from the transfectants appeared and non-transfected cells died when treated with geniticin. Transfectants were picked and transferred to a 25cm flask in order to expand the culture. For further verification of the selected cells, immunoblots and immunofluorescence techniques were performed to confirm the effectiveness of the transfection. Details of the antibiotics for the selection of are listed in Table 2.1.

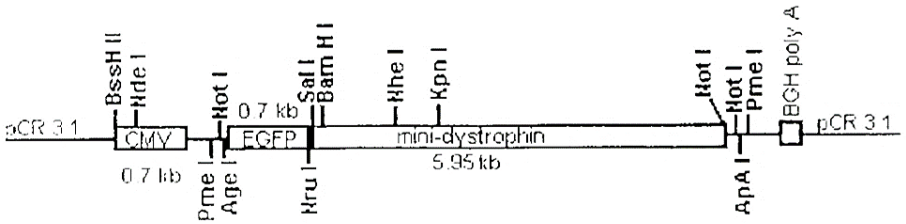

pCR3.1 EGFP-mini-dystrophin (pMDysE)

Figure 2.2: Schematic of pCR3.1 EGFP-minidystrophin
(From Chapdelaine et al., 2000)

Table 2.1: Plasmids used in this study and selection markers

Plasmids	Antibiotic selection markers	Gentamycin selection
pBRIT-Pax7-FLAG	Ampicillin	-
pBRIT His/FLAG		-
pCR3.1-minidystrophin-eGFP	Kanamycin	+
pCR3.1-eGFP		+

2.4 Preparation of Cells for Immunofluorescence

2.4.1 Preparation of Acid Etching Cover Slips

Cover slips (9 mm^2) were placed in a beaker without overlapping and concentrated nitric acid was carefully added onto the cover slips in a fume hood and left for 5 minutes. Used nitric acid was transferred into another beaker filled with water and poured down the sink with copious tap water. Acid-etched cover slips were washed under running tap water for at least 1 hour before soaking in methanol and transferring onto a tissue culture hood to allow complete evaporation overnight. Acid etched-cover slips were sterilised by baking.

2.4.2 Cell Fixation

Culture medium was removed and cells washed with PBS at room temperature for 5 minutes on a shaker. Cells were fixed by adding 4% paraformaldehyde (PFA) to each well and the cells were incubated at room temperature for 10 minutes on a shaker. Each well was rinsed twice in PBS containing 30mM glycine for 5 minutes and then PBS containing 50% glycerol + 0.01% sodium azide was added to each well. The plate was then sealed with tape and stored at 4°C for not more than one week.

2.4.3 Immunofluorescence - Single Labelling

After fixation cells were permeabilised with 0.25% triton X-100 for 5 minutes to allow the antibody to bind specifically. The cells were then washed three times for 5 minutes with PBS before blocking with 5% BSA at room temperature for 30 minutes. The blocking solution was removed and the cells incubated with the primary antibody according to the optimised dilution (

Table 2.2) at 4°C overnight.

The primary antibody was removed the next day and the cells washed three times for 10 minutes with PBST. The primary antibody was probed using a secondary antibody (biotinylated) according to the optimised dilution (

Table 2.2) for 1 hour at room temperature. The cells were washed three times with PBST for 10 minutes before being incubated with streptavidin-Texas red (1:1000) at room temperature for 1 hour in the dark. The cells were then counterstained with DAPI (1:100) for 3 minutes and washed three times with PBST for 10 minutes at room temperature in the dark before rinsing with PBS and mounted onto slides using DakoCytomation. The slides were wrapped in aluminium foil and stored at 4°C.

2.4.4 Immunofluorescence - Double Labelling

The same steps as for single labelling were applied up until the washing step following incubation with streptavidin-Texas red. The cells were washed three times with PBST for 10 minutes in the dark and then incubated with the secondary antibody again for 30 minutes to block the binding of the second primary antibody and avoid cross-reactions with the first primary antibody. The cells were washed three times with PBST for 10 minutes before being incubated with the second primary antibody according to the optimised dilution (

Table 2.2) at 4°C overnight.

The following day the primary antibody was removed and the cells washed three times with PBST for 10 minutes before being probed with the secondary antibody IgG-Alexa488/IgG-FITC at room temperature in the dark. The cells were counterstained with DAPI (1:100) for 3 minutes and washed with PBST three times for 10 minutes. The cells were rinsed with PBS before being mounted onto slides using DakoCytomation. The slides were wrapped in aluminium foil and stored at 4 °C.

Table 2.2: Antibodies used in immunofluorescence
The tertiary antibody for pax7 was streptavidin-Texas red (1:1000)

Primary Antibody (Titre)	Secondary Antibody (Titre)
Mouse monoclonal anti-pax7 (1:500)	Anti-mouse IgG biotinylated (1:1000)
Mouse monoclonal anti-myosin (Skeletal-Fast) (1:100)	Anti-mouse IgG-Alexa594
Rabbit polyclonal anti-Akt (1:500)	Anti-rabbit IgG-Alexa488 (1:500)
Rabbit polyclonal anti-Akt (Phospho-Ser473) (1:200)	
Rabbit polyclonal anti-GM130 (1:200)	
Rabbit polyclonal anti-Rab11 (1:200)	
Mouse polyclonal anti-Ca^{2+}ATPase (1:200)	Anti-mouse IgG-FITC (1:500)
Mouse polyclonal anti-CD107a (1:200)	
Mouse polyclonal Anti-KPNA2 (1:100)	

2.5 Protein-Protein Interaction Assay

2.5.1 Immunoprecipitation Assay

In this study, Pax7 and importin13 were immunoprecipitated using a protein A sepharose CL-4B bead slurry. KPNA2 and FLAG were immunoprecipitated using Dynabeads® Protein G magnetic beads.

2.5.1.1 Protein A Sepharose CL-4B Beads Slurry Preparation

Approximately 2.5 µg of protein A sepharose (powder form) was suspended in 50 mL distilled water in order to eliminate soluble stabilisation agents. The beads were spun down at 2500 rpm at room temperature and the supernatant discarded; this step was repeated 2 more times. The beads were then suspended in 20% ethanol to avoid them drying out.

2.5.1.2 Immunoprecipitation using a Protein A Sepharose CL-4B Beads Slurry

Approximately 100 µg of cell lysate was diluted with lysis buffer and about 20 µL of the protein A sepharose CL-4B beads slurry added to the lysate. The mixture was subjected to centrifugation at 2500 rpm for 1 minute, and the pellet discarded. Approximately 1 µg of antibody was added to the supernatant (pre-cleared lysate) and incubated at 4 °C for 2 hours on a rotator. Next, 30 µL of the protein A Sepharose CL-4B beads slurry was added into the antibody-protein complex and incubated at 4 °C overnight.

The mixture containing the complex-bound beads was subjected to centrifugation at 2500 rpm for 1 minute. The supernatant was discarded and the pellet washed with 30 µL TBS (50 mM Tris-HCl; 150 mM NaCl pH7.4). The centrifugation step was repeated and the pellet resuspended in 20 µL sample buffer and heat-denatured at 95 °C for 7 minutes. The mixture was subjected to centrifugation at 13000 rpm for 1 minute and the supernatant used in Western blot analysis.

2.5.1.3 Dynabeads® Protein G Magnetic Beads

Dynabeads® Protein G magnetic beads were vortexed for about 30 seconds and approximately 50 µL of Dynabeads transferred to a new tube and placed on a magnet to separate the beads from the solution. The supernatant was removed and antibody diluted in 200 µL PBST (PBS containing 0.02% Tween20) added, before being were incubated with rotation at room temperature for 10 minutes. The tube was placed on a magnet for bead separation and washed with 400 µL PBST. Approximately 500 µg cell lysate was added to the beads and the mixture incubated with rotation for 30 minutes at room temperature. Next, the tube was placed on a magnet and the supernatant discarded before washing the beads three times with ice-cold PBST. About 20 µL of sample buffer

was added to the cleaned beads which were resuspended before being boiled at 95°C for 7 minutes.

2.5.2 Antibody Crosslinking

Antibody crosslinking was performed to avoid non-specific binding of antibodies raised is the same host. The crosslinking step was performed at the beginning of immunoprecipitation procedure. After the Dynabeads had been incubated with the antibody for 10 minutes, the tube was placed on a magnet for bead-solution separation. The supernatant was discarded and the beads washed with PBST, followed by two washes in washing buffer (0.2 M triethanolamine, TEA; Sigma-Aldrich, UK, in PBS). The antibody-bound beads were resuspended in crosslinking buffer (20 mM dimethyl pimelidate dihydrochloride (DMP; Sigma-Aldrich, UK, in wash buffer) and incubated at room temperature for 30 minutes on a rotator. The tube was placed on a magnet for bead-solution separation and the supernatant discarded. The beads were washed three times with quenching buffer (0.05 M tris-HCl pH7.5) for 15 minutes on a rotator before approximately 500 µg of cell lysate (diluted in lysis buffer up to 1 mL) was added, and then incubated at room temperature for 30 minutes on a rotator. The tube containing the Dynabeads-Ab-antigen complex was washed three times with ice-cold PBS and the complex resuspended in sample buffer and boiled for 7 minutes at 95 °C prior to Western blot analysis.

2.6 Protein Assay

2.6.1 Total Protein Extraction

Protein was extracted from cells cultured in a 10 cm dish. The medium was removed and the cells washed twice with PBS before adding approximately 300 µL of lysis buffer (0.5% triton X-100, 0.5% deoxycholic acid; 0.15 M NaCL; 0.02 M Tris; 0.01 M

EDTA, pH 7.5) containing a protease inhibitor (complete ULTRA tablets, EDTA-free, protease inhibitor cocktail, Roche, UK). The cells were scraped and collected into a tube before being subjected to centrifugation at 14000 rpm for 15 minutes at 4 °C. The pellet was discarded and the supernatant transferred to a new tube and stored at -20 °C.

2.6.2 Protein Sub-Fractionation

The rapid efficient and practical (REAP) protocol was used for protein sub-fractionation (Suzuki et al. 2010). All reagents were chilled and kept on ice all times. The medium was removed and the cells washed three times with PBS before adding approximately 1 mL of ice-cold PBS. The cells were scraped and collected into a new tube and pop-spun for 10 seconds and the supernatant discarded. The pellet was resuspended in 900 µL of ice-cold PBS containing 0.1% nonyl-phenoxypolyethoxylethanol (NP-40) and approximately 300 µL was removed to a new tube labelled as whole cell lysate (WCL). The remaining cells were pop-spun for 10 seconds and approximately 300 µL was transferred to a new tube labelled as the cytosolic fraction, while the remainder of the supernatant was discarded. The pellet was washed with 1 mL of PBS containing 0.1% NP-40) and pop-spun for 10 seconds; this step was repeated 2 to 5 times to eliminate the cytosolic fraction. After washing was completed this was considered to be the nuclear fraction. The cytosolic fraction was also pop-spun 3 times to separate the remaining nuclear fraction. Both the WCL and nuclear fraction were sonicated three times for 10 seconds and boiled for 1 minute.

2.6.3 Determination of the Protein Yield

While working with protein it was placed on ice at all times to avoid sample denaturation and to maintain protein stability. To determine the protein yield, unknown samples were diluted and compared with serial dilutions of bovine serum albumin

standards (BSA; Pierce, UK). BSA standards were diluted in sterile distilled water to obtain concentrations of 1, 2, 5, 10, 15 and 25 µg/mL, while the unknown samples were diluted in sterile distilled water at the ratios 1:100 and 1:400. Approximately 100 µL of the standards and samples were added to a 96-well plate (Nunc plasticware, UK) in triplicate. An equal volume of Coomassie Protein assay reagent (Pierce, UK) was added to each well and mixed thoroughly with the protein samples. The plate was read at λ=595 nm on microplate reader. The samples were stored in aliquots of 40 µL to avoid freeze-thawing which could damage them.

2.7 Western Blot Analysis

2.7.1 SDS-Poly-Acrylamide Gel Electrophoresis

For specific protein detection, sodium dodecyl sulfate polyacrylamide gel electrophoresis (SDS-PAGE) was used for whole protein separation based on size through the use of different percentages of acrylamide within the gel. SDS with a net negative charge binds to polypeptide changes and is proportional to the molecular mass of the protein. It also destroys most of the complex structure of a protein. The percentage of acrylamide used depends on the size of the protein of interest (Table 2.3).

Table 2.3: Percentage of acrylamide in SDS-PAGE gels based on protein size

Percentage of acrylamide (%)	Range of protein separation (kDa)
6	180>
8	43 - 180
10	26 - 72
12	10 - 55
15	10 - 34

2.7.1.1 Electrophoresis

Before preparing the SDS-PAGE mixture, the Bio-Rad electrophoresis gel apparatus was set up. Both gel casts were cleaned using 70% ethanol and the spacers inserted between two gel casts which were clipped together using the clipper. The resolving gel mixture contained 3.24 mL of dH_2O, 1.84 mL of 30% acrylamide (Protogel, Geneflow, UK), 1.75 mL of 1.5 M Tris-HCl (pH8.8), 70 µL of 10% SDS, 70 µL of 10% sodium persulphate, and 7 µL of TEMED, which was thoroughly mixed and poured into the gel cast until three quarters full and left for 30 minutes until it polymerised. Onto the set resolving gel, the stacking gel was poured and a comb inserted into the gel. The resolving gel contained 1.4 mL of dH_2O, 0.33 mL of 30% acrylamide (Protogel, Geneflow, UK), 0.25 mL of 1.5 M Tris-HCl (pH8.8), 20 µL of 10% SDS, 20 µL of 10% sodium persulphate, and 8.5 µL of TEMED, which was thoroughly mixed and left to polymerise for 30 minutes.

Meanwhile the protein samples were prepared, and approximately 20 µg of each protein extract and 15 µg of embryonic samples were loaded into each well. The samples were mixed with 2.5 µL of 6X sample buffer and dH_2O was added to make up the final volume to 15 µL. The samples were boiled at 100°C for 5 minutes and placed on ice. The comb was slowly removed from the gel to avoid tearing the wells and the gel holder unclipped. The gel was placed in the middle of the electrophoresis tank with

the plastic plates slipped next to it, and the tank fully filled with SDS running buffer. Both the samples and pre-stained protein markers (New England Biolabs, Ltd, UK) were loaded using a pipette. The gel was run at 70V until the dye front reached the end of the gel.

2.7.2 Transfer Blotting using the Trans-Blot® Turbo™ Blotting System

After the samples had been separated on the gel, the glass plates were removed from the tank, the plates separated and the stacking gel removed using a scalpel. Distilled water was used while handling the gel as the running buffer contained detergent which made the gel slippery. The Trans-Blot Turbo^{TM} Transfer System was then used to transfer the separated proteins from the gel onto a nitrocellulose membrane.

2.7.3 Hybridisation, Detection and Analysis

The nitrocellulose membrane with the transferred proteins were blocked with blocking buffer (TBS, non-fat milk, Tween20) for 1 hour at room temperature on a shaker before incubating the membrane with primary antibody and sealed into a plastic bag at 4°C overnight on a shaker. The following day the membrane was washed three times with washing buffer (TBS with 0.1% Tween20) for 10 minutes. The membrane was probed with a biotinylated secondary antibody for 1 hour at room temperature on a shaker with vigorous agitation before washing three times with TBS for 10 minutes. The membrane was probed with the detection labelling agent streptavidin-conjugated DyLight 800 for 30 minutes at room temperature whilst protected from light and after three times washes, was ready to be examined using an Odyssey infrared imaging system (Li-Cor Biotech, UK). A list of the antibodies used with specific titre details is provided in Table 2.4.

Table 2.4: Antibodies used in Western blotting analysis
The tertiary antibody for all was DyLight(TM) 800 Conjugates-Streptavidin (1:20,000)

Primary Antibody (Titre)	Secondary Antibody (Titre)
Mouse monoclonal anti-pax7 (1:500)	Anti-mouse IgG biotinylated (1:10,000)
Mouse monoclonal anti-myosin (Skeletal-Fast) (1:1000)	
Mouse polyclonal Anti-Desmin (1:500)	
Monoclonal Anti-α-Tubulin antibody produced in mouse (1:10,000)	
CHOP monoclonal antibody produced in mouse (1:500)	
Mouse anti-PKC-ε (1:1000)	
Mouse monoclonal anti-ATF6 (1:1000)	
Rabbit polyclonal anti-PKC-ε (phospho-S729) (1:1000)	Anti-rabbit IgG biotinylated (1:10,000)
Rabbit polyclonal anti-PTEN (1:1000)	
Rabbit polyclonal anti-PI3K p85 (1:1000)	
Rabbit polyclonal anti-PI3K p85 (phospho-Tyr458) (1:1000)	
Rabbit polyclonal anti-Akt (1:1000)	
Rabbit polyclonal anti-Akt (phospho-Ser473) (1:1000)	
Rabbit polyclonal anti-Akt (phospho-Thr308) (1:1000)	
Rabbit monoclonal anti-Rictor (1:1000)	
Rabbit monoclonal anti-Rictor (phospho-Thr1135) (1:1000)	
Rabbit polyclonal anti-mTOR (1:1000)	
Rabbit polyclonal anti-mTOR (phospho-Ser2448) (1:1000)	
Rabbit polyclonal anti-p70S6K (phospho-Thr389) (1:1000)	
Rabbit polyclonal anti-p70S6K (1:1000)	
Rabbit monoclonal anti-FoxO3a (1:1000)	
Rabbit monoclonal anti-Beclin1 (1:1000)	
Rabbit monoclonal anti-Atg5 (1:1000)	
Rabbit monoclonal anti-Atg7 (1:1000)	
Rabbit monoclonal anti-LC3A/B (1:1000)	
Rabbit monoclonal anti-PLCγ1 (1:1000)	
Rabbit monoclonal PLC-γ1 (phospho-1248) (1:1000)	
Rabbit polyclonal anti-PKC-α/βII (phospho-Thr638/Thr641) (1:1000)	
Rabbit polyclonal anti-PKC-βII (pan) (phospho-Ser660) (1:1000)	
Rabbit polyclonal anti-ERK1/2 (1:1000)	
Rabbit polyclonal anti-Phospho-ERK1/2 (phospho-Thr202/Tyr204) (1:1000)	
Rabbit monoclonal anti-eIF2α (phospho-Ser51) (1:1000)	

2.8 Autophagy Assay - Live Cell Analysis by Flow Cytometry

2.8.1 Cell Labelling

An autophagy assay was performed using a CYTO-ID Autophagy Detection Kit (Enzo Life Science, Switzerland) and 1 x 10^5/mL myoblasts were added to every well in a 24-well plate and maintained via standard tissue culture practice. Cells were grown in a humidified incubator at 37 °C and 5% CO_2; cells were not allowed to become over-crowded and the density should not exceed 1 x 10^6 /mL. In this experiment 60 mM of chloroquine was used as positive control, while unstained cells were utilised as a negative control. Myoblasts were treated with chloroquine for 4 hours in a humidified incubator at 37 °C and 5% CO_2. At the end of the treatment cells were trypsinised and collected into a fresh 1.5 mL microtube. Cells were subjected to centrifugation for 5 minutes at 1000 rpm at room temperature and washed by re-suspending in 1x assay buffer and the centrifugation step repeated. Each cell pellet was then re-suspended in 250 µL of 1x assay buffer. Approximately 250 µL of the diluted CYTO-ID Green stain solution was added to all the cells except the negative control, and incubated for 30 minutes at room temperature in the dark. The cells were collected by centrifugation, washed with 1x assay buffer, and the pelleted cells re-suspended in 500 µL of 1x assay buffer. The samples were analysed using the green (FL1) channel of a flow cytometer.

2.8.2 Flow Cytometer

Experiments were performed using a FACS Analyser CyAn B (Beckman Coulter, USA) at the Institute of Biomedical Research, University of Birmingham. Samples were run using Summit V4.3 software and all data were saved in the fcs format developed by the Society of Analytical Cytology, thereby allowing further analysis using other software packages. Data were analysed using the software FCS Express 6 Plus (De Novo

Software, USA) for three parameters; side scatter (SS), forward scatter (FS) and Fluorescein Isothiocyanate (FITC). Gating was performed based on the size and complexity of the myoblasts as illustrated in density plots. Gated data were further analysed to count myoblasts labelled with FITC and the results presented in a histogram format.

2.9 Statistical Analysis

All Western blots were repeated at least three times for different protein samples obtained at different times/experiment. Statistical analyses were carried out using the student t-test (Microsoft Excel) and differences were considered significant at $p<0.05$ and $p<0.01$. Standard error was obtained using analysis of variance (ANOVA) in Microsoft excel.

2.10 Microscopy

Images were taken using a confocal microscope (Nikon A1R) under 60x magnification and were analysed/edited using the NIS element software provided by Nikon Corporation. The images were analysed using NIS-elements provided by Nikon® Instruments using object based overlap analysis (ROI). The image was first selected using ROI properties and then separated into a monochrome image and converted into a binary image prior to the threshold. Each binary image was processed using a binary operation to create binary overlays that only exist when the green and red channel signals overlap. Each analysis was repeated at least three times for different samples obtained at different times/experiment.

Chapter 3 - Mislocalisation of Pax7 and its Interaction with Importin-A1 (KPNA2) in Dystrophin-Deficient Myoblasts

3.1 Introduction

Earlier, our group has reported that Pax7 cell is attenuated in the *mdx* embryo during gestation. Pax7 cell fragments have also been found in dystrophic muscle, indicating that the cells are undergoing apoptosis. Immunoblot analysis of whole embryos showed that Pax7 expression was also substantially reduced with age (Merrick et al. 2009). This finding has led to the suggestion that dysregulation of Pax7 takes place in MD as early as during the embryonic stages. Therefore, in this study the Pax7 expression pattern has been further examined during the postnatal/juvenile stage in Pax7 myoblasts isolated from a 5-week old *mdx* mouse.

As a transcription factor, Pax7 is mainly found in the nucleus of myoblasts, but surprisingly, it has been found not only in the nucleus, but also found in cytoplasmic region (i.e. organelles) of dystrophin-deficient myoblasts. However, there are a lack of studies to show what actually happens to Pax7 in dystrophin-deficient myoblasts. There may be a problem in protein trafficking in or out of the nucleus which involves the importin and exportin mediated pathway, or there could be an alteration in the NLS which causes the failure of Pax7 to bind to importins. This could be the cause of the failure of these cells to be differentiated into mature myotubes prior to the development of muscle tissue.

Initially, the capacity of dystrophin-deficient myoblast differentiation was investigated. Analysis of myotube formation was performed by examining the morphology of myotubes and the expression of specific MyHC as a terminal

differentiation marker. The expression of Pax7 upon differentiation was determined. Furthermore, the cytoplasmic-Pax7 subcellular localisation, i.e. endoplasmic reticulum, golgi, recycling endosome and lysosome, for protein synthesis and degradation was examined using subcellular markers. Finally, protein prediction tools were utilised which suggested that a Pax7-karyopherin protein interaction is responsible for nuclear localisation.

3.2 Results

3.2.1 Dystrophin-Deficient Myoblasts Do Not Achieve Terminal Differentiation

In vitro differentiation of myoblasts can be induced in culture through the use of a low mitogen medium (2% horse serum) for a few days. In this study, both C2C12 (non-dystrophic) and dfd13 (dystrophin-deficient) myoblasts were cultured in low mitogen medium (differentiation medium; DM) for 10 days prior to determining their terminal differentiation capacity. Immunofluorescence analyses (Figure 3.1) showed both non-differentiated and differentiated myoblasts. Multinucleated myotube formation can be clearly seen on day 10 of differentiation in C2C12 (Figure 3.1A) myoblasts but is hardly/rarely found in dfd13 myoblasts where less multinucleated cells were observed (Figure 3.1B). This indicates that dfd13 differentiation capacity is impaired; however, the differentiating dfd13 myoblasts can be seen to be aligned and seem to be ready for cell fusion to become myotubes.

Myotube formation was determined by counting the myonuclei present in a myotube that expressed MyHC (fast-type II, F-MyHC) and then normalised against total nuclei. F-MyHC, also called ‘fast-twitch’ fibres, were chosen as the terminal differentiation marker based on the existence of a spectrum of fibre types, with type II

being the most developed form of myosin: type 1 ↔ 1/2A ↔ 2A ↔ 2A/2X ↔ 2X ↔ 2X/2B ↔ 2B (Schiaffino and Reggiani 2011). The number of myonuclei in C2C12 myotubes was 9-fold higher compared to myonuclei in differentiating dfd13 myoblasts ($p<0.01$; $p = 2.9x10^{-3}$). The percentage of myonuclei per total nuclei was 80.2% ± 8.2 in C2C12 myotubes and 8.2% ± 6.6 in differentiating dfd13 myoblasts (Figure 3.1C)

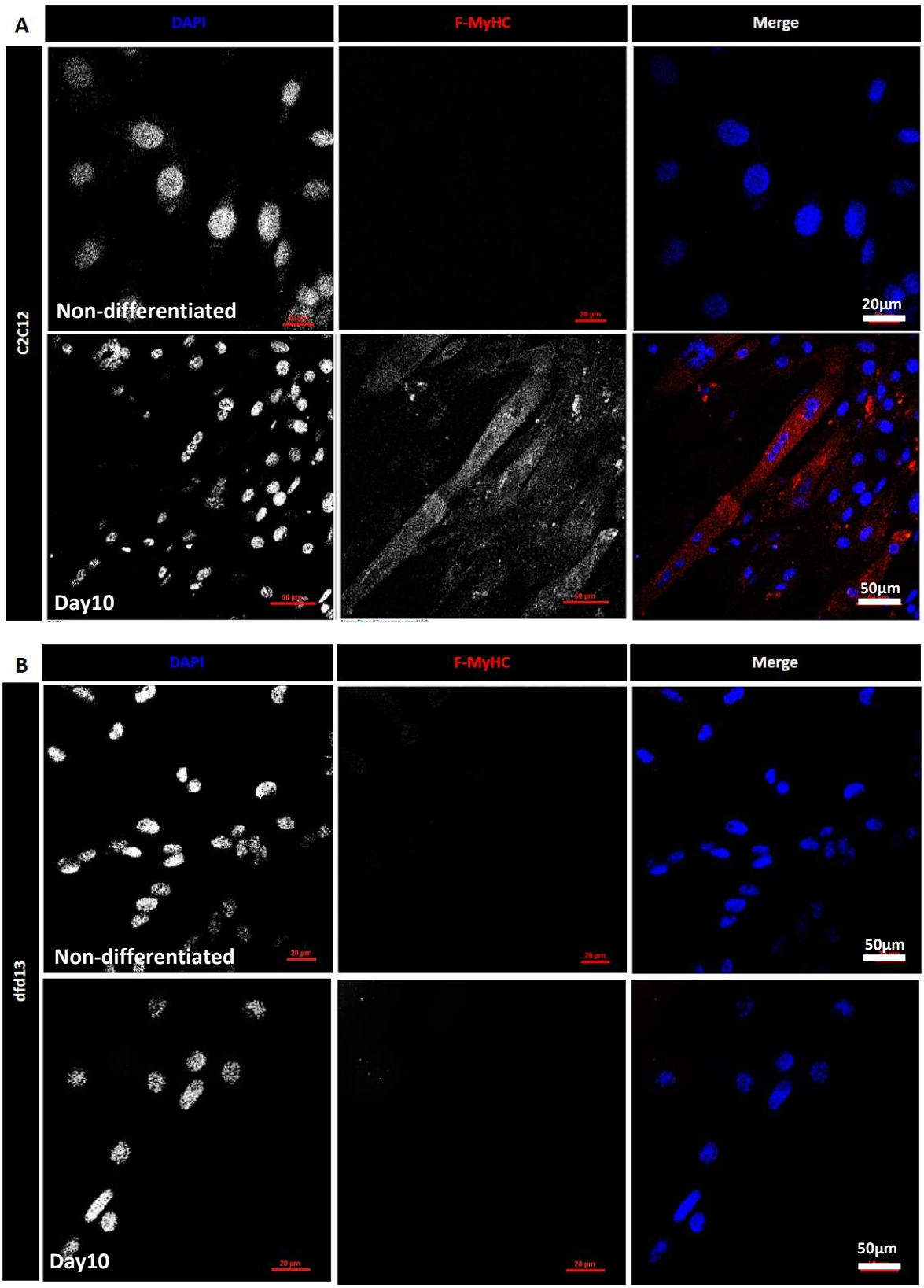
A
DAPI
F-MyHC
Merge
C2C12
Non-differentiated
Day10
20µm
50µm
B
DAPI
F-MyHC
Merge
dfd13
Non-differentiated
Day10
50µm
50µm

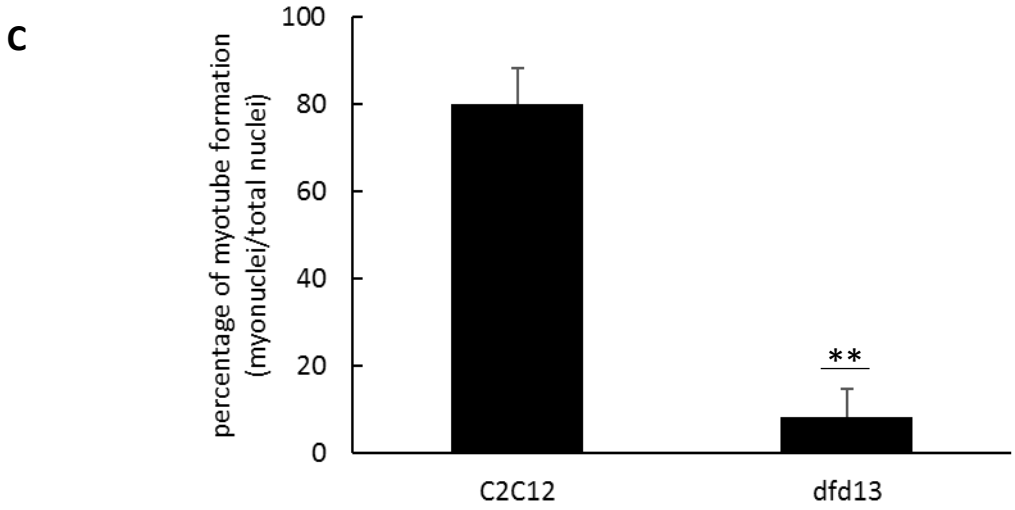

Figure 3.1: Dystrophin-deficient myoblasts formed less myotubes
Approximately 1.5 x 10^4 of both C2C12 (non-dystrophic) and dfd13 (dystrophin-deficient) myoblasts were cultured in GM before being transferred to DM and allowed to differentiate for 10 days in a 48-well plate (on acid-etched cover slip). On day 10 cells were fixed in 4% PFA and stained with an anti F-MyHC antibody, while DAPI was used as a nuclear counterstain. Immunofluorescence analysis of F-MyHC in (A) C2C12 and (B) dfd13 cells during the non-differentiated stage and after 10 days of differentiation. (C) Percentage myotube formation was calculated by counting the nuclei present in myotubes (myonuclei) per total nuclei from 10 random microscope fields. ND: non-differentiated; significant different: ** ($p<0.01$) compared to C2C12 myoblasts; GM: growth medium (DMEM + 10% FCS); DM: differentiation medium (DMEM + 2% horse serum); n=3.

Immunoblotting for F-MyHC, pan-myosin and desmin was performed on days 4, 7 and 10 of differentiation (Figure 3.2A). Generally, F-MyHC expression was increased upon differentiation in C2C12 myoblasts but none of the differentiating dfd13 myoblasts showed any expression (Figure 3.2B). However, pan-myosin was expressed at day 10 in dfd13 myoblasts (Figure 3.2C), and there was a significant difference in expression ($p<0.01$; $p = 7.78 \times 10^{-3}$) when compared to C2C12 myoblasts. Desmin expression in both myoblasts was also examined and was found to be drastically increased upon differentiation, in C2C12 myoblasts. In differentiating dfd13 myoblasts, desmin expression gradually increased over the 10 days and was significantly higher ($p<0.01$; $p = 2.24 \times 10^{-3}$) in comparison to levels in C2C12 myotubes (day 10) (Figure 3.2D). Desmin was used as an intermediate differentiation marker and is a muscle specific type

II intermediate filament that integrates the sarcolemma, Z-disk and nuclear membrane in myoblasts. An *in vivo* study by Smythe et al. (2001) indicated that desmin expression is up-regulated during myogenesis and demonstrated that desmin(-/-) showed delays in myotube regeneration 5 days after transplantation when compared to the control where desmin was detected (Smythe et al. 2001). Desmin also has been reported overexpressed at molecular level in DMD patient (Haslett et al. 2002).

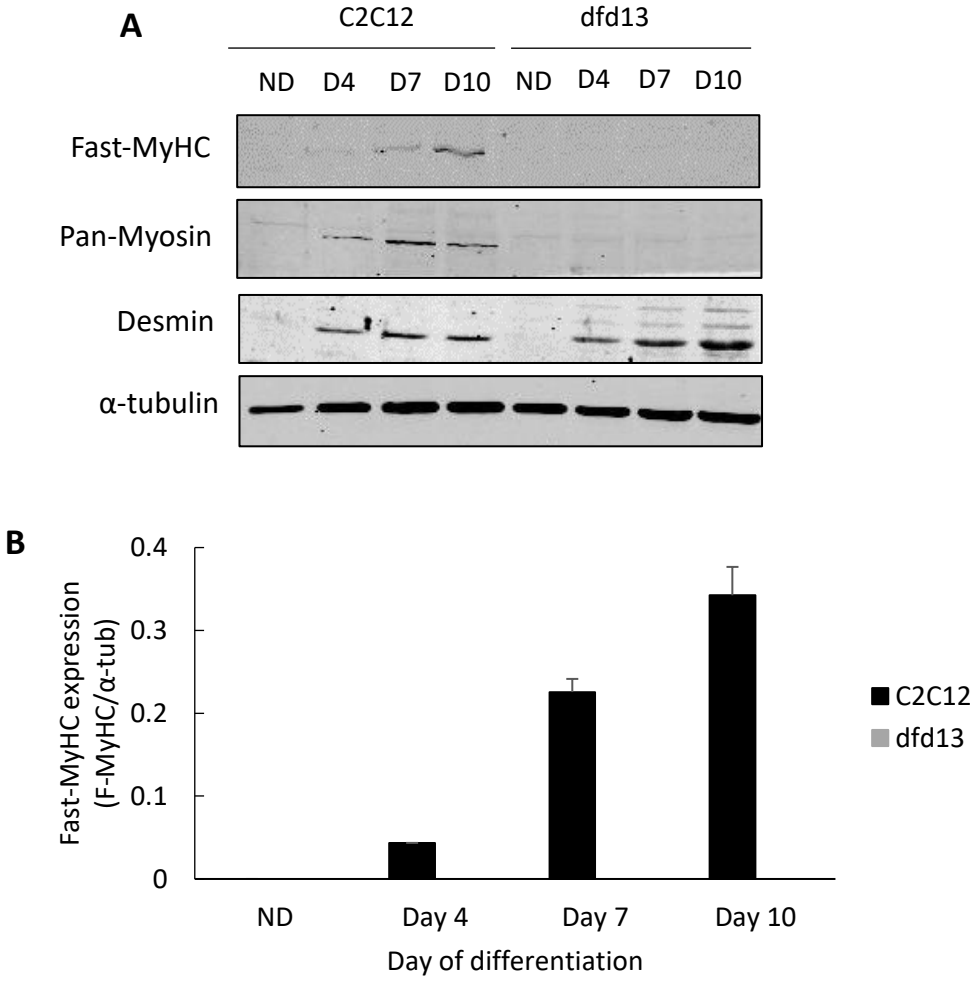

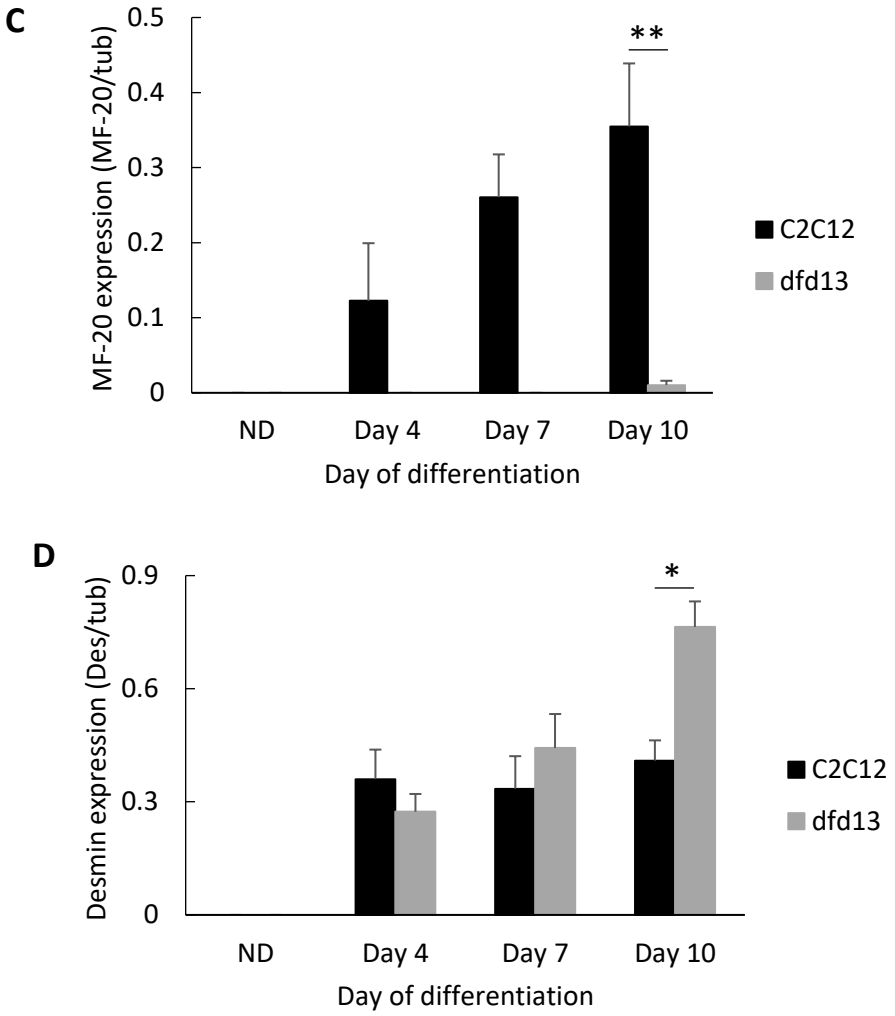

Figure 3.2: Dystrophin-deficient myoblasts do not express fast-myosin heavy chain during differentiation

Both C2C12 and dfd13 myoblasts were seeded in 10-cm dishes and cultured in GM until 80-90% confluent. The myoblasts were washed twice with PBS and then cultured in DM for 10 days, which was changed every 2 days. Total protein was extracted at the indicated time points and immunoblotted with antibodies recognising the proteins F-MyHC, pan-myosin (MF-20) and desmin. (A) Representative immunoblot of the proteins during myoblast differentiation with α-tubulin expression as a loading control. Densitometry analyses of (B) F-MyHC (MY-32), (C) pan-myosin (MF20) and (D) desmin expression. The graphs represent an average of three repeats from different samples. ND: non-differentiated; **: significantly different ($p<0.01$) compared to dfd13 myoblasts. GM: growth medium (DMEM + 10% FCS); DM: differentiation medium (DMEM + 2% horse serum); n=3.

3.2.2 Pax7 Expression Remains Higher in Differentiating Dystrophin-Deficient Myoblasts

As Pax7 cells and Pax7 expression was found to be attenuated in *mdx* embryos, its expression in the postnatal/juvenile stage was investigated. C2C12 and dfd13 myoblasts were initially cultured in GM overnight or until they reached 90% confluence before being replaced with DM. The cells were harvested and subjected to whole protein extraction for ND (non-differentiated) and after 4, 7 and 10 days of differentiation. Each sample was immunoblotted with an anti-Pax7 antibody to examine the level of Pax7 expression throughout the 10 days of differentiation.

Immunoblotting (Figure 3.3) showed that Pax7 is highly expressed in both types of undifferentiated myoblasts, although slightly lower in dfd13 myoblasts. Densitometry analysis showed that the level of Pax7 expression in differentiating dfd13 myoblasts was higher than in differentiating C2C12 myoblasts throughout the 10 days of differentiation. The level of Pax7 showed a significant reduction at day 4 ($p<0.01$; $p= 4.85x10^{-3}$) and day 7 ($p<0.05$; $p= 2.81x10^{-2}$) and was slightly increased at day 10 ($p<0.05$; $p=4.64x10^{-2}$) in the myogenic differentiation of C2C12 cells when compared to the non-differentiated state. However, Pax7 expression in differentiating dfd13 myoblasts remained high until day 7 and had decreased by day 10 ($p<0.05$; $p= 4.17x10^{-2}$). There was a significant difference in Pax7 expression between both the differentiating C2C12 and dfd13 myoblasts on day 7 ($p<0.05$; $p= 1.75 \times 10^{-2}$).

Pax7 is a transcription factor that plays role in gene regulation/activation during myogenesis. It has been reported that Pax7 directly regulates Myf5 (McKinnell et al. 2008; Günther et al. 2013) however, up-regulation of Pax7 expression inhibits myogenic differentiation due to the down-regulation of myogenin (Olguin et al. 2007;

Olguín and Pisconti 2011), and differentiation onset is delayed. In this study, Pax7 remained at a high level of expression 7 days after differentiation commenced, indicating that differentiation may be delayed in dfd13 myoblasts. However, there was a significant reduction in Pax7 on day 10 in dfd13 myoblasts, suggesting that dfd13 myoblasts are prone to apoptosis. Pax7 acts as a survival factor in myotubes (Olguin et al. 2007; Olguín and Pisconti 2011), thus down-regulation of Pax7 may cause apoptosis.

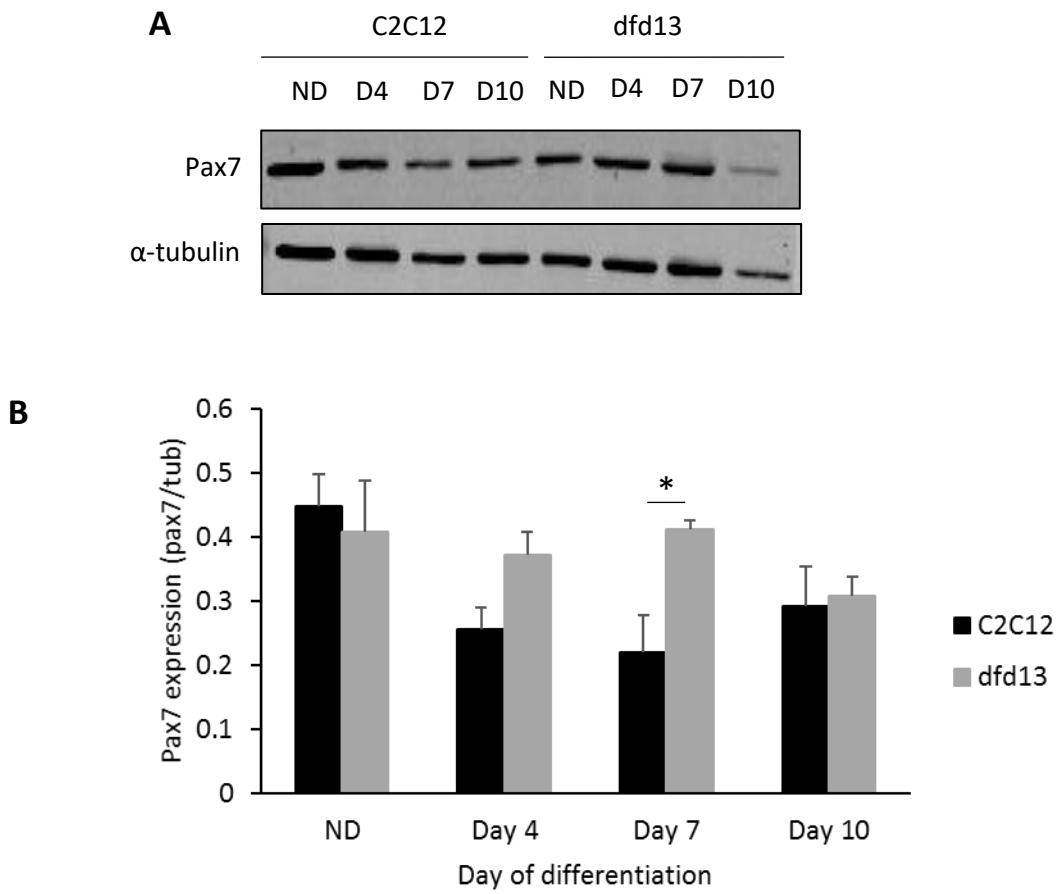

Figure 3.3: Pax7 expression remains high in differentiating myoblasts
Both C2C12 and dfd13 myoblasts were cultured in GM overnight. After reaching 90% confluence, myoblasts were washed with PBS and cultured for 10 days in DM which was changed every two days. Myoblasts were harvested at days 4, 7 and 10 and subjected to protein extraction prior to immunoblotting with an antibody recognising Pax7, with α-tubulin used as a loading control. (A) Representative immunoblot of Pax7 and α-tubulin expression. (B) Densitometry analysis of Pax7 expression. The graph represents an average of three repeats from different samples. ND: non-differentiated; Significant different: * ($p<0.05$) compared to C2C12 myoblasts. GM: growth medium (DMEM + 10% FCS); DM: differentiation medium (DMEM + 2% horse serum); PBS: phosphate-buffered saline; n=3.

3.2.3 Pax7 is Mislocalised in Proliferating Dystrophin-Deficient Myoblasts

To further examine the Pax7 expression pattern, both types of myoblasts were subjected to immunofluorescence and sub-fractionation analyses. Again there is a lack of studies on Pax7 regulation in myoblasts in terms of the post-translational modifications, i.e. phosphorylation events, as well as protein distribution. In this study, Pax7 expression

and its distribution was assessed in dystrophin-deficient myoblasts, with C2C12 myoblasts used as a control.

In line with the role of Pax7 as a transcription factor, the immunofluorescence data showed the localisation of Pax7 within the nucleus of both types of myoblasts (Figure 3.4). However, it also showed that Pax7 was localised outside the nucleus, within the cytoplasm compartment. The pattern of Pax7 distribution was mostly perinuclear, and in the dfd13 myoblasts it could also be found scattered within the cytoplasm (Figure 3.4). Pax7 was labelled with AlexaFlour®594 dye (red) in both types of myoblasts and counterstained with DAPI. The images were taken using a confocal microscope (Nikon A1R) and were analysed/edited using the NIS element software provided by Nikon Corporation. However, this analysis was not able to provide the exact amount of Pax7 expression in both compartments, thus immunoblotting analysis was performed.

Cellular fractionation was performed for both types of myoblast during the proliferative stage. For protein yield validation, specific markers were used, including the structure-specific recognition protein-1 (SSRP-1) and α-tubulin for nuclear and cytoplasmic fractions, respectively. Immunoblots showed that SSRP-1 was not present in the cytoplasmic fraction and α-tubulin was completely absent from the nuclear fraction, indicated that these fractions were not contaminated with each other (Figure 3.5A).

Immunoblot analysis on the subfractionated myoblasts showed that about 27.5% of Pax7 in C2C12 cells was localised to the nucleus, while only 11.1% of Pax7 in dfd13 myoblasts was localised to the nucleus (Figure 3.5B). Nuclear-Pax7 expression was normalised with SSRP-1, while cytoplasmic-Pax7 was normalised with α-tubulin. The

immunoblot data revealed that most Pax7 was found in the cytoplasm of both types myoblast (Figure 3.5B). The specific localisation distribution generally indicates that Pax7 is heading to an unknown protein event. For example, perinuclear Pax7 in C2C12 cells could be due to Pax7 being abundantly synthesised in the cytoplasm and then retained in the cell during the undifferentiated stage where it is maintained by cell proliferation.

Pax7 expression was found to be scattered throughout the cytoplasm of dfd13 myoblasts. This observation shows that Pax7 is extensively mislocalised in dfd13 myoblasts, suggesting that Pax7 is misregulated during the proliferative stage. Unpublished data from Chen (2013), showed that Pax7 was expressed at slightly higher levels in undifferentiated dfd13 myoblasts compared to undifferentiated C2C12 myoblasts. However, there no data has previously reported on the level of Pax7 expression in the nucleus and cytoplasm of myoblasts separately. Further examination of cytoplasmic-Pax7 in subcellular fraction was undertaken via co-localisation analysis.

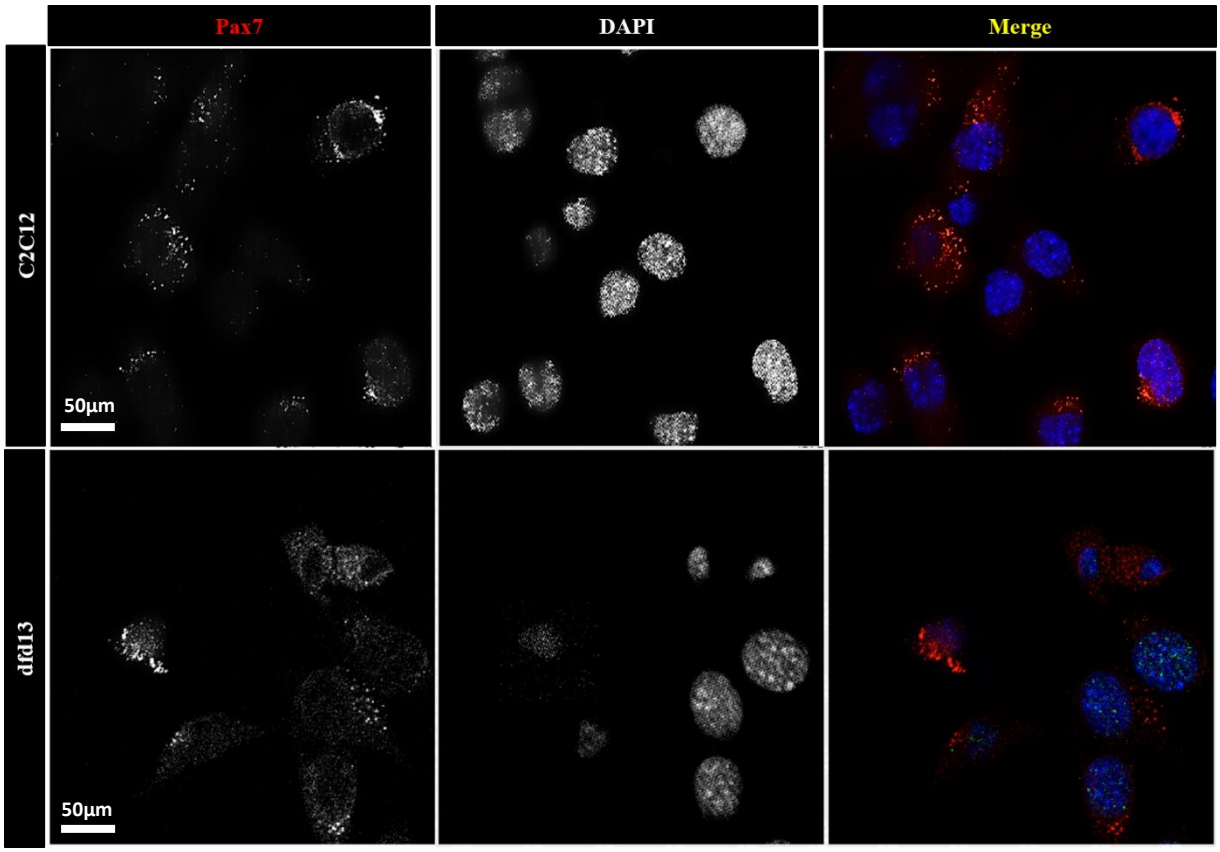

Figure 3.4: Pax7 is more widely scattered in the cytoplasm of dystrophin-deficient myoblasts

Approximately 1.5 x 10^4 C2C12 and dfd13 myoblasts were cultured in GM until 60-70% confluent in a 48-well plate. Both types of myoblast were fixed in 4% PFA and subjected to immunofluorescence labelling. Pax7 was labelled with AlexaFlour594 and the myoblasts were counterstained with DAPI. Immunofluorescence of Pax7 in C2C12 and dfd13 images were taken using a confocal microscope (Nikon A1R) and were analysed/edited using the NIS element software provided by Nikon Corporation. GM: growth medium (DMEM + 10% FCS); n=3.

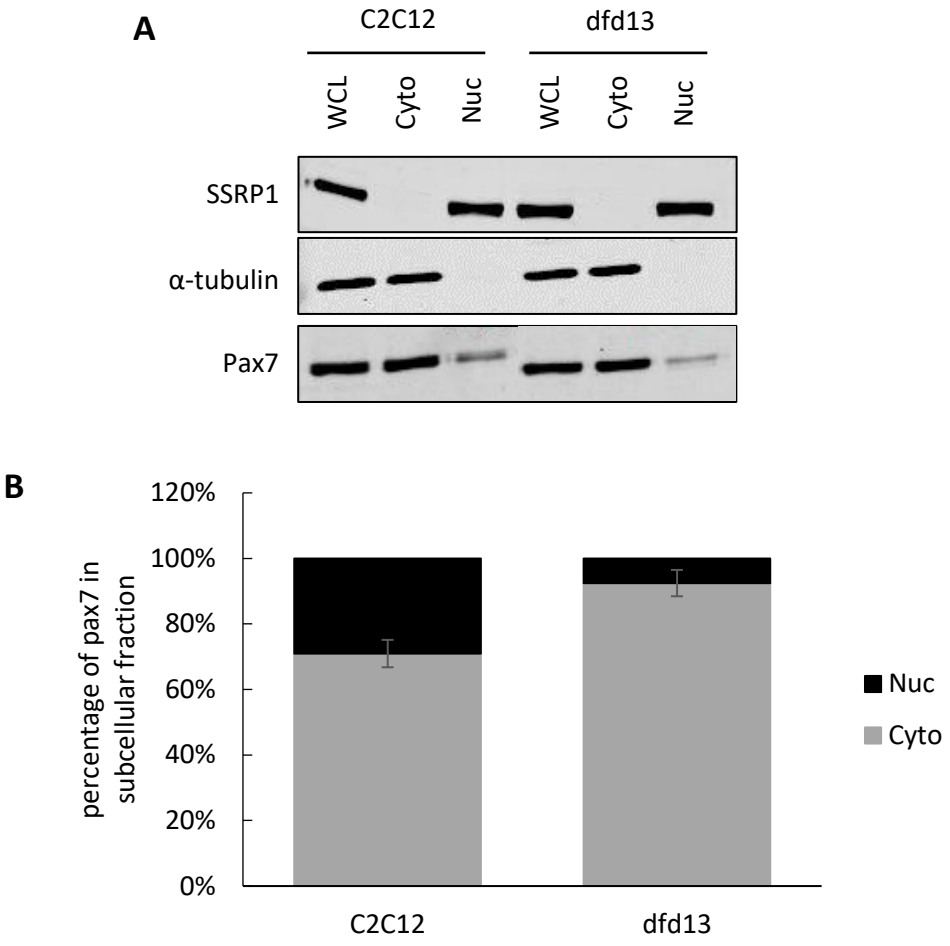

Figure 3.5: Pax7 expression within the subcellular compartments of myoblasts
Both C2C12 and dfd13 myoblasts were cultured in GM and when ~70% confluent were harvested and subjected to sub-fractionation prior to immunoblotting with an anti-Pax7 antibody. SSRP-1 and α-tubulin were used as nuclear and cytoplasmic fraction control markers, respectively. (A) Immunoblot for Pax7 expression. (B) Densitometry analysis of Pax7 expression in both types of myoblasts. WCL: whole cell lysate; Cyto: cytoplasmic; Nuc: nuclear; n=3.

3.2.4 Pax7 May Undergo Protein Modification and Be Recycled in Proliferating Dystrophin-Deficient Myoblasts

As indicated in Figure 3.4 and Figure 3.5, Pax7 was found to be expressed and more localised to the cytoplasm of dfd13 myoblasts compared to C2C12 myoblasts. To examine the exact location of Pax7 and identify the event that cytoplasmic-Pax7 might be involved in within proliferating dfd13 myoblasts, co-localisation of Pax7 with

subcellular components, i.e. endoplasmic reticulum, golgi, recycling endosome and lysosome, was performed. Co-localisation analysis via immunofluorescence double labelling using specific markers for each location was undertaken and the subcellular markers utilised are listed in Table 3.1.

Table 3.1: Subcellular markers utilised

Subcellular Marker	Functions
Ca^{2+}ATPase: Endoplasmic reticulum	Protein is synthesised and prepared for sending to the Golgi prior to integral modification, sorting and packaging.
Golgi Matrix protein-130kDa (GM130): Golgi	Involved in maintaining the cis-Golgi structure. Protein is ready to be dispatched to other parts of the cell.
Rab11: Recycling endosome	Transporting protein within the tubular network.
CD107a: Lysosome	Also known as lysosomal-associated membrane protein-1 (LAMP1), involved in the protein degradation pathway.

3.2.4.1 Cytoplasmic-Pax7 of Both Types of Proliferating Myoblasts are Co-Localised with Markers for the Endoplasmic Reticulum and Golgi

As depicted in Figure 3.6, Pax7 was labelled with Texas red (red) while the Ca^{2+}ATPase (ER) and GM130 (Golgi) markers were labelled with AlexaFlour®488 (green). From the images taken, it can be seen that Pax7 co-localised with Ca^{2+}ATPase and GM130 in both proliferating C2C12 and dfd13 myoblasts (Figure 3.6).

Based on the statistical co-localisation analysis, Pax7 was found to be co-localised with the ER and Golgi markers in proliferating C2C12 myoblasts and dfd13 myoblasts. The co-localisation of Pax7 with Ca^{2+}ATPase demonstrates that Pax7 is synthesised abundantly in proliferative C2C12 myoblasts in line with the expression levels detected previously (Figure 3.3A). Ca^{2+}ATPase is localised to the ER membrane and involved in transporting calcium ions from the cytosol into the ER. Co-localisation of Pax7 to Ca^{2+}ATPase corresponds to the current location of Pax7. It has been reported

that Pax7 expression is crucial for the maintenance and self-renewal of myoblasts (Kuang et al. 2006; Lepper, Conway, and Fan 2009). Maintaining Pax7 expression retains the transcriptional regulation of Pax7 for myogenesis and for down-regulation at the onset of muscle differentiation.

GM130 is a protein localised specifically at the cis-Golgi, where it faces the ER in order to receive biosynthetic output from the ER. Co-localisation of Pax7 with GM130 suggests two possible events. Pax7 which is not used may be packaged and ready to be despatched to the final destination, most probably to lysosomes for digestion. Alternatively, Pax7 may be ready to be despatched back to the ER and to be translocated to the nucleus for transcription purposes. As GM130 has been found to be involved in signal transduction regulating migration and cell polarisation via kinases (Preisinger et al. 2004; Millarte and Farhan 2012), it could be suggested that Pax7 is also involved in these events. Further analysis is therefore needed into the co-localisation of Pax7 with recycling endosomes and lysosomes.

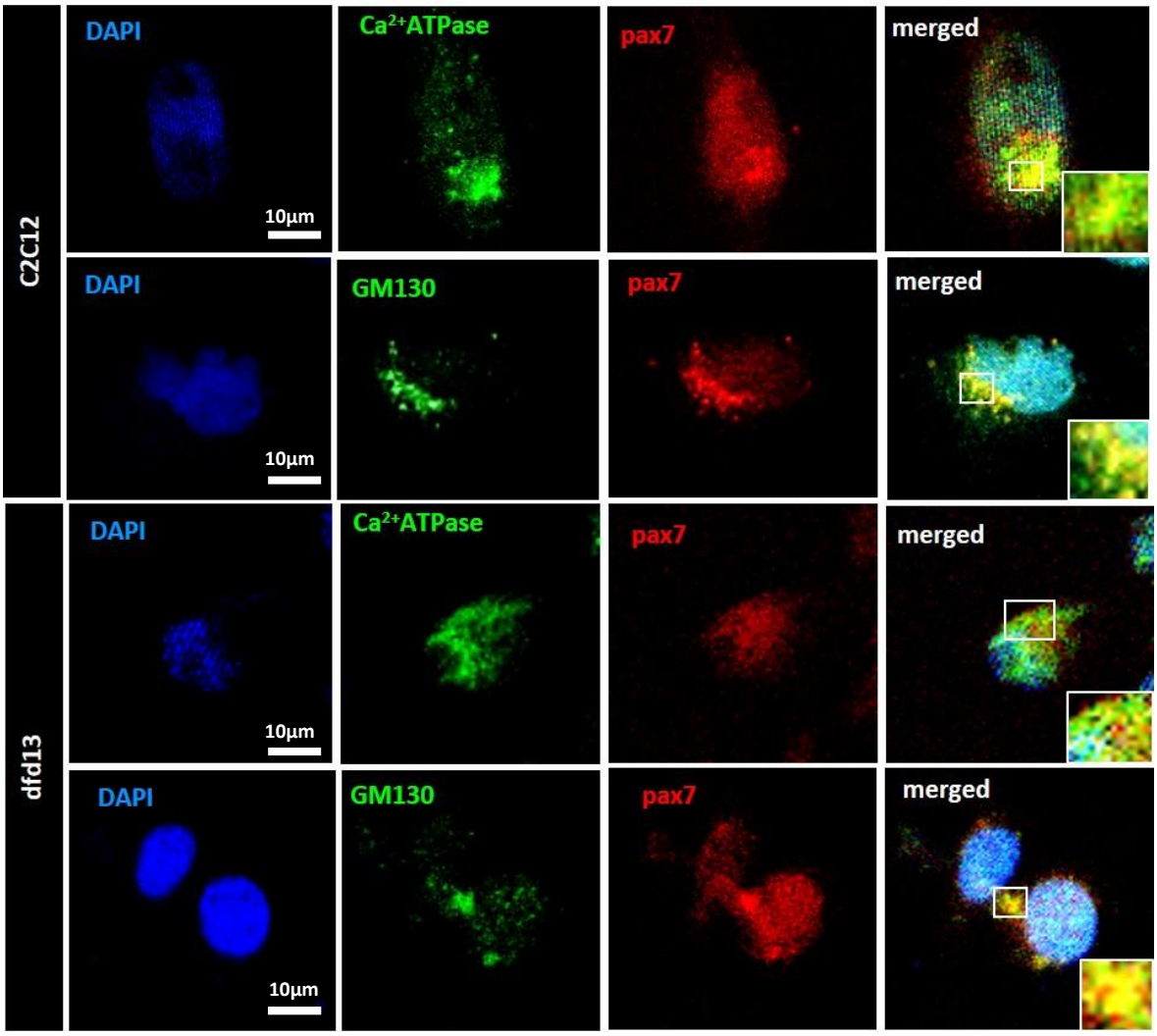

Figure 3.6: Cytoplasmic-Pax7 is co-localised in the ER and Golgi in both proliferating C2C12 and dfd13 myoblasts

Approximately 1.5 x 10^4 C2C12 (non-dystrophic) and dfd13 (dystrophin-deficient) myoblasts were cultured in GM until 60-70% confluent in a 48-well plate. Both types of myoblast were fixed in 4% PFA prior to double immunolabelling for Ca^{2+}ATPase or GM130 (green) and Pax7 (red). DAPI was used as a nuclear counterstain. Images were taken using a Nikon A1 confocal microscope and co-localisation analysis was performed using NIS element software provided by Nikon. GM: growth medium (DMEM + 10% FCS); n=3

3.2.4.2 Cytoplasmic-Pax7 in Proliferating Dystrophin-Deficient Myoblast is Co-Localised with Recycling Endosomes and Not Lysosomes

Cytoplasmic-Pax7 in both proliferative C2C12 and dfd13 myoblasts has been shown to localise to the Golgi, suggesting that Pax7 might be processed, packaged and ready to be translocated to another myoblast compartment. It was hypothesised that Pax7 would be digested/lysed rather than secreted for an external use as it plays a role as a transcription factor within the nucleus. In addition, Pax7 does not possess a signal peptide directing it towards a secretory pathway. To test this hypothesis, co-localisation of Pax7 within cells components, i.e. recycling endosome and lysosome, was explored. Rab11 and CD107a markers were used for recycling endosomes and lyososomes, respectively.

C2C12 myoblasts with cytoplasmic-Pax7 expression were chosen for this analysis. Co-localisation of Pax7 with recycling endosomes (Rab11) could be clearly seen in both proliferative C2C12 and dfd13 myoblasts (Figure 3.7). Rab11 is a small Ras-like GTPase regulatory protein which has a regulatory role in most membrane-transport steps, i.e. recycling of perinuclear proteins, the plasma membrane and golgi compartment endosomes. It is localised to the endocytic recycling compartment and trans-Golgi network. As Pax7 was found to co-localise with Rab11 in the perinuclear region, it can be suggested that here it is in the process of being transported from the Golgi to the ER following modification.

The co-localisation of Pax7 with lysosomes (CD107a) gave a lower score in both types of myoblasts (Table 3.2). CD107a, also known as lysosomal-associated membrane protein-1 (LAMP-1), is a type I transmembrane protein that has been widely used as a lysosome marker. As Pax7 was not co-localised with CD107a, this suggests that degradation of Pax7 may not occur to a significant extent. This result suggests that

cytoplasmic-Pax7 in both proliferative C2C12 and dfd13 myoblasts is active within recycling endosomes but not purposely for degradation.

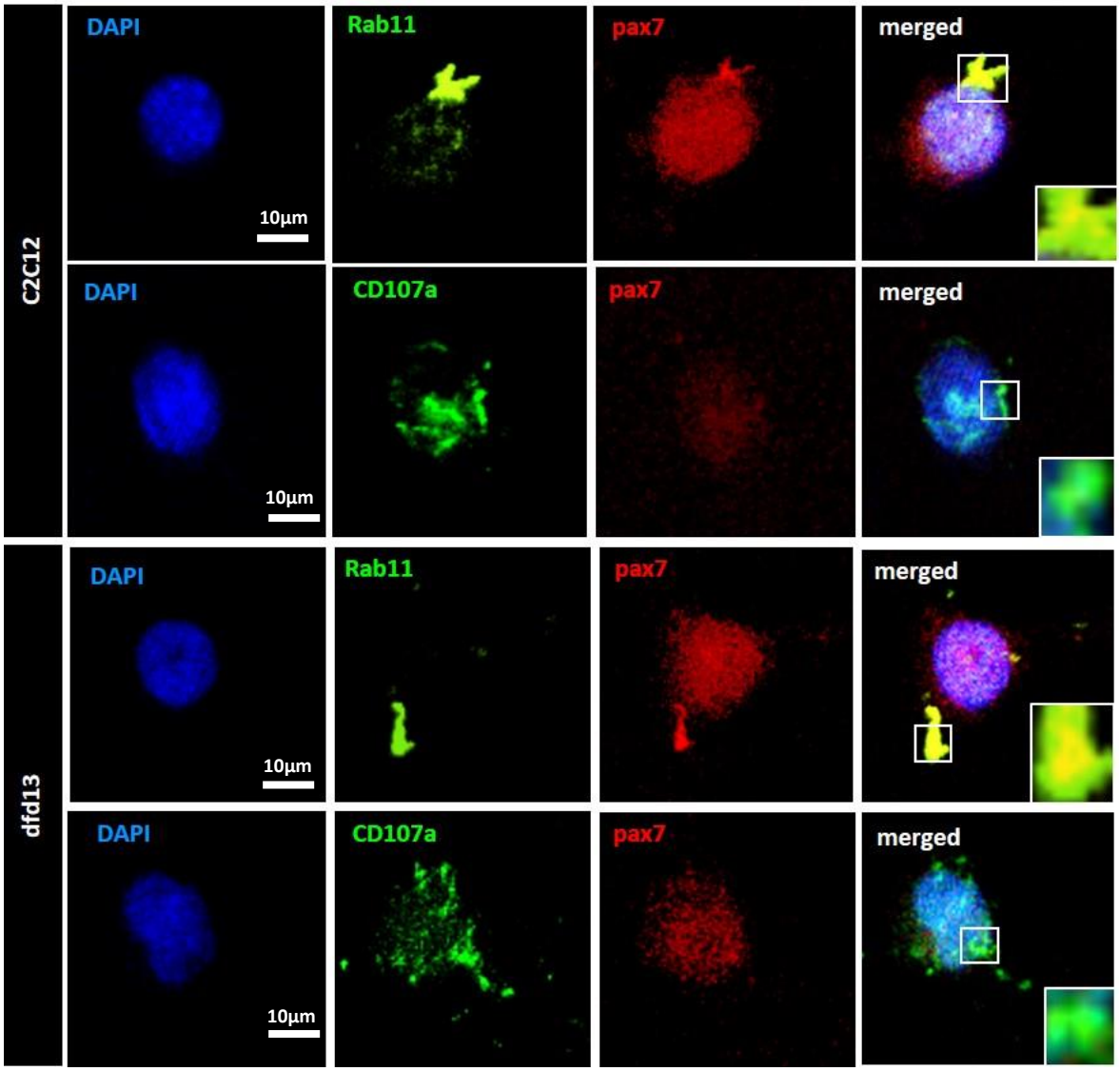

Figure 3.7: Cytoplasmic-Pax7 co-localises with recycling endosomes in both proliferating myoblasts

Approximately 1.5 x 10^4 C2C12 (non-dystrophic) and dfd13 (dystrophin-deficient) myoblasts were cultured in GM until 60-70% confluent in a 48-well plate. The myoblasts were fixed in 4% PFA prior to double immunolabelling for Rab11 or CD107a (green) and Pax7 (red). DAPI was used as a nuclear counterstain. Images were taken using a Nikon A1 confocal microscope and co-localisation analysis was performed using NIS element software provided by Nikon. GM: growth medium (DMEM + 10% FCS); n=3.

Table 3.2: Analysis of Pax7 co-localisation with subcellular markers

Stage/State of Myoblasts	Protein events with respect Subcellular markers	C2C12 myoblasts	dystrophin-deficient myoblasts
Proliferating	Protein synthesis/modification • Endoplasmic reticulum (Ca^{2+}ATPase) • Golgi (GM130)	Co-localised Co-localised	Co-localised Co-localised
	Protein transportation/degradation • Recycling endosome (Rab11) • Lysosome (CD107a)	Co-localised Not co-localised	Co-localised* ($p=2.62x10^{-2}$) Not co-localised

* Significantly higher ($p<0.05$) when compared to C2C12; (n=3).

3.2.5 Identification of the Nuclear Localisation of Pax7-KPNA2 Interaction

Synthesised protein that needs to be translocated into the nucleus needs a importin-α and importin-β recognition sequence within its NLS in order to form a complex. However, it remains unknown as to which protein adaptor is involved in shuttling Pax7 through the nuclear membrane.

3.2.5.1 In silico *Inspection of the Pax7 Sequence*

A) NES analysis

Based on the previous results, cytoplasmic-Pax7 has been found to be localised at higher levels in dfd13 myoblasts compared to C2C12 myoblasts. It appears that cytoplasmic-Pax7 is either from the nucleus or remains in the cytoplasm following translation process. It was therefore hypothesised that there must be an impairment in the nuclear-cytoplasmic transportation for Pax7 or other associated-proteins. The Pax7 protein sequence was obtained from the UniProt database (www.uniprot.org) and analysed to ascertain whether a NLS and/or nuclear export signal (NES) was present.

The NetNES 1.1 server developed by the Center for Biological Sequence Analysis (CBS), Technical University of Denmark

(http://www.cbs.dtu.dk/services/NetNES/) was used to predict the NES sequence in Pax7. The server predicts leucine-rich NES in eukaryotic proteins using combination of Hidden Markov Model (HMM) and Artificial Neural Network (ANN) scores in the prediction algorithm and verify the method on the most recently discovered NES (Figure 3.8) with 0.5 as a threshold. However, as the NES score was below the threshold, no residue is expected to participate in a NES.

A

CENTERFO RBIOLOGI CALSEQU ENCEANA LYSIS CBS

NetNES 1.1 Server - prediction results

Technical University of Denmark

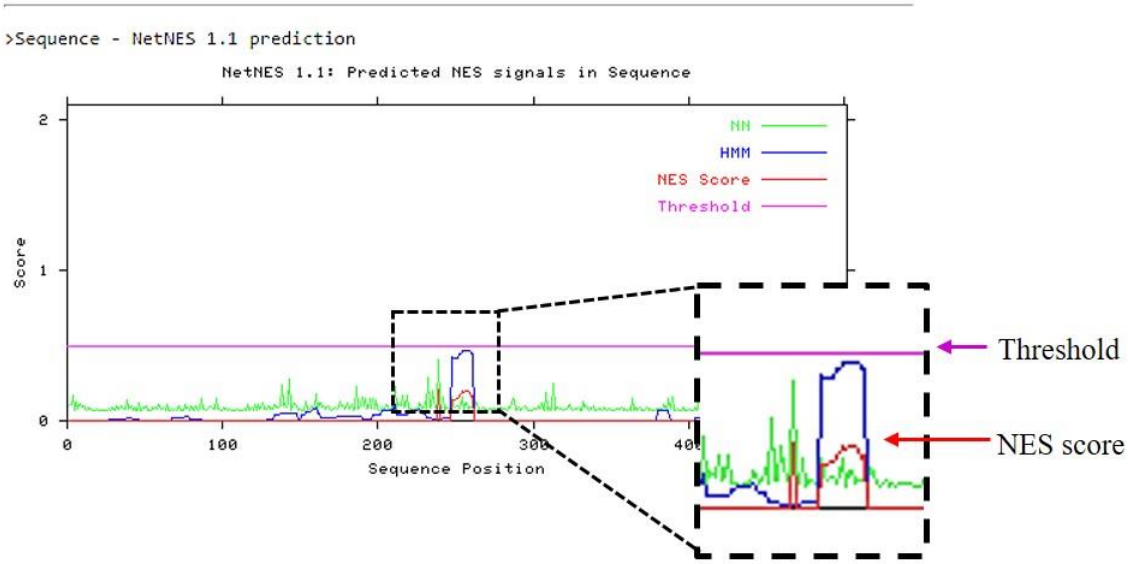

B

#Seq-Pos-Residue	ANN	HMM	NES	Predicted
Sequence-248-L	0.162	0.427	0.143	-
Sequence-249-A	0.101	0.419	0.141	-
Sequence-250-Q	0.091	0.419	0.141	-
Sequence-251-R	0.104	0.419	0.144	-
Sequence-252-T	0.077	0.448	0.173	-
Sequence-253-K	0.119	0.449	0.179	-
Sequence-254-L	0.162	0.463	0.193	-
Sequence-255-T	0.073	0.463	0.188	-
Sequence-256-E	0.118	0.463	0.194	-
Sequence-257-A	0.115	0.463	0.196	-
Sequence-258-R	0.076	0.463	0.196	-
Sequence-259-V	0.092	0.463	0.190	-
Sequence-260-Q	0.093	0.448	0.161	-
Sequence-261-V	0.086	0.448	0.164	-

Figure 3.8: NES analysis of the Pax7 sequence
Pax7 has no potential sequence for exportin to bind to for its export out of the nucleus to the cytoplasm. (A) Graphic of the NES analysis showing that no residue scored over the threshold. (B) Some of the residues analysed by the NetNES 1.1 server.

B) NLS analysis

The cNLS mapper is software for NLS predictions in protein sequences and was developed by Kasugi et al. (2009) to recognise specific NLS for the importin αβ pathway by calculating NLS scores (levels of NLS activities) (Kosugi et al. 2009). In this study, it was used to analyse the NLS residues in the Pax7 sequence. The Pax7

sequence was obtained from the UniProt database (www.uniprot.org) and loaded into the software with a cut-off score of 5.0 selected. The cut-off score indicates the strength of NLS activity, with higher activities at 10.0 and lower activities at 1.0, based on an experiment where the GUS-GFP reporter protein was fused to an NLS. Searching for a bipartite NLS with a long linker in the protein sequence was also performed by selecting the 'within terminal 60-amino-acids region' option, as this would help to identify a structure-dependent bipartite NLS which may be located close to each other in the tertiary structure (http://nls-mapper.iab.keio.ac.jp/). The analysis showed that a predicted bipartite NLS was present in the Pax7 sequence, starting at position 134 until residue 220, shown in red text in Figure 3.9A. The scores were 5.8, 5.5 and 5.1, which means that Pax7 has intermediate NLS activities, indicating it could be localised within both the nucleus and cytoplasm.

Analysis of phosphorylation sites was achieved using the NetPhos 2.0 server developed by the Center for Biological Sequence Analysis (CBS), Technical University of Denmark (http://www.cbs.dtu.dk/services/NetNES/). This server produces predictions for serine, threonine and tyrosine phosphorylation sites in eukaryotic proteins. The analysis shows that there are seven predicted serine phosphorylation sites within the NLS sequence, but no threonine or tyrosine phosphorylation sites were found (Figure 3.9B). These sites indicate the positions that have the highest probability for importin binding via a phosphorylation event.

A

Predicted NLSs in query sequence

```
MAALPGAVPRMMRPGPGQNYPRTGFPLEVSTPLGQGRVNQLGGVFINGRP 50
LPNHIRHKIVEMAHHGIRPCVISRQLRVSHGCVSKILCRYQETGSIRPGA 100
IGGSKPRQVATPDVEKKIEEYKRENPGMFSWEIRDRLLKDGHCDRSTVPS 150
VSSISRVLRIKFGKKEDDEEGDKKEEDGEKKAKHSIDGILGDKGNRLDEG 200
SDVESEPDLPLKRKQRRSRTTFTAEQLEELEKAFERTHYPDIYTREELAQ 250
RTKLTEARVQVWFSNRRARWRKQAGANQLAAFNHLLPGGFPPTGMPTLPP 300
YQLPDSTYPTTTISQDGGSTVHRPQPLPPSTMHQGGLAAAAAAADTSSAY 350
GARHSFSSYSDSFMNPGAPSNHMNPVSNGLSPQVMSILSNPSAVPPQPQA 400
DFSISPLHGGLDSASSISASCSQRADSIKPGDSLPTSQSYCPPTYSTTGY 450
SVDPVAGYQYSQYGQTAVDYLAKNVSLSTQRRMKLGEHSAVLGLLPVETG 500
QAY                                                  503
```

Predicted bipartite NLS

Pos.	Sequence	Score
134	RDRLLKDGHCDRSTVPSVSSISRVLRIKFGKKE	5.8
156	RVLRIKFGKKEDDEEGDKKEEDGEKKAKHSID	5.5
189	ILGDKGNRLDEGSDVESEPDLPLKRKQRRSRT	5.1

B

Sequence 146 **HCDRSTVPS** 0.577 *S*
Sequence 150 **STVPSVSSI** 0.932 *S*
Sequence 152 **VPSVSSISR** 0.811 *S*
Sequence 185 **KAKHSIDGI** 0.939 *S*
Sequence 201 **LDEGSDVES** 0.988 *S*
Sequence 205 **SDVESEPDL** 0.994 *S*
Sequence 218 **KRKQRRSRTTF** 0.989 *S*

Figure 3.9: NLS analysis of the Pax7 sequence
(A) Pax7 has NLS residues from 134 to 220 that are a potential site for importin to bind to, indicating that Pax7 is a nuclear protein that is translocated into the nucleus. (B) The NLS sequence highlighting the predicted residues for phosphorylation as analysed using the NetPhos 2.0 server.

3.2.5.2 Prediction of Importin-α1 and Importin13 as Pax7 Translocator in Myoblasts

There is a lack of studies on the interactions of Pax7 with proteins involved in it translocation to the nucleus. Since Pax7 was found to be more localised within the cytoplasm of dfd13 myoblasts, it was hypothesised that the translocation of Pax7 into the nucleus is impaired, resulting in more cytoplasmic-Pax7 in these myoblasts. Two

candidate proteins were chosen that may form a complex with Pax7, karyopherin-α (KPNA2) and karyopherin-β or importin13 (IPO13).

Karyopherin α1 has been shown to be involved in myoblast proliferation and differentiation, as a knockdown via siRNA targeting KPNA2 reduced both events (Hall et al. 2011). A study by Kovac et al. (2000) confirmed that importin α1 interacts with Pax5 via a NLS located at amino acids 195-201 within the central domain (Kovac et al. 2000). Therefore, it was hypothesised that importin α1 could also be the Pax7 escort protein enabling its translocation into the nucleus. The Pax5 and Pax7 sequences were aligned, revealing that 4 out of the 8 residues were similar within the binding site, suggesting that importin α1 could potentially interact with Pax7 (Figure 3.10). The NLS of both Pax7 and Pax5 was also analysed using NucPred by Brameier et al. (2007), which showed that both have a similar predicted NLS, suggesting that both proteins have a nuclear role (Figure 3.11) (Brameier, Krings, and MacCallum 2007).

Based on the STRING (Search Tool for the Retrieval of Interacting Genes/Proteins) database, no study has reported Pax7 (*Mus musculus*) protein interactions. However, it has been reported that Pax6 and Pax3 interact with IPO13, indicating that these are potential cargo proteins for IPO13 (Ploski, Shamsher, and Radu 2004). Thus, it was hypothesised that IPO13 may also play a role as a translocator for Pax7.

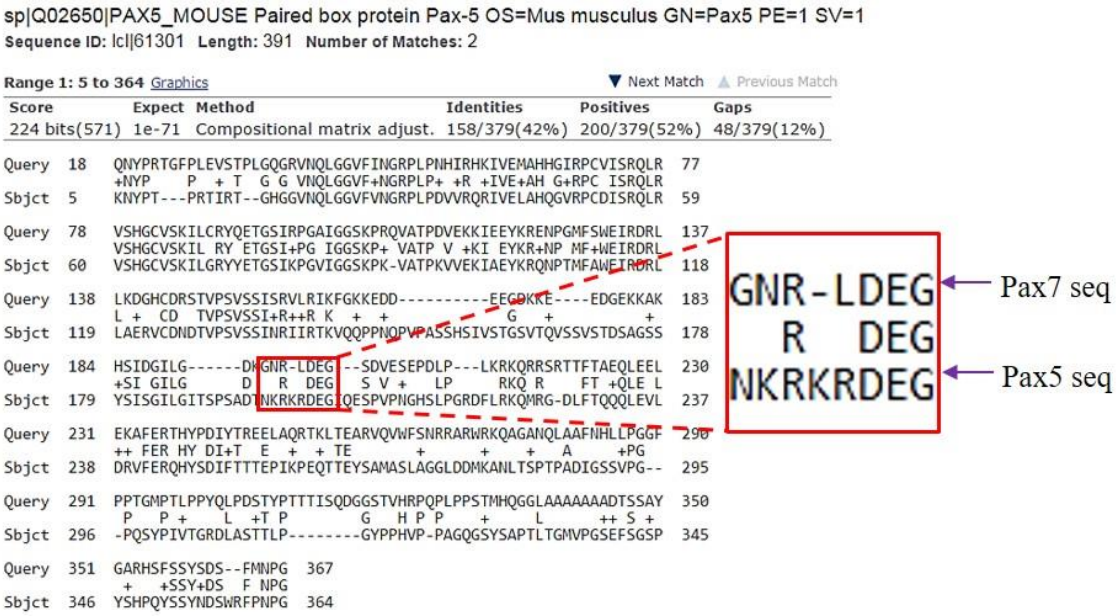

Figure 3.10: Alignment of Pax5 and Pax7 sequences

The alignment shows that only 4 out of 8 Pax7 residues are similar to the Pax5 residue binding site. Alignment of the two sequences was performed using blastp algorithm from the BLAST website.

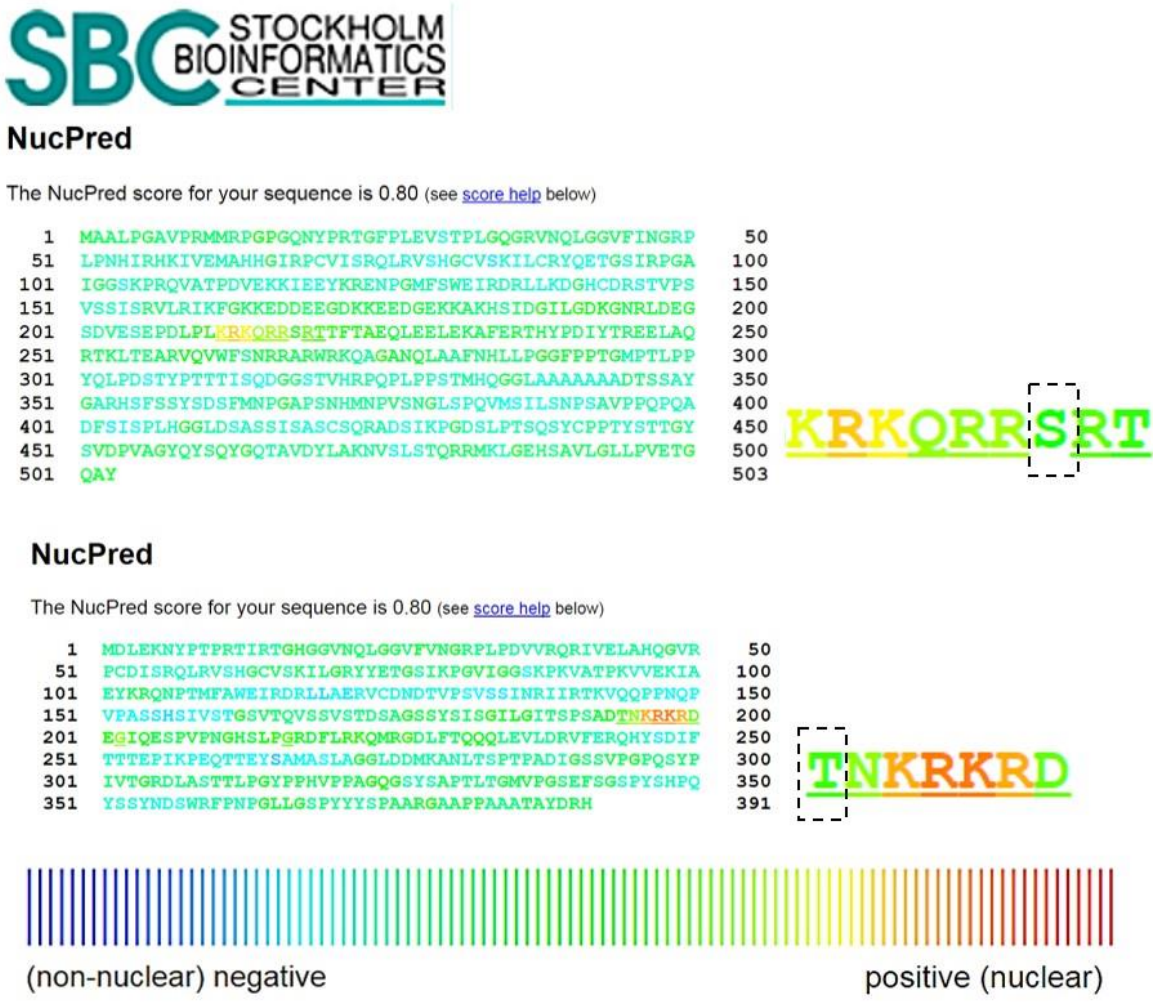

Figure 3.11: NLS analysis of the Pax7 sequence compared to the Pax5 sequence
Analysis of the NLS using NucPred by Brameier et al., 2007. The 'S' (serine) and 'T' (Threonine) are residue which are expected to be phosphorylated based on the prediction phosphorylation analysis using NetPhos2.0.
(https://www.sbc.su.se/~maccallr/nucpred/cgi-bin/single.cgi)

3.2.5.3 Endogenous Pax7 is Associated with Importin-α1 (KPNA2) But Not Importin13 (IPO13) in Myoblasts

The data has shown that cytoplasmic-Pax7 was found localised in the Golgi and recycling endosomes not in lysosomes. This provides evidence that high level expression of Pax7 in differentiating dfd13 myoblasts is recycled and not degraded, retaining its function during this stage. Therefore, it was suspected that Pax7 transportation regulation is impaired during proliferation and differentiation of dfd13 myoblasts. Further investigations were carried out to determine the functional interaction of Pax7 with importin-α1 (KPNA2) in myoblasts.

There is no data relating to the Pax7 nuclear transport protein (karyopherin) available; however, based on the analysis presented, it is predicted that Pax7 possesses a NLS that importin could bind to. Analysis of importin candidates could be a Pax7 protein partner, identified IPO13 and KPNA2. Co-immunoprecipitation analysis showed that only KPNA2 associates with Pax7 (Figure 3.12). Therefore to confirm this interaction, co-localisation analysis was undertaken. Co-localisation analysis also showed that Pax7 and KPNA2 are associated, suggesting that these proteins are interacting (Figure3.13).

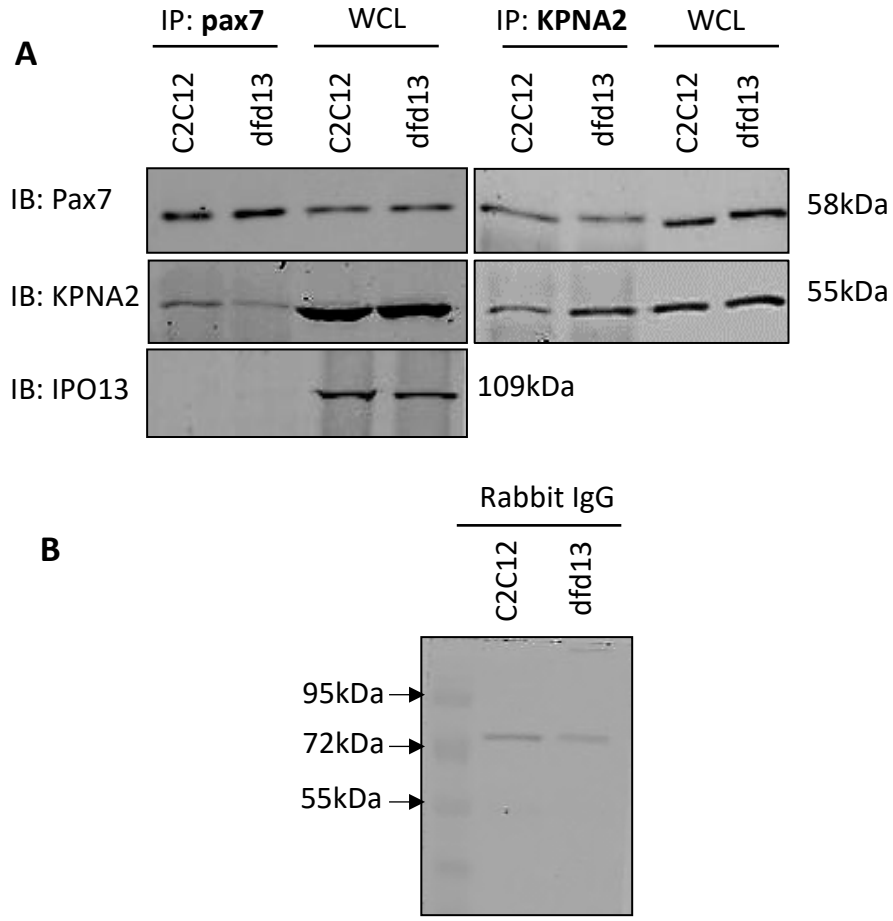

Figure 3.12: Endogenous Pax7 associates with KPNA2

Approximately 500 µg of whole cell lysates of C2C12 and dfd13 myoblasts were used for immunoprecipitation analysis. Endogenous Pax7 was pulled down using a protein A sepharose CL-4B bead slurry, and KPNA2 was pulled down using Dynabeads Protein G magnetic beads. Both purified proteins were blotted with anti-Pax7, KPNA2 and IPO13 antibodies. Whole cell lysate was used as a positive control and rabbit IgG (with sample buffer) as the negative control. WCL: whole cell lysate; n=3

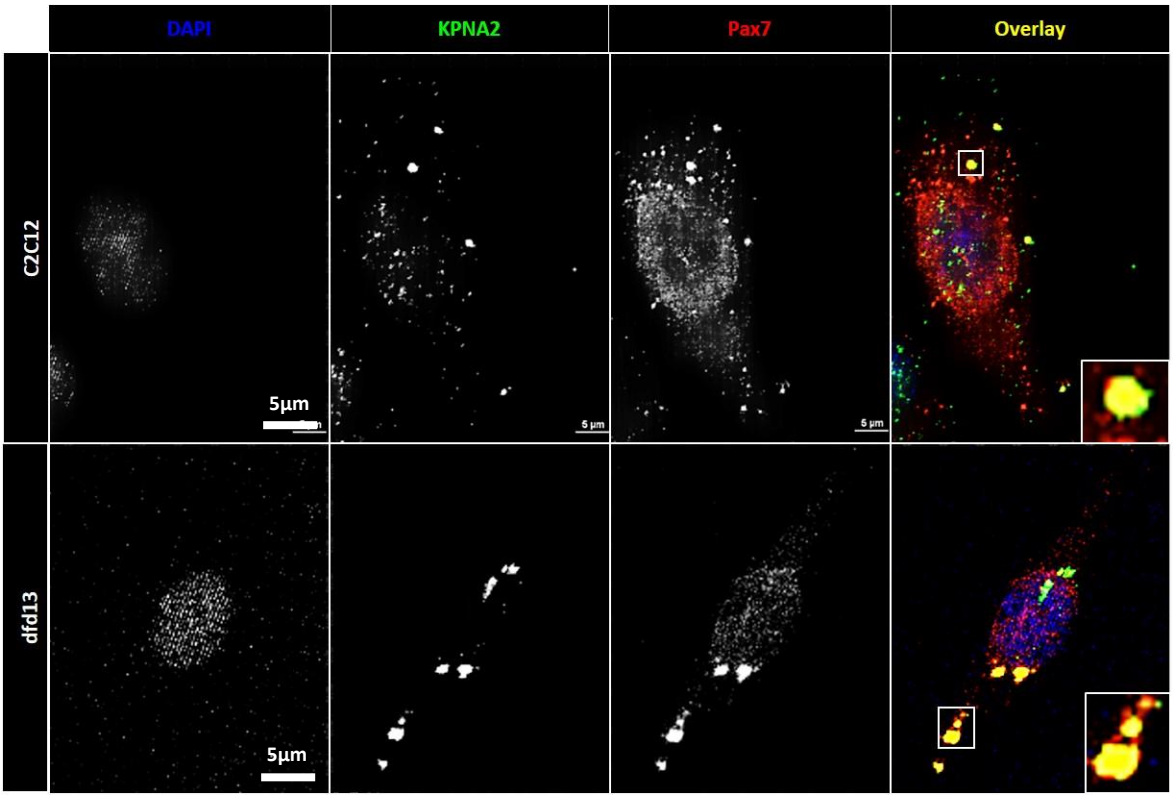

Figure 3.13: Endogenous Pax7 co-localises with KPNA2
Approximately 1.5 x 10^4 C2C12 and dfd13 myoblasts were cultured in GM in a 48-well plate overnight. The myoblasts were fixed in 4% paraformaldehyde prior to immunolabelling with for Pax7 and KPNA2. DAPI was used as a nuclear counterstain. The images were captured using a confocal microscope Nikon 1AR. Co-localisation analysis has performed using NIS element software provided by Nikon. GM: growth medium (DMEM + 10% FCS); n=3.

3.2.6 KPNA2 Expression Fluctuates in Differentiating Dystrophin-Deficient Myoblasts

It has been shown that KPNA2 knockdown decreases myoblast proliferation, indicating that KPNA2 plays a role in myoblast proliferation (Hall et al. 2011). Furthermore, it has also been suggested that KPNA2 may have a specific role in the nucleo-cytoplasmic import of cNLS proteins required for the positive regulation of myoblast proliferation. The results of further investigations in this study indicated that KPNA2 interacts with Pax7 and plays the role of the Pax7-transport protein.

Figure 3.14A presents an immunoblot demonstrating KPNA2 expression in non-differentiated and differentiated myoblasts. Generally, KPNA2 expression is decreased upon differentiation when compared to non-differentiated myoblasts. At day 10 of differentiation, KPNA2 has accumulated but is still lower than in non-differentiated C2C12 cells (Figure 3.14B). Densitometry analysis showed that there is a significant difference in expression ($p<0.05$; $p = 3.27 \times 10^{-2}$) on day 7 between the two types of myoblasts.

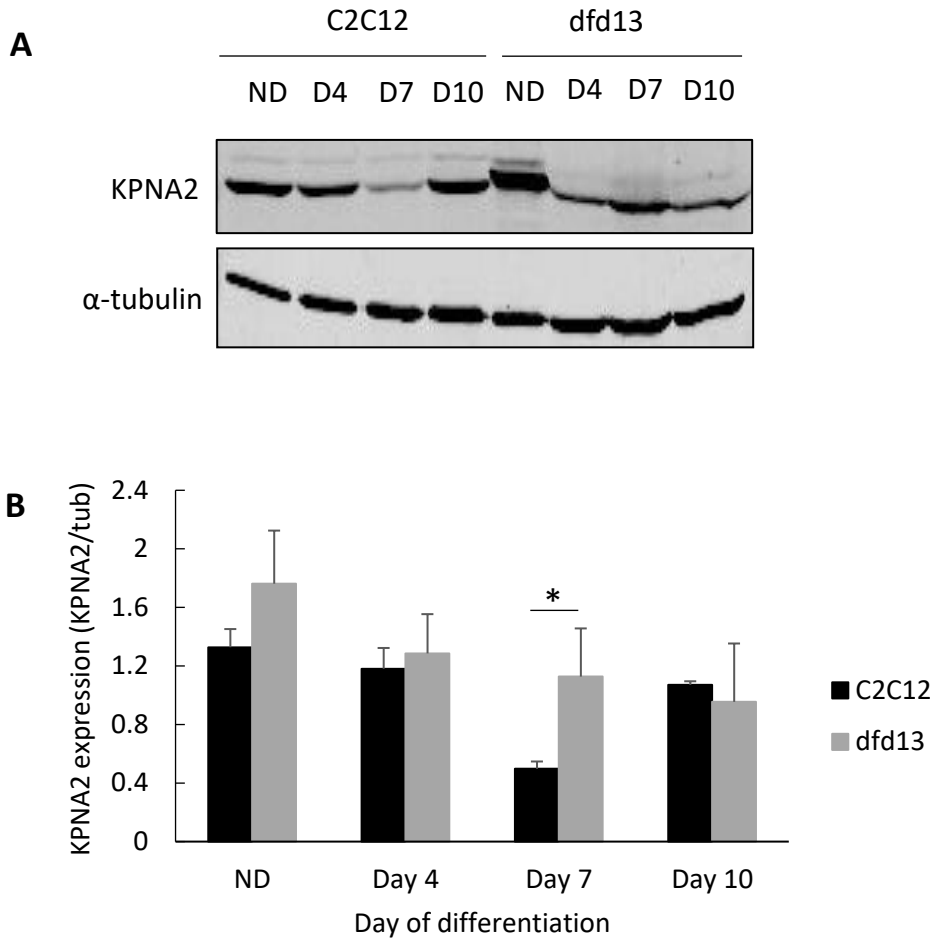

Figure 3.14: KPNA2 expression fluctuates in differentiating dystrophin-deficient myoblasts

Both C2C12 and dfd13 myoblasts were cultured in GM until 80-90% confluent before replacing with DM and cultured for 10 days, with the medium changed every two days. Total protein extraction was performed at the indicated time points prior to immunoblotting with antibodies recognising KPNA2 and α-tubulin protein. (A) Immunoblot of KPNA2 expression during differentiation with α-tubulin as a loading control. (B) Densitometry analysis of KPNA2 expression normalised against α-tubulin. The graph represents an average of three repeats from different samples. ND: non-differentiated; Significant different: * ($p<0.05$) compared to dfd13 myoblasts; GM: growth medium (DMEM + 10% FCS); DM: differentiation medium (DMEM + 2% horse serum); n=3.

3.3 Discussion

3.3.1 Dystrophin-Deficient Myoblasts Do Not Achieve Terminal Differentiation

In this chapter it has been established that dystrophin-deficient myoblast differentiation is impaired when in low mitogen medium for 10 days based on morphological analysis (Figure 3.1) and the detection of F-MyHC expression (Figure 3.2). Differentiation analyses showed that less myotubes were formed, and no/less F-MyHC expression was detected. However, pan-myosin was only expressed at the end of differentiation on day 10 in dfd13 myoblasts. Desmin expression levels were found to be higher at the end of the differentiation period. Desmin is a marker for newly formed fibres and is a class-III intermediate filament found in muscle cells that connect myofibrils to each other, as well as to the plasma membrane of myofibres. In this study, it can be suggested that the integrative element in myofibres was generated/developed earlier than myotube formation in the differentiating dystrophin-deficient myoblasts, although full/terminal differentiation was not achieved.

During myogenesis, proliferating myoblasts withdraw from the cell cycle and differentiate into myotubes. Cyclin-dependent Kinase (CDK) inhibitor p21 and retinoblastoma protein (Rb) have been shown to play a critical role in establishing the post-mitotic state by permitting the transcription of the S-phase promoting gene during myogenesis (Blagosklonny and Pardee 2002). Most mitogens have been shown to promote myoblast proliferation. In contrast, insulin-like growth factors (Igf-1 and Igf-2) trigger myoblast differentiation. It is unknown how Igf-2 is controlled during the initiation of differentiation. A previous study showed that Igf-2 up-regulates its own gene expression via the Akt/PKB pathway (Duan, Liimatta, and Bottum 1999).

Elevation of Igf-2 mRNA was found in C2 myoblasts after 24 hours' culture in differentiation medium containing 2-10% horse serum (Tollefsen et al. 1989), while Erbay et al. (2003) suggested that mTOR regulates Igf-2 production at the transcriptional level when cultured under low mitogen conditions (Erbay et al. 2003). There has also been a study suggesting that myoblasts under low mitogen conditions have elevated levels of IGFBP5, which helps concentrate IGF-2 to a threshold level which triggers the IGF-1R pathway leading to differentiation (James et al. 1993; Florini, Ewton, and Coolican 1996). However, in this study levels of Igf-1/2 could not be examined in the culture system utilised, i.e. Igf-1/2 secreted/present in the media. Therefore, further study needs to be undertaken to examine this aspect. a previous study by Chen (2013) showed that Igf-2 induction promotes dystrophin-deficient myoblast differentiation for 4 days, and differentiation was greater when induced by a combination of Igf-1/Igf-2/LIF factors (Hung-chih 2013).

3.3.2 Pax7 Mislocalisation/Misregulation May Affect Terminal Differentiation Achievement in Dystrophin-Deficient Myoblasts

The localisation of specific proteins, particularly transcription factors can be used to elucidate their specific functions and enable characterisation. Therefore, determinating the localisation of Pax7 was crucial to distinguishing and identifying whether this protein was functioning. As depicted in Figure 3.3, Pax7 levels remain highly expressed upon differentiation in dystrophin-deficient myoblasts. A previous study reported that overexpression of Pax7 inhibits myoblast differentiation by down-regulating MyoD, thus preventing myogenin induction (Olguin and Olwin 2004). Therefore, further analysis of Pax7 localisation and subcellular-localisation during the proliferating and differentiating state was performed. As depicted in Figure 3.4 and Figure 3.5, Pax7 distribution analysis revealed that it is in the ER, golgi and recycling endosome of

dystrophin-deficient myoblasts. However, only ROI analysis of the co-localisation of Pax7 with rab11 showed that co-localisation was significantly higher ($p = 2.6x10^{-2}$) in dfd13 myoblasts compared to C2C12 myoblasts (Table 3.2). This indicates that Pax7 is actively transported across the cytoplasm, thus explaining the extensive dispersion expression within the cytoplasm of dystrophin-deficient myoblasts. Significant co-localisation was defined as the percentage of Pax7 co-localised with rab11 in dfd13 myoblasts compared to C2C12 myoblasts via a binary overlay.

3.3.3 Association of Pax7 with KPNA2 as a Complex Suggests a Nuclear Localisation Vehicle

As Pax7 was found in ER, golgi and recycling endosomes of dystrophin-deficient myoblasts, it was hypothesised that the protein translocator karyopherin may be impaired. To date, no study has reported on karyopherin complexing with Pax7 for translocation into the nucleus. It was identified in this study that KPNA2 interacts with Pax7 in both types of myoblasts examined. However, there was no impairment in terms of Pax7 binding to KPNA2. Figure 3.5 and Figure 3.6 showed that endogenous Pax7 is associated with KPNA2 in both types of myoblast.

KPNA2 is a member of the karyopherin-α family of proteins which function as protein transporters to the nucleus. A study by Hall et al. (2011) demonstrated that KPNA2 is important for myoblast proliferation (Hall et al. 2011). Therefore, it can be suggested that high expression levels of KPNA2 reflect Pax7 levels, since the co-immunoprecipitation analysis showed that both proteins interact and are associated. KPNA2 expression (Figure 3.14) has the same pattern as Pax7 (Figure 3.3), thereby supporting the association between Pax7 and KPNA2. High level expression of Pax7 may also reflect high binding to β-catenin, which inhibits myoblast differentiation

(Zhuang et al. 2014). From the data obtained, it can be seen that F-MyHC appeared on day 4 and increased upon differentiation, while Pax7 and KPNA2 expression was decreased until day 7, but then had accumulated by day 10. Such an accumulation may be due to their function as survival factors for myotubes (Olguín and Pisconti 2011) however their regulation was found to be impaired in dfd13 myoblasts.

3.4 Conclusions

In this chapter, it has been demonstrated that Pax7 is misregulated/mislocalised in dystrophin-deficient myoblasts. For the first time, it has been established that KPNA2 is the karyopherin-α that may be responsible for Pax7 translocation to the nucleus.

Key finding(s):

- Pax7 is localised in ER, golgi and rab11 of dystrophin-deficient myoblasts.
- Pax7 associates with KPNA2 to form a translocation complex.

Chapter 4 - The PTEN-PI3K/Akt Signalling Pathway is Perturbed in Dystrophin-Deficient Myoblasts

4.1 Introduction

The absence of dystrophin has a massive impact on myotube as well as myofibre structure. The destabilisation of the plasma membrane in dystrophin-deficient myoblasts from an *mdx* mouse affects transmembrane protein stability, as well as the protein-anchored cytoplasmic layer of the cell membrane thus changing signalling. One of the conserved signalling pathways for skeletal muscle differentiation is the PI3K/Akt/mTOR pathway. The regulation is via insulin-like growth factor-1 receptor (IGF-1R) activation following IGF1 binding. IGF-1R plays a major role in the regulation of skeletal muscle growth and many researchers have reported on the impairment of the Igf-1 pathway and changed its downstream protein regulation in MD. However, PTEN expression and regulation is rarely studied since this protein is negatively regulated in the Igf-1 pathway. In this chapter, the elevation of PTEN perturbed PI3K/Akt/mTOR signalling is reported which causes protein translation deactivation, excessive activation of autophagy related genes via FoxO3, and subsequently a reduction in autophagic flux in dystrophin-deficient myoblasts (Chapter 5).

The PTEN-PI3K/Akt signalling pathway regulates multiple biological processes, such as cell proliferation, differentiation, autophagy and apoptosis. A disruption in this pathway can cause impairments to these processes, as can occur in cancers due to an increase in Akt activity caused by the down-regulation of PTEN expression which is affected by PI3K activation. However, there is a different scenario in dystrophin-deficient myoblasts where PTEN expression is significantly higher and

extensively expressed upon differentiation. PTEN, also known as a tumour suppressor, is mutated within cancer cells. PTEN acts as a lipid phosphatase and hydrolyses phosphates in the 3′ position of phosphoinositides. Previous studies have found that *PTEN* mRNA is elevated in the muscle of *mdx* mice (Dogra et al. 2006; Haslett et al. 2003). The elevation of PTEN expression and its activity due to the deregulation of the PI3K/Akt signalling pathway in dystrophin-deficient dog muscle has also been shown in the GRMD dog (Feron et al., 2009).

In this study the protein responsible for the conversion of PIP_2 and PIP_3 is examined via the synergistic function of PI3K and PTEN. The conversion of phosphoinositides is important in regulating Akt signalling and the downstream proteins which are responsible for the regulation of proliferation, differentiation and cell survival, especially in myoblasts. To understand the impaired regulation of PTEN-PI3K/Akt in dystrophin-deficient myoblasts, the downstream protein profiling of this pathway was investigated as this ultimately changes autophagy modulation and activation, as will be shown in Chapter 5. An overview of this chapter is illustrated in Figure 4.1.

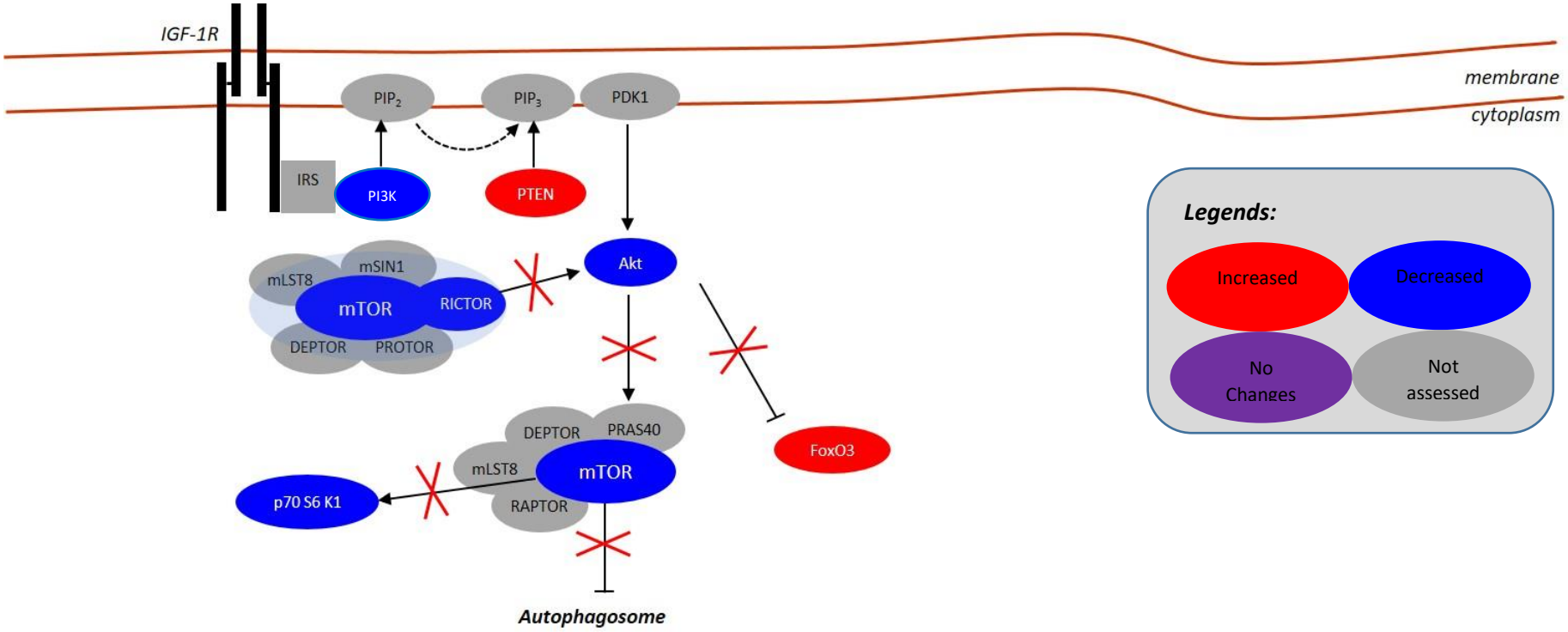

Figure 4.1: Chapter overview: perturbation of the PTEN-PI3K/Akt signalling pathway in dystrophin-deficient myoblasts
PTEN was found to be highly expressed in dystrophin-deficient myoblasts which leads to the reduction of activation of PI3K. Surprisingly, Akt was found not to be activated due to the inactivation of Rictor-mTORC2. Furthermore, downstream of Akt, i.e. p70S6K and FoxO3, there was defective activation. Activation of p70S6K was reduced, indicating that protein synthesis regulation is impaired. FoxO3 (unphosphorylated) expression accumulated thus increased FoxO3 nuclear translocation. Therefore, it can be implied that PI3K/Akt and downstream protein signalling is perturbed in dystrophin-deficient myoblasts.

4.2 Results

It was shown in Chapter 3 that the differentiation capacity of dystrophin-deficient (dfd13) myoblasts is diminished. The data showed that dfd13 myoblasts are unable to achieve terminal differentiation after culture in low-mitogen (2% horse serum) media for 10 days. In this chapter, the regulation of PTEN-PI3K is examined, as this is responsible for myoblast differentiation. PI3K/Akt regulation and regulation of the downstream protein pathway in myoblasts during differentiation is also investigated.

4.2.1 PTEN-PI3K Regulation is Perturbed in Differentiating Dystrophin-Deficient Myoblasts

Generally, PTEN expression was increased upon differentiation in both types of myoblasts. However, the accumulation of PTEN was found to be higher in differentiating dfd13 myoblasts compared to C2C12 myoblasts (

Figure 4.2A). The accumulation of PTEN throughout differentiation was not significant in C2C12 myoblasts but there were significant increases on day 7 ($p<0.05$; $p = 4.30x10^{-2}$) and day 10 ($p<0.05$; $p = 4.88x10^{-2}$) when compared to non-differentiated cells. Densitometry analysis showed that PTEN expression in differentiating dfd13 myoblasts were significantly higher compared to the differentiating C2C12 myoblasts ($p<0.01$; $p = 4.81x10^{-3}$) on day 4, ($p<0.05$), day 7 ($p = 1.29x10^{-2}$) and day 10 ($p = 1.95x10^{-2}$) (

Figure 4.2B).

PTEN has a negative effect on PI3K, as it concomitantly affects PI3K regulation. PI3K expression and its activity in both types of myoblasts was therefore examined. Generally, total PI3K expression was increased in dfd13 myoblasts throughout the differentiation period. However, significant accumulation of PI3K could

be seen by day 7 ($p<0.01$; $p = 1.04x10^{-3}$) and day 10 ($p<0.01$; $p = 1.65x10^{-3}$) when compared to the non-differentiated dfd13 myoblasts. There was a significant difference in total PI3K expression in C2C12 myoblasts on days 7 and 10 compared to non-differentiated myoblasts. Densitometry analysis showed that there were significant differences in total PI3K expression in dfd13 myoblasts on day 4 ($p<0.05$; $p = 1.70x10^{-2}$), day 7 ($p<0.01$; $p = 2.08x10^{-3}$), and day 10 ($p = 1.42x10^{-3}$) when compared to differentiating C2C12 myoblasts (

Figure 4.2C). As illustrated in

Figure 4.2D, densitometry analysis on relative PI3K activity was higher in dfd13 myoblasts at the non-differentiated stage ($p<0.01$; $p = 9.89x10^{-3}$), day 4 ($p<0.01$; $p = 1.69x10^{-3}$) and reduced at day 10 of differentiation ($p<0.05$; $p = 3.25x10^{-2}$) when compared to C2C12 myoblasts. However, the actual activity of PI3K is increased (Figure 4.2E).

In this study, phosphorylation of PI3K-p85 (regulatory subunit) was examined in order to observe PI3K activation. When cells are stimulated by the receptor, intrinsic tyrosine kinase phosphorylates p85 at Tyr458, causing a conformational change to p110 (the catalytic subunit) which increases its enzymatic activity for PIP_2. From this data, it seems that high PTEN expression decreased PI3K activity, thus affecting its downstream protein activation.

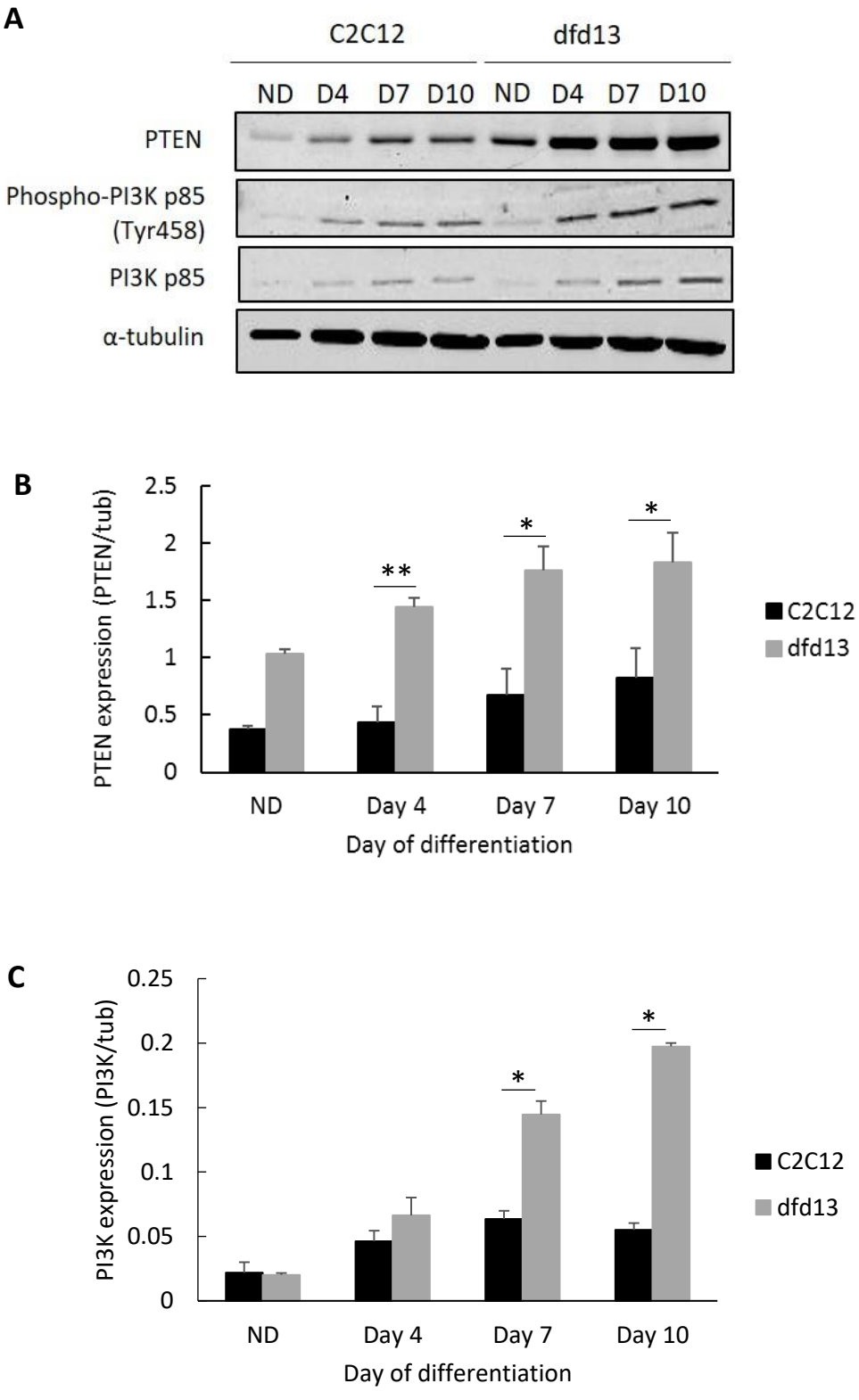
A
C2C12
dfd13
ND D4 D7 D10 ND D4 D7 D10
PTEN
Phospho-PI3K p85 (Tyr458)
PI3K p85
α-tubulin
B
PTEN expression (PTEN/tub)
2.5
2
1.5
1
0.5
0
**
*
*
ND
Day 4
Day 7
Day 10
Day of differentiation
C2C12
dfd13
C
PI3K expression (PI3K/tub)
0.25
0.2
0.15
0.1
0.05
0
*
*
ND
Day 4
Day 7
Day 10
Day of differentiation
C2C12
dfd13

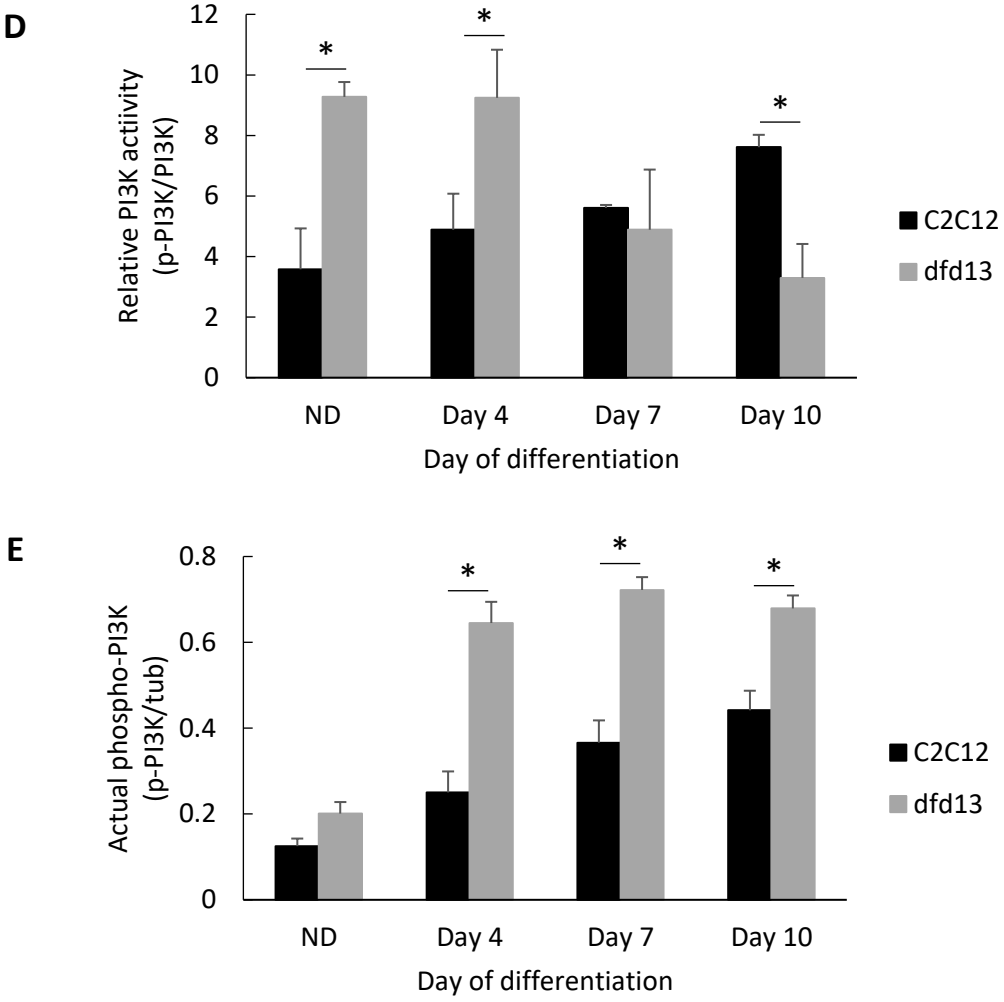

Figure 4.2: PTEN expression is higher while PI3K activation is decreased in dystrophin-deficient myoblasts

Myoblasts were cultured in GM until 80 to 90% confluent before washing twice with PBS and culturing in DM for 10 days with the media being changed every 2 days. Total protein extraction was performed at the indicated time points prior to immunoblot analysis. (A) Immunoblot analysis of PTEN, phospho-PI3K (p85) and total PI3K during myoblasts differentiation with α-tubulin expression as a loading control. Densitometry analysis of (B) PTEN expression, (C) total PI3K expression, and (C) PI3K activity. The graphs represent an average of three repeats from different samples. ND: non-differentiated; Significant different: * ($p<0.05$) and ** ($p<0.01$) compared to C2C12 myoblasts. GM: growth medium (DMEM + 10% FCS); DM: differentiation medium (DMEM + 2% horse serum); n=3.

4.2.2 Akt Is inactivated in Dystrophin-Deficient Myoblasts

As PTEN has been shown to be highly expressed in dfd13 myoblasts, it is predicted that Akt is inactivated, as PTEN has previously been reported to modulate Akt activation in rhabdomyosarcomas cells; skeletal muscle cancer (Wan and Helman 2003). In this study phosphorylation of Akt was not detected at Ser473 or Thr308 in dfd13 myoblasts during differentiation (Figure 4.3A). It has been reported that phosphorylation of Akt by PDK1 at Thr308 partially activates Akt while full activation requires phosphorylation of Ser473 which can be catalysed by multiple protiens including rictor-mTORC2 (Sarbassov et al. 2005). These activation is responsible for myoblast proliferation as well as differentiation.

As depicted in Figure 4.3B, total Akt expression increased in both types of myoblast during differentiation, with slightly higher levels present in dfd13 myoblasts (not significantly different). Densitometry analysis of Akt activation via phosphorylation at Ser473 (Figure 4.3C) showed a significant difference when compared to C2C12 myoblast at all stages (non-differentiated $p<0.05$; $p = 3.90x10^{-2}$, day 4 $p<0.05$; $p = 1.17x10^{-2}$, day 7 $p<0.05$; $p = 1.25x10^{-2}$ and day 10 $p<0.01$; $p = 1.39x10^{-3}$). There was also a significant difference in Akt activation at Ser473 in C2C12 myoblasts when compared to the non-differentiated stage (day 4 $p<0.05$; $p = 2.06x10^{-2}$, day 7 $p<0.05$; $p = 3.31x10^{-2}$ and day 10 $p<0.01$; $p = 1.41x10^{-3}$).

Akt is a downstream protein of PI3K. Its plays an important role and is recognised as one of the most critical pathways in the regulation of cell viability and maintenance in skeletal muscle mass (Egerman and Glass 2014). Therefore, its expression pattern in dystrophin-deficient myoblasts was investigated, as previously dfd13 myoblasts have been reported to undergo apoptosis when cultured in DM (Chen

2013). As expected, the immunoblot data showed that Akt was inactivated in differentiating dfd13 myoblasts. Surprisingly, it was found that Akt was only activated by phosphorylation at Ser473 in C2C12 myoblasts. Akt was not phosphorylated at Thr308 in either type of myoblasts and consequently mouse embryonic fibroblast (MEF) cells were used as a positive control (gift from Adil Rashid, University of Birmingham) for this activation site (Figure 4.3A).

Immunofluorescence analysis was performed to localise Akt phosphorylated at Ser473 in myoblasts during differentiation. As illustrated in Figure 4.4, phosphorylated-Akt can be observed on the membrane of both non-differentiated myoblasts and myotubes. However, less phospho-Akt was found in non-differentiated dfd13 myoblasts and some was localised on the membrane at day10 of differentiation.

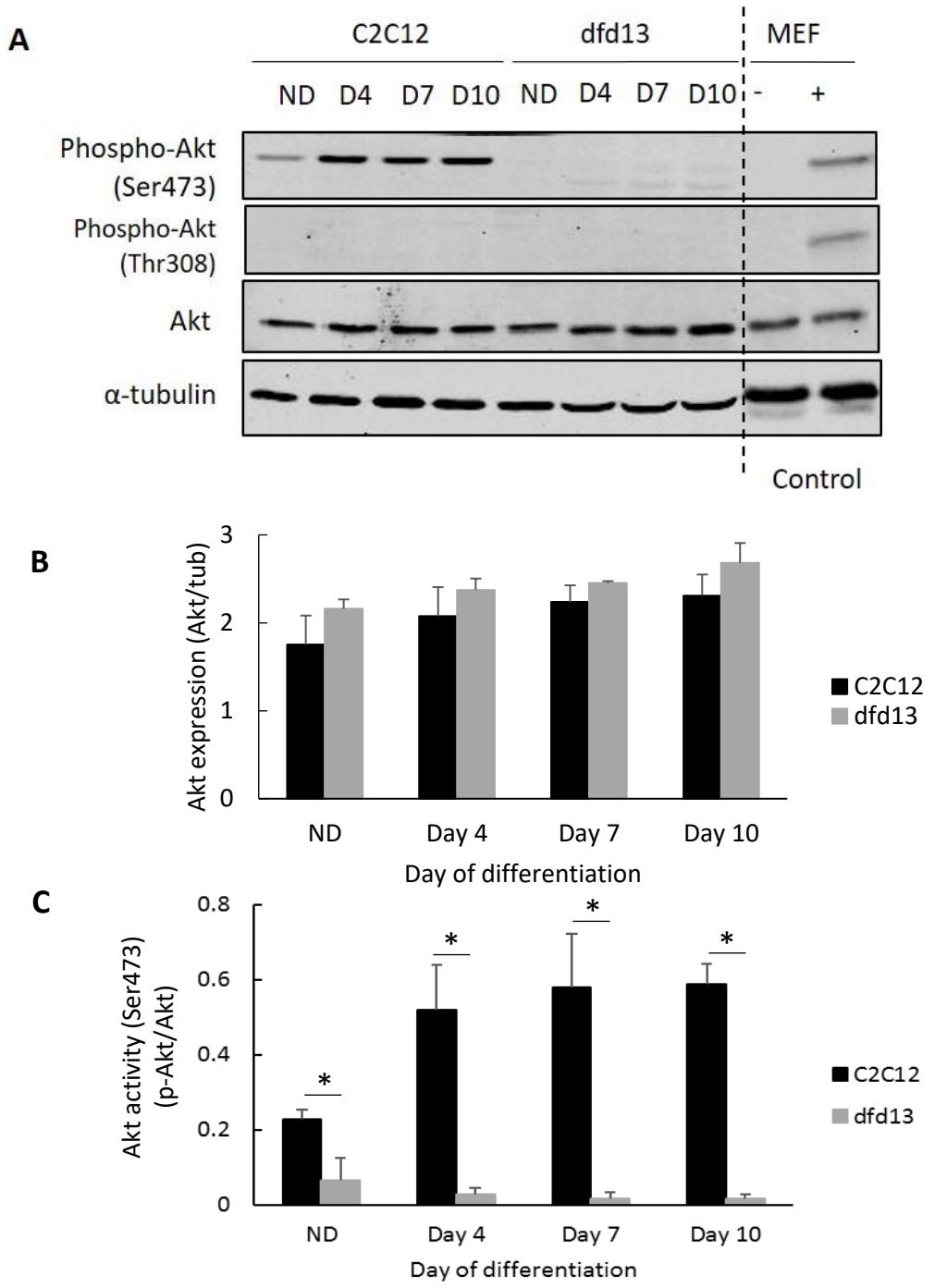

Figure 4.3: Akt is inactivated in dystrophin-deficient myoblasts

Myoblasts were cultured in GM until 80 to 90% confluent before washing twice with PBS and culturing in DM for 10 days with the media being changed every 2 days. Untreated- and PDGF-treated MEF cells were used as a control for Akt phosphorylation at both Ser473 and Thr308. Total protein was extracted at the indicated time points prior to immunoblotting with antibodies recognising Akt, phospho-Akt (Ser473) and phospho-Akt (Thr308). (A) Immunoblot analysis during myoblast differentiation with α-tubulin expression as a loading control. Densitometry analysis of (B) Akt expression and (C) Akt activation at Ser473. The graphs represent an average of three repeats from different samples. ND: non-differentiated; +: PDGF-treated; -: non-treated; *: significantly different ($p<0.05$) compared to C2C12 myoblasts. GM: growth medium (DMEM + 10% FCS); DM: differentiation medium (DMEM + 2% horse serum); n=3.

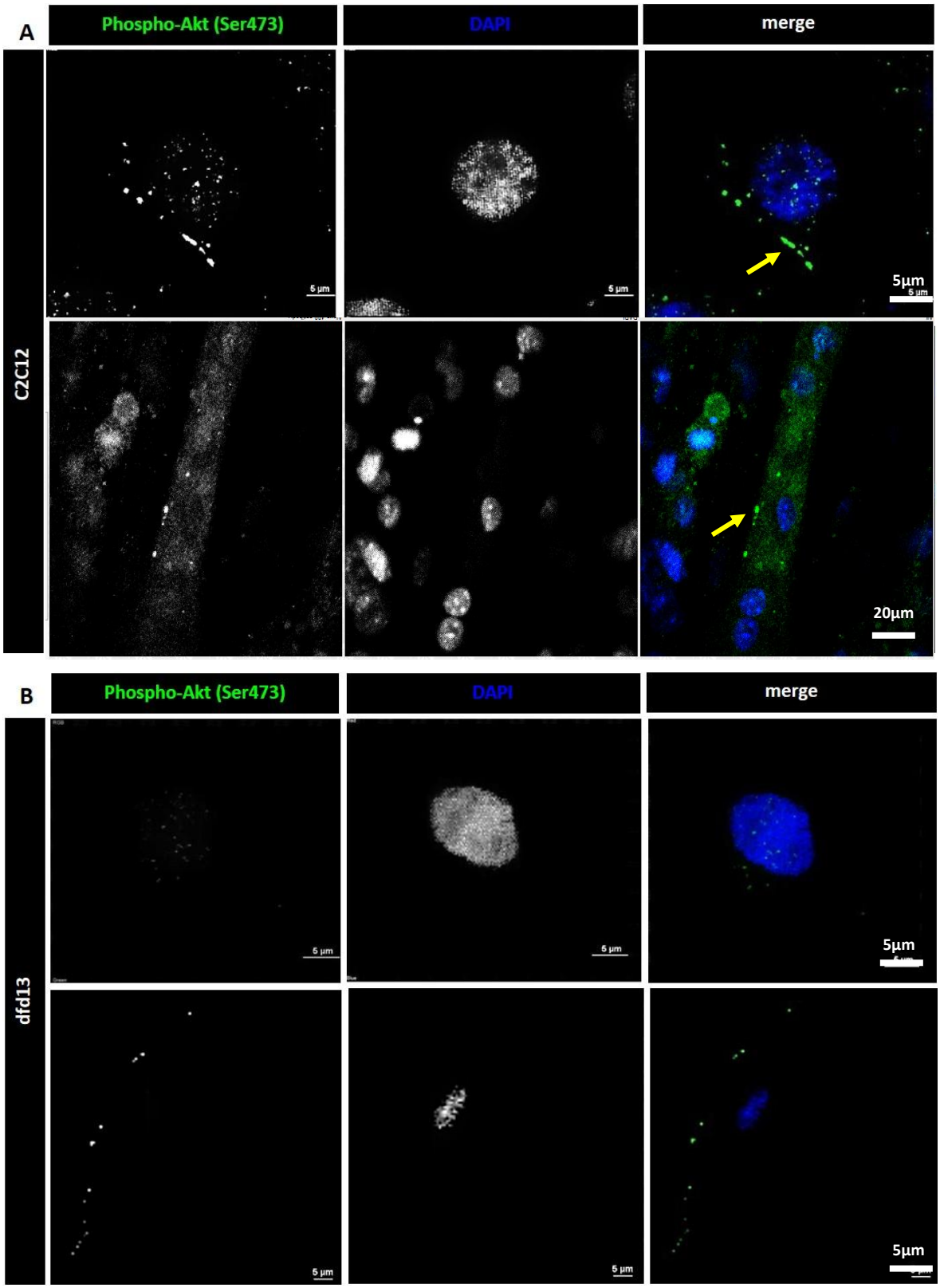
A
Phospho-Akt (Ser473)
DAPI
merge
C2C12
5 µm
5µm
20µm
B
Phospho-Akt (Ser473)
DAPI
merge
dfd13
5 µm
5µm

Figure 4.4: Phosphorylated-Akt is not localised to the membrane in dystrophin-deficient myoblasts

Approximately 1.5 x 10^4 non-dystrophic and dystrophin-deficient myoblasts were cultured in GM before differentiated for 10 days in DM in a 48-well plate. Myoblasts (undifferentiated) and myotubes (Day10) were fixed in 4% PFA and blocked with 5% BSA for 30 minutes before staining with anti-phospho-Akt (Ser473) antibody. DAPI was used as a nuclear counterstain. Immunofluorescence analysis of (A) phospho-Akt (ser473) in C2C12 myoblasts and (B) dfd13 myoblasts at the non-differentiated stage and day 10 of differentiation. Yellow arrow showed phospho-Akt(Ser473) on membrane. GM: growth medium (DMEM + 10% FCS); DM: differentiation medium (DMEM + 2% horse serum); n=3.

4.2.3 Rictor-mTORC2 is inactivated in Dystrophin-Deficient Myoblasts

A previous study reported that mTORC2 is essential for terminal myogenic differentiation (Shu and Houghton 2009). It was also reported that it participates in actin cytoskeleton arrangements, which might be involved in dystrophin functionality in myoblasts. Therefore, it was hypothesised that Akt inactivation is affected by rictor, a subunit of mTORC2, upstream of Akt and responsible for Ser473 phosphorylation. However, the upstream protein that regulates rictor-mTORC2 remains unclear. In this study both total rictor and mTOR expression was examined as well as its activation. However, it was impossible to classify the specific complexes of mTOR activity as phosphorylation at Ser2448 can cause the binding to both raptor and rictor (Rosner et al. 2010).

As depicted in Figure 4.5A, immunoblot analysis of total rictor, mTOR and their phosphorylated forms was performed. Phosphorylated-rictor at Thr1135 was virtually not detected in dfd13 myoblasts throughout the differentiation period. However, rictor expression was increased upon differentiation in both types of myoblasts. Densitometry analysis showed that there was no significance difference in its accumulation in the two types of myoblasts (Figure 4.5B). Rictor expression only showed a significant increase ($p<0.05$; $p = 2.75x10^{-2}$) in dfd13 myoblasts at day 10 compared to non-differentiated dfd13 myoblasts. Densitometry analysis of rictor

activation by phosphorylation at Thr1135 (Figure 4.5C) showed a significant difference in C2C12 myoblasts compared to dfd13 myoblasts at all stages; non-differentiated $p<0.05$; $p = 2.22x10^{-2}$, day 4 $p<0.05$; $p = 3.52x10^{-2}$, day 7 $p<0.05$; $p = 1.01x10^{-2}$ and day 10 $p<0.01$; $p = 3.23x10^{-3}$).

Figure 4.5D shows that total mTOR expression was increased in dfd13 myoblasts during differentiation but remained the same in C2C12 myoblasts. A significant accumulation was seen in dfd13 myoblasts on day 4 ($p<0.05$; $p = 2.93x10^{-2}$), day 7 ($p<0.05$; $p = 1.23x10^{-2}$), and day 10 ($p<0.01$; $p = 8.55x10^{-3}$) when compared to C2C12 myoblasts. Relative mTOR activity was significantly higher in non-differentiated dfd13 myoblasts when compared to non-differentiated C2C12 myoblasts ($p<0.05$; $p = 4.15x10^{-2}$). Relative activity showed a significant reduction upon differentiation in dfd13 myoblasts while C2C12 myoblasts showed a significant accumulation when compared to dfd13 myoblasts on day4 ($p<0.05$; $p = 2.23x10^{-2}$), day 7 ($p<0.01$; $p = 6.78x10^{-3}$) and day 10 ($p<0.05$; $p = 1.29x10^{-2}$) (Figure 4.5E). The actual of mTOR activity in dfd13 myoblast also showed reduction throughout differentiation day (Figure 4.5F).

From these results it can be suggested that inactivation of Akt is caused by the inactivation of rictor in dfd13 myoblasts. This impairment is thought to affect other kinases, such as protein kinase C (PKC) (Chapter 6) and focal adhesion proteins, such as integrin-linked-kinase (ILK). Alterations to these kinases have been reported as one of the factors that causes MD. Expression and activation of mTOR was considered to represent endogenous levels of mTOR within both complexes i.e. mTORC1 or mTORC2, where distinct activation occurred. Phosphorylation of mTOR at Ser2448

makes it a major target for p70S6 kinase activation and is also an important event for raptor and rictor binding (Rosner et al., 2010).

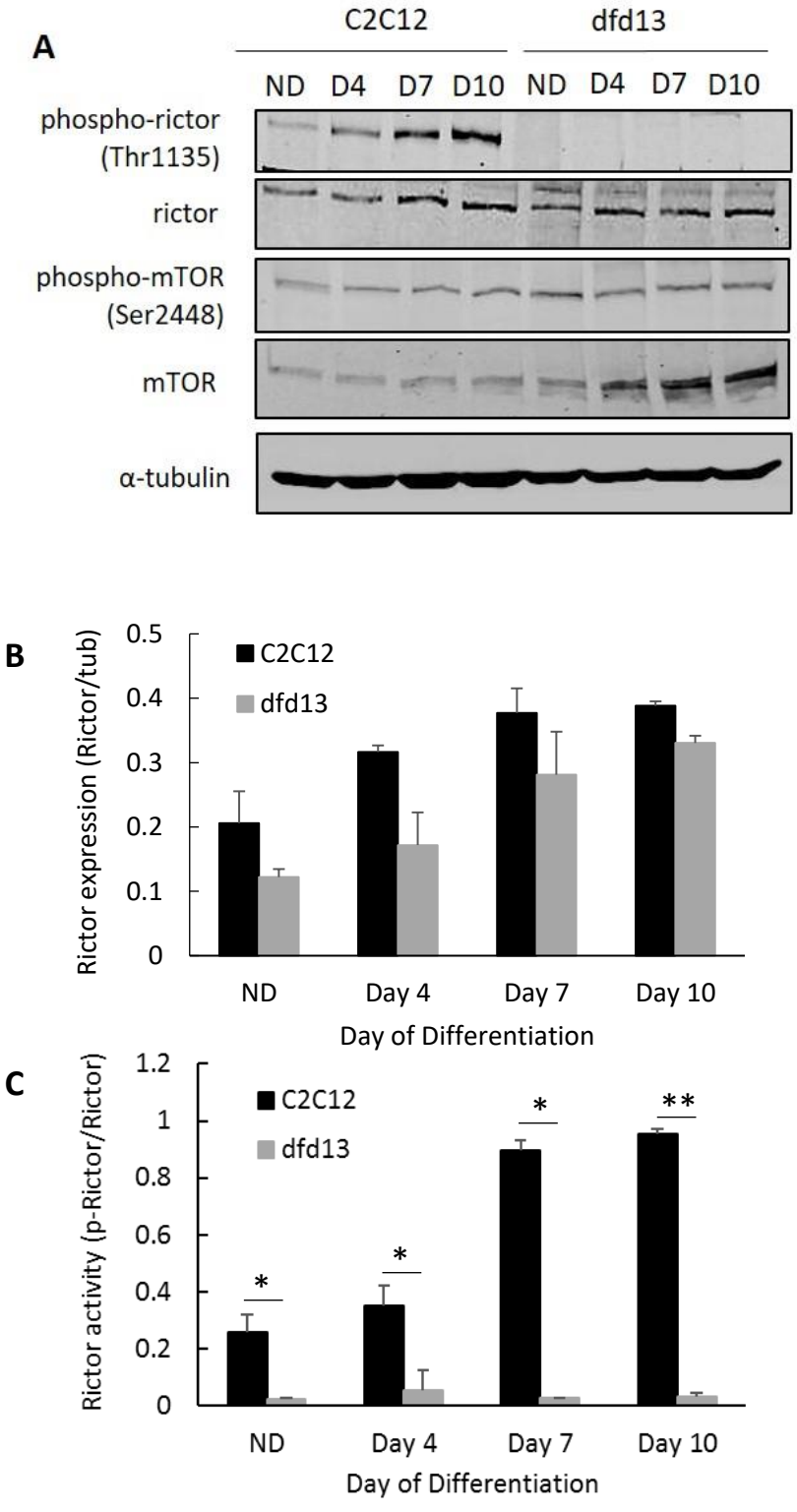

D

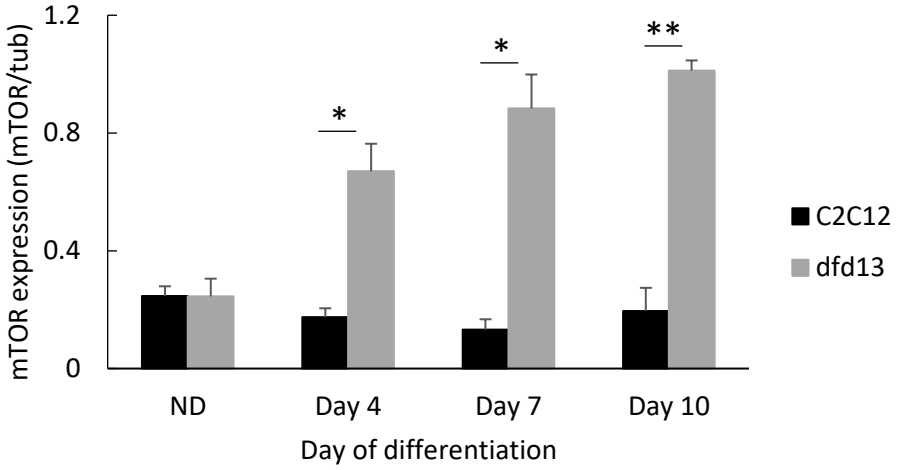
1.2
0.8
0.4
0
mTOR expression (mTOR/tub)
*
*
**
ND
Day 4
Day 7
Day 10
Day of differentiation
C2C12
dfd13

E

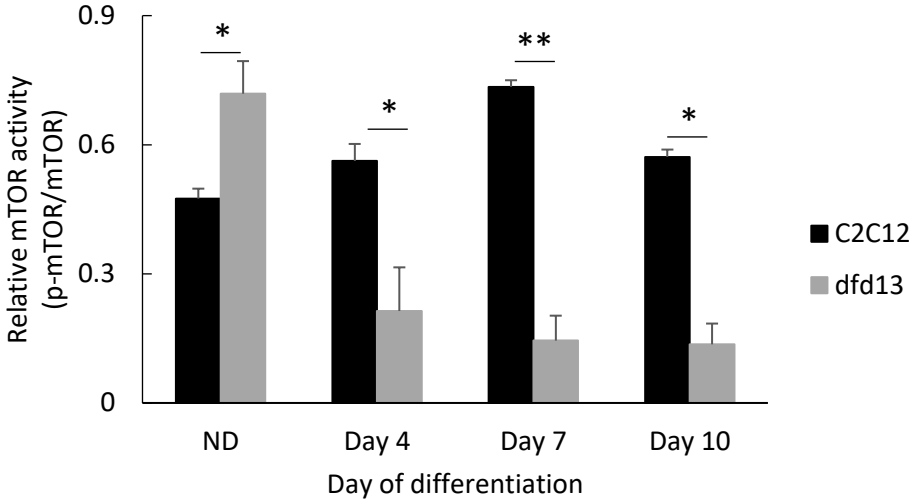
0.9
0.6
0.3
0
Relative mTOR activity
(p-mTOR/mTOR)
*
*
**
*
ND
Day 4
Day 7
Day 10
Day of differentiation
C2C12
dfd13

F

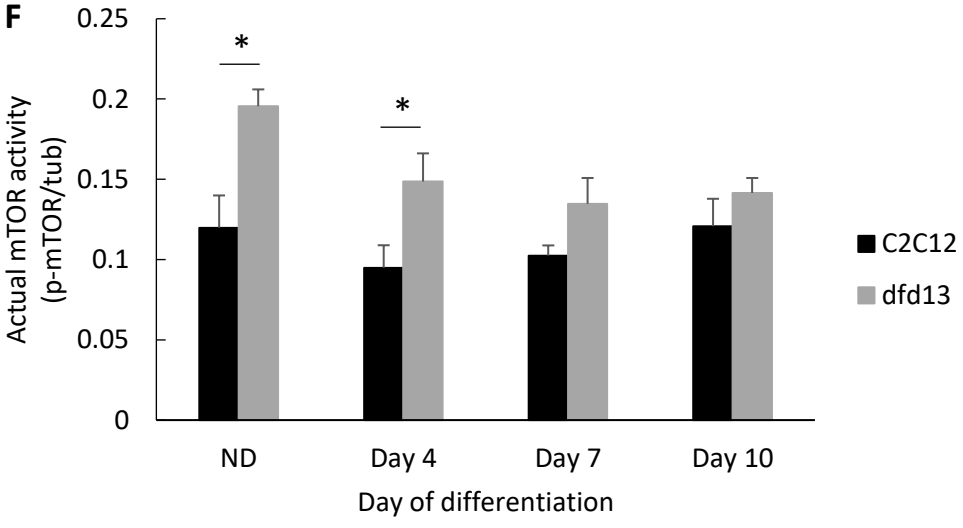
0.25
0.2
0.15
0.1
0.05
0
Actual mTOR activity
(p-mTOR/tub)
*
*
ND
Day 4
Day 7
Day 10
Day of differentiation
C2C12
dfd13

Figure 4.5: Rictor-mTORC2 activation is lower in dystrophin-deficient myoblasts
Myoblasts were cultured in GM until 80 to 90% confluent before washing twice with PBS and culturing in DM for 10 days with the media being changed every 2 days. Total protein was extracted at the indicated time points prior to immunoblotting with antibodies recognising phospho-rictor (Thr1135), rictor, phospho-mTOR (Ser2448) and mTOR proteins. (A) Immunoblot analysis during myoblast differentiation with α-tubulin expression as a loading control. Densitometry analyses of (B) total rictor expression (C) rictor activity (D) total mTOR expression, and (E) mTOR activity. The graphs represent an average of three repeats from different samples. ND: non-differentiated; *: significantly different ($p<0.05$) compared to dfd13 myoblasts. GM: growth medium (DMEM + 10% FCS); DM: differentiation medium (DMEM + 2% horse serum); n=3.

4.2.4 p70S6 Kinase Activity Is Completely Reduced in Differentiating Dystrophin-Deficient Myoblasts

Rictor has been shown inactivated in undifferentiated and differentiating dfd13 myoblasts. Following the mTORC2 impairment, mTORC1 activity was investigated through the analysis of the downstream protein, pS6 kinase. pS6 kinase has two isoforms; p70S6K and p85S6K. Expression and activation of both isoforms in undifferentiated and differentiated myoblasts were examined.

As depicted in Figure 4.6A, an immunoblot panel showed that phospho-p70S6K (Thr389) and p70S6K was detected in both types of myoblasts. The phopsho-kinase blot also detected endogenous levels of p85S6K when phosphorylated at the analogous site (Thr412) (Figure 4.6A). Densitometry analysis showed that both p85 and p70 S6 kinase expression remained the same throughout the differentiation period in C2C12 myoblasts, but in contrast, both kinases were significantly increased in dfd13 myoblasts. p70S6K was significantly increased in dfd13 myoblasts compared to C2C12 myoblasts on day 4 ($p<0.05$; $p = 4.74\text{x}10^{-2}$), day 7 ($p<0.05$; $p = 1.29\text{x}10^{-2}$), and day 10 ($p<0.05$; $p = 1.01\text{x}10^{-2}$ and $p<0.05$; $p = 2.45\text{x}10^{-2}$) (Figure 4.6B). Similarly, p85S6K was significantly increased in dfd13 myoblasts compared to C2C12 myoblasts on day 4

($p<0.05$; $p = 4.84x10^{-2}$), day 7 ($p<0.05$; $p = 3.36x10^{-2}$), and day 10 ($p<0.05$; $p = 1.01x10^{-2}$ and $p<0.05$; $p = 2.21x10^{-2}$) (Figure 4.6C).

Figure 4.6D shows p70S6K activation when phosphorylated at Thr389, which can be seen to have increased significantly ($p<0.05$; $p = 4.69x10^{-2}$) on day 4 in C2C12 myoblasts compared to dfd13 myoblasts. This activity was found to be reduced on day 7 ($p<0.05$; $p = 4.49x10^{-2}$) and day 10 ($p<0.05$; $p = 4.70x10^{-2}$) of differentiation, but remained higher when compared to dfd13 myoblasts. In contrast, p70S6K activation was only found in non-differentiated dfd13 myoblasts and decreased over the differentiation period (Figure 4.6D). Phosphorylated-p85S6Kwas not detected in either type of myoblasts.

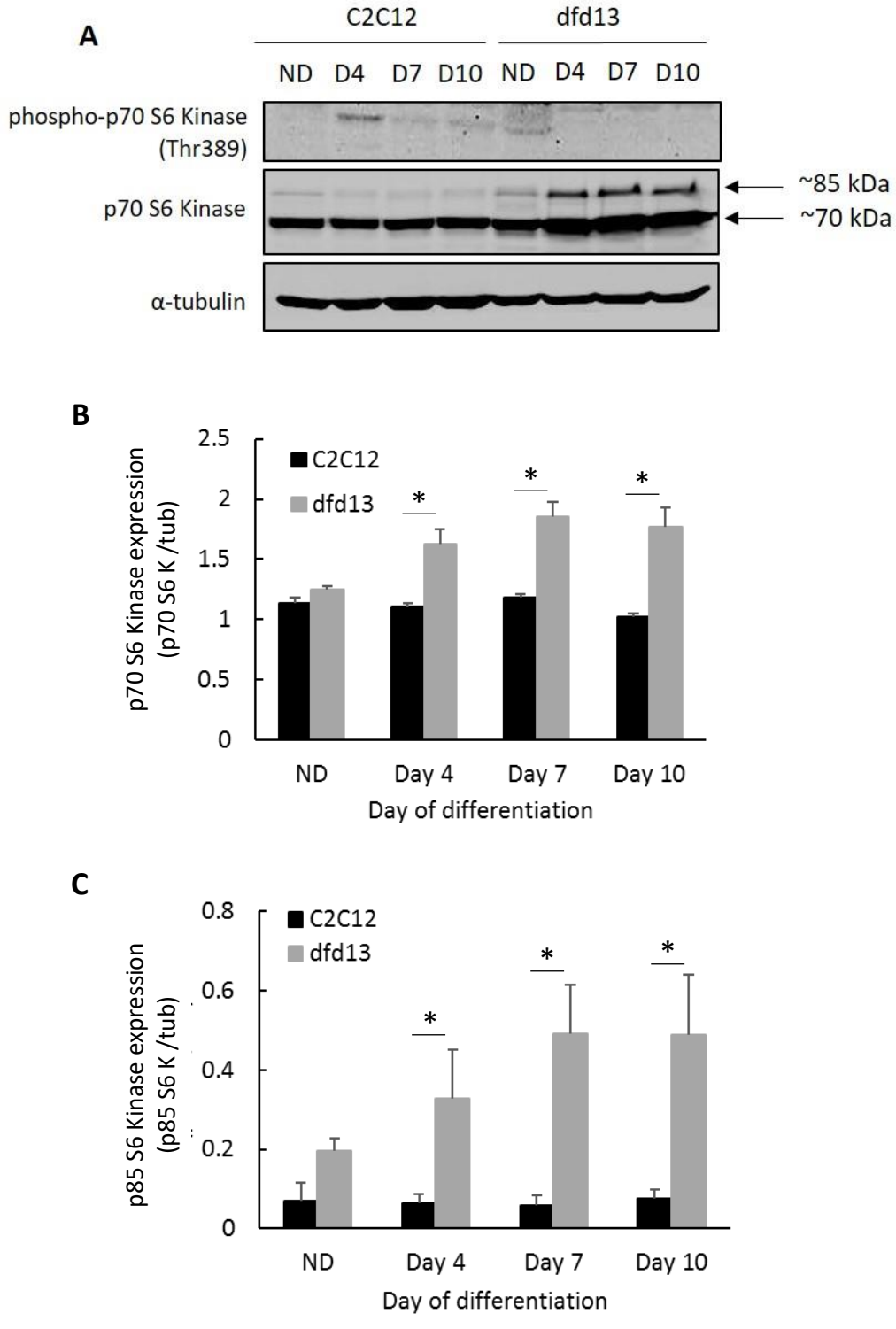
A
C2C12
dfd13
ND D4 D7 D10 ND D4 D7 D10
phospho-p70 S6 Kinase (Thr389)
p70 S6 Kinase
α-tubulin
~85 kDa
~70 kDa
B
p70 S6 Kinase expression (p70 S6 K /tub)
C2C12
dfd13
2.5
2
1.5
1
0.5
0
*
ND
Day 4
Day 7
Day 10
Day of differentiation
C
p85 S6 Kinase expression (p85 S6 K /tub)
C2C12
dfd13
0.8
0.6
0.4
0.2
0
*
ND
Day 4
Day 7
Day 10
Day of differentiation

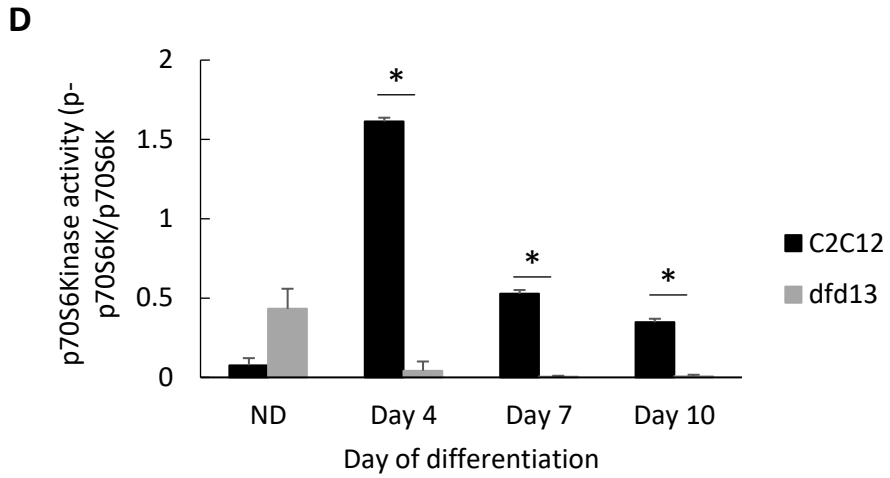

Figure 4.6: p70S6 kinase activation is reduced in differentiating dystrophin-deficient myoblasts

Myoblasts were cultured in GM until 80 to 90% confluent before washing twice with PBS and culturing in DM for 10 days with the media being changed every 2 days. Total protein was extracted at the indicated time points prior to immunoblotting with antibodies recognising phosho-p70S6K, p70S6K and p85S6K protein. (A) Immunoblot of the proteins during myoblast differentiation with α-tubulin expression as a loading control. Densitometry analysis representing (B) p70S6K expression, (C) p85S6K, and (D) phospho-p70S6K (Thr389) activation. The graphs represent an average of three repeats from different samples. ND: non-differentiated; *: significantly different ($p<0.05$) compared to dfd13 myoblasts. GM: growth medium (DMEM + 10% FCS); DM: differentiation medium (DMEM + 2% horse serum); n=3.

4.2.5 FoxO3 Expression Is Highly Increased in Differentiating Dystrophin-Deficient Myoblasts

Besides p70S6K, inactivation of Akt also had an effect on another downstream protein, FoxO3 (Forkhead box O3), which is a target protein of Akt. FoxO3 is a transcription factor responsible for the activation of autophagy genes involved in the autophagy machinery. A previous study showed that FoxO3 controls autophagy in skeletal muscle *in vivo* and induced multiple autophagy genes, including LC3B transcription in skeletal muscle (Mammucari et al. 2007). In this study, FoxO3 expression in myoblasts was examined.

Immunoblot analyses (Figure 4.7A) showed that FoxO3 expression was increased in both types of myoblasts during differentiation. However, there was only a

slight increase in FoxO3 in C2C12 myoblasts on day 4, and it remained at the same level until day 10. In non-differentiated dfd13 myoblasts FoxO3 levels were found to be significantly lower ($p<0.01$; $p = 6.63x10^{-3}$) compared to C2C12 myoblasts. FoxO3 then increased throughout the differentiation period and there was a significant difference in dfd13 myoblasts ($p<0.01$; $p = 4.45x10^{-3}$) on day 10 compared to C2C12 myoblasts (Figure 4.7B).

Akt plays a role in inhibiting FoxO3 through phosphorylation at Thr24, Ser256 and Ser319, which leads to nuclear exclusion and activation. As Akt is inactive in dfd13 myoblasts, it is thought that FoxO3 is not phosphorylated. Therefore, the non-phosphorylated FoxO3 is translocated to the nucleus and activates the gene involved in autophagy i.e., Becn1, Atg5 and Atg7.

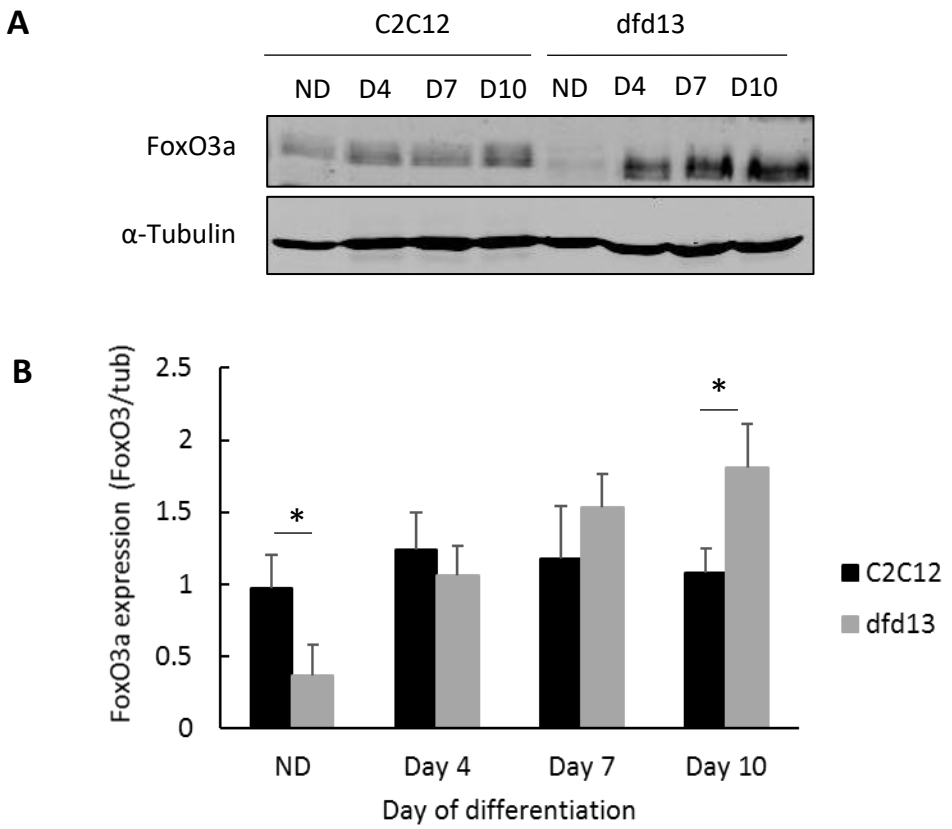

Figure 4.7: FoxO3a is highly increased in differentiating dystrophin-deficient myoblasts
Myoblasts were cultured in GM until 80 to 90% confluent before washing twice with PBS and culturing in DM for 10 days with the media being changed every 2 days. Total protein was extracted at the indicated time points prior to immunoblotting with antibodies recognising FoxO3a. (A) Immunoblot analysis of proteins during myoblast differentiation with α-tubulin expression as a loading control. Densitometry analysis representing (B) FoxO3a expression. The graph represents an average of three repeats from different samples. ND: non-differentiated; *: significantly different ($p<0.05$) compared to dfd13 myoblasts. GM: growth medium (DMEM + 10% FCS); DM: differentiation medium (DMEM + 2% horse serum); n=3.

4.3 Discussion

4.3.1 Elevation of PTEN Affects PI3K/Akt Regulation in Dystrophin-Deficient Myoblasts

The PI3K/Akt pathway is a highly-conserved pathway for the regulation of skeletal muscle growth and is activated by the binding of Igf-1 to its receptor, Igf1-r. This binding leads to intrinsic tyrosine kinase activation, as well as auto-phosphorylation, which can generate a docking site for IRS. Phosphorylated-IRS then becomes a docking site for PI3K, thus activating PI3K/Akt signalling for myoblast differentiation via a series of phosphorylation events. This signalling is negatively regulated by PTEN.

In this study PTEN was shown to be elevated in dfd13 myoblasts, which might affect PI3K activity upon PIP_3 production, as it was found to be decreased during differentiation (

Figure 4.2), indicating that PI3K regulation is altered in dfd13 myoblasts. PTEN acts as lipid phosphatase and plays a role in removing the phosphate group present on the inositol ring of PIP_3 to produce PIP_2. In contrast, PI3K reverses this event by phosphorylating PIP_2 to become PIP_3.

PI3K exists as a heterodimer consisting of two subunits (p85 and p110) regulatory and catalytic. When cells are stimulated, p85 binds to tyrosine-phosphorylated IRS, and phosphorylated-p85 changes the conformation of p110 and thus mediates the p110 subunit to translocate to the membrane and increases its enzymatic activity such as PIP_2 phosphorylation. PIP_3 helps to recruit Akt by binding the plekstrin homolog (PH) domain at the N-terminal of Akt to the cell membrane. PTEN in turn acts as a negative regulator by dephosphorylating PIP_3 to form PIP_2, and thereby reduces the available docking sites for Akt to bind to prior to activation. PTEN

is mainly found in the cytosol and nucleus. The N-terminal possess a PIP_2-binding motif while the C-terminal contains a serine/threonine phosphorylation, Ser380, which regulates its stability and activity, as well as membrane recruitment. The main C2 domain, contains basic residues that are essential for membrane binding. Phosphorylation of PTEN is considered result in a closed conformation which is the inactive form. In this conformation it has been proposed that the phosphorylated C-terminal interacts with the positively charged C2 domain and remains in the cytoplasm (Vazquez et al. 2006).

Feron and colleagues (2009) reported that increased PTEN expression caused deregulation of the PI3K/Akt pathway in dystrophin-deficient muscle present in GRMD dogs. This was also observed in muscle sections from 3- to 36-month old animals and indicates that the PI3K/Akt pathway is a long-term alteration. A more recent study by Alexander et al. (2014) proposed that overexpression of micro-RNA-486 improved muscle physiology and performance in dystrophin-deficient mice. Micro-RNA-486 is a muscle-enriched micro-RNA that is markedly reduced in the muscle of dystrophin-deficient mice and DMD patient muscles (Eisenberg et al. 2007; Alexander et al. 2011). Micro-RNA-486 targets DOCK3 (dedicator of cytokinesis 3) which modulates PTEN/Akt signalling in skeletal muscle. As DOCK3 was increased in dystrophic muscle (Alexander et al. 2014), it is suggested that high PTEN activation also occurred in dystrophin-defieicent myoblasts.

4.3.2 Inactivation of Akt is Caused By Impaired Rictor-mTORC2 in Dystrophin-Deficient Myoblasts

In this study it was found that Akt is inactivated in dfd13 myoblasts, as phosphorylation at Ser473 or Thr308 was not detected. However, in C2C12 myoblasts Akt was

phosphorylated at Ser473 and the activated form accumulated upon differentiation. Immunofluorescence analysis showed that phosphorylated-Akt (Ser473) is localised to the membrane of C2C12 myotubes but found less often in dfd13 myoblasts. During biosynthesis, nascent Akt is phosphorylated at Thr450 within the turn motif site and localised to the cytosol when in its inactive conformation. In the presence of signals via PI3K activation, Akt is recruited to the membrane through the binding of plekstrin homolog (PH) to PIP_3. Once bound, the conformation is changed and this event unmasks two residues for phosphorylation, Ser473 and Thr308. In this study, less Akt-phosphorylated at Ser473 was detected in dystrophin-deficient myoblasts, indicating that Akt is inactivated. According to Sarbassov et al. (2005), PDK1 has a better target on Akt phosphorylated at Ser473 than non-phosphorylated Akt. In line with the results shown in

Figure 4.2, there is no Thr308 phosphorylation if Ser473 phosphorylation does not occur. However, the expression of total Akt did not show any significant difference when compared between both types of myoblast.

Since Akt was found to only be phosphorylated at Ser473 the protein responsible for this phosphorylation event was investigated. It is known that mTORC2, specifically, rictor, can directly phosphorylate Akt at Ser473 *in vitro* and this facilitated Thr308 phosphorylation by PDK1 in Drosophila (Sarbassov et al., 2005). In this study it was found that rictor is inactivated in both undifferentiated and differentiated dfd13 cells, which explains the absence of phosphorylated-Akt (Ser473) observed; however, the regulator for rictor activation in myoblasts remains unknown. Rictor phosphorylation has been shown to require mTORC1-activated p70S6K in MEF, HEK293 and HeLa cells (Julien et al. 2010). Recently, it has been showed that PTEN negatively regulates

mTORC2 signalling in glioma (Bhattacharya, Maiti, and Mandal 2016). As PTEN was found to be highly expressed in dfd13 myoblasts, inactivation of rictor can be seen as a consequence of this event and presumably represents the same scenario as in myoblasts.

4.3.3 Reduction of p70S6 Kinase Activation Indicates Less mTORC1 Activation and Suggests Inactivation of Akt in Dystrophin-Deficient Myoblasts

Akt is not activated in dystrophin-deficient myoblasts which alters downstream protein regulation, as Akt is a key regulator of a diverse array of cellular functions, such as cell proliferation, differentiation, apoptosis and metabolism. One of the downstream proteins it regulates is p70S6K, which together with 4E-BP1 is responsible for protein synthesis. This is the best characterised substrate of mTORC1 kinase activity. Akt controls mTORC1 activation via a series of other protein activations i.e. PRASS40, and protein inhibitions, i.e. TSC1/2-RHEB complexes.

The data showed that phosphorylated-p70S6K at Thr389 is decreased in dfd13 myoblasts after differentiation. This indicates that mTORC1 is inactivated, in line with the inactivation of Akt (Figure 4.3), and there is less phosphorylated-mTOR at Ser2448 Figure 4.4 upon differentiation. This suggests that protein synthesis regulation is disturbed thus impairing myoblast differentiation regulation. As p70S6K showed a decrease in activation, it can be suggested that rictor phosphorylation is mTORC1-activated p70S6K dependent within myoblasts, which is in line with what occurs in reports for other cells (Julien et al., 2010). To the best of our knowledge, this is the first report describing the inactivation of Akt which is mTORC1-activated p70S6K dependent in dystrophin-deficient myoblasts and could be one of the causes for dystrophin-deficient myoblasts not achieving terminal differentiation.

4.4 Conclusions

PTEN-PI3K/Akt and its downstream proteins are perturbed in dystrophin-deficient myoblasts.

Key finding(s):

- PTEN overexpression impairs PI3K/Akt signalling.
- Activation of Akt (Ser473) is mTORC1-activated p70S6K dependent.
- Protein synthesis and FoxO3 regulation is defective.

Chapter 5 - Autophagy is Defective in Dystrophin-Deficient Myoblasts

5.1 Introduction

It is known that the transcription factor FoxO3 controls autophagy in skeletal muscle; however, it remains unknown how autophagy is modulated in the *mdx* mouse as well as in DMD humans. In this study, dystrophin-deficient myoblasts were used to reveal the mechanism for this event. In Chapter 4 it was reported that PI3K/Akt and its downstream proteins are impaired in differentiating dystrophin-deficient myoblasts, and FoxO3 expression was shown to increase in dfd13 myoblasts after 10 days of differentiation.

A previous study has demonstrated that in carcinoma cells an increase in Akt activity promotes nuclear exclusion of FoxO thus preventing FoxO-DNA binding and transcriptional activity (Brunet et al. 1999). Similarly, in colon and renal cancer cells which do not express PTEN, the accumulation of FoxO3 in the cytoplasm results in arrest in the G1 phase of the cell cycle (Nakamura et al., 2000). However, the situation may be different in dystrophin-deficient myoblasts where PTEN is excessively expressed upon differentiation. It has also been reported that autophagy is defective in *mdx* mice but can be rescued by long-term exposure to a low-protein diet (Clara De Palma et al. 2014).

To further understand the impaired regulation of autophagy in dystrophin-deficient myoblasts, the protein profiling of this pathway has been determined which provides information on autophagy modulation and activation. An overview of this chapter is presented in Figure 5.1.

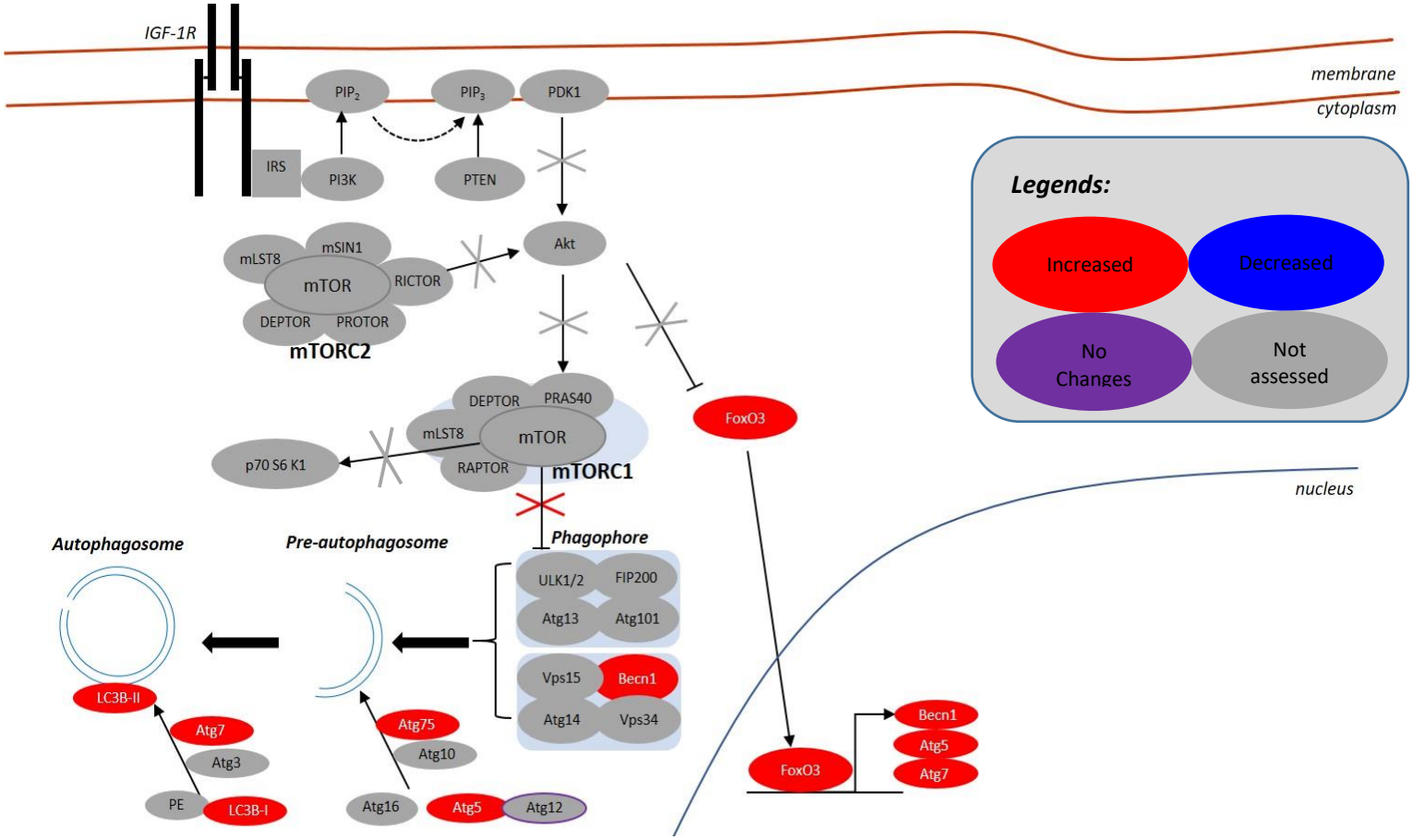

Figure 5.1: Chapter overview: accumulation of nuclear-FoxO3 increases autophagosome formation but exhibits an autophagy flux reduction in dystrophin-deficient myoblasts

Accumulation of translocated-FoxO3 to the nucleus increases the expression autophagy related proteins, i.e. Atg5, Atg7, Beclin1. As a result, phagophore formation is increased and the maturation of autophagosome by Atgs; however, autophagic flux is reduced. The perturbation of PI3K/Akt increases nuclear-FoxO3, thus modulating excessive autophagosome formation while reducing autophagic flux in dystrophin-deficient myoblasts.

5.2 Results

5.2.1 FoxO3 Is Predominantly Localised in the Nucleus of Differentiating Dystrophin-Deficient Myoblasts

Akt represses FoxO3 via phosphorylation resulting in nuclear exclusion. As Akt is not activated in dfd13 myoblasts, it was speculated that unphosphorylted-FoxO3 translocates into the nucleus and binds to the promoter, thus up-regulating autophagy related genes such as LC3B, Atg5 and Atg7. Therefore, FoxO3 expression and localisation needed to be examined within subcellular fractions, i.e. the nucleus and cytoplasm.

FoxO3 was found to be localised more to the nucleus of dfd13 myoblasts (Figure 5.2A), with approximately 81.6% of FoxO3 present in the nucleus of dfd13 myoblasts compared to only ~47.6% in C2C12 myoblasts during the undifferentiated stage. Surprisingly, on day 10 of differentiation, levels in the nucleus had accumulated in both types of myoblast; C2C12 ~78.2%, and dfd13 ~94.4%.

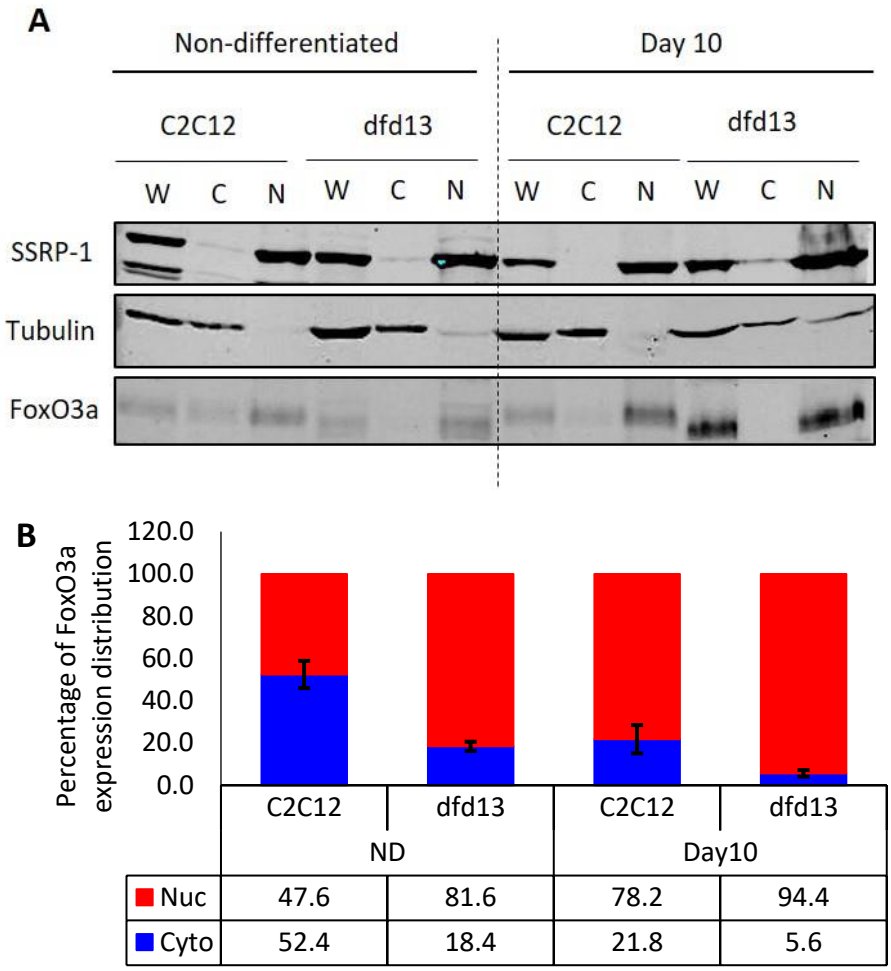

Figure 5.2: FoxO3a is predominantly localised in the nucleus of differentiating dystrophin-deficient myoblasts

Myoblasts were cultured in GM until 80 to 90% confluent before washing twice with PBS and culturing in DM for 10 days with the media being changed every 2 days. Subcellular protein extraction was performed at the indicated time points using the REAP protocol prior to immunoblotting with an antibody which recognises FoxO3a. (A) Immunoblot of the proteins during myoblast differentiation with α-tubulin and SSRP1 expression as loading controls. Densitometry analysis representing (B) FoxO3a expression in the cytoplasm and nucleus. ND: non-differentiated; GM: growth medium (DMEM + 10% FCS); DM: differentiation medium (DMEM + 2% horse serum); W: whole cell lysate; C: cytoplasm; N: nucleus; n=3.

5.2.2 Autophagy Related Proteins Are Highly Increased in Differentiating Dystrophin-Deficient Myoblasts

It has been shown that FoxO3 is highly expressed and primarily localised to the nucleus of differentiating dfd13 myoblasts. Within the nucleus, FoxO3 acts as a transcriptional activator that can recognise and bind to DNA sequences resulting in the activation of

genes involved in autophagy, such as those for Beclin1 and Atgs. It was hypothesised that autophagy is highly activated in differentiating dystrophin-deficient myoblasts.

Figure 5.3 presents immunoblot and densitometry analyses of autophagy related proteins involved in autophagosome formation. Beclin1 expression was slightly increased in C2C12 myoblasts and highly increased in dfd13 myoblasts upon differentiation (Figure 5.3A). Densitometry analysis of Beclin1 expression showed significant accumulation on day 4 ($p<0.05$; $p = 2.07x10^{-2}$), day 7 ($p<0.05$; $p = 1.56x10^{-2}$) and day 10 ($p<0.01$; $p = 5.70x10^{-3}$) in dfd13 myoblasts compared to C2C12 myoblasts (Figure 5.3B).

Atg5 was found to be expressed at low levels in C2C12 myoblasts (Figure 5.3A). It can be seen that Atg5 expression was increased upon differentiation in dfd13 myoblasts, and expression was significantly increased on day 4 ($p<0.01$; $p = 6.36x10^{-3}$), day 7 ($p<0.01$; $p = 6.13x10^{-4}$) and day 10 ($p<0.01$; $p = 1.96x10^{-3}$) compared to the non-differentiated stage. Densitometry analysis also showed significant differences ($p<0.01$) for dfd13 myoblasts at every time point compared to C2C12 myoblasts (Figure 5.3C).

Densitometry analysis of Atg7 expression in dfd13 myoblasts showed its accumulation throughout the differentiation period; however, there was no significant difference in expression when compared to the non-differentiated stage in C2C12 myoblasts. Expression showed a significant increase in dfd13 myoblasts when compared to the non-differentiated stage and also significant on day 4 ($p<0.05$; $p = 1.43x10^{-2}$), day 7 ($p<0.05$; $p = 4.54x10^{-2}$) and day 10 ($p<0.05$; $p = 2.74x10^{-2}$) compared to C2C12 myoblasts (Figure 5.3D).

Autophagy is responsible for the removal of unfolded protein as well as dysfunctioning organelles, and has been reported to be constantly active within skeletal muscle (De Palma et al., 2014). Beclin1 is the protein responsible for the initiation of autophagosome formation and is also known as phagophore, while Atg5 and Atg7 are ubiquitin-like enzymes involved in the autophagosome elongation process. In this study, Beclin1, Atg5 and Atg7 showed enhanced expression in dfd13 myoblasts. However, in C2C12 myoblasts there was only a slight increase in the expression of Beclin1 and Atg7 which persisted throughout the differentiation period. Consequently, autophagosome formation (maturation) and autophagic flux during myoblast differentiation were investigated via immunoblotting and flow cytometry analysis, respectively.

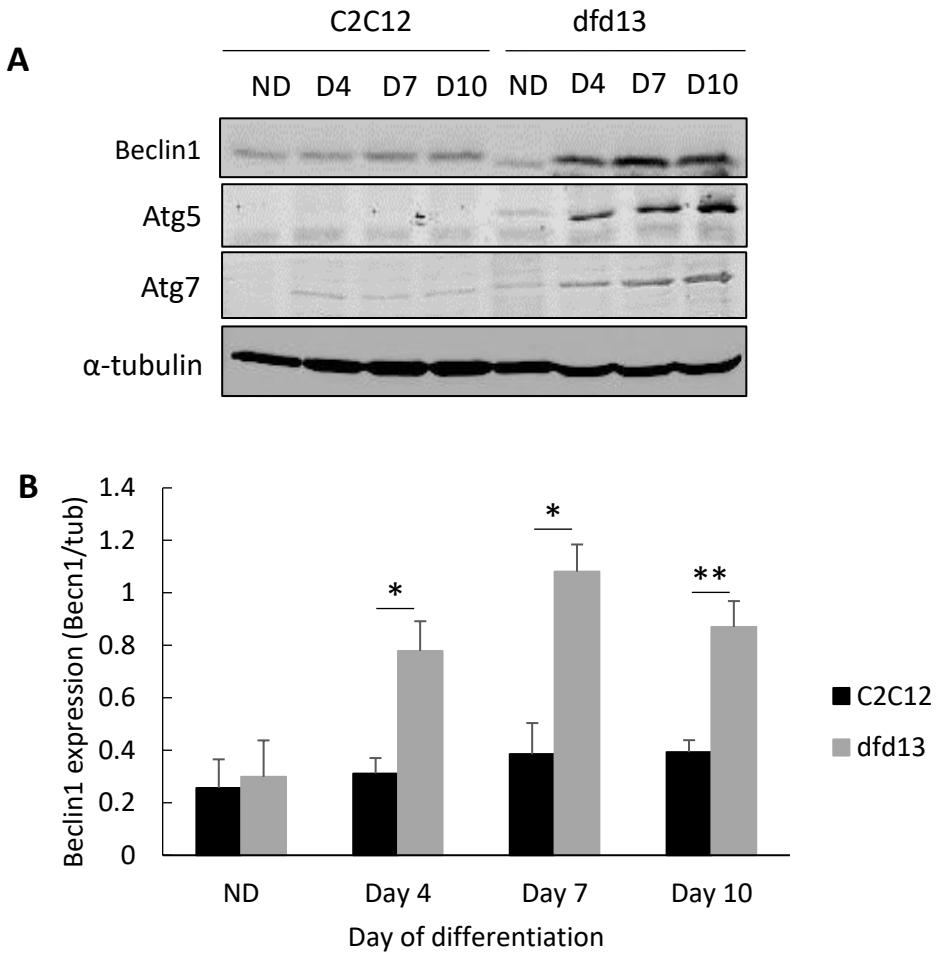

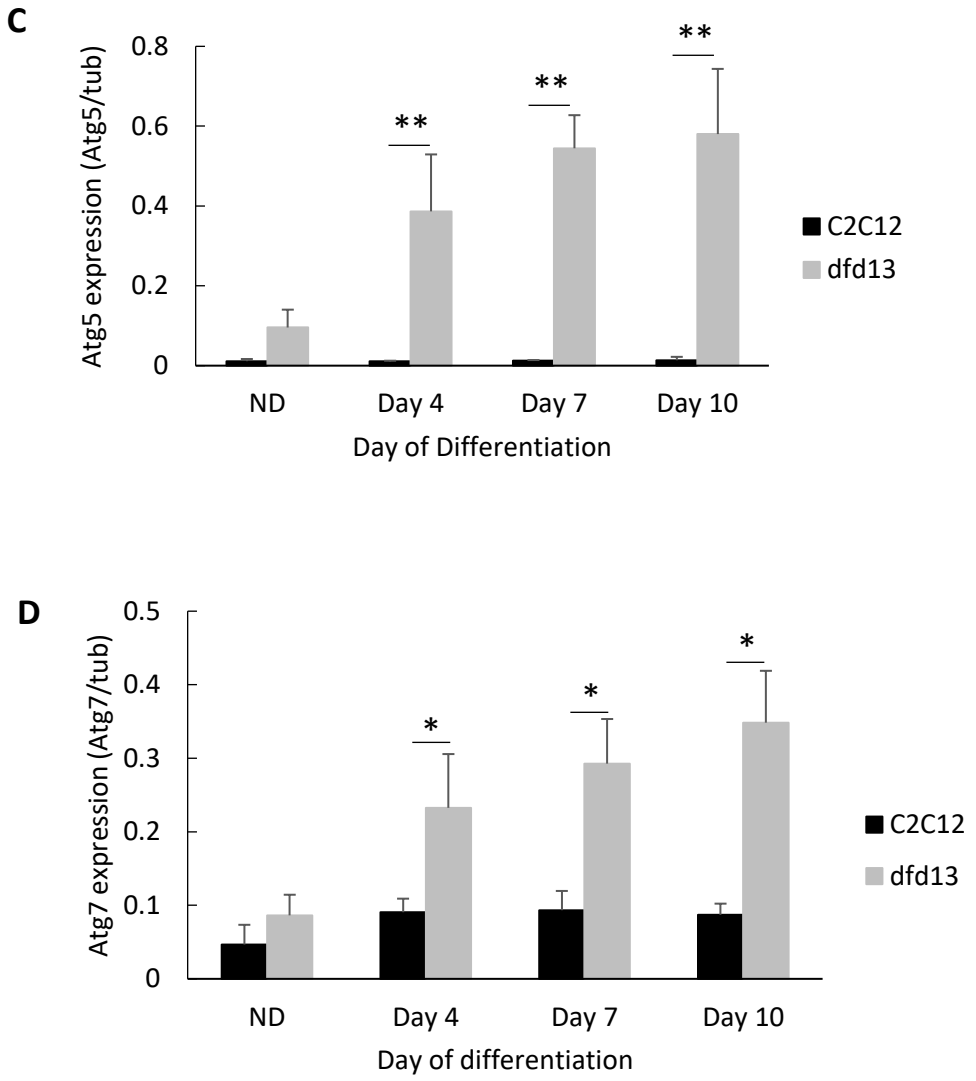

Figure 5.3: Expression of autophagy related proteins is highly increased in differentiating dystrophin-deficient myoblasts

Myoblasts were cultured in GM until 80 to 90% confluent before washing twice with PBS and culturing in DM for 10 days with the media being changed every 2 days. Protein extraction was performed at the indicated time points. (A) Immunoblot analysis of Beclin1, Atg5 and Atg7 expression with α-tubulin expression as a loading control. Densitometry analysis representing (B) Beclin1, (C) Atg5, and (D) Atg7 expression. The graphs represent an average of four repeats from different samples. ND: non-differentiated; Significantly different: * ($p<0.05$) and ** ($p<0.01$) compared to C2C12 myoblasts; n=4.

5.2.3 Microtubule-Associated Light Chain-3B Conversion Is Increased in Differentiating Dystrophin-Deficient Myoblasts

Autophagy related genes had been shown to be highly activated, and the next step was to determine whether a double-membraned vesicle, known as autophagosome, had been formed. The conversion of Light Chain-3B (LC3B-I) to LC3B-II can be considered to represent total autophagosome formation in myoblasts during differentiation.

As shown in Figure 5.4A, expression of LC3B-I and LC3B-II is increased in both differentiating C2C12 and dfd13 myoblasts when compared to the respective non-differentiated myoblasts. LC3B-I expression in differentiated dfd13 myoblasts was significantly higher ($p<0.01$; $p = 3.41 \times 10^{-3}$) at day 10 when compared to differentiated C2C12 myoblasts (Figure 5.4B). LC3B-II was found to accumulate upon differentiation in both types of myoblasts, but was higher in dfd13 myoblasts, with a significant difference on day 10 ($p<0.05$; $p = 1.69 \times 10^{-2}$) when compared with to C2C12 myoblasts (Figure 5.4C). However, the LC3B-II/LC3B-I ratio showed a reduction in dfd13 myoblasts compared to C2C12 myoblasts upon differentiation, and was significantly different ($p<0.05$; $p = 5.33 \times 10^{-2}$) (Figure 5.4D).

LC3B-II levels correlate with the number of autophagosomes formed; however, this could indicate either the up-regulation of autophagosome formation or a blockage in autophagic degradation. In addition, it does not conclusively indicate autophagic degradation. Therefore, further analysis was performed to determine autophagic flux, with a lysosome inhibitor used as a positive control.

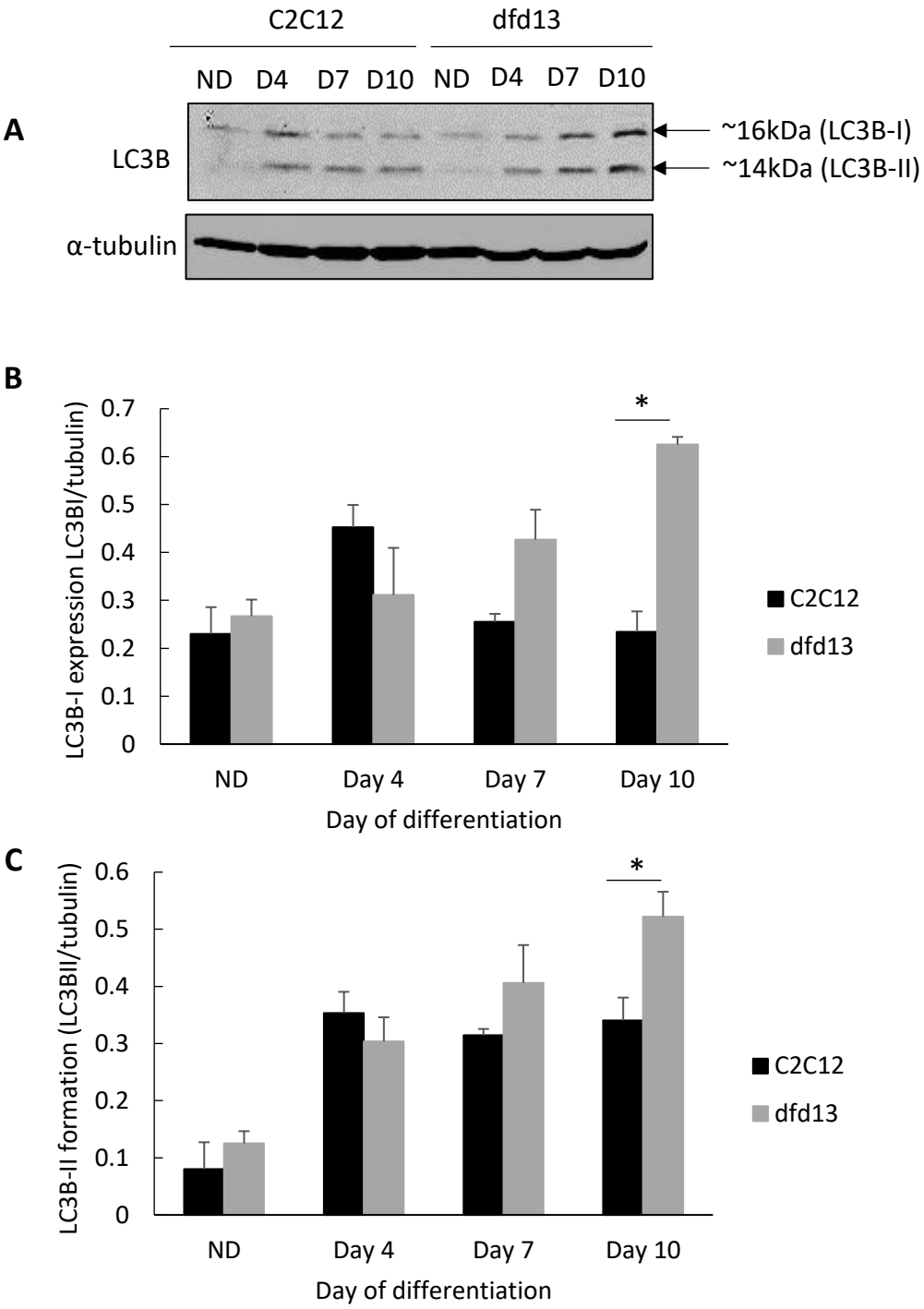
A
C2C12
dfd13
ND D4 D7 D10 ND D4 D7 D10
LC3B
α-tubulin
~16kDa (LC3B-I)
~14kDa (LC3B-II)
B
LC3B-I expression LC3BI/tubulin)
0.7
0.6
0.5
0.4
0.3
0.2
0.1
0
*
ND
Day 4
Day 7
Day 10
Day of differentiation
C2C12
dfd13
C
LC3B-II formation (LC3BII/tubulin)
0.6
0.5
0.4
0.3
0.2
0.1
0
*
ND
Day 4
Day 7
Day 10
Day of differentiation
C2C12
dfd13

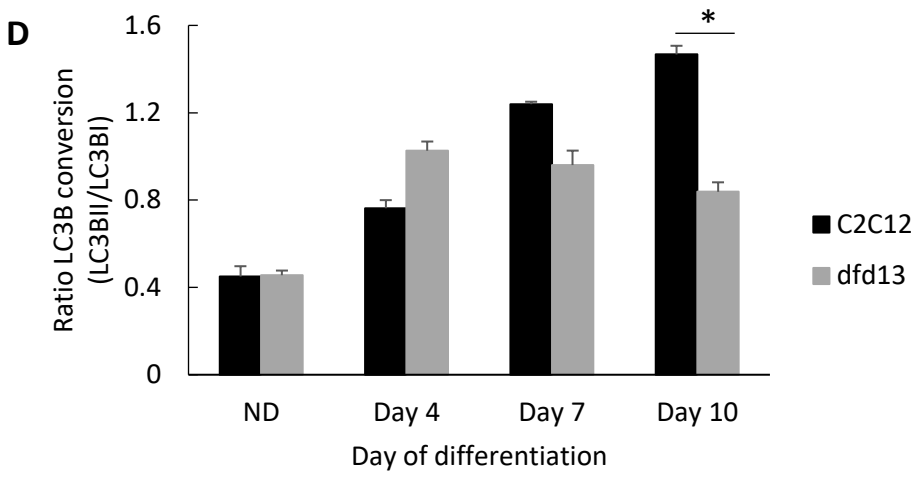

Figure 5.4: LC3B-II expression is decreased in differentiating dystrophin-deficient myoblasts

Myoblasts were cultured in GM until 80 to 90% confluent before washing twice with PBS and culturing in DM for 10 days with the media being changed every 2 days. Total protein was extracted at the indicated time points prior to immunoblotting with an antibody recognising LC3B with α-tubulin expression as a loading control. Densitometry analysis of (B) LC3B-I expression, (C) LC3B-II expression, and (D) the ratio of LC3B-II/LC3B-I. The graphs represent an average of four repeats from different samples. ND: non-differentiated; significantly different: * ($p<0.05$) and ** ($p<0.01$) compared to C2C12 myoblasts; n=4.

5.2.4 Autophagic Flux Is Decreased During Dystrophin-Deficient Myoblast Differentiation

In order to accurately determine autophagic activity, measuring the increase in the number of autophagosomes is required. Previous data showed that LC3B conversion was increased in C2C12 but reduced in dfd13 myoblasts upon differentiation; however, the results from measuring LC3B conversion alone could be inappropriately interpreted. LC3B-II itself has been reported to be degraded by autophagy and also tends to be more sensitive than LC3B-I during immunoblotting analysis (Mizushima and Yoshimori 2007). Autophagosome formation is an intermediate stage of autophagy, and there could be either the generation of autophagosomes or the blocked conversion of autolysosomes. Therefore, the accurate measurement of autophagic flux is required. In this study a Cyto-ID autophagy detection kit was utilised which selectively labelled

autophagic vacuoles independent of the LC3B protein, thus eliminating the need for transfection. This detection kit employs a 488nm-exitable green-emitting fluorescent probe to highlight various vacuolar components of autophagy. Chloroquine was used as a control as it passively diffuses into lysosomes and increases the pH, thus inhibiting lysosome function and blocking fusion with autophagosomes to become an autolysosome.

Figure 5.5 presents the density plots (A-D) and histograms (E-H) from flow cytometry-based profiling for both C2C12 and dfd13 myoblasts in the non-differentiated and differentiated state. From the density plot images, the size and complexity of each myoblasts can be determined. When the laser beam strikes the stream, a photon passes through unobstructed, but when it strikes a cell there are two different sizes of angle produced. When a photon strikes the cytoplasm, which is less dense and translucent, a small angle of reflection is generated and which can be detected by the forward scatter detector. In contrast, when a photon strikes an organelle such as nucleus or ER (denser), then a wide angle of reflection is generated which is detected by side scatter detector. The forward scatter (FS: X-axis) is proportional to the size, meaning that the bigger a cell the more light that will be scattered and a higher signal will be detected. The side scatter (SS: Y-axis) is proportional to the complexity of the myoblasts.

Based on the density plot images, it can be seen that the dfd13 myoblasts (Figure 5.5B) are smaller and less complex than C2C12 myoblasts (Figure 5.5A), although the differences between these cells are not obvious. After differentiation it can be seen that C2C12 cells become more complex (Figure 5.5C) while dfd13 cells remain the same (Figure 5.5D). As both myoblasts were labelled with FITC (green fluorescence), this

analysis was taken beyond the basic characteristics of myoblasts, as the specific protein behaviour of the antibody-tagged protein can be accurately measured. The signal was collected and measured/read by using a specific filter/channel based on the size of the emission and excitation of the fluorochrome used.

A Cyto-ID autophagy detection kit and FITC was utilised to label/stain autophagosomes. The collected data was gated and analyses were performed based on the myoblasts in the gated region. Histograms were then plotted, as shown in Figure 5.5E-H; the black line indicates the unstained myoblasts (negative control), the blue line stained myoblasts, and the red line stained myoblasts treated with chloroquine (positive control). From the histograms data were gated based on the intensity (10^1-10^3) (X-axis) and then the percentage obtained.

Generally, both treated and non-treated myoblasts showed a reduction in autophagosome counts after 10 days of differentiation. Non-treated myoblasts had less autophagosomes when compared to treated myoblasts, which is due to chloroquine acting as a lysosome inhibitor, preventing autophagosome from fusing with lysosomes and causing the accumulation of autophagosomes. As illustrated in Figure 5.5I, the number of autophagosomes was significantly decreased after 10 days of differentiation in both non-treated C2C12 myoblasts ($p= 1.98x10^{-2}$) and dfd13 myoblasts ($p= 1.59x10^{-2}$) when compared to non-differentiated stage. It was also significantly decreased in treated C2C12 myoblasts ($p= 2.34x10^{-3}$) and dfd13 myoblasts ($p= 3.44x10^{-3}$) after 10 days of differentiation. There was a significant reduction in autophagosomes in dfd13 myoblasts when compared to C2C12 myoblasts at the equivalent stages and treatment.

From these results autophagy flux can be determined. Autophagic flux can be calculated by subtracting the chloroquine-treated from the untreated myoblasts, which

enables the total number of non-fused autophagosomes to be measured and also the total number of autophagosomes formed. As depicted in Figure 5.5J, autophagic flux was increased in C2C12 myoblasts after 10 days of differentiation, whereas it was reduced in dfd13 myoblasts. When compared to non-differentiated C2C12 myoblasts, the number of autophagosomes in dfd13 myoblasts was significantly higher ($p= 3.64x10^{-2}$) and was slightly higher in differentiated dfd13 myoblasts compared to differentiated C2C12 myoblasts.

Overall, autophagy activity was decreased upon differentiation in dystrophin-deficient myoblasts. Based on the flow cytometry analysis, autophagic flux was decreased, as the total number of autophagosomes detected was higher in dfd13 myoblasts (both non-differentiated and differentiated) when compared to C2C12 myoblasts. In addition, autophagy was 2-fold higher in non-differentiated myoblasts (proliferation state) compared to the differentiated state.

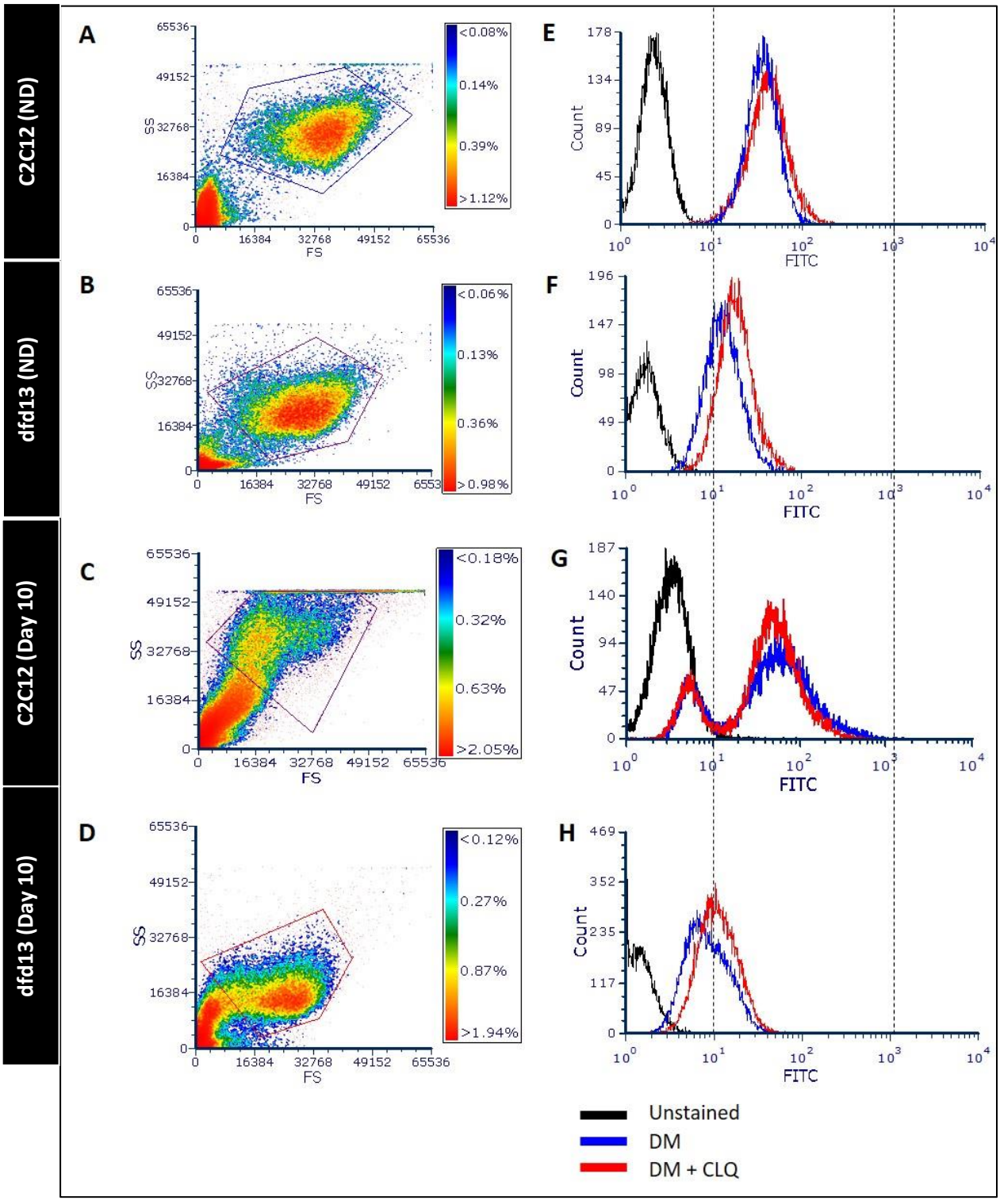
C2C12 (ND)
dfd13 (ND)
C2C12 (Day 10)
dfd13 (Day 10)
A
B
C
D
E
F
G
H
SS
FS
Count
FITC
<0.08%
0.14%
0.39%
>1.12%
<0.06%
0.13%
0.36%
>0.98%
<0.18%
0.32%
0.63%
>2.05%
<0.12%
0.27%
0.87%
>1.94%
Unstained
DM
DM + CLQ

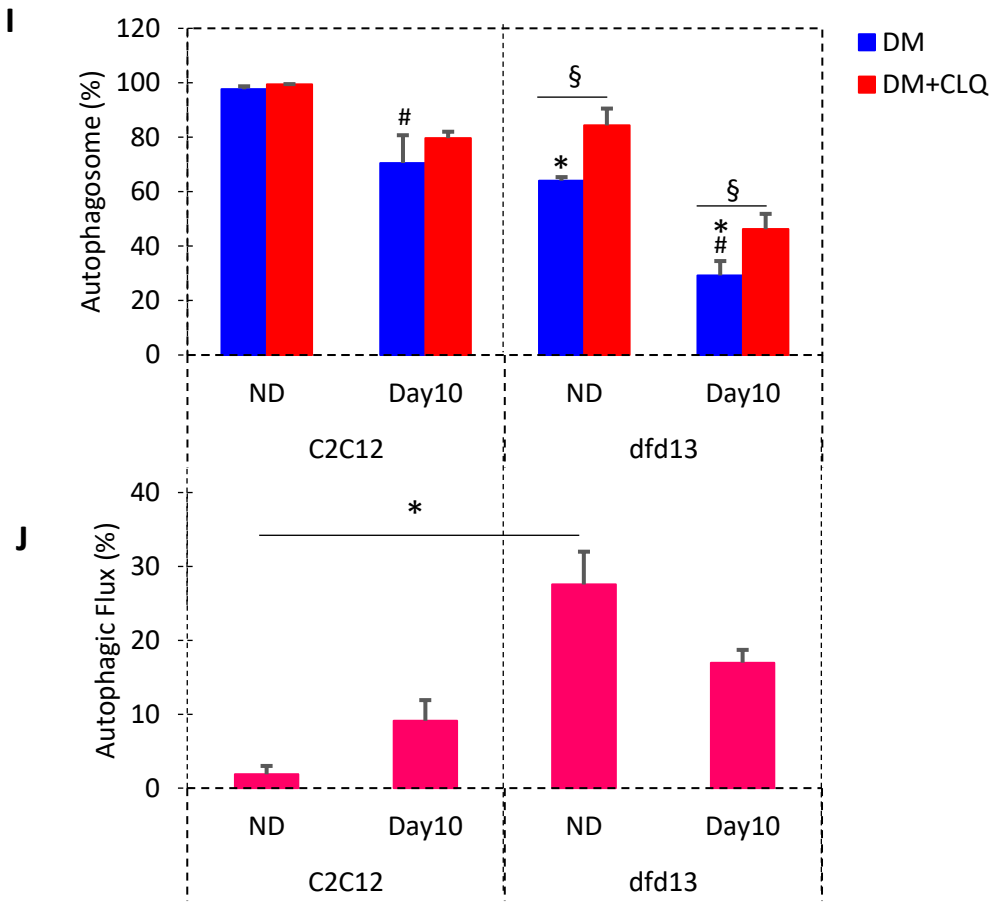

Figure 5.5: Autophagic flux is reduced in differentiating dystrophin-deficient myoblasts
Myoblasts were cultured in GM until 80 to 90% confluent before washing twice with PBS and culturing in DM for 10 days with the media being changed every 2 days.. Three different conditions were set up for each stage: 1) unstained cells (negative control); 2) stained cells; and 3) stained cells with chloroquine treatment (positive control). Chloroquine treatment was consisted of 3 hours' incubation at 37°C. Cells were trypsinised and incubated with Cyto-ID Green stain solution prior to analysis using the FITC channel of a CyAn B flow cytometer (Beckman Coulter, USA). Data analysis was performed using FCS Express 6 Plus Research Edition De Novo Software, USA). The density plot images represent non-differentiated (A) C2C12 myoblasts, (B) dfd13 myoblasts; day10 differentiation (C) C2C12 myoblasts and(D) dfd13 myoblasts. The histogram overlays (E-H) represent each neighbouring dot plot. (I) The percentage of autophagosomes detected in myoblasts and (J) percentage of autophagic flux within myoblasts. All bar graphs represent an average of three repeats from different samples. DM: differentiation medium; ND: non-differentiated; * ($p<0.05$) significantly difference when compared to C2C12 myoblasts. # ($p<0.05$) when compared with ND; § ($p<0.05$) when compared to DM+CLQ; n=3.

5.3 Discussion

5.3.1 Excessive Formation of Autophagosome in Dystrophin-Deficient Myoblast via FoxO3-Mediated Regulation

In skeletal muscle, autophagy is transiently activated and continues for only a few days (Mizushima 2004; Clara De Palma et al. 2014) it is regulated via FoxO3. Generally, it can be seen that autophagosomes are formed in both types of myoblast during differentiation, as the autophagy related protein involved in the initiation and elongation process was found to be increased (Figure 5.3). The ratio of LC3B-I converted to LC3B-II also reflected the formation of autophagosomes during differentiation (Figure 5.4).

The data presented here suggest that autophagosome formation is modulated via FoxO3 in dfd13 myoblasts. Inactivation of Akt allowed the active-form of FoxO3 (unphosphorylated) to translocate into the nucleus and trigger the expression of autophagy related genes. FoxO3 is required for the transcriptional regulation of LC3B. and also for transcriptional regulation of MAFbx and MuRF1. This transcriptional regulation leads to protein degradation via the autophagy-lysosome pathway and ubiquitin-proteosome pathway, respectively. However, autophagy in C2C12 myoblasts seems to be only partially FoxO3-mediated, as subsequent activation of Akt inhibited FoxO3 and suppressed its translocation to the nucleus and the targeting of autophagy-related gene activation. Activated-Akt, through phosphorylation at Ser473 by rictor-mTORC2, also contributes to autophagy activation during C2C12 myoblast differentiation (Shu and Houghton 2009; Ge and Chen 2012).

5.3.2 Modulation of Atg5-Dependent Autophagy During Differentiation of Dystrophin-Deficient Myoblasts

Autophagy is responsible for removing unfolded proteins as well as dysfunctioning organelles, and has been reported to be constantly active within skeletal muscle. Recently, increased autophagy has been reported to protect differentiating myoblasts from apoptotic cell death (McMillan and Quadrilatero 2014). Several autophagy related genes are known to be involved in the formation of autophagosomes, and FoxO3 has been shown to induce multiple autophagy related genes, including LC3B transcription in skeletal muscle (Mammucari et al., 2007). LC3B is an isoform of LC3 which plays a critical role in autophagy via post-translational modification.

LC3B is a subunit of microtubule-associated protein 1 (MAP1LC3B), and LC3 is cleaved by Atg4 to become cytosolic LC3B-I. LC3B-I is then converted to lipidated-LC3B-II through the conjugation of membrane lipid phosphatidylethanoleamine (PE), which involves the E1-like enzyme ubiquitin, Atg7 and the E2-like enzyme, Atg10. LC3B-II then binds to the isolation membrane and mediates membrane elongation until the edges fuse to form an autophagosome. The isolation membrane appears when cells are placed under starvation conditions. Atg7 also conjugate Atg5 to Atg12 to form the Atg5-Atg12 complex and then bind to the isolation membrane with Atg16. This complex binding is necessary for autophagosome formation.

In this study, the results showed that LC3B-I was increased in both types of myoblast due to the up-regulation of Beclin1 by nuclear-FoxO3, which is increased in dystrophin-deficient myoblasts (Figure 5.3). Beclin1 forms a complex with Vsp34 and becomes a core component during the pre-autophagosome stage. This complex then binds to the ULK1/Atg13/FIP200/Atg101 complex before entering the elongation stage,

when Atg7 catalyses the ligation of Atg5 to Atg12 to become the Atg5-Atg12 complex. With the aid of the Atg5-Atg12 complex, Atg7 catalyses the transfer of PE to LC3B-I, converting it to LC3B-II, resulting in the accumulation of LC3B-II within dfd13 myoblasts (Figure 5.4). Therefore, autophagosomes can be formed even when Atg5 is not present and so it can be suggested that Atg5 plays a booster role for autophagosome formation in dfd13 myoblasts. Autophagy in C2C12 myoblasts might also activated via PERK-mediated CHOP (Matsumoto et al., 2013), which is investigated in Chapter 6. Although the expression of both LC3B-I and LC3B-II in differentiating dfd13 myoblasts accumulates until day 10, the conversion ratio of LC3B-I to LC3B-II was reduced in dystrophin-deficient myoblasts, indicating that autophagy regulation is impaired (Figure 5.5).

It has been reported that autophagy is induced upon myoblast differentiation in order to eliminate pre-existing structures and proteins. This elimination occurs concomitantly with the myoblast fusion process prior to the formation of multinucleated myotubes. Based on the results presented, autophagy is activated in both types of myoblasts; however, over expression of Atg7 and Atg5 in dystrophin-deficient myoblasts suggests that the ubiquitin-like system is impaired. This could affect cascade activation which in turn will affect autophagosome formation, as well as autophagic flux in dystrophin-deficient myoblasts.

5.3.3 Reduction in Autophagic Flux suggests there is Defective Autophagy in Dystrophin-Deficient Myoblasts

From the data obtained the increased expression of autophagy related genes (Atg5, Atg7 & Beclin1) demonstrates excessive autophagosome formation in dfd13 myoblasts during differentiation; however, the conversion ratio of LC3B-I to LC3B-II was reduced

in dystrophin-deficient myoblasts. Furthermore, although activation was higher, autophagic flux analysis showed a reduction upon differentiation and revealed that autophagy activity is decreased upon differentiation in dfd13 myoblasts. Therefore, it was suggested that after excessive autophagosome formation in non-differentiated dfd13 myoblasts could potentially undergo apoptosis during differentiation. Previously, our group has shown that the ratio of cleaved caspase-3 to uncleaved caspase-3 is increased in a derivative of dfd13 myoblasts, PD50A when cultured in DM (Chen, 2013). This finding fits with the current data obtained and in the next chapter it is shown that dystrophin-deficient myoblasts are prone to apoptosis via PERK-mediated CHOP under ER stress conditions.

DMD is mostly characterised by ~2 years of age and it progresses until the early 30s. Therefore, the applicability of this finding to the understating of DMD patients may fit with the actual scenario. During the early stage of life (new born to below 2 years), deficient myoblasts survive as most cells are actively proliferating and high levels of autophagy activation is able to prevent apoptosis. As age increases (>2 years old), most of the deficient myoblasts have been triggered for differentiation as the body develops and muscle size and functionality increases, but now autophagy starts to decrease and apoptosis begins. This is the most common period for when DMD is diagnosed. At the later stage (~10 years-old), there is progressive disruption to the muscle due to loss/damage and support (wheelchair) is needed for mobility and undertaking daily life tasks. This state will worsen and patients will eventually die, commonly as a complication of respiratory muscle damage and cardiomyopathy (Figure 5.6)

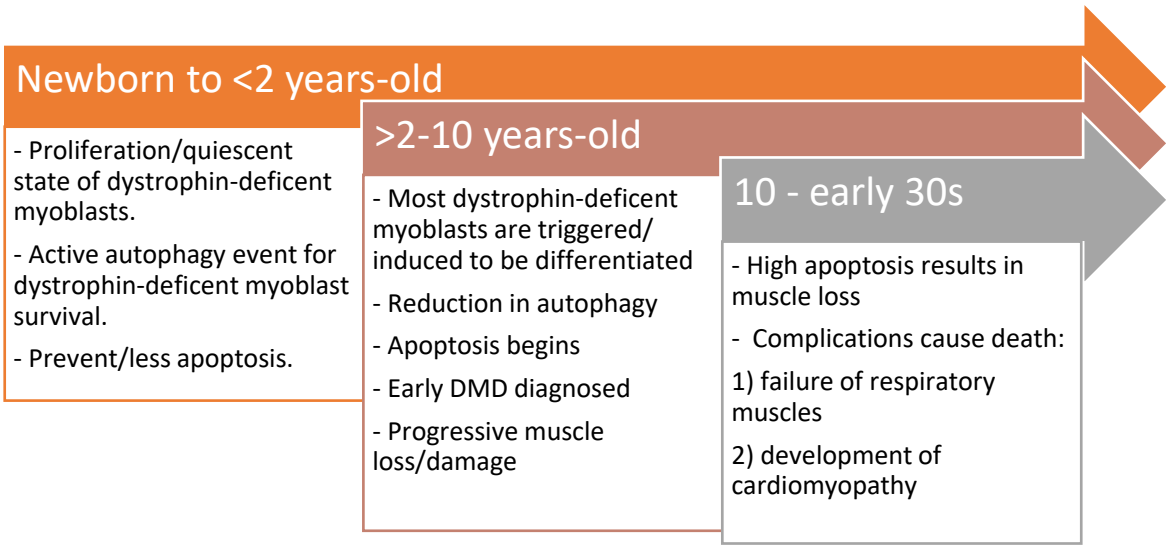

Figure 5.6: Proposed sequence of autophagy events in DMD patients

5.4 Conclusions

From the data obtained, dystrophin-deficient myoblasts exhibit the high expression of autophagy related proteins. However, a reduction in autophagy activity, as well as autophagy flux upon differentiation, indicates that autophagy is defective. This finding suggests the reduction of autophagy in dystrophin-deficient myoblasts. The perturbation of the PTEN-PI3K/Akt pathway initially triggers excessive autophagosome formation, and subsequently there is a reduction in autophagic flux within dystrophin-deficient myoblasts.

Key finding:

- Autophagy regulation is defective in differentiating dystrophin-deficient myoblasts.

Chapter 6 - Unfolded Protein Response is Impaired in Differentiating Dystrophin-Deficient Myoblasts

6.1 Introduction

During muscle fibre development there are series of myoblast conversions, i.e. alignment and fusion, before the formation of multinucleated fibres called myotubes. Myotubes re-organised and form muscle fibres which spontaneously contract once maturation is achieved. Each series of conversions is coordinated by the activation of various signalling pathways. For instance, during myoblast fusion to form multinucleated myotubes, cell surface proteins, as well as intracellular proteins, require the activation of signalling pathways, which then modulate membrane changes and cytoskeletal rearrangements. In addition to the fusion event, unfolded or misfolded proteins accumulate in the ER (Nakanishi, Dohmae, and Morishima 2007), which is known as ER stress and is essential for successful myotube formation. Therefore, a dynamic unfolded protein response needs to be achieved in order to maintain ER homeostasis.

ER stress has been reported to be involved during myotube formation (Nakanishi et al., 2007) and been proven to be required during myoblast differentiation (Rayavarapu, Coley, and Nagaraju 2012; Screen et al. 2014). ER stress is triggered due to the loss of homeostasis in ER lumen during the transition when myoblasts become multinucleated. Under these circumstances myoblasts exhibit two types of response which lead to survival and/or apoptosis. The ER is a storage location for Ca^{2+} which plays a role as a second messenger in regulating several cellular functions. The correct concentration of this ion is extremely important, especially for the formation of disulphide bonds and correct protein folding, together with maintaining protein

regulation during differentiation. This is finely regulated by a complex machinery, including plasma membrane Ca^{2+}ATPase (PMCA), Na^{+}/Ca^{2+} exchanger (NCX), inositol 1,4,5-triphospate receptor ($InsP_3R$) and sarcoplasmic reticulum Ca^{2+}ATPase (SERCA). In this study, it is suggested that Ca^{2+} leaks via $InsP_3R$ into the cytosolic space which is affected by high PLC-γ1 activation in dystrophin-deficient myoblasts.

The absence of dystrophin has also been thought to affect this myoblast fusion via PIP_2 regulation on the membrane; however, the signalling cascade that modulates this process remains unclear although inositide regulation/signalling is also thought to be disturbed/impaired during differentiation. In Chapter 4 it was reported that PTEN is highly expressed in differentiating dystrophin-deficient myoblasts, which causes the abundant production of PIP_2 which is a substrate for PLC. PLC catalyses the hydrolysis of PIP_2 to diacyl glycerol (DAG) and IP_3, with the latter triggering SERCA to open allowing Ca^{2+} to be released into the cytoplasmic compartment. This change to the ER stress level stimulates the activation of the unfolded protein response (UPR). Meanwhile, DAG binds to PKC, and binding of Ca^{2+} will also change PKC regulation.

Therefore, it was hypothesised that high PLC activation disturbs the ER stress level subsequently affected UPR activation at the same time disturbs PKC regulation and thus impairs dystrophin-deficient myoblast differentiation. In this chapter how the elevation of PTEN conveys a signal to C/EBP homolog protein (CHOP) via UPR regulation during myoblast differentiation *in vitro* is investigated. These mechanisms could support and explain the elevation of Ca^{2+} in *mdx* mice and in DMD human fibres, as has been reported (Mallouk, Jacquemond, and Allard 2000; Han, Grounds, and Bakker 2006). An overview of the chapter is presented in Figure 6.1.

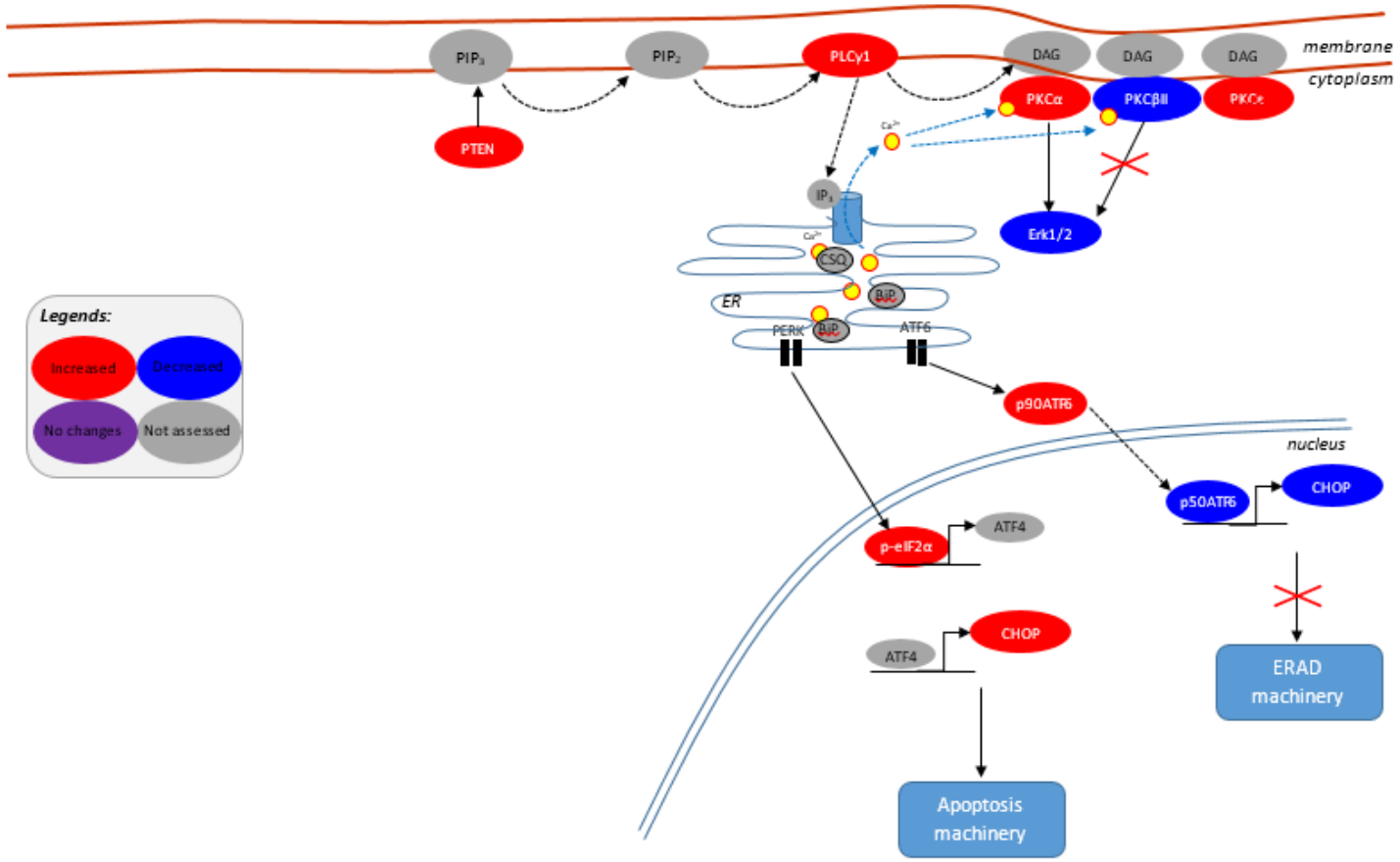

Figure 6.1: Chapter overview: elevation of PTEN expression contributes to the perturbation of PLC and PKC signalling and subsequently changes UPR modulation in dystrophin-deficient myoblasts

PTEN overexpression increases PLC-γ1 activation which causes a reduction in the ER stress level. Subsequently, modulation of UPR is changed and activation of CHOP tends to results in the activation of apoptosis rather than ERAD machinery activation. Meanwhile, phosphorylated-PKC levels are altered, which effects downstream protein activation, i.e. ERK1/2. From this chapter, it can be concluded that dystrophin-deficient myoblasts show a tendency for apoptosis modulated by PERK-mediated CHOP. ERAD: ER-associated degradation

6.2 Results

6.2.1 Phospholipase C Gamma-1 Activation Is Increased in Differentiating Dystrophin-Deficient Myoblasts

A study by Valdes et al. (2013) demonstrated that PI3K also regulates PLC-γ1 activation when myoblast was induced by Igf-1 (Valdés et al. 2013). In Chapter 4 it was shown that PTEN is highly expressed in dystrophin-deficient myoblasts during differentiation, which leads to an abundance of PIP_2 and triggers the high level activation of PLC signalling. There are different subfamilies/isotypes of PLC, known such as beta, gamma, delta, epsilon, eta and zeta. However, in this study, PLC-γ1 is the only isotype that is examined because its activator is known to be either a non-receptor or protein receptor tyrosine kinase which is involved in myoblast differentiation.

The activity of PLC, specifically subunit γ1, was measured, as this has previously been reported to be activated during myoblast differentiation (Gaboardi et al. 2010; Valdés et al. 2013). Figure 6.2A shows an immunoblot of PLC-γ1 expression and its phosphorylated form at Tyr783. Figure 6.2B and Figure 6.2C show the densitometry analysis of PLC-γ1 expression and activity, respectively. Total PLC-γ1 was constantly expressed in C2C12 myoblasts compared to the non-differentiated state. However, in dfd13 myoblasts there was a significant accumulation on day 7 ($p<0.05$; $p = 4.67 \times 10^{-2}$) and day 10 ($p<0.05$; $p = 4.52 \times 10^{-2}$) compared to non-differentiated dfd13 myoblasts.

In C2C12 myoblasts it can be clearly seen that PLC-γ1 activity remains constant in both non-differentiated and differentiated cells throughout the differentiation period. However, in dfd13 myoblasts PLC-γ1 activity was accumulated following differentiation, and a significant increase in activation was noted on day 7 ($p = 1.44 \times$

10^{-2}) and day 10 ($p = 2.27 \times 10^{-2}$) compared to the non-differentiated state. PLC-γ1 activation in dfd13 myoblasts also showed a significant increase after differentiation on day 4 ($p<0.01$; $p = 4.52 \times 10^{-3}$), day 7 ($p<0.01$; $p = 4.82 \times 10^{-5}$) and day 10 ($p<0.01$; $p = 9.49 \times 10^{-3}$) compared to C2C12 myoblasts.

The elevation of PLC-γ1 activation was thought to be due to the conversion of PIP_2 produced by elevated PTEN levels. PIP_2 is a minor membrane component that is exclusively located in the cytoplasmic leaflet of the plasma membrane. PLC hydrolyses PIP_2 into IP_3 and DAG, which subsequently activate IP_3R and PKC, respectively.

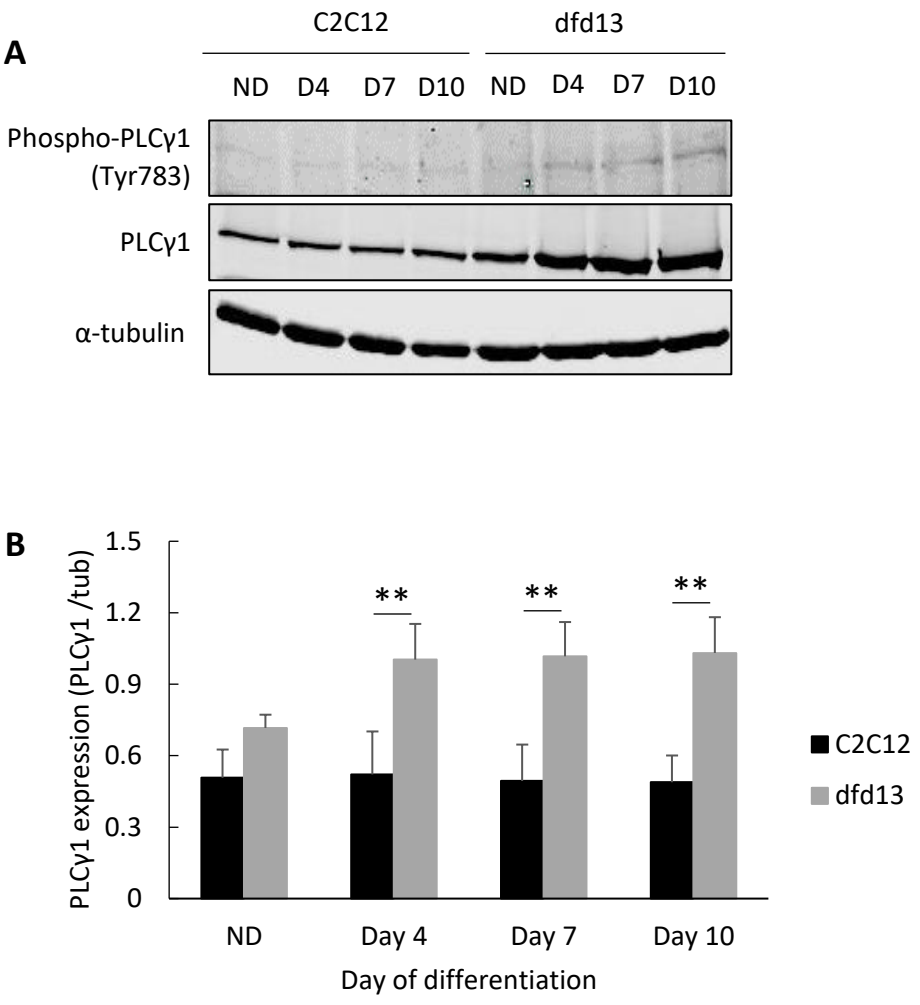

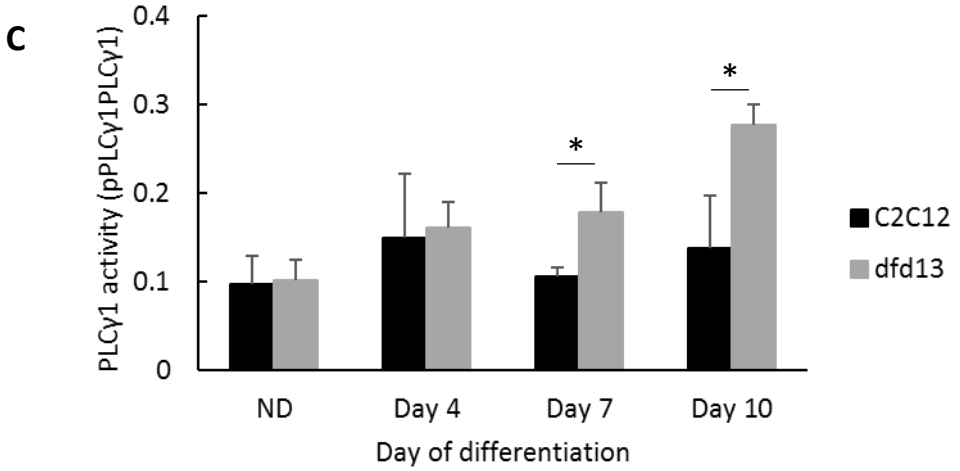

Figure 6.2: PLC-γ1 is highly activated in differentiating dystrophin-deficient myoblasts
Myoblasts were cultured in GM until 80 to 90% confluent before washing twice with PBS and culturing in DM for 10 days with the media being changed every 2 days. Total protein was extracted at the indicated time points prior to immunoblotting with antibodies recognising phospho-PLC-γ1 and PLC-γ1. (A) Immunoblot analysis during myoblast differentiation with α-tubulin expression as a loading control. Densitometry analysis of (B) PLC-γ1 expression and (C) PLC-γ1 activity. The graphs represent an average of three repeats from different samples. ND: non-differentiated; *: significantly different ($p<0.05$) compared to dfd13 myoblasts. **: significantly different ($p<0.01$) compared to dfd13 myoblasts; GM: growth medium (DMEM + 10% FCS); DM: differentiation medium (DMEM + 2% horse serum); n=3.

6.2.2 CHOP Expression is Reduced in Early Differentiating Dystrophin-Deficient Myoblasts

Previous studies have shown that ER stress occurs during myoblast differentiation (Nakanishi et al., 2007; Rayavarapu et al., 2012); consequently, the UPR is activated. During ER stress, unfolded and misfolded proteins accumulate in the ER lumen and in the short term, the UPR inhibits protein synthesis, whereas in the longer term, the UPR leads to adaptive changes, such as an increase in ER protein folding chaperones; if this is not sufficient to alleviate the stress, then apoptosis will occur. It was hypothesised that UPR regulation is impaired in dystrophin-deficient myoblasts. Therefore, CHOP expression together with the activation of transmembrane receptor markers, i.e. phospho-eIF2α and ATF6, were examined throughout the myoblast differentiation period.

A control experiment was performed to determine CHOP expression following induction with 10 µg/mL of tunicamycin (Figure 6.3). Tunicamycin is an antibiotic that inhibits glycoprotein synthesis (inhibitor of N-glycosylation) and subsequently causes ER stress. Generally, both types of myoblast showed the accumulation of CHOP following 8 hours of tunicamycin treatment (Figure 6.3A). However, there was higher expression in C2C12 myoblasts after 4 hours ($p<0.05$; $p = 4.42x10^{-2}$) and the highest level of CHOP expression was observed after 8 hours ($p<0.05$; $p = 2.95x10^{-2}$) of tunicamycin treatment (Figure 6.3B). Expression was decreased in C2C12 myoblasts after 16 hours, but remained the same in dfd13 myoblasts. After 24 hours of tunicamycin treatment both types of myoblast were observed to detach from the plate surface (not shown). From this control experiment it can be suggested that dfd13 myoblasts exhibited lower ER stress after treated with tunicamycin, indicating that UPR regulation may be impaired.

Immunoblot analysis (Figure 6.4A) showed an elevation in CHOP expression upon differentiation in both C2C12 and dfd13 myoblasts compared to their respective non-differentiated myoblasts. However, there was a non-identified band present on the blot, with a size of ~25 kDa. Densitometry analysis (Figure 6.4B) showed that CHOP expression was significantly increased ($p<0.05$; $p = 4.39x10^{-2}$) on day 4 and even more so on day7 ($p = 8.81x10^{-4}$) and day10 ($p = 1.43x10^{-2}$) in differentiating C2C12 myoblasts compared to non-differentiated myoblasts. However, in differentiating dfd13 myoblasts, the accumulation of CHOP expression only showed a significant increase on day 7 ($p<0.01$; $p = 1.44x10^{-3}$) which continued to increase until day 10 ($p<0.01$; $p = 3.45x10^{-4}$) compared to non-differentiated myoblasts. There was a significant difference

($p<0.05$; $p = 2.74x10^{-2}$) in CHOP expression in C2C12 myoblasts compared to dfd13 myoblasts on day 4 of differentiation.

Generally, the pattern of CHOP expression seems to be different between the two types of differentiating myoblasts. CHOP expression remained stable in differentiating C2C12 myoblasts, was slightly decreased on day 10 of differentiation, and was expected to decrease further over time. In contrast, CHOP expression in differentiating dfd13 myoblasts increased continuously until day 10 of differentiation and was expected to be increased further over time. Therefore, the next step is to investigate UPR markers in order to reveal which receptor is activated and conveys the signal.

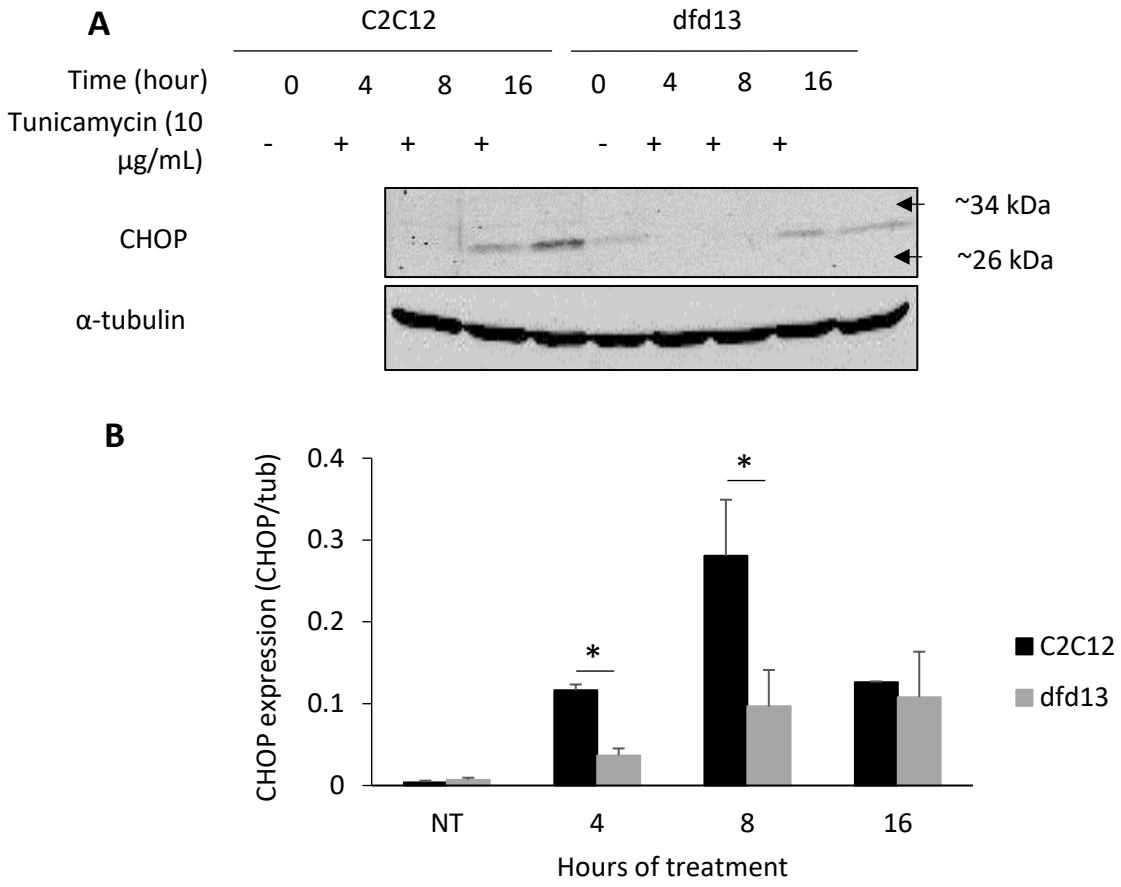

Figure 6.3: Dystrophin-deficient myoblasts have reduced CHOP expression following tunicamycin treatment

Myoblasts were cultured in GM until 80 to 90% confluent and then treated with 10µg/mL of tunicamycin (LKT laboratories, UK). Total protein was extracted at the indicated time points prior to immunoblotting with an antibody which recognises CHOP. (A) Immunoblot analysis of CHOP expression in myoblasts during tunicamycin treatment/induction with α-tubulin expression as a loading control. (B) Densitometry analysis of CHOP expression. The graph represents an average of three repeats from different samples. NT: Non-treated; *: significantly different ($p<0.05$) compared to dfd13 myoblasts. GM: growth medium (DMEM + 10% FCS); n=3.

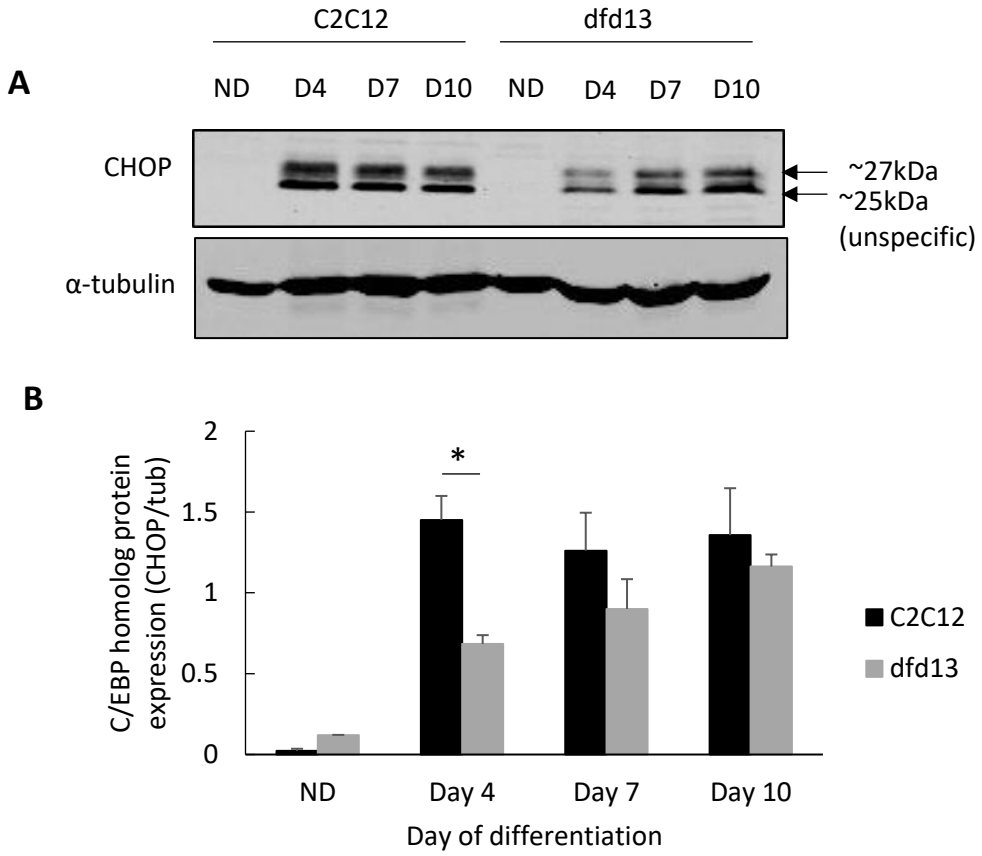

Figure 6.4: CHOP expression is lower in early differentiating dystrophin-deficient myoblasts

Myoblasts were cultured in GM until 80 to 90% confluent before washing twice with PBS and culturing in DM for 10 days with the media being changed every 2 days. Total protein was extracted at the indicated time points prior to immunoblotting with antibodies which recognise CHOP and α-tubulin. (A) Immunoblot analysis of CHOP expression during differentiation with α-tubulin as a loading control. (B) Densitometry analysis of CHOP expression. The graph represents an average of four repeats from different samples. ND: non-differentiated; Significant different: * ($p<0.05$) compared to dfd13 myoblasts; GM: growth medium (DMEM + 10% FCS); DM: differentiation medium (DMEM + 2% horse serum); n=3.

6.2.3 ER Stress Activates the Phosphorylation of eIF2α via PERK Receptor and Deactivates ATF6 Transmission in Differentiating Dystrophin-Deficient Myoblasts

ER stress signalling has been reported to be transmitted through the activation of transcription factor-6 (ATF6) in C2C12 myoblasts during differentiation (Nakanishi, Sudo, and Morishima 2005). It can also be transmitted via the protein kinase RNA-like endoplasmic reticulum kinase (PERK) receptor, with subsequent phosphorylation of

eukaryotic initiation factor 2-α (eIF2α) prior to the attenuation of the translational process and cell cycle arrest at the G1 phase. However, some ATF4 triggers CHOP production and it can therefore be used as a marker of ER stress.

CHOP expression has been shown to be lower in dfd13 myoblasts, suggesting that transmission activation may be impaired. Immunoblot analysis (Figure 6.5A) showed that phospho-eIF2α is increased in differentiating dfd13 myoblasts compared to C2C12 myoblasts, where it remains the same. There was a significantly lower level ($p<0.01$; $p = 4.26x10^{-4}$) in non-differentiated dfd13 myoblasts compared to non-differentiated C2C12 myoblasts. Phosphorylated-eIF2α increased significantly throughout the differentiation period and there was a significant difference in expression in dfd13 myoblasts on day 4 ($p<0.01$; $p = 9.73x10^{-3}$), day 7 ($p<0.01$; $p = 1.55x10^{-2}$) and day 10 ($p<0.01$; $p = 6.56x10^{-3}$) compared C2C12 myoblasts (Figure 6.5B). This indicates that PERK is less activated in proliferating dfd13 myoblasts. In the differentiation state it is auto-phosphorylated and subsequently phosphorylates eIF2α at Ser51. Higher levels of the phospho-form indicate high activation of PERK following ER stress induction.

ATF6 is a unique transcription factor which is embedded in the ER and acts as a transmembrane protein. Activated ATF6 translocates to the Golgi and is subsequently cleaved by proteases to form an active 50 kDa fragment. This protein fragment activates the target genes for the UPR during ER stress. From the immunoblot data shown, it can be clearly seen that ATF6 signal activation is decreasing while eIF2α receptor activation increases in dfd13 myoblasts upon differentiation. ATF6 activity was measured using the ratio of cleaved ATF6 (50kDa) to total ATF6 (90kDa), and this showed a significant reduction of activation at day 4 ($p = 3.49x10^{-3}$), day 7 ($p = 3.74x10^{-2}$) and day 10 ($p =$

$2.10x10^{-2}$) of dfd13 myoblast differentiation compared to C2C12 myoblasts (Figure 6.5C). Although one of the receptor was turned down, a significant increase in phospho-eIF2α can compensate for ATF6, and thus explains the high level of CHOP expression at the end of the differentiation period.

From this analysis it can be suggested that ER stress in differentiating dfd13 myoblasts switched the UPR signals for activation from ATF6 to the PERK receptor. During ER stress the majority of the phosphorylated-eIF2α will block ribosome 80s assembly, thus preventing protein translation and synthesis and causing cell cycle arrest. Under other conditions, phosphorylated-eIF2α can also trigger ATF4 translation, which in turn up-regulates CHOP. Therefore, this explains the lower CHOP expression in dfd13 myoblasts at day 4 of differentiation. CHOP acts as a dominant-negative inhibitor of DNA-binding when it is heterodimerised to another C/EBP partner.

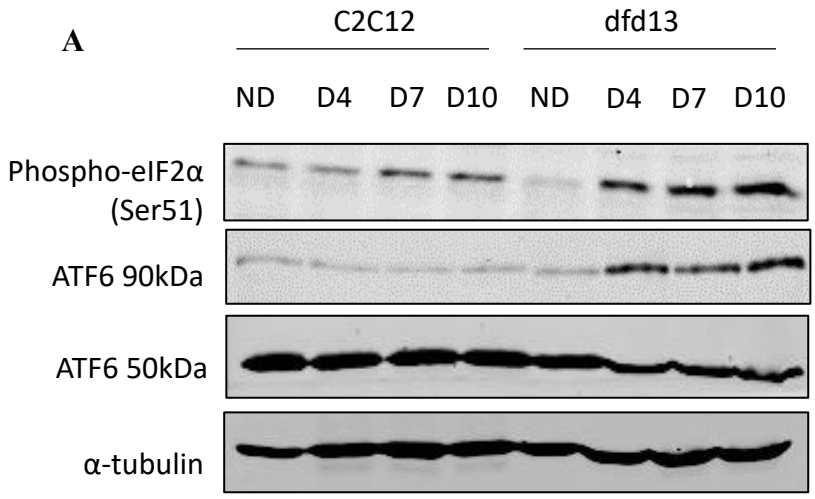

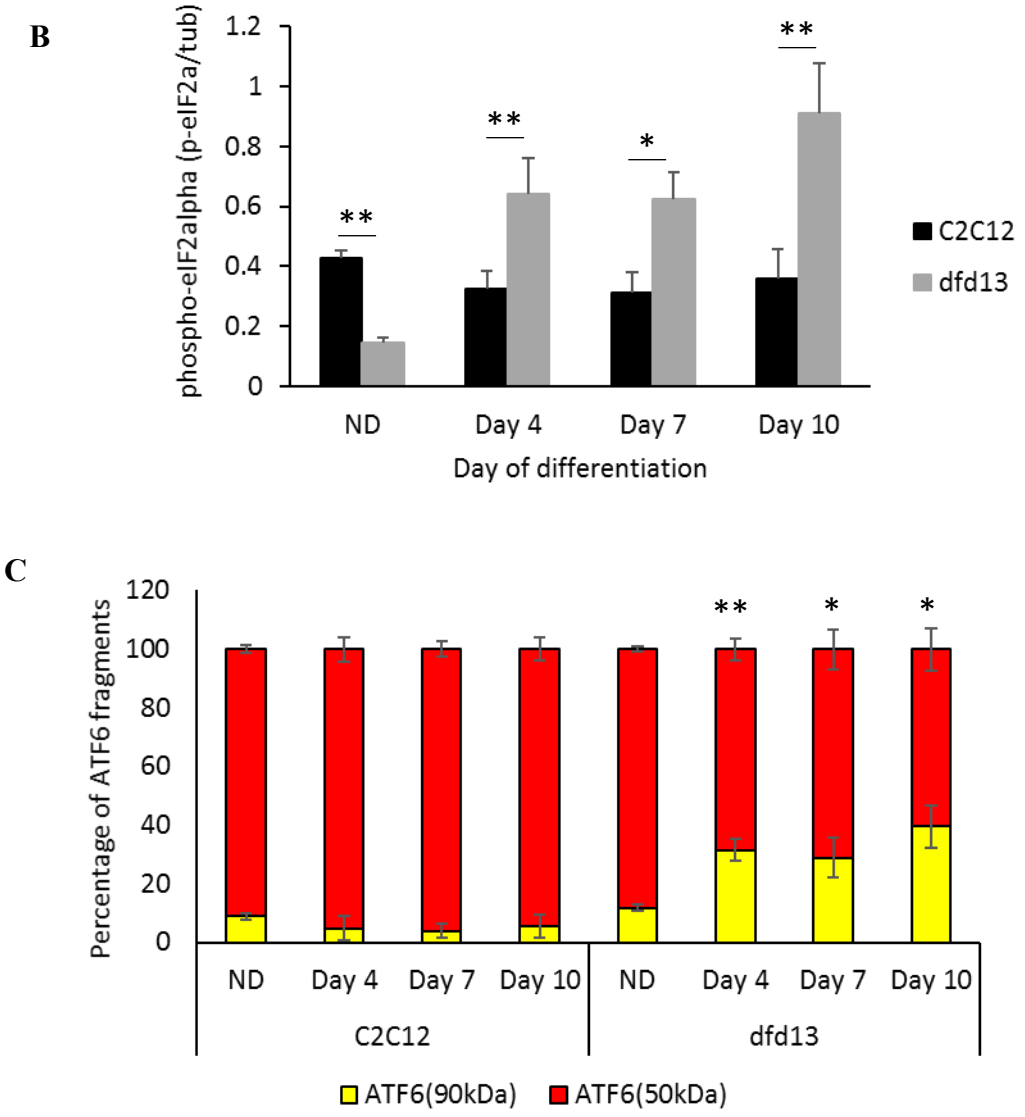

Figure 6.5: ER stress activates the eIF2α receptor and deactivates the ATF6 signal in differentiating dystrophin-deficient myoblasts

Myoblasts were cultured in GM until 80 to 90% confluent before washing twice with PBS and culturing in DM for 10 days with the media being changed every 2 days. Total protein was extracted at the indicated time points prior to immunoblotting with antibodies recognising phospho-eIF2α, ATF6 and α-tubulin. (A) Immunoblot analysis of phospho-eIF2α and ATF6-90kDa and ATF6-50kDa expression during differentiation with α-tubulin as a loading control. (B) Densitometry analysis of phospho-eIF2α protein and (C) percentage of ATF6 according to fragment size. The graphs represent an average of three repeats from different samples. ND: non-differentiated; Significant different: * ($p<0.05$) and ** ($p<0.01$) compared to C2C12 myoblasts; GM: growth medium (DMEM + 10% FCS); DM: differentiation medium (DMEM + 2% horse serum); n=3.

6.2.4 Protein Kinase C Alpha Remains Activated While Protein Kinase C Beta II is Selectively Activated in Differentiating Dystrophin-Deficient Myoblasts

PKC activation requires a series of maturation steps before it can be catalytically function. This maturation steps consist of series of phosphorylation at the specific site based on type of isoform. It is thought that PKC could have high activation since PLC-γ1 has been shown gave massive catalytic mechanism generating DAG and IP_3 (Ca^{2+} released intracellularly). In order to confirm this hypothesis PKC phosphorylation was assessed by focussing on two different isoforms, PKC-α and PKC-β. These isoforms were chosen based on the report that they are involved in myoblast proliferation and differentiation (Capiati, Téllez-Iñón, and Boland 1999).

Immunoblot analysis of PKC-α and PKC-βII and their phosphorylated forms is shown in Figure 6.6A. Densitometry analysis (Figure 6.6B-D) of both PKC isoforms showed that the degree of phosphorylation revealed maturation prior to being catalytically activated. Densitometry analysis of PKC-α phosphorylation at Thr638 showed an increase throughout the differentiation period, with a significant increase in phosphorylation in C2C12 myoblasts seen after 10 day of differentiation ($p<0.01$; $p = 8.15 \times 10^{-3}$) compared to the non-differentiated state. A significant increase was shown for all time points in dfd13 myoblasts compared to the non-differentiated state; day 4 ($p<0.05$; $p = 1.62 \times 10^{-2}$), day 7 ($p<0.05$; $p = 1.08 \times 10^{-2}$) and day 10 ($p<0.01$; $p = 7.77 \times 10^{-3}$) (Figure 6.6B). Both types of myoblasts showed a significant difference in phosphorylation throughout the differentiation period when compared to each other; day 4 ($p<0.05$; $p = 1.87 \times 10^{-2}$), day 7 ($p<0.01$; $p = 6.16 \times 10^{-3}$) and day 10 ($p<0.05$; $p = 1.06 \times 10^{-2}$) (Figure 6.6B).

Rapid phosphorylation of PKC-βII was observed and the activation pattern of the two different activation sites, Thr641 and Ser660, was assessed to confirm PKC-βII maturation. Densitometry analysis showed that phosphorylated-PKC-βII at Thr641 was decreased in C2C12 myoblasts whilst it remained the same in dfd13 myoblasts upon differentiation. The difference in this phosphorylation event continued to be significant as the C2C12 myoblasts differentiated; day 4 ($p<0.05$; $p = 4.12 \times 10^{-2}$), day 7 ($p<0.01$; $p = 5.09 \times 10^{-3}$) and day 10 ($p<0.01$; $p = 7.42 \times 10^{-5}$) compared to non-differentiated stage (Figure 6.6C). The level was significantly different in non-differentiated stage ($p<0.01$; $p = 1.01 \times 10^{-3}$) and day 4 ($p<0.05$; $p = 2.17 \times 10^{-2}$) of differentiation when compared to dfd13 myoblasts (Figure 6.6C).

Phosphorylated-PKC-β at Ser660 was found to be significantly lower ($p<0.05$; $p = 1.54 \times 10^{-2}$) in dfd13 myoblasts compared to C2C12 myoblasts in the non-differentiated state. Phosphorylation was increased in dfd13 myoblasts while it remained the same in C2C12 myoblasts upon differentiation. There was a significant difference in phosphorylated-PKC-βII found on day 7 ($p<0.05$; $p = 3.33 \times 10^{-2}$) and day 10 ($p<0.05$; $p = 3.69 \times 10^{-2}$) in dfd13 myoblasts compared to C2C12 myoblasts (Figure 6.6D).

Generally, the physiological function of PKC can be achieved via three events, maturation, catalytic activation and targeting. Maturation consists of a series of phosphorylations at specific sites depending on the type of PKC. Catalytic activation occurs when DAG, Ca^{2+} and other substrates bind to a specific site within the C2 domain of PKC causing the conformational change required for its catalytic function. Then, activated PKC is targeted to a specific subcellular location. In this study, the maturation of PKC-α and PKC-ßII was determined before further DAG and Ca^{2+} binding.

Phosphorylation of the Thr638 residue in PKC-α and of Thr641 and Ser660 in PKC-βII was observed in both types of myoblasts. mTORC2 has been reported to target Thr638 in PKC-α during myogenic differentiation (Jaafar et al. 2011). Inactivation of mTORC2 (rictor-mTORC) is thought to impair the phosphorylation of PKC-α at Thr657, as it has been shown to not be activated in dfd13 myoblasts (Chapter 4). Phosphorylation of PKC-α at Ser657 was not observed and phosphorylation of Thr500 was not assessed as this is a prerequisite for subsequent activation to occur. Therefore, it can also be suggested that non-phosphorylation of Akt at Thr308 in dfd13 myoblasts is not caused by a PDK1 impairment, as phosphorylation of PKC at Thr641 revealed its functionality (Figure 6.6C). PDK1 is responsible for phosphorylating PKC-βII at Thr500.

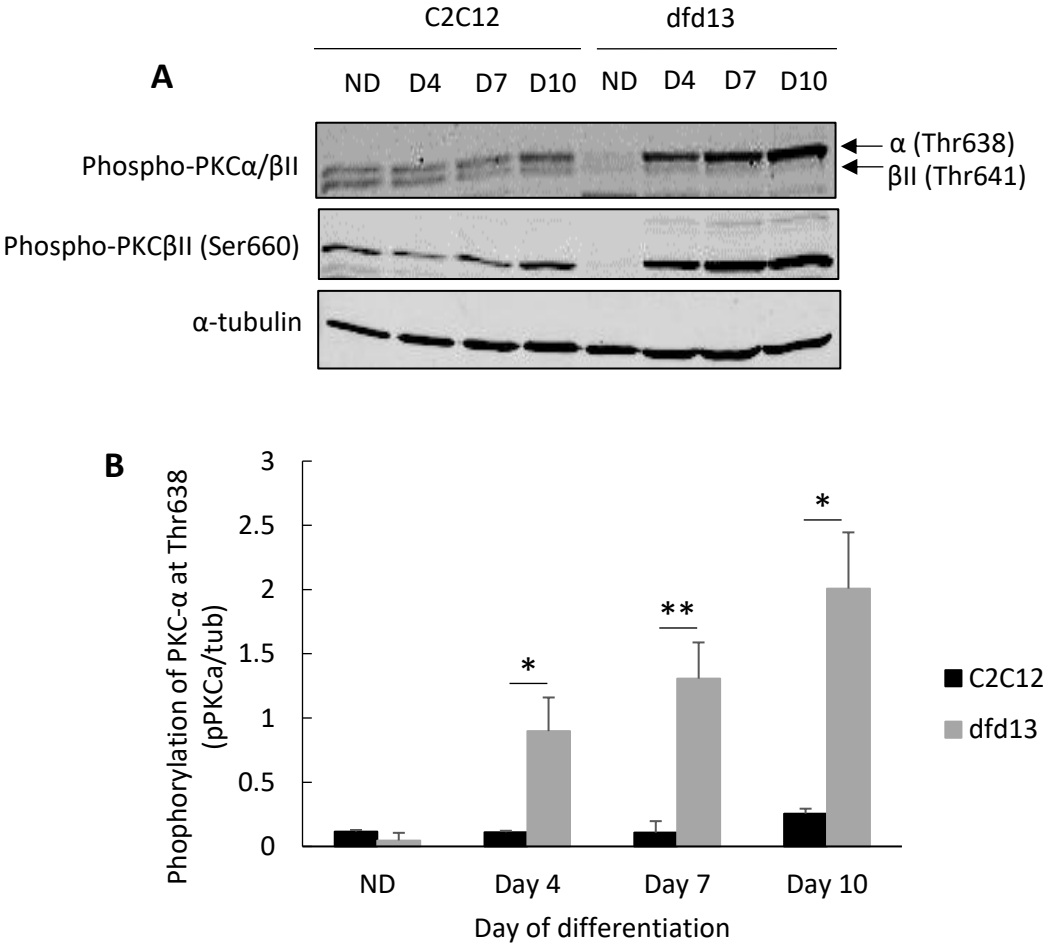

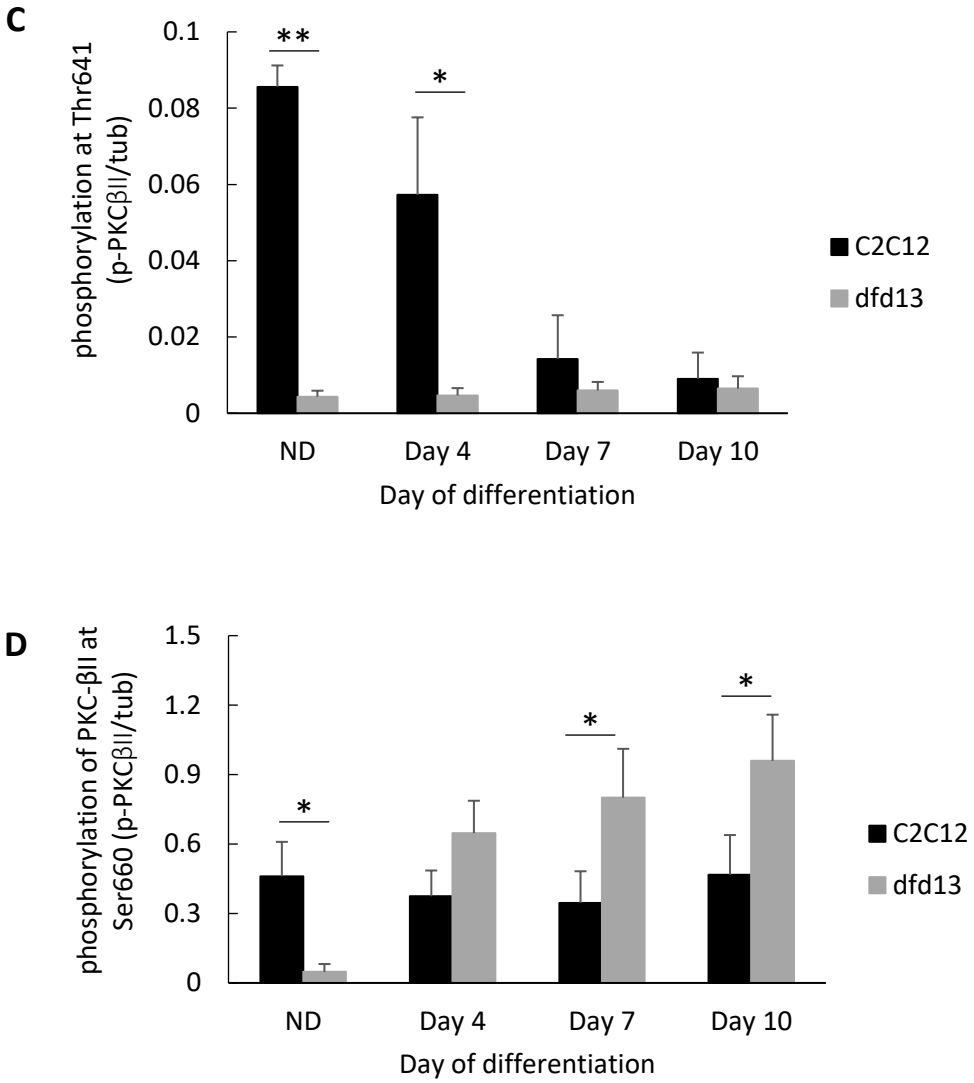

Figure 6.6: PKC-α and PKC-βII regulation is impaired in differentiating dystrophin-deficient myoblasts

Myoblasts were cultured in GM until 80 to 90% confluent before washing twice with PBS and culturing in DM for 10 days with the media being changed every 2 days. Total protein was extracted at the indicated time points prior to immunoblotting with antibodies recognising phospho-PKC-α/βII (Thr638/Thr641) and phospho-PKC-βII (Ser660). (A) Immunoblot analysis during myoblast differentiation with α-tubulin expression as a loading control. Densitometry analysis of (B) phosphorylation of PKC-α at Thr638, (C) phosphorylation of PKC-βII at Thr641, and (D) phosphorylation of PKC-βII at Ser660. The graphs represent an average of three repeats from different samples. ND: non-differentiated; *: significantly different ($p<0.05$) compared to dfd13 myoblasts. **: significantly different ($p<0.01$) compared to dfd13 myoblasts; GM: growth medium (DMEM + 10% FCS); DM: differentiation medium (DMEM + 2% horse serum); n=3.

6.2.5 Protein Kinase C Epsilon Is Highly Expressed in Differentiating Dystrophin-Deficient Myoblasts

Levels of the ε-isoform of PKC were determined in order to investigate DAG-dependent PKC activity, since PLC-γ1 was shown to have high activity in dfd13 myoblasts. A study by Gaboardi et al. (2009) demonstrated that PKC-ε levels and its activity is increased in differentiated myoblasts after being administered via insulin. In this study, total PKC-ε expression was found to be increased in both types of myoblast. However, dfd13 myoblasts showed significantly higher expression and activity compared to C2C12 myoblasts; though detected at very low levels.

Figure 6.7A presents the immunoblot analysis of the phosphorylated form of PKC-ε and total PKC-ε expression. Densitometry analysis of total PKC-ε expression (Figure 6.7B) showed the significant accumulation in dfd13 myoblasts compared to the C2C12 myoblasts; day 4 ($p<0.01$; $p = 8.58x10^{-3}$), day 7 ($p<0.05$; $p = 1.14x10^{-2}$) and day 10 ($p<0.05$; $p = 1.33x10^{-2}$). Expression was also significantly increased when compared to the non-differentiated state at day 4 ($p<0.01$; $p = 3.31x10^{-3}$), day 7 ($p<0.01$; $p = 8.10x10^{-3}$) and day 10 ($p<0.05$; $p = 6.36x10^{-3}$) (Figure 6.7B). Total PKC-ε expression in C2C12 myoblasts only showed a significant increase at day 10 when compared to the non-differentiated state (Figure 6.7B).

The PKC-ε was found not activated in C2C12 myoblasts. PKC-ε activation showed a significant increase throughout the differentiation period; non-differentiated ($p<0.05$; $p = 1.59x10^{-2}$), day 4 ($p<0.01$; $p = 1.78x10^{-3}$), day 7 ($p<0.01$; $p = 2.98x10^{-3}$) and day 10 ($p<0.01$; $p = 2.66x10^{-4}$) compared to C2C12 myoblasts (Figure 6.7B). This data indicates the elevation of DAG from the high activity of PLC-γ1 which is a substrate for PKC-ε and thus activates the kinase catalytic domain.

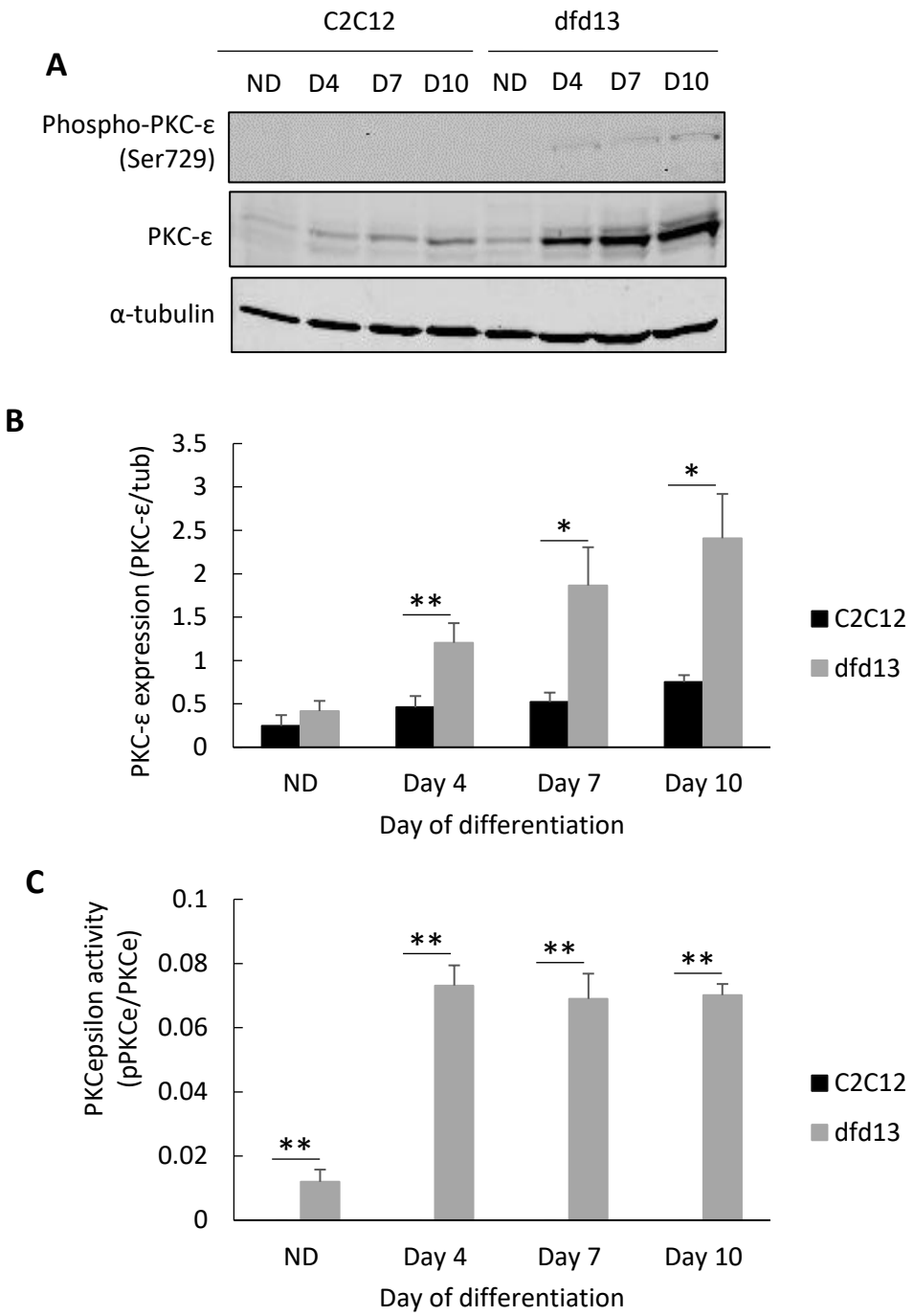

Figure 6.7: PKC-ε is highly activated in differentiating dystrophin-deficient myoblasts
Myoblasts were cultured in GM until 80 to 90% confluent before washing twice with PBS and culturing in DM for 10 days with the media being changed every 2 days. Total protein was extracted at the indicated time points prior to immunoblotting with antibodies which recognise phospho-PKC-ε (Ser729) and PKC-ε. (A) Immunoblot analysis during myoblast differentiation with α-tubulin expression as a loading control. Densitometry analysis of (B) PKC-ε expression and (C) PKC-ε activity. The graphs represent an average of three repeats from different samples. ND: non-differentiated; *: significantly different ($p<0.05$) compared to dfd13 myoblasts. **: significantly different ($p<0.01$) compared to dfd13 myoblasts; GM: growth medium (DMEM + 10% FCS); DM: differentiation medium (DMEM + 2% horse serum); n=3.

6.2.6 ERK1/2 Activity Is Decreased in Differentiating Dystrophin-Deficient Myoblasts

ERKs have been reported to be activated when myogenesis is promoted by mitogen removal in C2C12 myoblasts (Gredinger et al. 1998). Activation of ERK by PKC-α via MEF activation is also a possible mechanism of MAPK activation in myoblasts (Schönwasser et al. 1998). Therefore, ERK activation was examined to determine whether high activation of PLC-γ1 affected ERK activation during dfd13 myoblast differentiation. Previous data has shown that PKC activation is disturbed in dystrophin-deficient myoblasts. ERK consists of two similar protein kinases, known as ERK1 and ERK2, and phosphorylation activates kinase activity for protein translation in myoblasts.

Figure 6.8 presents the analysis of ERK1/2 in both types of myoblasts during the non-differentiated and differentiated stages. An immunoblot of ERK1/2 expression and activation is shown in Figure 6.8A. Densitometry analysis (Figure 6.8B) of ERK1 expression (approximately 44 kDa) showed its significant accumulation in both types of myoblasts upon differentiation compared to non-differentiated cells. There was also a significant difference between the two types of myoblast; ERK2 expression (approximately 42 kDa) was shown to accumulate in dfd13 myoblasts while expression remained the same in C2C12 myoblasts. A significant increase was found on day 7 ($p<0.05$; $p = 3.61 \times 10^{-2}$) and day 10 ($p<0.05$; $p = 2.31 \times 10^{-2}$) compared to non-differentiated dfd13 myoblasts (Figure 6.8C). A significant difference in expression on day 7 ($p<0.05$; $p = 1.58 \times 10^{-2}$) and day 10 ($p<0.05$; $p = 1.12 \times 10^{-2}$) was also shown in comparison to C2C12 myoblasts (Figure 6.8C).

As illustrated in Figure 6.8D, the activation of ERK1 was decreased in dfd13 myoblasts upon differentiation, while in C2C12 myoblasts it was constantly expressed at the same level upon differentiation. A significant reduction was found on day 4 ($p<0.05$; $p = 4.03x10^{-2}$) when compared to non-differentiated dfd13 myoblasts, and a significant difference in the expression level was seen on day 4 ($p<0.05$; $p = 3.82x10^{-2}$) day 7 ($p<0.05$; $p = 3.44x10^{-2}$) and day 10 ($p<0.05$; $p = 3.99x10^{-2}$) compared to C2C12 myoblasts (Figure 6.8D).

ERK2 activation showed a massive reduction in differentiating dfd13 myoblasts which was significant on day 4 ($p<0.01$; $p = 7.39x10^{-3}$), day 7 ($p<0.05$; $p = 1.87x10^{-2}$) and day 10 ($p<0.05$; $p = 1.09x10^{-2}$) compared to the non-differentiated state (Figure 6.8E). The significant accumulation of ERK2 activation was seen in C2C12 myoblasts on day 4 ($p<0.05$; $p = 1.98x10^{-2}$) but activation was significantly reduced on day 7 ($p<0.01$; $p = 3.09x10^{-3}$) and day 10 ($p<0.05$; $p = 4.42x10^{-2}$) compared to non-differentiated C2C12 myoblasts. A significant difference in ERK2 activation was found on day 4 ($p<0.01$; $p = 1.75x10^{-3}$), day 7 ($p<0.01$; $p = 7.53x10^{-3}$) and day 10 ($p<0.05$; $p = 8.28x10^{-2}$) when compared between the two types of myoblasts (Figure 6.8E).

From the data obtained, ERK1/2 activation was reduced in dfd13 myoblasts during differentiation. ERK1/2 is phosphorylated by MEK at Thr202 and Thr204 in response to external stimuli, such as insulin. This phosphorylation is required for activation and conformational changes which enable interactions with substrates.

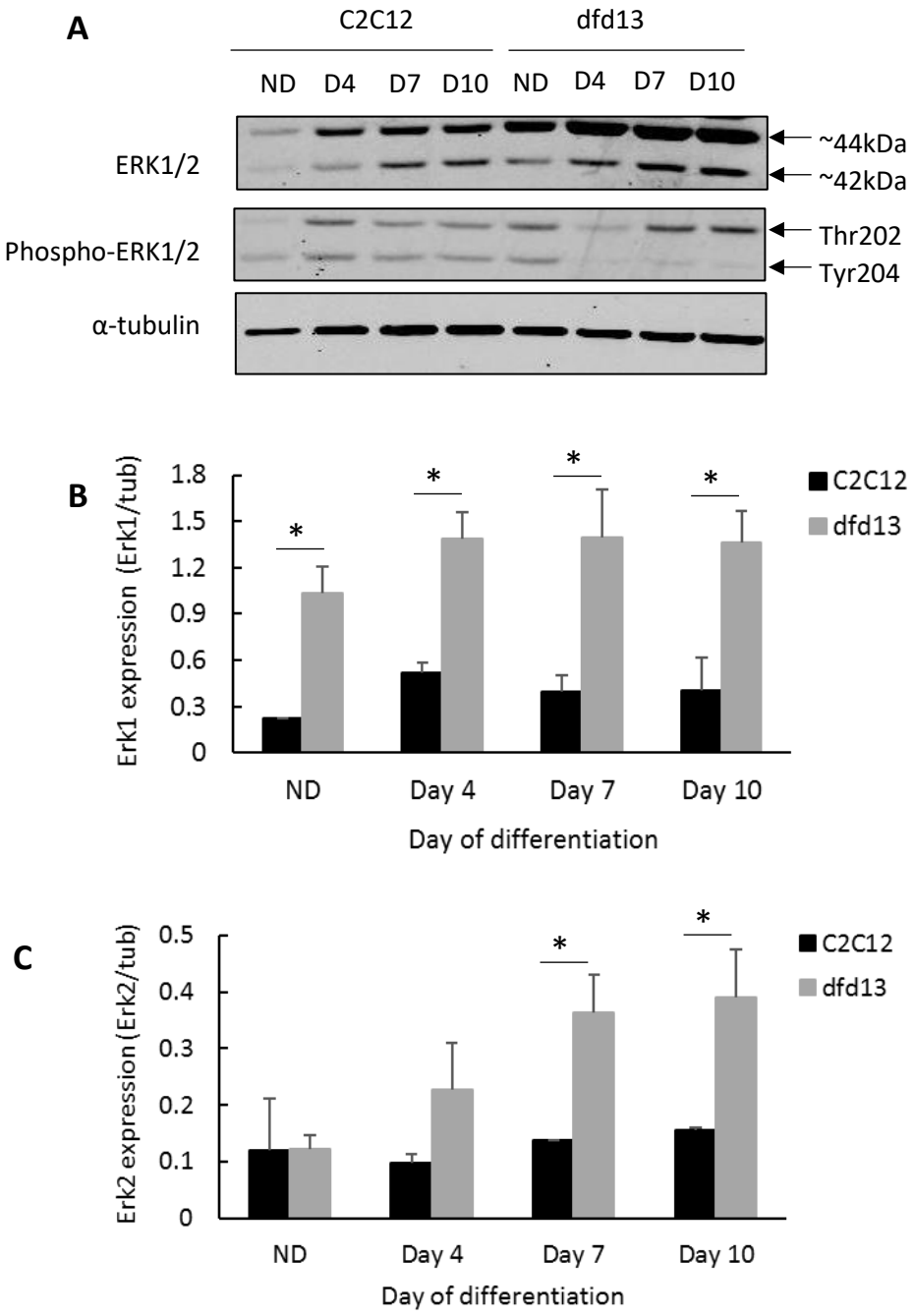
A
C2C12
dfd13
ND D4 D7 D10 ND D4 D7 D10
ERK1/2
~44kDa
~42kDa
Phospho-ERK1/2
Thr202
Tyr204
α-tubulin
B
Erk1 expression (Erk1/tub)
1.8
1.5
1.2
0.9
0.6
0.3
0
*
C2C12
dfd13
ND
Day 4
Day 7
Day 10
Day of differentiation
C
Erk2 expression (Erk2/tub)
0.5
0.4
0.3
0.2
0.1
0
*
C2C12
dfd13
ND
Day 4
Day 7
Day 10
Day of differentiation

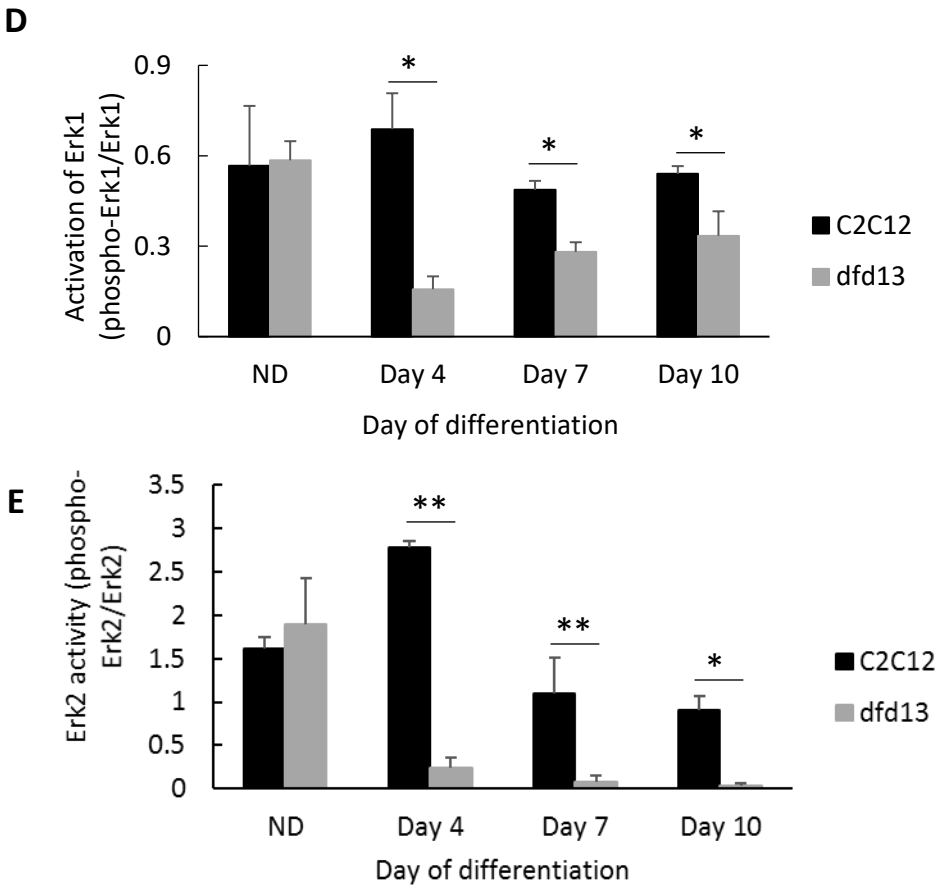

Figure 6.8: ERK1/2 is down-regulated in differentiating dystrophin-deficient myoblasts
Myoblasts were cultured in GM until 80 to 90% confluent before washing twice with PBS and culturing in DM for 10 days with the media being changed every 2 days. Total protein was extracted the indicated time points prior to immunoblotting with antibodies which recognise phospho-ERK1/2 and ERK1/2. (A) Immunoblot analysis during myoblast differentiation with α-tubulin expression as a loading control. Densitometry analysis of (B) ERK1, (C) ERK2 expression, and (D) phospho-ERK1, (E) phopsho-ERK2 activity. The graphs represent an average of three repeats from different samples. ND: non-differentiated; *: significantly different ($p<0.05$) compared to dfd13 myoblasts. GM: growth medium (DMEM + 10% FCS); DM: differentiation medium (DMEM + 2% horse serum); n=3.

6.3 Discussion

6.3.1 Increased PLC Activity Increases the Cytosolic Calcium Concentration which Impairs Endoplasmic Reticulum Stress in Differentiating Dystrophin-Deficient Myoblasts

One of the problematic conditions faced in dystrophic muscle is the loss of membrane integrity causing an increase in Ca^{2+} permeability, known as Ca^{2+} leakage. Ca^{2+} leaks into the cell through the damaged membrane causes an elevation in cytosolic Ca^{2+} within muscle fibre. It also has been reported that Ca^{2+} leakage occurs from the ER to the cytosolic space, as SERCA activity is found to be reduced which suggests a reduction of ER stress in dystrophic muscle (Divet and Huchet-Cadiou 2002; Goonasekera et al. 2011). However, the mechanism/signalling/regulation of Ca^{2+} leakage from the ER to the cytosolic space through IP_3R remains uncertain. In this study it has been shown that the reduction of ER stress might be caused by high PLC activity derived from the overexpression of PTEN.

In Chapter 4 it was shown that PTEN expression is highly increased in differentiating dfd13 myoblasts and this has an effect on the PI3K/Akt pathway (

Figure 4.2). In this chapter, the regulation of PLC and PKC was examined, together with ER stress, which are all thought to be affected by the high expression of PTEN in dystrophin-deficient myoblasts. PTEN is known to be a tumour suppressor which plays a role in the conversion of PIP_3 to PIP_2 via a dephosphorylation event. As PTEN is highly expressed (

Figure 4.2), a high level of PIP_2 is presumed to formed which will subsequently increase PLC activity. A study by Hong et al. (2001) reported that PLC plays a role in IGF-1 induced muscle differentiation, and the isoform PLC-γ1 has been widely reported

to be involved in this event. PLC-γ1 is also involved in the activation of focal adhesion kinase (FAK), which is required in cytoskeletal organisation as it directly interacts with the cytoplasmic tail of integrin-β1 (Hong et al. 2001; Choi et al. 2007). This indicates that the absence of dystrophin could also impair PLC regulation.

During myoblast differentiation PI3K is activated via a series of phosphorylation events following Igf-1 induction. In addition to Akt activation, PI3K has also been shown to control the activation of the PLC-γ1/IP_3 pathway, as inhibition of PI3K blocks PLC-γ1 activation. Valdes et al. (2013) reported that during myoblast differentiation, calcium is released from intracellular stores, which is mediated by the PLC signalling pathway. This has been coordinated dynamically such that over activation will cause excessive calcium to be released from the ER via the IP_3R into the intracellular space. Since the calcium concentration has been reported to be elevated in *mdx* mice and DMD human fibres, this finding regarding the high activation of PLC being affected by high PTEN expression may be cause. High activation of PLC produces IP_3 and DAG, which bind to IP_3R and PKC, respectively. Once bound to IP_3R, the channel is opened and subsequently causes calcium to be released into the cytoplasm. Concurrently, DAG bound to PKC will open its active site, enabling phosphorylation of its substrates, such as RAF. The downstream proteins of MAP kinase will also be affected, such as ERK1/2 expression and activation.

Although previous studies have shown that a lack of dystrophin causes calcium leakage from the extracellular space into the cell through the damaged membrane, this study suggests that elevation of cytosolic calcium concentration due to leakage from the ER may also occur. Calcium homeostasis is regulated by the presence of protein chaperons, known as Ca^{2+} binding proteins. The chaperons, such as binding

immunoglobulin protein (BiP/Grp78) and calreticulin, function as buffers which have a low-affinity and large-capacity for Ca^{2+} binding (Kaufman and Malhotra 2014). In this case, released calcium will cause a reduction of Ca^{2+}/BiP and/or Ca^{2+}/calreticulin thus reducing the ER stress level (Figure 6.5). However, the actual calcium concentration in the ER could not be measured and instead expression of the ER stress protein marker, CHOP, as well as its receptor activation on the ER was assessed in order to determine the stress level. It was found that CHOP expression is low initially and increases upon differentiation in dystrophin-deficient myoblasts, indicating that ER homeostasis is impaired (Figure 6.5).

6.3.2 Expression of CHOP via PERK May Leads to Dystrophin-Deficient Myoblasts Apoptosis

CHOP is induced by nutrient depletion and a previous study has shown that ER stress occurs during myoblast differentiation (Nakanishi et al., 2005). In this study, myoblasts were cultures in serum-deprived medium by using a low percentage of horse serum which can considerably slow down proliferation and switch myoblasts to differentiate into multinucleated myotubes. This condition can disrupt/change ER homeostasis and subsequently cause ER stress. By activating the UPR mechanism, ER stress can be countered and ER homeostasis restored. The UPR is used to alleviate the effects of ER stress via receptor-based activation, but excessive activation causes apoptosis. There are three classic specific responses involving three ER stress sensors: 1) PERK, 2) ATF6 and 3) IRE1. The activation of UPR via these sensors up regulates ER stress proteins such as BiP/Grp78 (binding immunoglobulin protein) and CHOP (GADD153; growth arrest DNA damage inducible protein 153) in order to increase the protein folding capacity within the ER. The up-regulation of all the proteins involved will restore ER homeostasis.

In C2C12 myoblasts both receptors are constantly activated upon myoblast differentiation; however, dfd13 myoblasts showed a different pattern of UPR activation. In non-differentiated state, UPR activation is highly exhibited via the ATF6 receptor rather than PERK; upon differentiation, this is a switch to PERK and ATF6 shows less activation. This may explain the lower levels of CHOP expression observed 4 and 7 days after differentiation. ATF6 is a transmembrane-transcription factor embedded in the ER membrane where Grp78/BiP binds to it. During ER stress, Grp78/BiP is dissociated and ATF6 become activated before being translocated to the Golgi and cleaved by proteases (S1P and S2P) to become a 50kDa-ATF6 (N-terminal cyclic AMP-dependent) fragment. This fragment then translocates to the nucleus and activates the transcription of genes involved in the UPR. From the data (Figure 6.5), ATF6-50 kDa was found to be reduced in differentiated dfd13 myoblasts, suggesting that ATF6 is less activated.

The elevation of UPR activation via PERK/phospho-eIF2α blocks ribosome 80s assembly and protein synthesis, consequently causing cell cycle arrest. This also explains the translational attenuation through the inactivation of p70S6K, as previously reported (Figure 4.6). However, some phospho-eIF2α also activates ATF4 and thus up-regulates CHOP expression. CHOP activates GADD34 (protein phosphatase 1 regulatory subunit 15A) which can dephosphorylate phospho-eIF2α and reversing the blockage of protein synthesis. This may be the cause of lower CHOP expression on day 4 of differentiation in dfd13 myoblasts. However, the increase in CHOP expression upon differentiation can be explained by the increase in phospho-eIF2α expression which up-regulates CHOP via ATF4 activation. A previous study reported that UPR activation via PERK is enriched in mitochondria-associated ER membranes which

promotes ER-stress induced apoptosis (Verfaillie et al. 2012). As both mitochondria and ER regulate calcium signalling, it is possible that the same scenario occurs.

The accumulation of CHOP expression in dfd13 myoblasts could also lead to prolonged ER stress and eventually could cause apoptosis. In differentiating C2C12 myoblasts CHOP protein expression is retained throughout the differentiation period, suggesting that ER stress could be well-alleviated by the UPR mechanism, i.e. via ATF6 and phospho-eIF2α regulation as shown in this study (Figure 6.6). Persistent CHOP expression can mediate programmed cell death by suppressing the transcription factor anti-apoptotic Bcl-2. The interaction of CHOP with FoxO3a has been shown to regulate the expression of BH3-only, i.e. BAD in neuronal cells (Ghosh 2012) and this may also occur in myoblasts. Therefore, it can be concluded that the accumulation of FoxO3a (Figure 4.7), reduction of autophagic flux (Figure 5.5) and PERK-mediated CHOP (Figure 6.4) suggest the dfd13 myoblasts are prone to apoptosis.

6.3.3 Increased PKC Activation Reflects Increased PLC Activity in Differentiating Dystrophin-Deficient Myoblasts

PKC is a serine/threonine kinase that is involved in cell proliferation, as well as cell differentiation. It consists of three subfamilies i.e. conventional/classic, novel and atypical. Each subfamily requires different activators for their activation and in this study, two isoforms from the classic PKC (cPKC) and one isoform from the novel PKC (nPKC) subfamilies were examined during differentiation. These isoforms were chosen based on the PLC products DAG and IP_3, which are highly produced as a result of PTEN overexpression. As discussed, high IP_3 could cause the release of Ca^{2+} into the cytosol thereby increasing the Ca^{2+} concentration. Therefore, excessive PKC activation in dfd13 myoblasts could reflect the existence/production of high DAG and Ca^{2+} in the

cytosol. The binding of DAG to the C1 domain and Ca^{2+} binding to the C2 domain of cPKC, PKC-α and PKC-βII results in its catalytic activation. The nPKC, PKC-ε, only requires DAG binding to its C1 domain for catalytic activation.

Before the binding of activators, phosphorylation of PKC at a specific residue will occur. From the data obtained, phosphorylated PKCs increased throughout the differentiation period in both types of myoblast. However, one of the phosphorylation residues of PKCβII, Thr641, was shown to be not phosphorylated in dystrophin-deficient myoblasts. A previous study reported that PKC-β is involved in myogenic differentiation and expression is increased upon differentiation. This indicates that non-phosphorylation of one residue in PKC-β could contribute to the deterioration of myotube development. It could be possible that PKC-β interacts with dystrophin as its target location on the membrane. It has also been previously shown to be localised to the cytoskeleton of a T-cell (Black and Black 2012).

This study provided information about the involvement of isoforms of PKC during the transition event. It can be seen that high levels of activated PKC-ε also reflects the accumulation of DAG in dystrophin-deficient myoblasts (Figure 6.8). In this case PKC-ε is almost never activated (low level detected), even though total PKC-ε expression showed a significant accumulation in C2C12 myoblasts (Figure 6.8). However, further analysis on Ca^{2+} concentration needs to be carried out prior to confirm PKC activation. A study by Gaboardi et al. (2009) reported that not only was PKC-ε expression increased but also activation following culture in a serum-free medium supplemented with insulin. In this case, it can be assumed that PKC-ε is also activated in C2C12 myoblasts but at lower levels which might be increased under insulin-induced conditions.

6.3.4 Reduced Activation of PKC-βII Contributes to the Instability of Its Catalytic Domain in Dystrophin-Deficient Myoblasts

The newly translated PKC-βII is associated with the cytoskeleton, and once phosphorylated, it starts to mature and is ready to act as a kinase. The regulation of PKC-βII involves two distinct phosphorylation events: 1) trans-phosphorylation at Thr500 to provide catalytic competency, via PDK1; and 2) auto-phosphorylation at C-terminus Thr641 which stabilises the catalytic conformation and auto-phosphorylation at Ser660, which releases PKC into the cytosol. However, this conformation remains inactive as the pseudo-substrate position is still occupied within the substrate-binding cavity. DAG and Ca^{2+} binding will release the pseudo-substrate and provide the open-formed catalytic site ready for substrate binding (substrate phosphorylation).

There is a lack of study regarding the involvement of PKC in myogenic differentiation. From the data obtained (Figure 6.6), PKC-βII has been shown to be selectively activated during myoblast differentiation. In this study the phosphorylation of PKC-βII at Thr641 was decreased but was increased at Ser660, suggesting that there is different regulation of these phosphorylation sites during differentiation of C2C12 myoblasts (Figure 6.6). Both phosphorylation sites occur within the C-terminus of the PKC-βII kinase domain; however, regulation is disturbed in dystrophin-deficient myoblasts. Phosphorylation of PKC-βII at Ser660 is found to be highly increased while phosphorylation at Thr641 is far less in dfd13 myoblasts throughout the differentiation period (Figure 6.6).

This phosphorylation event takes place at a hydrophobic motif and plays role in stabilising the catalytic competent conformation of PKC-βII before being released into the cytosol. As Thr641 is found to be less activated in dystrophin-deficient myoblasts,

it can be proposed that the released PKC-βII has an unstable catalytic component which impairs its role as a protein kinase. It also can be proposed that unphosphorylated Thr641 may disturb DAG and Ca^{2+} binding to the C1 and C2 domains, respectively, and subsequently alter the conformation change for the release of the pseudo-substrate prior to its kinase activity. This also impairs the stability of the PKC-membrane binding due to the high phosphorylation at the Ser660 site.

The phosphorylation of PKC-α at Thr638 corresponds to phosphorylation of PKC-βII at Thr641 in the turn motif of the catalytic region. Surprisingly, this phosphorylation showed a massive accumulation in dystrophin-deficient myoblasts, indicating that its regulation is impaired. Another suggestion that may support the reduced activation at Thr641 is the inactivation of rictor-mTORC2 as reported in Chapter 4, which may not be able to phosphorylate PKC-βII. It has been reported that mTORC2 may be responsible for both phosphorylation sites; however, it is unknown whether it is directly or indirectly involved (Alexandre and Thrower, 2012).

A previous study has shown that down-regulation of PKC-α inhibits myoblast proliferation. In contrast, PKC-β expression is increased during myoblast differentiation. From this study, again it can be implied that the accumulation of PKC-α activation and reduction in PKC activation are necessary during myoblast differentiation. In proliferating chick embryo myoblasts treatment with a PKC activator, TPA (phorbol ester), inhibited DNA synthesis and down-regulated PKC expression, suggesting that PKC-α plays a role in myoblast proliferation (Capiati et al., 1999). A study by Komati et al. (2004) demonstrated that TPA also can induce myogenic differentiation at nano molar concentrations (Komati et al. 2004). PKC can promote cell

growth by phosphorylating and activating RAF1, which mediates the activation of the MAPK/ERK signalling cascade.

6.3.5 Instability of PKC Reduces ERK1/2 Activation in Dystrophin-Deficient Myoblasts

According to the immunoblot analysis of PKC activation in dfd13 myoblasts, it can be suggested that the phosphorylated-form reflects the high release of DAG and Ca^{2+}. PKC-ε also showed the same effects which was caused by high levels of DAG being produced from the conversion of PLC-γ1. However, PKC-βII activity is down-regulated than in C2C12 myoblasts, suggesting that PKC-βII is not regulated/activated by high DAG and Ca^{2+}. It can also be suggested that low/down-regulated of PKC-βII activity is caused by impaired rictor-mTORC2 (Chapter 4) as a previous study showed that this complex regulates PKC in myoblasts. As ERK1/2 is also a downstream protein for PKC, ERK1/2 activity is thought to also be impaired.

Phosphorylation of PKC-βII at Thr641 stabilises the catalytic conformation while phosphorylation at Ser660 releases PKC from a detergent-insoluble fraction into the cytosol. In this study, the results showed a lack of phosphorylation at Thr641 (in PKC-βII) in differentiating dfd13 myoblasts potentially disturbed the stability of the kinase catalytic domain at the C-terminus, although it was released into the cytosol following phosphorylation at Ser660. This impairs the catalytic activity/kinase activity (phosphorylation) of its downstream protein. It has been reported that PKC controls RAF-1 activation, thus activating the MAPK cascade. In this study it was shown that the ERK1/2 expression, as well activation, is down-regulated in dystrophin-deficient myoblasts. Down-regulation of ERK1/2 also contributes to the down-regulation of protein translation. This in line with the impairment of p70S6K activity, as reported in

Chapter 4. ERK1/2 is a serine/threonine kinase that participates in the Raf/Ras/MEK cascade, and plays a role in catalysing the phosphorylation of various substrates, such as transcription factors during protein translation. Therefore, it is important to examine its phosphorylation level for effective functionality.

6.4 Conclusions

Elevation of PLC activation contributes to a reduction in the ER stress level and subsequently changes the UPR in differentiating dystrophin-deficient myoblasts.

Key finding(s):

- PTEN overexpression triggers high PLC activation and PKC regulation and disturbs the ER stress level in dystrophin-deficient myoblasts.
- A disturbed ER stress level alters activation of the UPR and leads to apoptosis via PERK-mediated CHOP.
- PKC maturation is disturbed thus reduced ERK1/2 activation in dystrophin-deficient myoblasts.

Chapter 7 - Minidystrophin$^{\Delta H2\text{-}R19}$ Partly Improved Protein Signalling in Dystrophin-Deficient Myoblasts

7.1 Introduction

The gene encoding dystrophin is one of the largest genes, and results in a rod-shaped dystrophin protein that is responsible for connecting the cytoskeleton to the extracellular matrix. The absence of full-length dystrophin in DMD has previously been shown causes impaired PTEN/PI3K/Akt (Chapter 4), which alters autophagy modulation (Chapter 5) and PLC/PKC signalling (Chapter 6), as well as causing a reduction is ER stress; therefore, the restoration of this protein is hoped to compensate for these effects. However, full-length dystrophin restoration is extremely difficult due to the large size of the dystrophin protein, and consequently mini-dystrophin has been utilised.

In this study, stable minidystrophin-eGFP tagged transfected myoblasts were used. Both C2C12 (non-dystrophic) and dfd13 (dystrophin-deficient) myoblasts were transfected with pCR3.1 eGFP-mini dystrophin (pMDysE), which is ~5.8 kb and kindly provided by Jacque P. Tremblay (Faculté of Médecine, Université Laval, Quebec, Canada). Minidystrophin lacks exons 17-48 of full-length dystrophin, which is ~220 kDa. A schematic of minidystrophin compared to full-length dystrophin is depicted in Figure 7.1, and stable transfectants are presented in Figure 7.2. An overview of the chapter is presented in Figure 7.3.

.

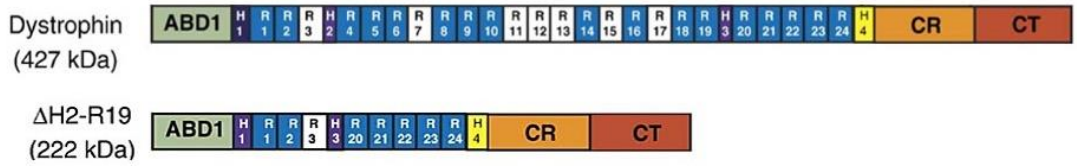

Figure 7.1: Schematic of full-length dystrophin and mini-dystrophin ΔH2-R19
Dystrophin begins with an actin-binding domain (ABD1) that binds to actin filaments. The central domain consists of long rod spectrin repeats, which are interspersed with hinge regions, and is followed by a cysteine-rich domain (CR) for dystroglycan binding. The C terminus (CT) domain binds members of the syntrophin and dystrobrevin protein families.

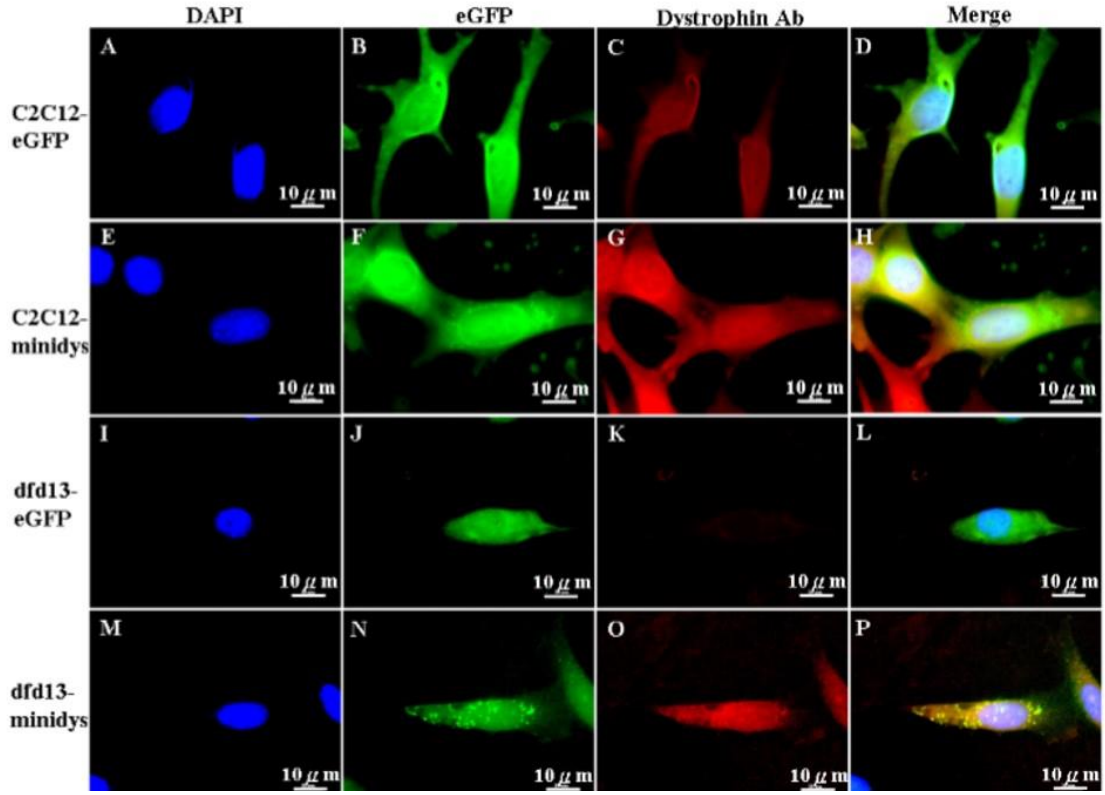

Figure 7.2: Minidystrophin-eGFP expression in C2C12 and dfd13 myoblasts
Human minidystrophin tagged with eGFP was introduced into C2C12 and dfd13 myoblasts. Stable clones were selected with geniticin for use in differentiation studies. Immunofluorescence and immunoblot analyses were performed prior to determining the capacity of both myoblasts to be terminally differentiated. Immunofluorescence analysis showed that minidystrophin$^{\Delta H2\text{-}R19}$ had been successfully introduced in C2C12 and dfd13 myoblasts. The eGFP plasmid was used as a control. Transfection of myoblasts with minidystrophin-eGFP was undertaken by Dr. Chen Hung-Chih during his doctoral research in Dr. Janet Smith's Lab (Chen, 2013).

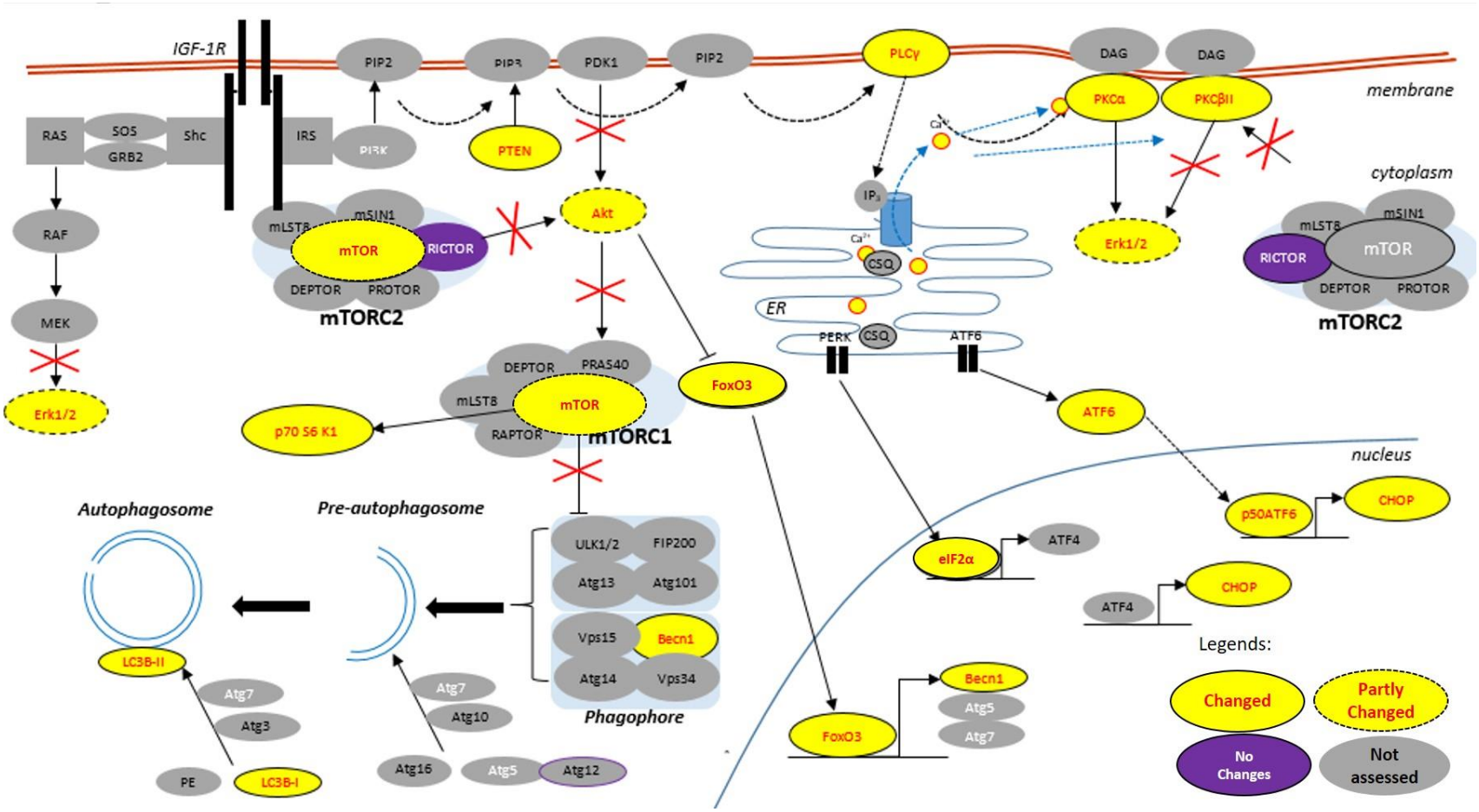

Figure 7.3: Chapter overview: mini-dystrophinΔH2-R19 partly improves proteins signalling in dystrophin-deficient myoblasts.
In this chapter, minidystrophin transfected myoblasts resulted in improvements to protein signalling. The accumulation of Akt was shown during the non-differentiated stage, with increased p70S6K activation throughout the differentiation period. Autophagy activation also increased as the LC3B conversion ratio was increased; however FoxO3 expression was decreased.

7.2 Results

7.2.1 dfd13 Minidystrophin$^{\Delta H2\text{-}R19}$ Myoblasts Did Not Achieve Terminal Differentiation

In Chapter 3 it was shown that dfd13 myoblasts failed to achieve terminal differentiation. Unfortunately, the introduction of minidystrophin into dfd13 myoblasts also showed the same pattern, and MyHC and MF-20 were expressed late compared to C2C12-eGFP myoblasts. Immunoblot analysis (Figure 7.4A) showed that both proteins were expressed at day 7 in C2C12-minidystrophin myoblasts, whereas in C2C12-eGFP myoblasts expression commences as early as day 4 of differentiation. Based on the densitometry analysis (Figure 7.4B), there were significant differences in MyHC expression between C2C12-minidystrophin and C2C12-eGFP myoblasts on day 7 ($p<0.01$; $p = 5.00 \times 10^{-3}$), and day 10 ($p<0.01$; $p = 2.34 \times 10^{-3}$).

As shown in Figure 7.4C, MF-20 was also expressed later in C2C12-minidystrophin myoblasts. Densitometry analysis showed that MF-20 was expressed significant lower than in C2C12-eGFP myoblasts on day 7 ($p<0.01$; $p = 7.64 \times 10^{-4}$), and day 10 ($p<0.01$; $p = 7.39 \times 10^{-3}$). From this analysis, it can be seen that minidystrophin delayed C2C12 myoblast terminal differentiation. It is also showed that minidystrophin is unable to rescue dfd13 myoblasts to achieve terminal differentiation. Therefore, potentially full-length of dystrophin may be required to improve differentiation in dystrophin-deficient myoblasts.

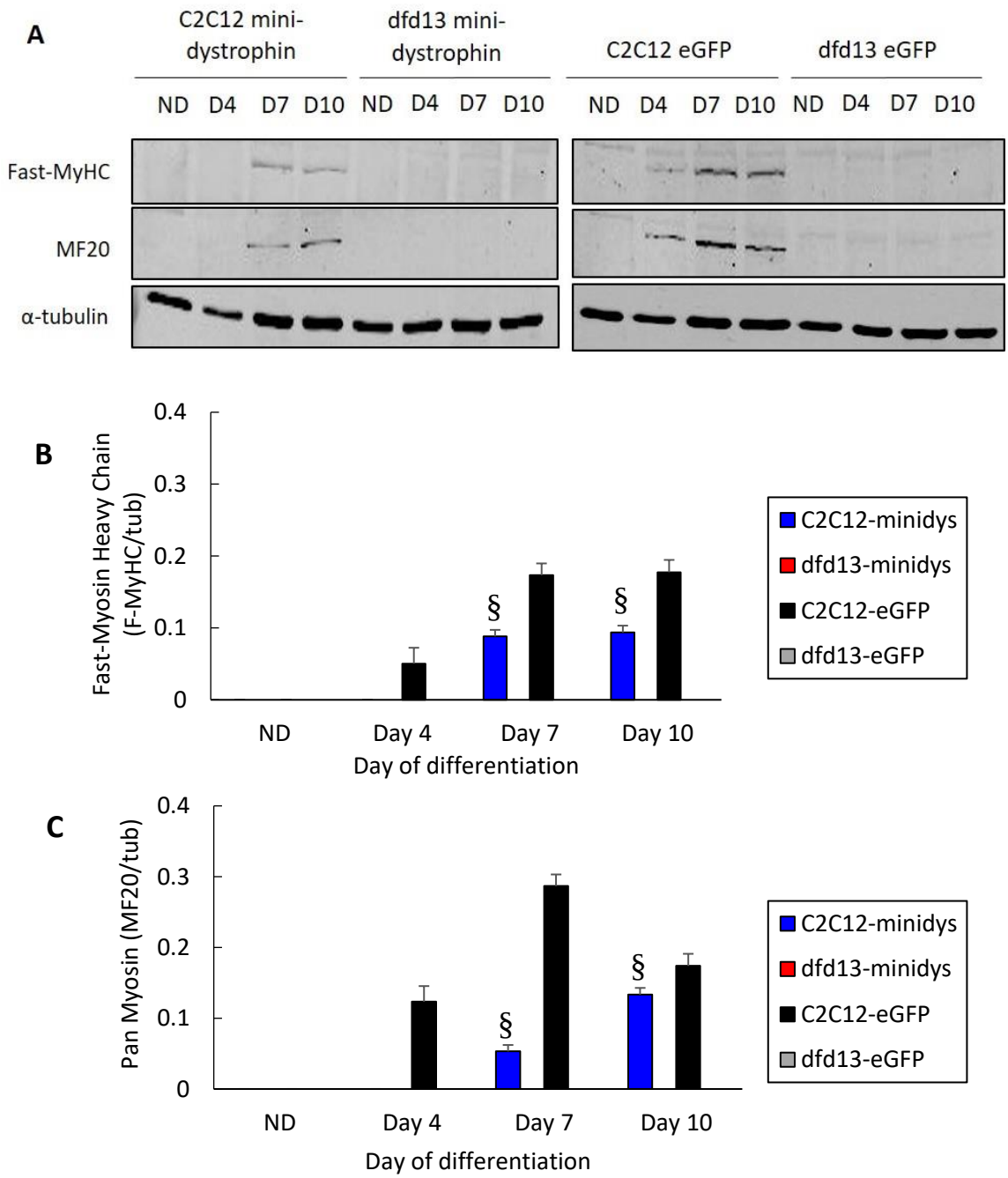

Figure 7.4: Myosin heavy chain is expressed later in C2C12 minidystrophinΔH2-R19 myoblasts

Myoblasts were cultured in GM until 80 to 90% confluent before washing twice with PBS and culturing in DM for 10 days with the media being changed every 2 days. Total protein was extracted at the indicated time points prior to immunoblotting with antibodies recognising-MyHC and pan-myosin (MF20). (A) Immunoblot analysis during myoblast differentiation with α-tubulin expression as a loading control. Densitometry analysis of (B) F-MyHC and (C) pan-myosin (MF20) expression. The graphs represent an average of three repeats from different samples. ND: non-differentiated; Significantly different: § ($p<0.01$) compared to C2C12-eGFP myoblasts. GM: growth medium (DMEM + 10% FCS); DM: differentiation medium (DMEM + 2% horse serum).

7.2.2 Minidystrophin$^{\Delta H2\text{-}R19}$ Improves Akt Expression During the Undifferentiated Stage and Increases p70S6 Kinase Activation During Dystrophin-Deficient Myoblasts Differentiation

In Chapter 4 it was shown that the PTEN-PI3K/Akt pathway is impaired in dfd13 myoblasts where the downstream proteins, i.e. p70S6K, FoxO3a, were affected. In dfd13-minidystrophin myoblasts PTEN expression was found to be reduced upon differentiation. Akt was found to be highly activated at the undifferentiated stage, while p70S6K showed activation upon differentiation. Immunoblot analysis of protein expression in minidystrophin-transfected myoblasts is shown in Figure 7.5A .

Densitometry analysis of PTEN expression showed significant accumulation of PTEN in C2C12-minidystrophin myoblasts when compared to C2C12-eGFP myoblasts; ND ($p<0.01$; $p = 1.20 \times 10^{-3}$) and day 4 ($p<0.01$; $p = 4.81 \times 10^{-4}$). In contrast, PTEN expression was found to be significantly reduced on day 7 ($p<0.01$; $p = 9.81 \times 10^{-4}$) and day 10 ($p<0.01$; $p = 7.37 \times 10^{-3}$) in dfd13-minidystrophin myoblasts when compared to dfd13-eGFP myoblasts. Rictor was inactivate in dfd13 myoblasts before and after the introduction of minidystrophin, but rictor expression and activity remained increased in C2C12-minidystrophin myoblasts upon differentiation.

mTOR expression was found significantly increased in minidystrophin-myoblasts when compared to eGFP-myoblasts; day 4 ($p<0.05$; $p = 2.08 \times 10^{-2}$) and day 7 ($p<0.05$; $p = 1.36 \times 10^{-2}$) (Figure7.5E). However, mTOR activity was showed a massive reduction in C2C12-minidystrophin when compared to C2C12-eGFP; ND ($p<0.01$; $p = 4.59 \times 10^{-3}$), on day 4 ($p<0.01$; $p = 1.41 \times 10^{-4}$), day 7 ($p<0.01$; $p = 6.24 \times 10^{-3}$), and day 10 ($p<0.01$; $p = 5.38 \times 10^{-3}$). Whilst, mTOR activity remained the same in dfd13-minidystrophin with slightly increased on day 10.

Akt activation was found to be significantly increased ($p<0.01$; $p = 6.73 \times 10^{-4}$) in undifferentiated dfd13-minidystrophin myoblasts compared to dfd13-eGFP myoblasts. However, its expression was found reduced upon differentiation to levels comparable with dfd13-eGFP myoblasts. Significant accumulation of Akt activity was found in C2C12-minidystrophin myoblasts compared to C2C12-eGFP myoblasts; ND ($p<0.01$; $p = 7.98 \times 10^{-4}$), on day 4 ($p<0.01$; $p = 3.46 \times 10^{-4}$), day 7 ($p<0.01$; $p = 1.66 \times 10^{-4}$), and day 10 ($p<0.01$; $p = 3.51 \times 10^{-3}$).

Surprisingly, p70S6K showed significant massive activation in dfd13-minidystrophin myoblasts compared to dfd13-eGFP myoblasts. Although the total expression reduced, it remained active in dfd13-minidystrophin myoblasts upon differentiation. There was a significant level of activation throughout the differentiation period compared to dfd13-eGFP myoblasts; day 4 ($p<0.05$; $p = 1.36 \times 10^{-2}$), day 7 ($p<0.05$; $p = 2.26 \times 10^{-2}$), and day 10 ($p<0.01$; $p = 3.45 \times 10^{-3}$). C2C12-minidystrophin also showed the same pattern where the p70S6K activity showed significant increased when compared to C2C12-eGFP; day 4 ($p<0.01$; $p = 7.71 \times 10^{-3}$), day 7 ($p<0.01$; $p = 2.64 \times 10^{-3}$), and day 10 ($p<0.01$; $p = 9.84 \times 10^{-4}$).

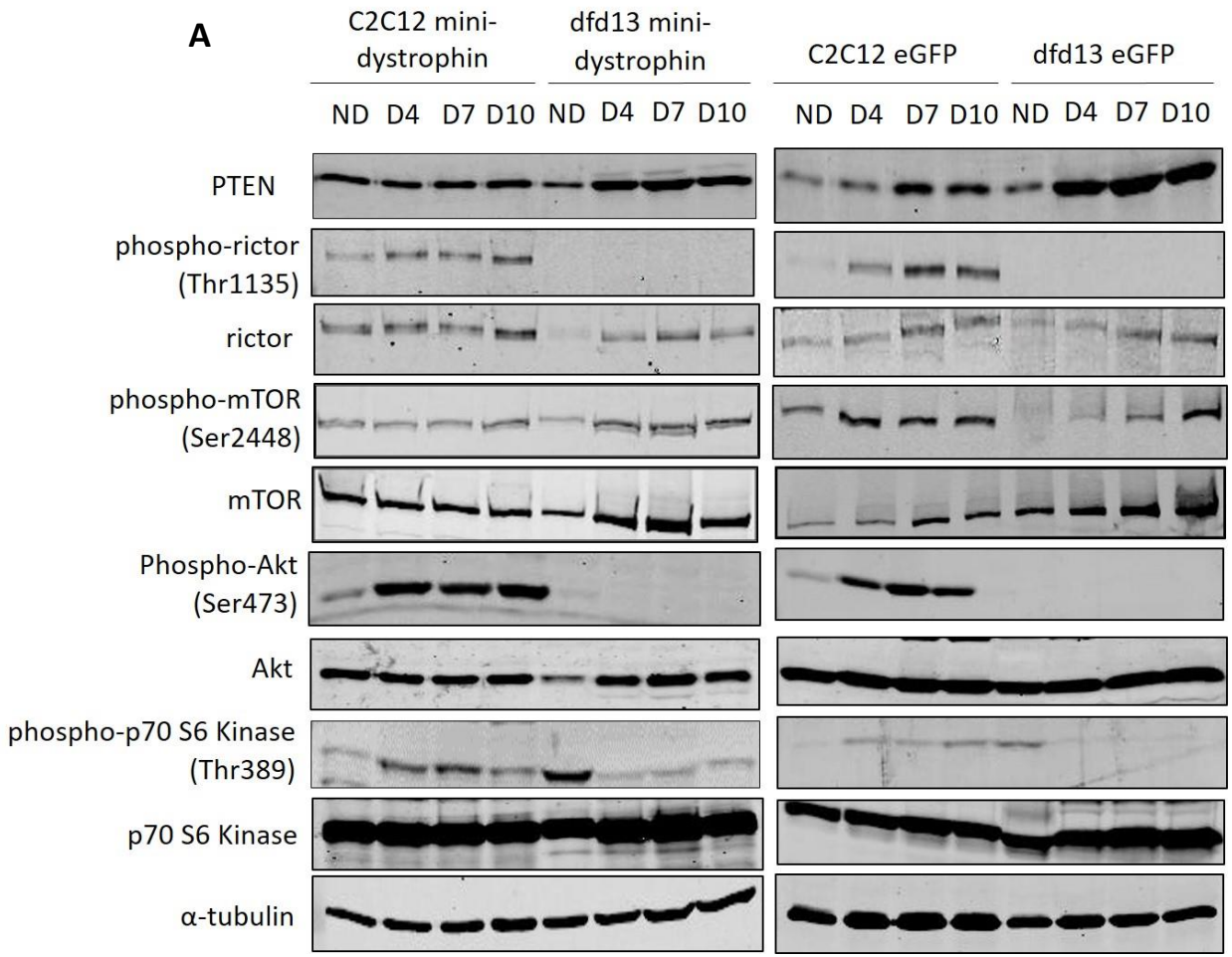
A
C2C12 mini-dystrophin
dfd13 mini-dystrophin
C2C12 eGFP
dfd13 eGFP
ND D4 D7 D10 ND D4 D7 D10
ND D4 D7 D10 ND D4 D7 D10
PTEN
phospho-rictor (Thr1135)
rictor
phospho-mTOR (Ser2448)
mTOR
Phospho-Akt (Ser473)
Akt
phospho-p70 S6 Kinase (Thr389)
p70 S6 Kinase
α-tubulin

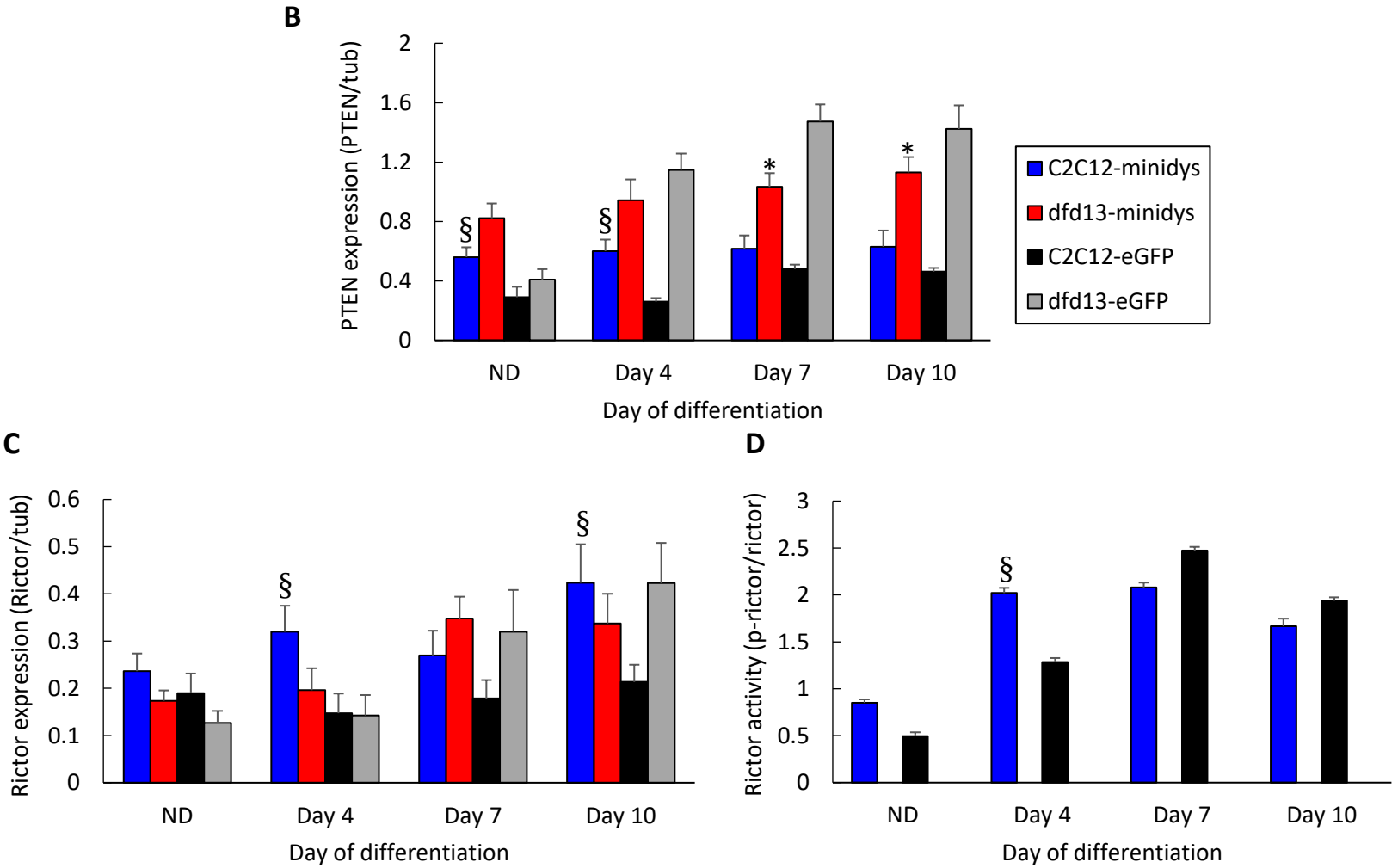
B
PTEN expression (PTEN/tub)
2
1.6
1.2
0.8
0.4
0
§
§
*
*
C2C12-minidys
dfd13-minidys
C2C12-eGFP
dfd13-eGFP
ND
Day 4
Day 7
Day 10
Day of differentiation
C
Rictor expression (Rictor/tub)
0.6
0.5
0.4
0.3
0.2
0.1
0
§
§
ND
Day 4
Day 7
Day 10
Day of differentiation
D
Rictor activity (p-rictor/rictor)
3
2.5
2
1.5
1
0.5
0
§
ND
Day 4
Day 7
Day 10
Day of differentiation

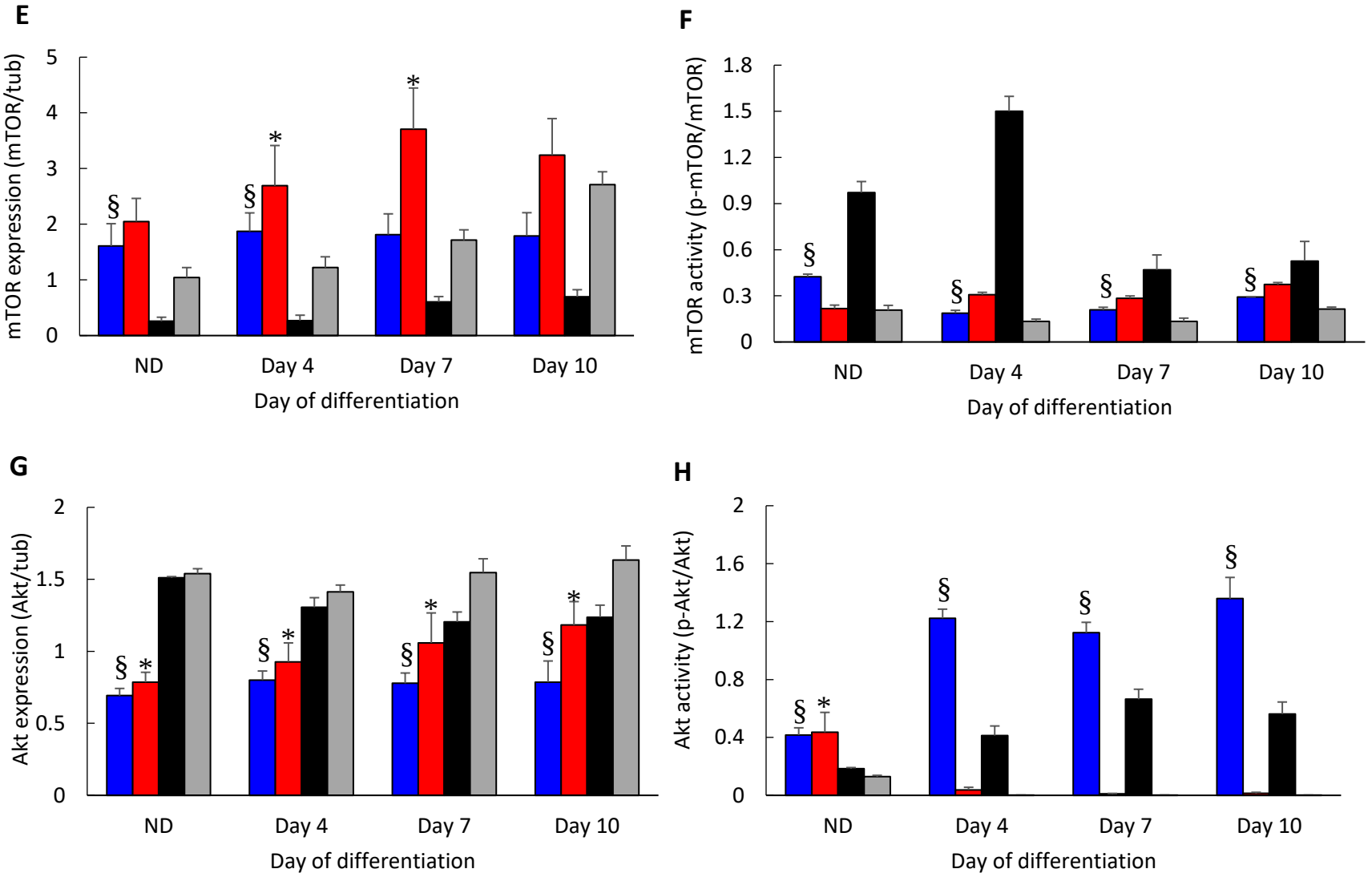
E
mTOR expression (mTOR/tub)
0
1
2
3
4
5
§
*
ND
Day 4
Day 7
Day 10
Day of differentiation
F
mTOR activity (p-mTOR/mTOR)
0
0.3
0.6
0.9
1.2
1.5
1.8
§
ND
Day 4
Day 7
Day 10
Day of differentiation
G
Akt expression (Akt/tub)
0
0.5
1
1.5
2
§
*
ND
Day 4
Day 7
Day 10
Day of differentiation
H
Akt activity (p-Akt/Akt)
0
0.4
0.8
1.2
1.6
2
§
*
ND
Day 4
Day 7
Day 10
Day of differentiation

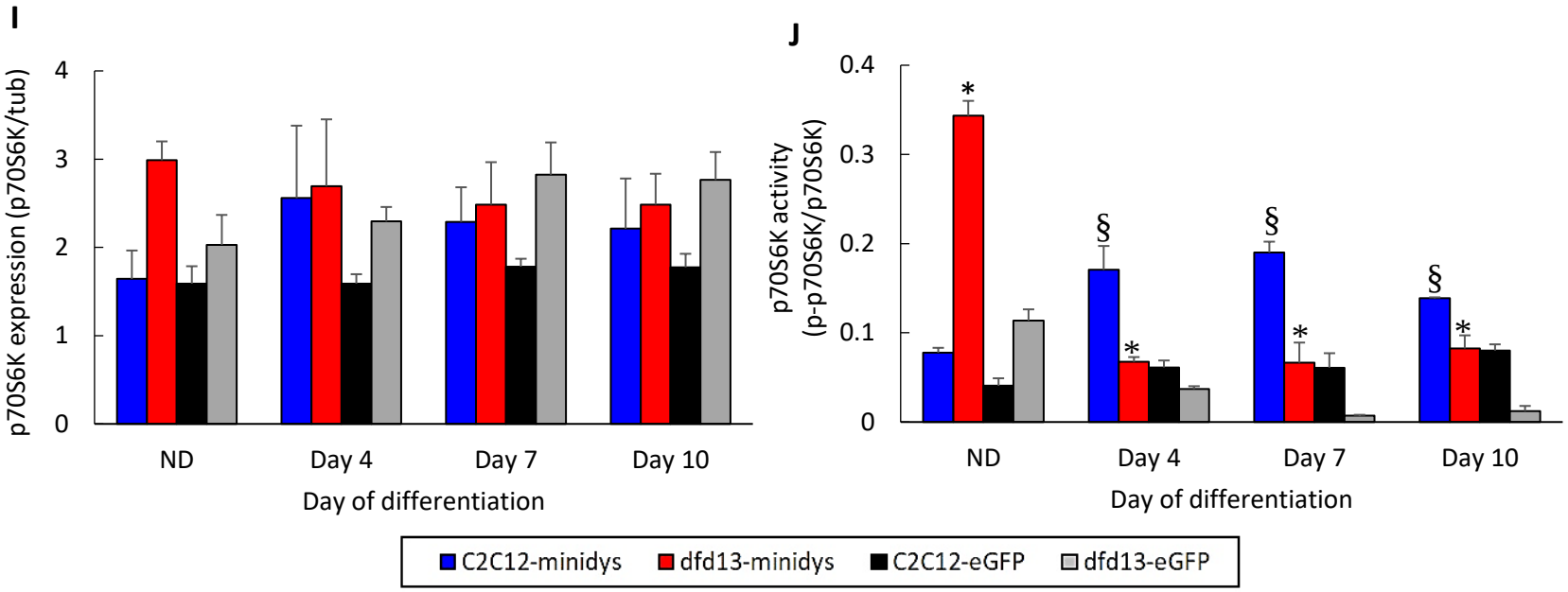

Figure 7.5: MinidystrophinΔH2-R19 improved Akt at undifferentiated stage and increases the p70S6 Kinase activation of dystrophin-deficient myoblasts during differentiation

Myoblasts were cultured in GM until 80 to 90% confluent before washing twice with PBS and culturing in DM for 10 days with the media being changed every 2 days. Total protein was extracted at the indicated time points prior to immunoblot analysis. (A) Immunoblot analysis of PTEN, phospho-Rictor, Rictor, phospho-Akt (Ser473), Akt, phospho-p70S6K and p70S6K expression during myoblast differentiation with α-tubulin expression as a loading control. Densitometry analysis of (B) PTEN expression, (C) Rictor expression, (D) Rictor activity, (E) mTOR expression, (F) mTOR activity, (G) Akt expression, (H) Akt activity, (I) p70S6K expression and (J) p70S6K activation. The graphs represent an average of three repeats from different samples. ND: non-differentiated; Significantly different: § ($p<0.01$) compared to C2C12-eGFP myoblasts; * ($p<0.01$) compared to dfd13-eGFP myoblasts; GM: growth medium (DMEM + 10% FCS); DM: differentiation medium (DMEM + 2% horse serum)

7.2.3 Autophagosome Formation Increases in dfd13 Minidystrophin$^{\Delta H2\text{-}R19}$ Myoblasts

As previously reported in Chapter 5, the conversion of the LC3B ratio correlates with the autophagy flux in dfd13 myoblasts during differentiation. Therefore, immunoblotting analysis was performed to determine the effects of minidystrophin in dfd13 myoblasts as well as in C2C12 myoblasts. Figure 7.6A shows the immunoblot analysis of FoxO3, Becn1 and LCB expression, and Figure 7.6B-F shows the densitometry analysis for the expression of each protein.

Surprisingly, FoxO3a was highly expressed in C2C12-minidystrophin myoblasts compared to dfd13-minidystrophin myoblasts, and there was a significant difference in the expression level; ND ($p<0.01$; $p = 2.01 \times 10^{-3}$), on day 4 ($p<0.01$; $p = 1.16 \times 10^{-3}$), day 7 ($p<0.01$; $p = 2.73 \times 10^{-3}$), and day 10 ($p<0.01$; $p = 5.16 \times 10^{-3}$). The data also showed that FoxO3a expression in dfd13-minidystrophin myoblasts was reduced in dfd13-eGFP myoblasts. This indicates that the presence of minidystrophin had a massive impact on FoxO3a expression (unphosphorylated form). Beclin1 also showed higher expression in C2C12-minidystrophin myoblasts compared to C2C12-eGFP myoblasts. There was also an accumulation of expression in dfd13-minidystrophin myoblasts, although this was significantly lower at day 10 ($p<0.01$; $p = 1.04 \times 10^{-3}$) compared to dfd13-eGFP myoblasts.

Figure 7.6D & E show the densitometry analysis for LC3B-I and LC3B-II expression, respectively. LC3B-I was highly expressed in C2C12-minidystrophin myoblasts throughout the differentiation period compared to C2C12-eGFP myoblasts and dfd13-minidystrophin myoblasts. This is in line with the high expression level of Beclin1 and FoxO3a noted previously. LC3B-I expression was increased in dfd13-

minidystrophin myoblasts but still lower than in dfd13-eGFP myoblasts and proportional to the low FoxO3a expression level described. Densitometry analysis of the LC3B conversion ration showed a reduction in conversion in C2C12-minidystrophin myoblasts. In contrast, dfd13-minidystrophin myoblasts showed increased LC3B conversion, indicating that autophagosome formation actively increased upon differentiation. It can also be seen that the LC3B conversion ratio was altered in both control myoblasts (eGFP-transfectants), where there was a reduction in conversion, indicating that autophagosome formation is reduced upon differentiation.

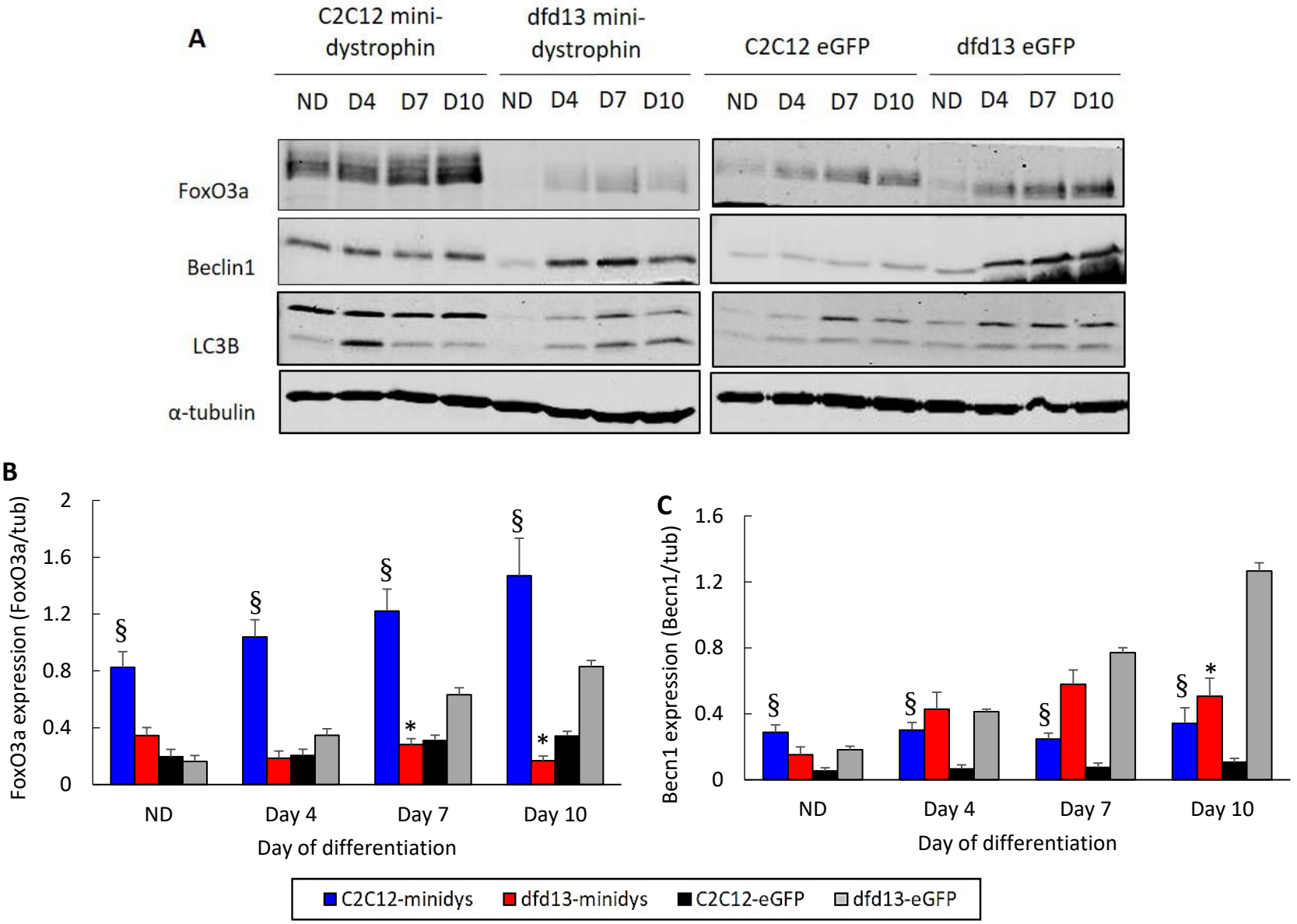
A
C2C12 mini-dystrophin
dfd13 mini-dystrophin
C2C12 eGFP
dfd13 eGFP
ND D4 D7 D10 ND D4 D7 D10 ND D4 D7 D10 ND D4 D7 D10
FoxO3a
Beclin1
LC3B
α-tubulin
B
FoxO3a expression (FoxO3a/tub)
2
1.6
1.2
0.8
0.4
0
§
*
ND
Day 4
Day 7
Day 10
Day of differentiation
C
Becn1 expression (Becn1/tub)
1.6
1.2
0.8
0.4
0
§
*
ND
Day 4
Day 7
Day 10
Day of differentiation
C2C12-minidys
dfd13-minidys
C2C12-eGFP
dfd13-eGFP

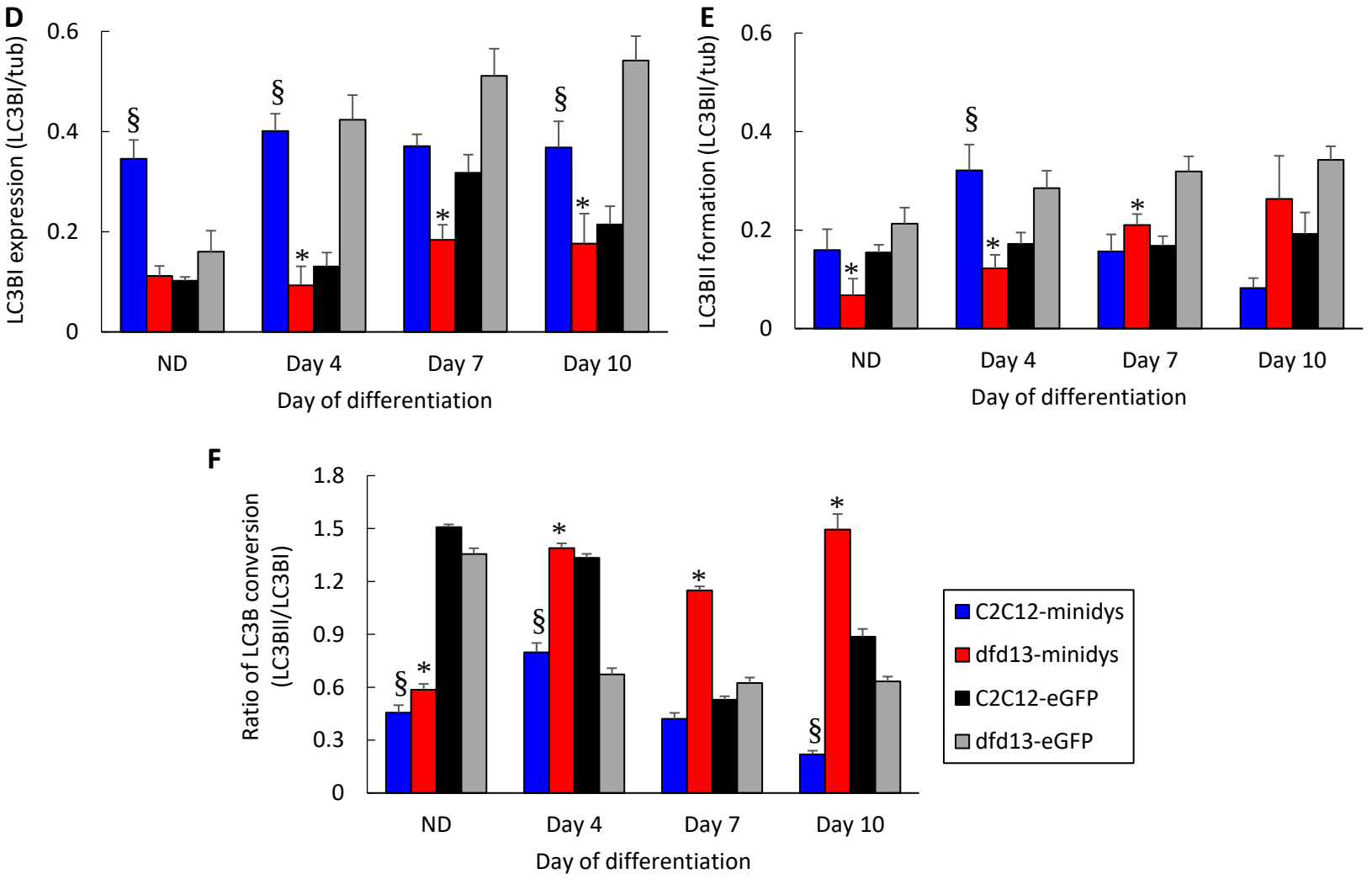
D
LC3BI expression (LC3BI/tub)
0.6
0.4
0.2
0
§
*
ND
Day 4
Day 7
Day 10
Day of differentiation
E
LC3BII formation (LC3BII/tub)
0.6
0.4
0.2
0
§
*
ND
Day 4
Day 7
Day 10
Day of differentiation
F
Ratio of LC3B conversion (LC3BII/LC3BI)
1.8
1.5
1.2
0.9
0.6
0.3
0
§
*
ND
Day 4
Day 7
Day 10
Day of differentiation
C2C12-minidys
dfd13-minidys
C2C12-eGFP
dfd13-eGFP

Figure 7.6: MinidystrophinΔH2-R19 reduces the FoxO3a expression and increases the LC3B conversion ratio in dfd13 during differentiation. Myoblasts were cultured in GM until 80 to 90% confluent before washing twice with PBS and culturing in DM for 10 days with the media being changed every 2 days. Total protein was extracted at the indicated time points prior to immunoblot analysis. (A) Immunoblot analysis of FoxO3a, Beclin1 and LC3B expression during myoblasts differentiation with α-tubulin expression as a loading control. Densitometry analysis of (B) FoxO3a expression, (C) Beclin1 expression, (D) LC3B-I expression, (E) LC3B-II formation, (F) Ratio of LC3B conversion. The graphs represent an average of three repeats from different samples. ND: non-differentiated; Significantly different: § ($p<0.01$) compared to C2C12-eGFP myoblasts; * ($p<0.01$) compared to dfd13-eGFP myoblasts; GM: growth medium (DMEM + 10% FCS); DM: differentiation medium (DMEM + 2% horse serum); n=3

7.2.4 Minidystrophin$^{\Delta H2\text{-}R19}$ Reduces PLC Activation and Changes the ER Stress Level

In Chapter 6 it was suggested that PLC-γ1 activation is affected by PTEN expression, as well as PI3K activity in myoblasts. Previously, (Figure 7.5), PTEN has been shown to be expressed at a lower level in dfd13-minidystrophin myoblasts than in dfd13-eGFP myoblasts. As predicted, even though there is increased activation of PLC-γ1 in dfd13-minidystrophin myoblasts, this is less than in dfd13-eGFP myoblasts upon differentiation, with a significant difference observed at day 10 ($p<0.05$; $p = 4.44 \times 10^{-2}$) (Figure 7.7B and C).

Surprisingly, CHOP was expressed at a low level in dfd13-minidystrophin myoblasts and even lower (almost not expressed) in C2C12-minidystrophin myoblasts (Figure 7.7). There was a significant difference in expression between the two types of myoblast during differentiation; day 4 ($p<0.01$; $p = 5.91 \times 10^{-4}$), day 7 ($p<0.01$; $p = 4.21 \times 10^{-3}$), and day 10 ($p<0.01$; $p = 2.35 \times 10^{-3}$). The level of CHOP expression showed a significant reduction ($p<0.01$; $p = 1.04 \times 10^{-3}$) in dfd13-eGFP myoblasts when compared to C2C12-eGFP myoblasts at day 7. This showed that the introduction of the eGFP-plasmid changed the ER stress level, as well as CHOP expression. It can be seen that the non-specific band sized approximately 25 kDa was also reduced, but this could not be identified. Furthermore, level of phospho-eIF2α was found significantly reduced in dfd13-minidystrophin day 7 ($p<0.05$; $p = 1.77 \times 10^{-2}$), and day 10 ($p<0.01$; $p = 3.48 \times 10^{-3}$).

The ATF6 cleavage ratio was examined since it is a downstream protein that is up-regulated by phospho-eIF2α. Figure 7.7F shows the percentage of ATF6 based on the 90 kDa and 50 kDa fragments. Fragmented/cleaved ATF6 represents the level of

ATF6 activation following cleavage in the Golgi during differentiation. As reported in Chapter 6, ATF6 is less activated in differentiating dfd13 myoblasts in line with the control dfd13-eGFP myoblasts. Interestingly, dfd13-minidystrophin myoblasts showed significantly higher activation of ATF6 compared to dfd13-eGFP myoblasts during differentiation; day 4 ($p<0.01$; $p = 1.13 \times 10^{-4}$) and day 10 ($p<0.01$; $p = 9.15 \times 10^{-4}$). In C2C12-minidystrophin myoblasts ATF6 showed a slight reduction in activation compared to C2C12-eGFP myoblasts but there was no significant difference.

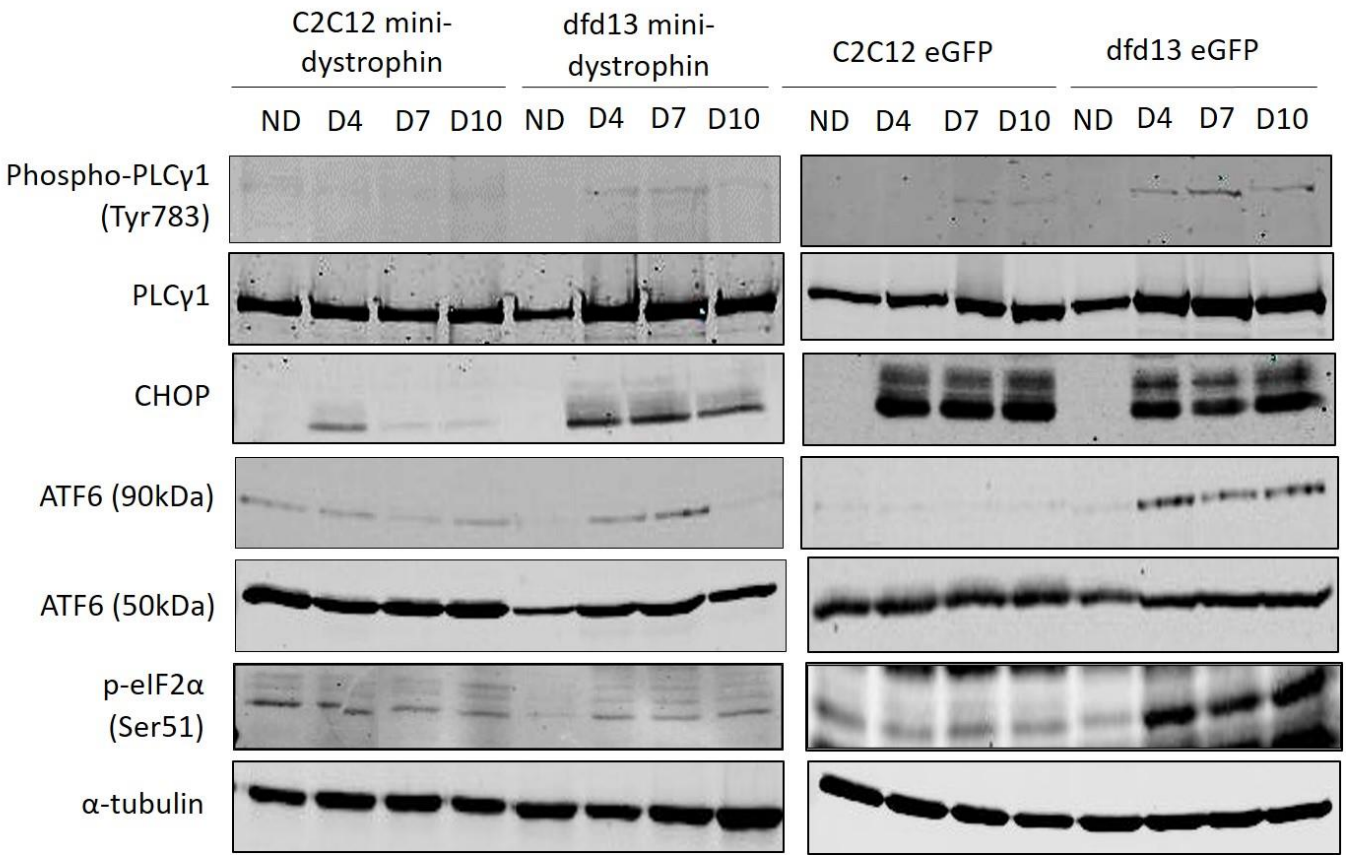
C2C12 mini-dystrophin
dfd13 mini-dystrophin
C2C12 eGFP
dfd13 eGFP
ND D4 D7 D10 ND D4 D7 D10 ND D4 D7 D10 ND D4 D7 D10
Phospho-PLCγ1 (Tyr783)
PLCγ1
CHOP
ATF6 (90kDa)
ATF6 (50kDa)
p-eIF2α (Ser51)
α-tubulin

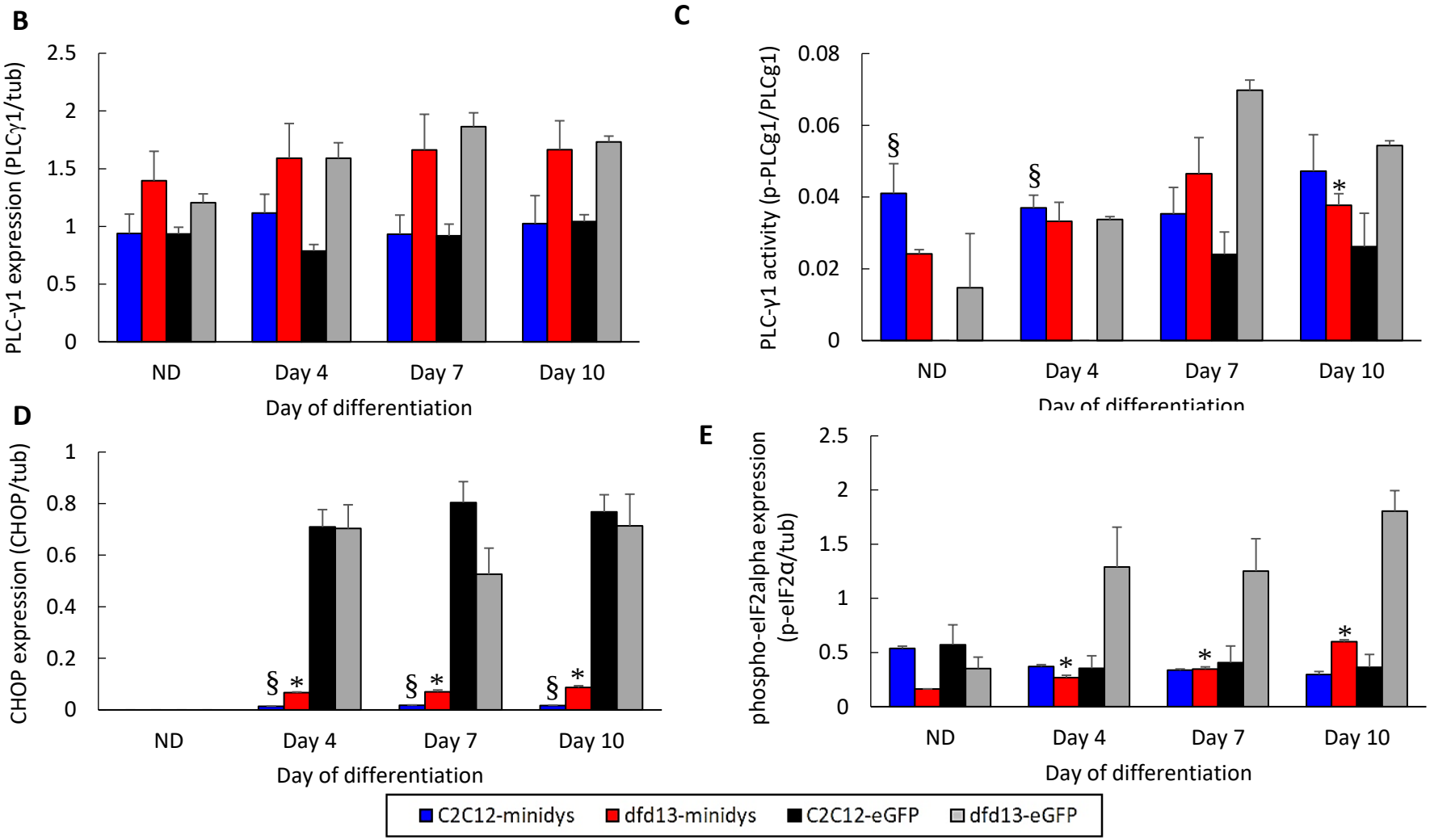
B
PLC-γ1 expression (PLCγ1/tub)
2.5
2
1.5
1
0.5
0
ND
Day 4
Day 7
Day 10
Day of differentiation
C
PLC-γ1 activity (p-PLCg1/PLCg1)
0.08
0.06
0.04
0.02
0
§
§
*
ND
Day 4
Day 7
Day 10
Day of differentiation
D
CHOP expression (CHOP/tub)
1
0.8
0.6
0.4
0.2
0
§
*
§
*
§
*
ND
Day 4
Day 7
Day 10
Day of differentiation
E
phospho-eIF2alpha expression (p-eIF2α/tub)
2.5
2
1.5
1
0.5
0
*
*
*
ND
Day 4
Day 7
Day 10
Day of differentiation
C2C12-minidys
dfd13-minidys
C2C12-eGFP
dfd13-eGFP

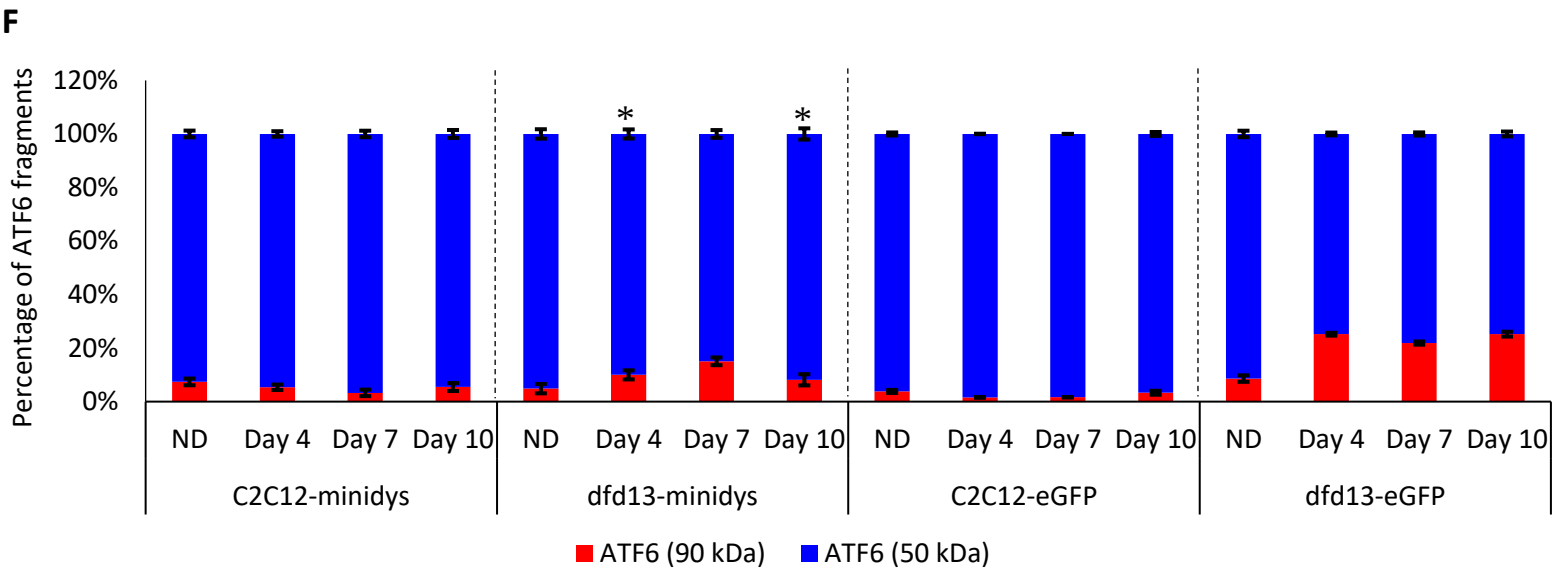

Figure 7.7: PLC activation and ER stress were reduced in dfd13-minidystrophin during differentiation

Myoblasts were cultured in GM until 80 to 90% confluent before washing twice with PBS and culturing in DM for 10 days with the media being changed every 2 days. Total protein was extracted at the indicated time points prior to immunoblot analysis. (A) Immunoblot analysis of phospho-PLC-γ1, PLC-γ1, CHOP, ATF6 expression during myoblasts differentiation with α-tubulin expression as a loading control. Densitometry analysis of (B) PLC-γ1 expression, (C) PLC-γ1 activity, (D) CHOP expression, (E) phospho-eIF2α (F) ATF6 fragmented percentage. The graphs represent an average of three repeats from different samples. ND: non-differentiated; Significantly different: § ($p<0.01$) compared to C2C12-eGFP myoblasts; * ($p<0.01$) compared to dfd13-eGFP myoblasts; GM: growth medium (DMEM + 10% FCS); DM: differentiation medium (DMEM + 2% horse serum); n=3.

7.2.5 Minidystrophin$^{\Delta H2\text{-}R19}$ Changes PKC and ERK1/2 Signalling

Previously, PKC and ERK1/2 have been shown to be impaired in dfd13 myoblasts (Chapter 5). PKC and ERK1/2 signalling was therefore examined in mindystrophin-transfected myoblasts. Figure 7.8A shows the immunoblot analysis for the expression of each protein in minidystrophin- and eGFP-transfected myoblasts. Densitometry analysis (Figure 7.8B) for the phosphorylation of PKC-α at Thr638 was found to be high during the non-differentiated state of C2C12-minidystrophin myoblasts compared to C2C12-eGFP myoblasts ($p<0.05$; $p = 1.26 \times 10^{-2}$). Expression was accumulated upon differentiation in both minidystrophin myoblasts and was even greater in eGFP myoblasts.

PKC-βII phosphorylation at Thr641 showed a reduction in C2C12-minidystrophin myoblasts and no expression in dfd13-minidystrophin myoblasts during differentiation. There was a significant reduction in the phosphorylation level in C2C12-minidystrophin myoblasts compared to C2C12-eGFP myoblasts; ND ($p<0.01$; $p = 9.78 \times 10^{-4}$), day 4 ($p<0.01$; $p = 2.20 \times 10^{-4}$), day 7 ($p<0.01$; $p = 5.49 \times 10^{5}$), and day 10 ($p<0.01$; $p = 4.20 \times 10^{-3}$) (Figure 7.8C). Phosphorylation of PKC-βII at Ser660 increased in minidystrophin myoblasts and showed the same pattern of expression as in both eGFP-myoblasts at a lower level.

As depicted in Figure 7.8E-H, ERK1/2 was also affected by minidystrophin. ERK1 is highly expressed in both C2C12-minidystrophin myoblasts and dfd13-minidystrophin myoblasts and showed the same expression pattern in eGFP-myoblasts. However, ERK1 activation could only be seen in C2C12-eGFP myoblasts with a reduction upon differentiation. ERK2 expression also showed the same pattern as in eGFP-myoblasts but at a higher level (Figure 7.8G); however, its activation was only

significantly higher ($p<0.01$; $p = 1.40 \times 10^{-3}$) in dfd13-minidystrophin myoblasts during the non-differentiated stage compared to C2C12-minidystrophin myoblasts. Upon differentiation, ERK2 was found to be less activated in dfd13-minidystrophin myoblasts compared to C2C12-minidystrophin myoblasts; day 4 ($p<0.01$; $p = 7.12 \times 10^{-4}$), day 7 ($p<0.01$; $p = 8.34 \times 10^{4}$), and day 10 ($p<0.01$; $p = 2.63 \times 10^{-4}$) (Figure 7.8H).

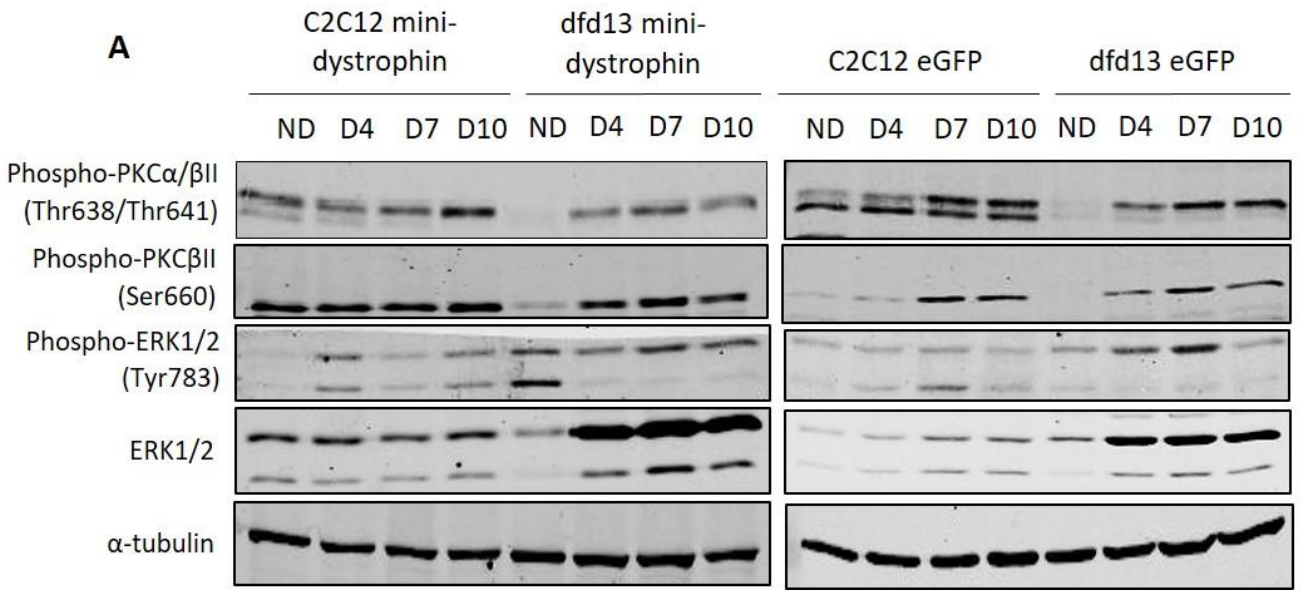
A
C2C12 mini-dystrophin
dfd13 mini-dystrophin
C2C12 eGFP
dfd13 eGFP
ND D4 D7 D10 ND D4 D7 D10 ND D4 D7 D10 ND D4 D7 D10
Phospho-PKCα/βII (Thr638/Thr641)
Phospho-PKCβII (Ser660)
Phospho-ERK1/2 (Tyr783)
ERK1/2
α-tubulin

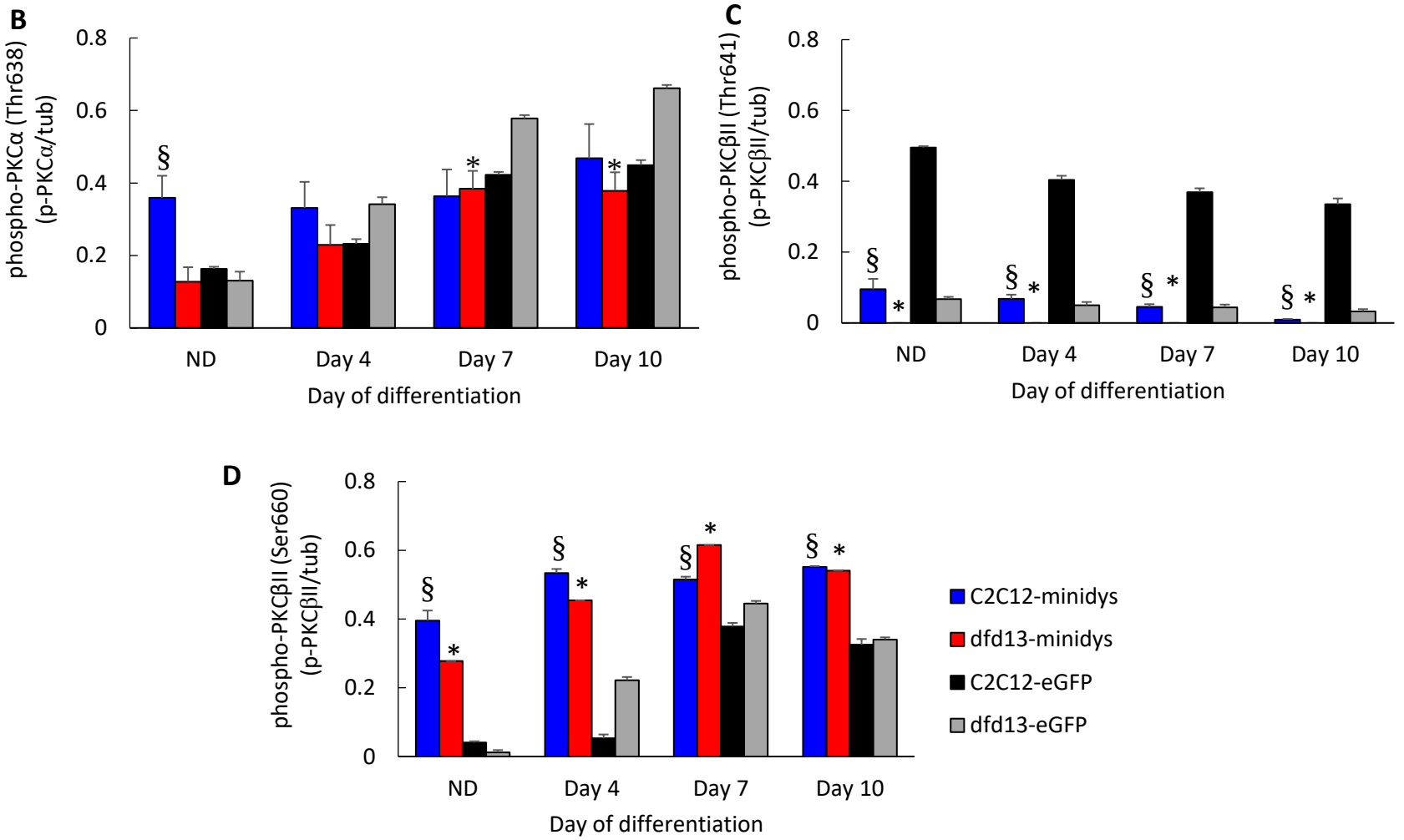
B
phospho-PKCα (Thr638)
(p-PKCα/tub)
0.8
0.6
0.4
0.2
0
§
*
ND
Day 4
Day 7
Day 10
Day of differentiation
C
phospho-PKCβII (Thr641)
(p-PKCβII/tub)
0.8
0.6
0.4
0.2
0
§
*
ND
Day 4
Day 7
Day 10
Day of differentiation
D
phospho-PKCβII (Ser660)
(p-PKCβII/tub)
0.8
0.6
0.4
0.2
0
§
*
ND
Day 4
Day 7
Day 10
Day of differentiation
C2C12-minidys
dfd13-minidys
C2C12-eGFP
dfd13-eGFP

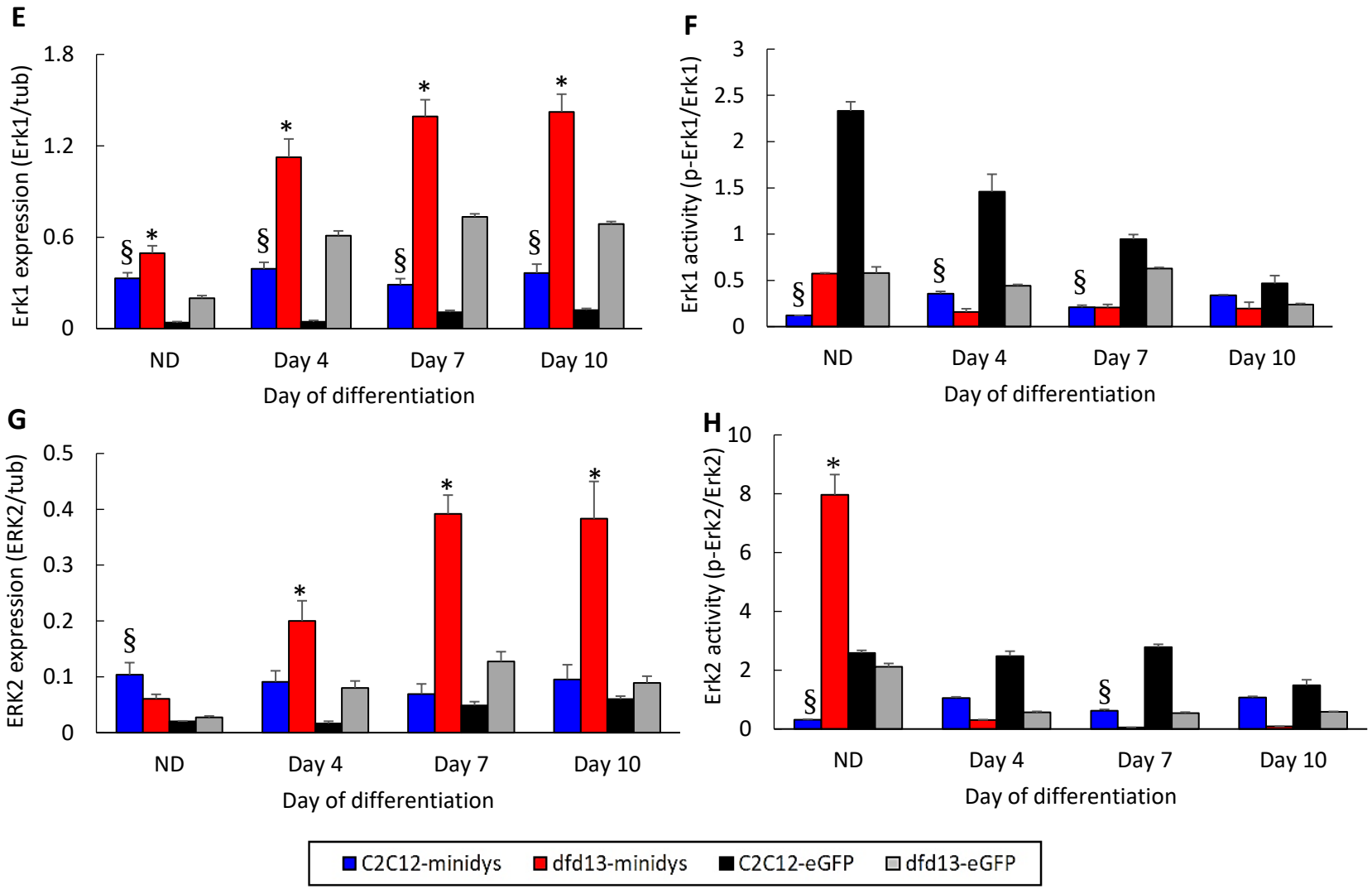
E
Erk1 expression (Erk1/tub)
1.8
1.2
0.6
0
ND
Day 4
Day 7
Day 10
Day of differentiation
F
Erk1 activity (p-Erk1/Erk1)
3
2.5
2
1.5
1
0.5
0
ND
Day 4
Day 7
Day 10
Day of differentiation
G
ERK2 expression (ERK2/tub)
0.5
0.4
0.3
0.2
0.1
0
ND
Day 4
Day 7
Day 10
Day of differentiation
H
Erk2 activity (p-Erk2/Erk2)
10
8
6
4
2
0
ND
Day 4
Day 7
Day 10
Day of differentiation
C2C12-minidys
dfd13-minidys
C2C12-eGFP
dfd13-eGFP

Figure 7.8: MinidystrophinΔH2-R19 changed PKC and ERK1/2 activation in myoblasts during differentiation.
Myoblasts were cultured in GM until 80 to 90% confluent before washing twice with PBS and culturing in DM for 10 days with the media being changed every 2 days. Total protein was extracted at the indicated time points prior to immunoblot analysis. (A) Immunoblot analysis of phospho-PKCα/βII (Thr638/Thr641), phospho-PKCβII (Ser660), phospho-ERK1/2 and ERK1/2 expression during myoblasts differentiation with α-tubulin expression as a loading control. Densitometry analysis of (B) phospho-PKCα (Thr638) expression, (C) phospho-PKC-βII (Thr641), (D) phospho-PKCβII (Ser660), (E) ERK1 expression, (F) ERK1 activation, (G) ERK2 expression and (H) ERK2 activity. The graphs represent an average of three repeats from different samples. ND: non-differentiated; Significantly different: § ($p<0.01$) compared to C2C12-eGFP myoblasts; * ($p<0.01$) compared to dfd13-eGFP myoblasts; GM: growth medium (DMEM + 10% FCS); DM: differentiation medium (DMEM + 2% horse serum); n=3.

7.3 Discussion

7.3.1 Minidystrophin$^{\Delta H2\text{-}R19}$ Ameliorates Protein Synthesis Regulation in Dystrophin-Deficient Myoblasts

From the results obtained, MyHC has been shown to be expressed later in C2C12-minidystrophin myoblasts than in C2C12-eGFP myoblasts. It is not expressed in dfd13 myoblast transfectants after 10 days of differentiation, indicating that dfd13 myoblasts have impaired differentiation ability/capacity even following the introduction of minidystrophin. Nevertheless, by introducing minidystrophin into dfd13 myoblasts Akt activation is increased compared to the control myoblasts (dfd13-eGFP) during the non-differentiated stage. There is no evidence concerning whether dystrophin and Akt directly interact. Based on the fact that dystrophin anchors the extracellular matrix to the cytoskeleton which stabilises the sarcolemma membrane, it is thought that it controls signalling conveyance, particularly the Igf-PI3K/Akt pathway. Igf-1 binds to Igf-1R which is embedded in the plasma membrane/sarcolemma membrane. Minidystrophin seems to improve PI3K/Akt signalling in dystrophin-deficient myoblasts by increasing myoblast stabilisation so that Igf-1R can function correctly. The use of minidystrophin may be the reason why Akt activation could not be fully recovered, as it is less activated upon differentiation (Figure 7.4).

Activation of Akt by doxycycline (DOX) treatment to control Akt1 expression via a transgene expression system has been shown to promotes myofibre regeneration and improve muscle function in dystrophin-deficient *mdx* mice (Kim et al. 2011). They also reported that the induction of Akt activation after the onset of peak pathology (>6 weeks) was even better, as Akt was found to have a faster regenerative response within the muscle. Akt has also been reported to be associated with integrin-linked kinase

(ILK), which can phosphorylate Akt. As ILK expression is found to be ncreased in the *mdx* mouse due to α7β1 integrin elevation, this may also have contributed to the accumulation of the phosphorylated-Akt during the non-differentiated stage.

The expression of p70S6K was shown to increase in minidystrophin-myoblasts when compared to eGFP-myoblasts. The expression pattern remained the same, indicating that minidystrophin has raised the activation level (Figure 7.4G). p70S6K is controlled by Akt via a series of phosphorylation events by mTORC1. Phosphorylation of p70S6K at Thr389 is important for further phosphorylation prior to full activation. Activation/phosphorylation of p70S6K stimulates its activity for several substrates, including translation initiation factor eIF-4B which is involved in the translation pre-initiation complex (Tchevkina and Komelkov 2012). This occurrence indicates that protein synthesis regulation in dystrophin-deficient myoblasts is improved after the introduction of minidystrophin.

7.3.2 Minidystrophin$^{\Delta H2\text{-}R19}$ Reduces FoxO3a Expression and Increases the LC3B Conversion Ratio in dfd13 Myoblasts During Differentiation

Autophagy is inhibited in MD and is emerging as an important process, especially during myoblast differentiation through the elimination of proteins and organelles. The conversion of LC3B as well as autophagy flux has been shown to be reduced in dystrophin-deficient myoblasts and minidystrophin was introduced in order to assess whether this scenario could be improved. The data showed that the introduction of minidystrophin into dystrophin-deficient myoblasts increased autophagy. FoxO3a as reduced while Beclin1 was increased which might balance autophagy activation during differentiation. C2C12-minidystrophin myoblasts exhibited high levels of FoxO3a and Beclin1 and consequently, LC3B was also expressed at a higher level (Figure 7.6) since

both FoxO3a and Beclin1 regulate LC3BI for autophagy activation (Mammucari et al., 2007).

Autophagy has been identified as a new therapeutic target in DMD and by Palma and colleagues (2012) demonstrated that a low-protein diet in *mdx* mice ameliorates dystrophic features after 3 months' consumption. In their study, the low-protein diet was characterised by a low amino-acid intake and autophagy reactivation was shown to improve the dystrophic phenotype in *mdx* mice, together with enhance LC3BII and FoxO3 expression.

7.3.3 Minidystrophin$^{\Delta H2\text{-}R19}$ Reduces PLC-γ1 Activation and Alters the ER Stress Level and UPR Activation in Dystrophin-Deficient Myoblasts

A study by Sabourin et al. (2012) demonstrated that the entry of Ca^{2+} is regulated by PLC activation, as well as PKC regulation (Sabourin et al. 2012). PLC activation leads to PIP_2 cleavage to become IP_3 and DAG. The released IP_3 has a high affinity to bind to IP_3-R on the ER and subsequently causes Ca^{2+} release into cytoplasm. The release of Ca^2 disturbs the interaction between Ca^{2+} and Ca^{2+} protein chaperons, and thus impairs protein folding in the ER. From the data obtained, PLC activation is reduced in dfd13-minidystrophin myoblasts compared to dfd13-eGFP myoblasts, indicating that minidystrophin affects PLC activation in dystrophin-deficient myoblasts (Figure 7.7). As a result, the Ca^{2+} concentration is constantly kept in the appropriate range and subsequently maintains the ER stress level during myoblasts differentiation.

ER stress is affected by Ca^{2+} concentration regulation, which is connectively associated with protein folding. Ca^{2+} and Ca^{2+} protein chaperons stabilise protein folding intermediates; therefore, protein signalling that controls Ca^{2+} regulation, as well as UPR activation, is important in order for myoblasts to dynamically achieve terminal

differentiation. Over the last decade there have been many reports of the reduction of Ca^{2+} in the ER (Burr and Molkentin 2015). In addition, various methods have been used to increase or restore Ca^{2+} level in the ER, i.e. overexpression of SERCA1a, which can increase Ca^{2+} intake into the ER.

In this study minidystrophin was used to restore the ER stress level. However, from the data obtained (Figure 7.7), CHOP expression in dfd13-minidystrophin myoblasts is lower when compared to dfd13-eGFP myoblasts, indicating that minidystrophin causes a reduction in the ER stress level. This was much worse in C2C12-minidystrophin myoblasts, where CHOP expression was almost undetectable. It is also thought that high levels of CHOP and FoxO3a could lead to cell cycle arrest and/or apoptosis. It has been reported that the interaction of CHOP with FoxO3a regulates BH3-only protein expression, such as BAD protein. From the data obtained, it can be seen that dfd13 myoblasts, including dfd13-eGFP myoblasts, exhibit high levels of FoxO3 and CHOP at the end of the differentiation period (day 10), suggesting that these myoblasts are prone to apoptosis. This is in line with the defective autophagy mentioned previously. From this study it can also be suggested that C2C12-minidystrophin myoblasts, as well C2C12-eGFP myoblasts are invulnerable to apoptosis.

Furthermore, UPR activation via ATF6 and PERK showed a reduction in activation. However, the level of activation is higher compared to dfd13-eGFP myoblasts, indicating that minidystrophin improves ATF6 activation. As CHOP is less expressed, it is thought that ATF6 up-regulates other ER stress markers and UPR proteins, such as Grp78. ATF6 is a transcription factor that is activated during ER stress and is capable of binding to ER stress-response elements (ERSE) to control the

expression of ER-localised molecular chaperons, such as BiP/Grp78, for unfolded protein refolding in the ER. ATF6 also regulates other UPR genes, such as XBP-1. Although both the ATF6 and IRE1 pathways can up-regulate CHOP, the PERK pathway predominates its expression through ATF4 translation (reviewed in Li et al., 2014). From data obtained, reduction of PERK activation via phospho-eIF2α improves dfd13 survival.

7.3.4 Minidystrophin$^{\Delta H2\text{-}R19}$ Changes PKC Phosphorylation and Subsequently Changes ERK1/2 Activity

There has been a lack of study on PKC expression and activation, especially concerning specific isoforms, within myoblasts. PKC has not been shown to be correlated directly with dystrophin; however, it has been reported to be involved in cation entry in dystrophin-deficient myoblasts (Sabourin et al., 2012). It has been demonstrated that inhibition of PLC and PKC in dystrophin-deficient myoblasts restores elevated cation entry to the normal level. Nascent PKC is needed to achieve full maturation via a series of phosphorylation events involving HSP90 (Heat-shock protein-90), PDK1 and mTORC2. HSP90, PDK1 and mTORC2 bind to the kinase domain, c-terminus and the turn and hydrophobic motif, respectively. Fully mature PKC is released into the cytoplasm with pseudo-substrate blocking until the specific substrate, i.e. Ca^{2+} and DAG, binds to it for activation.

The phosphorylation of PKC-α at Thr638 is higher in C2C12-minidystrophin myoblasts compared to C2C12-eGFP myoblasts, while dfd13-minidystrophin myoblasts exhibit a similar level as in dfd13-eGFP myoblasts until day 7 of differentiation. However, unlike dfd13-eGFP myoblasts, expression at day 10 remains the same as at day 7 (Figure 7.8). From this data, minidystrophin can be suggested to

indirectly control the phosphorylation of PKC-α in dfd13 myoblasts at an appropriate level, since the substrate (Ca^{2+} and DAG) is finely regulated by PLC-γ1.

PKC-βII also showed a reduction of phosphorylation at Thr641 and increased phosphorylation at Ser660 in dfd13-minidystrophin myoblasts. This indicates that minidystrophin affects PKC phosphorylation. Increased phosphorylation at Ser660 is in line with increased rictor activity as previously mentioned (Figure 7.5). Minidystrophin also increases the phosphorylation of PKC-βII at Ser660 in non-differentiated dfd13-minidystrophin myoblasts and thus increases downstream protein i.e. ERK2, activity (Figure 7.8H). Phosphorylation at Ser660 is important in order for PKC to be released into the cytoplasm where its kinase activity is activated by DAG and Ca^{2+}. In addition, rictor-mTORC2 was not activated in dfd13 myoblasts (Figure 7.5), yet phosphorylation could still be detected, indicating that other proteins in addition to mTORC2 may be able to phosphorylate this site.

Minidystrophin had an impact on the phosphorylation of PKC-βII at Ser660 , which was increased in both types pf minidystrophin myoblasts, even in dfd13 myoblasts where rictor is not active. This indicates that phosphorylation of PKC-βII at Ser660 is regulated by minidystrophin; however, it is uncertain whether direct or indirect regulation occurs.

7.4 Conclusions

Minidystrophin$^{\Delta H2\text{-}R19}$ can partly improve protein signalling in dystrophin-deficient myoblasts.

Key finding(s):

- Minidystrophin$^{\Delta H2\text{-}R19}$ does not increase differentiation in dfd13

- Increases protein synthesis activation.
- Increases autophagy activation/modulation.
- Reduces PLC-γ1 activation and the ER stress level.
- Increases ERK2 activation during the non-differentiated/proliferation stage.

Chapter 8 - Final Discussion

Duchenne muscular dystrophy is the most prevalent muscle disease characterised by muscle degeneration, loss of muscle regeneration and premature death. It is caused by mutation in DMD gene on X-chromosome mostly deletions of one or more exons that disrupt the reading frame and lead to complete loss of dystrophin expression. Dystrophin expressed in differentiated myofibres plays important role to connects extracellular matrix with cystoskeleton through the dystrophin-associated glycoprotein complex (DGC). However, the underlying protein signalling pathway in dystrophin-deficient myoblast that could contribute to DMD pathogenesis are still remains to be elucidated.

In this study, dystrophin-deficient myoblasts (dfd13) isolated from muscle of 5-week-old *mdx* mouse has been used as a model for dystrophic myoblasts. In chapter 3, it has been shown that the myoblast did not achieve the terminal differentiation characterised by lower myotube formation and absent of fast-myosin heavy chain expression but higher desmin expression after 10 days culture under low mitogen conditions. This pax7-expressing myoblasts also exhibit high pax7 expression and was found localised to ER, golgi and recycling endosome suggesting that pax7 is misregulated. For the first time, it is suggested that KPNA2 associated with pax7 to form a translocation complex. Current database from STRING showed that KPNA2 interacts with SUMO-protein ligase where it was reported that SUMOylation occurred on lys85 of pax7 (Luan et al. 2013) thus pax7-KPNA2 interaction is suggested occurred.

The Igf-1/PI3K/Akt is conserved pathway and has been reported impaired in skeletal muscle *mdx* mouse. In chapter 4, it was showed that high PTEN expression may caused the reduction of PI3K activation relatively, while the actual activity showed

accumulation. It also has been found that Akt was inactivated (Ser473) due to inactivation of rictor-mTOR. Therefore, subsequent downstream protein of Akt; mTORC1 and p70S6K, were shown inactivated indicating that protein synthesis regulation is impaired.

Due to inactivation of Akt, It can be suggested that pax7 signalling is also impaired. In this study, it is hypothesized that glycogen synthase kinase-3 (GSK3), one of the Akt downstream protein targets, is not to be completely activated. A previous study proved that Pax7 interacts with GSK3 through Wnt signalling. Therefore, it can be suggested that Pax7 involvement in GSK3/β-catenin signalling may be impaired.

GSK3 is a downstream protein in the Igf-1 pathway and generally known as a regulator of glycogen metabolism. Under Igf-1 stimulation, activated-Akt (protein kinase B) is responsible for directly phosphorylating GSK3β at the Ser9 residue. This phosphorylation suppresses its activation and thus changes downstream activities. In unstimulated conditions, GSK3β is present in its active form (non-phosphorylated). which targets primed substrates such as phosphorylated-β-catenin, which has previously been phosphorylated by casein kinase (CK1) at the Ser45 residue. GSK3β subsequently phosphorylates β-catenin at Ser33, Ser37 and Thr41 prior to proteasome degradation.

Recently, a study by Zhuang et al. (2014) demonstrated that Pax7 also interacts with β-catenin in the regulation of Wnt Signalling. This binding inhibits myoblast differentiation by repressing activation of T-cell factor/lymphoid enhancer factor (TCF/LEF). TCF/LEF protein is responsible for activating promoters to induce target genes that are involved in myoblast differentiation (Zhuang et al., 2014). It is also has been reported that wnt expression is reduced in *mdx* mouse indicating that wnt signalling impairment thus could cause ubiquitin-proteosome system activation in

dystrophin-deficient myoblasts. Consequently, active GSK3β could phosphorylates β-catenin (destabilises) and targets it for ubiquitination and subsequent proteasomal degradation.

Evidence from many groups has suggested that autophagy is impaired in *mdx* mouse (De Palma et al. 2012; Sandri et al. 2013; Neel et al. 2013). In this study, inactivation of Akt also may caused autophagy impairment in dystrophin-deficient myoblasts. There were two possible pathway has been suggested involved in this regulation; 1) Accumulation of autophagy related genes; Becn1, Atg5 and Atg7, as it highly expressed via FoxO3a-mediated, and 2) inactivation of mTORC1 that fail to inhibit autophagosome initiation complex formation; Becn1/Vps34/FIP200. The results of this study demonstrate an excessive autophagosome formation with reduction of autophagy flux indicated that autophagy is defective in dystrophin-deficient myoblast (chapter 5).

In chapter 6, it has been suggested that accumulation of PTEN expression has caused high activation of PLCγ1 subsequently increased enzymatic activity for PIP_2 cleavage. As consequences, this study also suggested that Ca^{2+} leakage from ER lumen via the opening of IP_3R due to IP_3 binding. This finding may supported an accumulation of Ca^{2+} concentration in cytoplasmic region in line with previous study (Burr and Melketin, 2015). In regard to Ca^{2+} leakage, ER stress level (CHOP expression level) has been shown reduced at the beginning of differentiation. In the meantime, activation of PERK (phospho-eIF2α expression level) was increased whilst ATF6 was decreased indicating that dystrophin-deficient myoblast is prone to apoptosis and has defects ERAD machinery. Altered PKC maturation also demonstrated that PKC could not

function well as Erk, the downstream protein of PKCα, showed reduction of activation via RAF-MEK pathway.

Due to several impairment described above, it can be concluded that dystrophin-deficient myoblast has impaired ability to differentiate prior to play role in muscle development as well as muscle regeneration in *mdx* mouse, and this could be the same happened in DMD patient.

Chapter 9 - Future Work

This sections describe future work that could be conducted to further the understanding.

9.1 Pax7 Study

From the data obtained in Chapter 3, it is unclear as to whether KPNA2 is the actual protein that functions as the protein translocator. Therefore, further experiments need to be performed in order to reveal its function, i.e. a nuclear transport assay, live cell imaging. It would also be beneficial to know whether the high expression of KPNA2 resembles high expression of Pax7, which may be a reason why dystrophin-deficient myoblasts are unable to achieve terminal differentiation.

As discussed in Section 3.3.2.2, future work on Pax7 protein signalling is proposed. A study by Zhuang et al. (2014) demonstrated that Pax7 interacts with β-catenin during Wnt signalling. In Wnt signalling, GSK3β is a subunit of the β-catenin destruction complex, and it is protein found downstream of Akt, (previously shown to be inactive in PI3K/Akt signalling) which is activated. Therefore, it is proposed that Wnt signalling is also impaired in dystrophin-deficient myoblasts.

9.2 Improving Minidystrophin Functionality

As previously mentioned, minidystrophin can only partly improve protein signalling, i.e. protein synthesis regulation and autophagy modulation. Therefore, it is suggested that full-dystrophin may have the potential to improve protein signalling and ameliorate the dystrophic phenotype in the *mdx* mouse as well as in DMD patients. As full-length dystrophin restoration confronted a massive problem as the large size of dystrophin protein, new method has to be developed.

References

Alexander, Matthew S, Juan Carlos Casar, Norio Motohashi, Jennifer a Myers, Iris Eisenberg, Robert T Gonzalez, Elicia a Estrella, Peter B Kang, Genri Kawahara, and Louis M Kunkel. 2011. "Regulation of DMD Pathology by an Ankyrin-Encoded miRNA." *Skeletal Muscle* 1 (1): 27. doi:10.1186/2044-5040-1-27.

Alexander, Matthew S, Juan Carlos Casar, Norio Motohashi, Natássia M Vieira, Iris Eisenberg, Jamie L Marshall, Molly J Gasperini, et al. 2014. "MicroRNA-486-Dependent Modulation of DOCK3/PTEN/AKT Signaling Pathways Improves Muscular Dystrophy-Associated Symptoms." *The Journal of Clinical Investigation* 124 (6). American Society for Clinical Investigation: 2651–67. doi:10.1172/JCI73579.

Allamand, Valerie, and Kevin Campbell. 2000. "Animal Models Formuscular Dystrophy: Valuable Tools for the Development of Therapies." *Journal of Artificial Intelligence Research*.

Angelini, Corrado, and Enrico Peterle. 2012. "Old and New Therapeutic Developments in Steroid Treatment in Duchenne Muscular Dystrophy." *Acta Myologica : Myopathies and Cardiomyopathies : Official Journal of the Mediterranean Society of Myology / Edited by the Gaetano Conte Academy for the Study of Striated Muscle Diseases* 31 (1): 9–15. http://www.pubmedcentral.nih.gov/articlerender.fcgi?artid=3440806&tool=pmcentrez&rendertype=abstract.

Bajard, Lola, Frédéric Relaix, Mounia Lagha, Didier Rocancourt, Philippe Daubas, and Margaret E Buckingham. 2006. "A Novel Genetic Hierarchy Functions during Hypaxial Myogenesis: Pax3 Directly Activates Myf5 in Muscle Progenitor Cells in the Limb." *Genes & Development* 20 (17). Cold Spring Harbor Laboratory Press: 2450–64. doi:10.1101/gad.382806.

Banduseela, Varuna C, Yi-Wen Chen, Hanna Göransson Kultima, Holly S Norman, Sudhakar Aare, Peter Radell, Lars I Eriksson, Eric P Hoffman, and Lars Larsson. 2013. "Impaired Autophagy, Chaperone Expression, and Protein Synthesis in Response to Critical Illness Interventions in Porcine Skeletal Muscle."

Physiological Genomics 45 (12): 477–86. doi:10.1152/physiolgenomics.00141.2012.

Bhattacharya, K, S Maiti, and C Mandal. 2016. "PTEN Negatively Regulates mTORC2 Formation and Signaling in Grade IV Glioma via Rictor Hyperphosphorylation at Thr1135 and Direct the Mode of Action of an mTORC1/2 Inhibitor." *Oncogenesis*. Macmillan Publishers Limited. http://dx.doi.org/10.1038/oncsis.2016.34.

Black, Adrian R., and Jennifer D. Black. 2012. "Protein Kinase C Signaling and Cell Cycle Regulation." *Frontiers in Immunology*. doi:10.3389/fimmu.2012.00423.

Blagosklonny, Mikhail V., and Arthur B. Pardee. 2002. "The Restriction Point of the Cell Cycle." *Cell Cycle (Georgetown, Tex.)*. doi:10.4161/cc.1.2.108.

Blake, Derek J., Andrew Weir, Sarah E. Newey, and Kay E. Davies. 2002. "Function and Genetics of Dystrophin and Dystrophin-Related Proteins in Muscle." *Physiol Rev* 82 (2): 291–329. doi:DOI 10.1152/physrev.00028.2001.

Blake, Judith A, and Melanie R Ziman. 2014. "Pax Genes: Regulators of Lineage Specification and Progenitor Cell Maintenance." *Development* 141 (4): 737 LP-751. http://dev.biologists.org/content/141/4/737.abstract.

Bononi, Angela, and Paolo Pinton. 2015. "Study of PTEN Subcellular Localization." *Methods* 77: 92–103. doi:10.1016/j.ymeth.2014.10.002.

Boppart, Marni D, Dean J Burkin, and Stephen J Kaufman. 2011. "Activation of AKT Signaling Promotes Cell Growth and Survival in α7β1 Integrin-Mediated Alleviation of Muscular Dystrophy." *Biochimica et Biophysica Acta* 1812 (4): 439–46. doi:10.1016/j.bbadis.2011.01.002.

Brameier, Markus, Andrea Krings, and Robert M MacCallum. 2007. "NucPred--Predicting Nuclear Localization of Proteins." *Bioinformatics (Oxford, England)* 23 (9): 1159–60. doi:10.1093/bioinformatics/btm066.

Bridge, J A, R Streblow, R W Frayer, P Dal Cin, A Rosenberg, A Meloni-Ehrig, and J Sumegi. 2010. "Recurrent (2; 2) and (2; 8) Translocations in Rhabdomyosarcoma without the Canonical PAX-FOXO1 Fuse PAX3 to Members of the Nuclear Receptor Transcriptional Coactivator (NCOA) Family." In *LABORATORY*

INVESTIGATION, 90:16A–16A. NATURE PUBLISHING GROUP 75 VARICK ST, 9TH FLR, NEW YORK, NY 10013-1917 USA.

Brunet, Anne, Azad Bonni, Michael J Zigmond, Michael Z Lin, Peter Juo, Linda S Hu, Michael J Anderson, Karen C Arden, John Blenis, and Michael E Greenberg. 1999. "Akt Promotes Cell Survival by Phosphorylating and Inhibiting a Forkhead Transcription Factor University of California at San Diego." *Cell* 96: 857–68.

Buckingham, Margaret, and Frederic Relaix. 2015. "PAX3 and PAX7 as Upstream Regulators of Myogenesis." In *Seminars in Cell & Developmental Biology*, 44:115–25. Elsevier.

Buckingham, Margaret, and Frédéric Relaix. 2007. "The Role of Pax Genes in the Development of Tissues and Organs: Pax3 and Pax7 Regulate Muscle Progenitor Cell Functions." *Annual Review of Cell and Developmental Biology* 23: 645–73. doi:10.1146/annurev.cellbio.23.090506.123438.

Burr, A R, and J D Molkentin. 2015. "Genetic Evidence in the Mouse Solidifies the Calcium Hypothesis of Myofiber Death in Muscular Dystrophy." *Cell Death and Differentiation* 22 (9). Nature Publishing Group: 1402–12. doi:10.1038/cdd.2015.65.

Capiati, Daniela A., Maria T. Téllez-Iñón, and Ricardo L. Boland. 1999. "Participation of Protein Kinase C α in 1,25-Dihydroxy-Vitamin D3 Regulation of Chick Myoblast Proliferation and Differentiation." *Molecular and Cellular Endocrinology* 153 (1–2): 39–45. doi:10.1016/S0303-7207(99)00093-3.

Chen, Xi, Jingshi Shen, and Ron Prywes. 2002. "The Luminal Domain of ATF6 Senses Endoplasmic Reticulum (ER) Stress and Causes Translocation of ATF6 from the ER to the Golgi." *Journal of Biological Chemistry* 277 (15). ASBMB: 13045–52.

Choi, J, Y Yang, S Lee, I Kim, S Ha, E Kim, Y Bae, S Ryu, and P Suh. 2007. "Phospholipase C-γ1 Potentiates Integrin-Dependent Cell Spreading and Migration through Pyk2/paxillin Activation." *Cellular Signalling* 19 (8): 1784–96. doi:10.1016/j.cellsig.2007.04.002.

Collins, Charlotte A, Viola F Gnocchi, Robert B White, Luisa Boldrin, Ana Perez-Ruiz, Frederic Relaix, Jennifer E Morgan, and Peter S Zammit. 2009. "Integrated

Functions of Pax3 and Pax7 in the Regulation of Proliferation, Cell Size and Myogenic Differentiation." Edited by Christophe Herman. *PLoS ONE* 4 (2). San Francisco, USA: Public Library of Science: e4475. doi:10.1371/journal.pone.0004475.

Cossu, G, S Tajbakhsh, M Buckingham, Giulio Cosso, Nt Jcglgfdl, G Cossu, S Tajbakhsh, and M Buckingham. 1996. "How Is Myogenesis Initiated in the Embryo?" *Trends in Genetics : TIG* 12 (6): 218–23. doi:10.1016/0168-9525(96)10025-1.

Diao, Yarui, Xing Guo, Yanfeng Li, Kun Sun, Leina Lu, Lei Jiang, Xinrong Fu, et al. 2012. "Pax3/7BP Is a Pax7- and Pax3-Binding Protein That Regulates the Proliferation of Muscle Precursor Cells by an Epigenetic Mechanism." *Cell Stem Cell* 11 (2). Elsevier: 231–41. doi:10.1016/j.stem.2012.05.022.

Dietz, Kevin N., Patrick J. Miller, Aditi S. Iyengar, Jacob M. Loupe, and Andrew D. Hollenbach. 2011. "Identification of Serines 201 and 209 as Sites of Pax3 Phosphorylation and the Altered Phosphorylation Status of Pax3-FOXO1 during Early Myogenic Differentiation." *International Journal of Biochemistry and Cell Biology* 43 (6): 936–45. doi:10.1016/j.biocel.2011.03.010.

Divet, Alexandra, and Corinne Huchet-Cadiou. 2002. "Sarcoplasmic Reticulum Function in Slow- and Fast-Twitch Skeletal Muscles from Mdx Mice." *Pflugers Archiv European Journal of Physiology* 444 (5): 634–43. doi:10.1007/s00424-002-0854-5.

Dogra, Charu, Harish Changotra, Jon E Wergedal, and Ashok Kumar. 2006. "Regulation of Phosphatidylinositol 3-Kinase (PI3K)/Akt and Nuclear Factor-Kappa B Signaling Pathways in Dystrophin-Deficient Skeletal Muscle in Response to Mechanical Stretch." *Journal of Cellular Physiology* 208 (3): 575–85. doi:10.1002/jcp.20696.

Du, Keyong, and Philip N Tsichlis. 2005. "Regulation of the Akt Kinase by Interacting Proteins." *Oncogene* 24: 7401–9. doi:10.1038/sj.onc.1209099.

Duan, C., M. B. Liimatta, and O. L. Bottum. 1999. "Insulin-like Growth Factor (IGF)-I Regulates IGF-Binding Protein-5 Gene Expression through the

Phosphatidylinositol 3-Kinase, Protein Kinase B/Akt, and p70 S6 Kinase Signaling Pathway." *Journal of Biological Chemistry* 274 (52): 37147–53. doi:10.1074/jbc.274.52.37147.

Duddy, William, Stephanie Duguez, Helen Johnston, Tatiana V Cohen, Aditi Phadke, Heather Gordish-Dressman, Kanneboyina Nagaraju, Viola Gnocchi, SiewHui Low, and Terence Partridge. 2015. "Muscular Dystrophy in the Mdx Mouse Is a Severe Myopathy Compounded by Hypotrophy, Hypertrophy and Hyperplasia." *Skeletal Muscle* 5: 16. doi:10.1186/s13395-015-0041-y.

Eagle, Michelle, Simon V. Baudouin, Colin Chandler, David R. Giddings, Robert Bullock, Kate Bushby, and M Egle. 2002. "Survival in Duchenne Muscular Dystrophy: Improvements in Life Expectancy since 1967 and the Impact of Home Nuctural Ventilation." *Neuromuscular Disorders* 12: 926–29. doi:10.1016/S0960-8966(02)00140-2.

Egerman, Marc A, and David J Glass. 2014. "Signaling Pathways Controlling Skeletal Muscle Mass." *Critical Reviews in Biochemistry and Molecular Biology* 49 (1). Informa Healthcare USA, Inc.: 59–68. doi:10.3109/10409238.2013.857291.

Eisenberg, Iris, Alal Eran, Ichizo Nishino, Maurizio Moggio, Costanza Lamperti, Anthony A Amato, Hart G Lidov, et al. 2007. "Distinctive Patterns of microRNA Expression in Primary Muscular Disorders." *Proceedings of the National Academy of Sciences of the United States of America* 104 (43): 17016–21. doi:10.1073/pnas.0708115104.

Erbay, Ebru, In Hyun Park, Paul D. Nuzzi, Christopher J. Schoenherr, and Jie Chen. 2003. "IGF-II Transcription in Skeletal Myogenesis Is Controlled by mTOR and Nutrients." *Journal of Cell Biology* 163 (5): 931–36. doi:10.1083/jcb.200307158.

Ervasti, James M., and Kevin P. Campbell. 1991. "Membrane Organization of the Dystrophin-Glycoprotein Complex." *Cell* 66 (6): 1121–31. doi:10.1016/0092-8674(91)90035-W.

Feron, Marie, Laetitia Guevel, Karl Rouger, Laurence Dubreil, Marie-Claire Arnaud, Mireille Ledevin, Lynn A Megeney, Yan Cherel, and Vehary Sakanyan. 2009. "PTEN Contributes to Profound PI3K/Akt Signaling Pathway Deregulation in

Dystrophin-Deficient Dog Muscle." *The American Journal of Pathology* 174 (4). Elsevier: 1459–70. doi:10.2353/ajpath.2009.080460.

Fiorillo, Alyson A., Christopher R. Heier, James S. Novak, Christopher B. Tully, Kristy J. Brown, Kitipong Uaesoontrachoon, Maria C. Vila, et al. 2015. "TNF-??-Induced microRNAs Control Dystrophin Expression in Becker Muscular Dystrophy." *Cell Reports* 12 (10): 1678–90. doi:10.1016/j.celrep.2015.07.066.

Florini, J R, D Z Ewton, and S A Coolican. 1996. "Growth Hormone and the Insulin-like Growth Factor System in Myogenesis." *Endocrine Reviews* 17 (5): 481–517. doi:10.1210/edrv-17-5-481.

Gaboardi, Gian Carlo, Giulia Ramazzotti, Alberto Bavelloni, Manuela Piazzi, Roberta Fiume, Anna Maria Billi, Alessandro Matteucci, Irene Faenza, and Lucio Cocco. 2010. "A Role for PKC?? During C2C12 Myogenic Differentiation." *Cellular Signalling* 22 (4): 629–35. doi:10.1016/j.cellsig.2009.11.017.

Ge, Yejing, and Jie Chen. 2012. "Mammalian Target of Rapamycin (mTOR) Signaling Network in Skeletal Myogenesis." *The Journal of Biological Chemistry* 287 (52): 43928–35. doi:10.1074/jbc.R112.406942.

Ghosh, Arindam P. 2012. "Regulation of Neuronal Cell Death by BH3-Only Molecules." The University of Alabama at Birmingham.

Glick, Danielle, Sandra Barth, and Kay F Macleod. 2010. "AutophagGlick, D., Barth, S., & Macleod, K. F. (2010). Autophagy : Cellular and Molecular Mechanisms. Journal of Pathology The, 221, 3–12. http://doi.org/10.1002/path.2697.Autophagyy : Cellular and Molecular Mechanisms." *Journal of Pathology The* 221: 3–12. doi:10.1002/path.2697.Autophagy.

Goonasekera, Sanjeewa A., Chi K. Lam, Douglas P. Millay, Michelle A. Sargent, Roger J. Hajjar, Evangelia G. Kranias, and Jeffery D. Molkentin. 2011. "Mitigation of Muscular Dystrophy in Mice by SERCA Overexpression in Skeletal Muscle." *Journal of Clinical Investigation* 121 (3): 1044–52. doi:10.1172/JCI43844.

Gredinger, E, a N Gerber, Y Tamir, S J Tapscott, and E Bengal. 1998. "Mitogen-Activated Protein Kinase Pathway Is Involved in the Differentiation of Muscle

Cells." *The Journal of Biological Chemistry* 273 (17): 10436–44. doi:10.1074/jbc.273.17.10436.

Grumati, Paolo, and Paolo Bonaldo. 2012. "Autophagy in Skeletal Muscle Homeostasis and in Muscular Dystrophies." *Cells* 1 (3). Molecular Diversity Preservation International: 325–45. doi:10.3390/cells1030325.

Grumati, Paolo, Luisa Coletto, Patrizia Sabatelli, Matilde Cescon, Alessia Angelin, Enrico Bertaggia, Bert Blaauw, Anna Urciuolo, Tania Tiepolo, and Luciano Merlini. 2010. "Autophagy Is Defective in Collagen VI Muscular Dystrophies, and Its Reactivation Rescues Myofiber Degeneration." *Nature Medicine* 16 (11). Nature Publishing Group: 1313–20.

Günther, Stefan, Johnny Kim, Sawa Kostin, Christoph Lepper, Chen-Ming Fan, and Thomas Braun. 2013. "Myf5-Positive Satellite Cells Contribute to Pax7-Dependent Long-Term Maintenance of Adult Muscle Stem Cells." *Cell Stem Cell* 13 (5): 590–601. doi:10.1016/j.stem.2013.07.016.

Hall, Monica N., Christine A. Griffin, Adriana Simionescu, Anita H. Corbett, and Grace K. Pavlath. 2011. "Distinct Roles for Classical Nuclear Import Receptors in the Growth of Multinucleated Muscle Cells." *Developmental Biology* 357 (1): 248–58. doi:10.1016/j.ydbio.2011.06.032.

Han, Renzhi, Miranda D Grounds, and Anthony J Bakker. 2006. "Measurement of Sub-Membrane [Ca 2+] in Adult Myofibers and Cytosolic [Ca 2+] in Myotubes from Normal and Mdx Mice Using the Ca 2+ Indicator FFP-18." *Cell Calcium* 40 (3). Elsevier: 299–307.

Haslett, Judith N, Despina Sanoudou, Alvin T Kho, Richard R Bennett, Steven A Greenberg, Isaac S Kohane, Alan H Beggs, and Louis M Kunkel. 2002. "Gene Expression Comparison of Biopsies from Duchenne Muscular Dystrophy (DMD) and Normal Skeletal Muscle." *Proceedings of the National Academy of Sciences* 99 (23): 15000–5. doi:10.1073/pnas.192571199.

Haslett, Judith N, Despina Sanoudou, Alvin T Kho, Mei Han, Richard R Bennett, Isaac S Kohane, Alan H Beggs, and Louis M Kunkel. 2003. "Gene Expression Profiling of Duchenne Muscular Dystrophy Skeletal Muscle." *Neurogenetics* 4 (4): 163–71.

doi:10.1007/s10048-003-0148-x.

Hawke, Thomas J, and Daniel J Garry. 2001. “Myogenic Satellite Cells: Physiology to Molecular Biology.” *Journal of Applied Physiology* 91 (2). Am Physiological Soc: 534–51.

Hoffman, Eric P., Robert H. Brown, and Louis M. Kunkel. 1987. “Dystrophin: The Protein Product of the Duchenne Muscular Dystrophy Locus.” *Cell* 51 (6). Elsevier: 919–28. doi:10.1016/0092-8674(87)90579-4.

Hong, Feng, Keun-ai Moon, Sam Soo Kim, Young Seol Kim, Young Kil Choi, Yun Soo Bae, Pann Ghill Suh, Sung Ho Ryu, Eui-Ju Choi, and Joohun Ha. 2001. “Role of Phospholipase C-γ1 in Insulin-like Growth Factor I-Induced Muscle Differentiation of H9c2 Cardiac Myoblasts.” *Biochemical and Biophysical Research Communications* 282 (3). Elsevier: 816–22.

Hung-chih, Chen. 2013. “Function of Caveolin-1 and Caveolin-3 I Muscular Dystrophy.” University of Birmingham.

Hyatt, Jon-Philippe K, Gary E McCall, Elizabeth M Kander, Hui Zhong, Roland R Roy, and Kimberly A Huey. 2008. “PAX3/7 Expression Coincides with MyoD during Chronic Skeletal Muscle Overload.” *Muscle & Nerve* 38 (1). Wiley Online Library: 861–66.

Ichimura, Yoshinobu, Takayoshi Kirisako, Toshifumi Takao, Yoshinori Satomi, Yasutsugu Shimonishi, Naotada Ishihara, Noboru Mizushima, Isei Tanida, Eiki Kominami, and Mariko Ohsumi. 2000. “A Ubiquitin-like System Mediates Protein Lipidation.” *Nature* 408 (6811). Nature Publishing Group: 488–92.

Jaafar, Rami, Caroline Zeiller, Luciano Pirola, Antonio Di Grazia, Fabio Naro, Hubert Vidal, Etienne Lefai, and Georges Némoz. 2011. “Phospholipase D Regulates Myogenic Differentiation through the Activation of Both mTORC1 and mTORC2 Complexes.” *The Journal of Biological Chemistry* 286 (25). 9650 Rockville Pike, Bethesda, MD 20814, U.S.A.: American Society for Biochemistry and Molecular Biology: 22609–21. doi:10.1074/jbc.M110.203885.

James, P L, S B Jones, W H Busby, D R Clemmons, and P Rotwein. 1993. “A Highly Conserved Insulin-like Growth Factor-Binding Protein (IGFBP-5) Is Expressed

during Myoblast Differentiation." *The Journal of Biological Chemistry* 268 (30): 22305–12. http://www.ncbi.nlm.nih.gov/pubmed/7693664.

Julien, L A, A Carriere, J Moreau, and P P Roux. 2010. "mTORC1-Activated S6K1 Phosphorylates Rictor on Threonine 1135 and Regulates mTORC2 Signaling." *Mol Cell Biol* 30 (4): 908–21. doi:10.1128/MCB.00601-09.

Kau, Tweeny R, Jeffrey C Way, and Pamela A Silver. 2004. "Nuclear Transport and Cancer: From Mechanism to Intervention." *Nature Reviews Cancer* 4 (2). Nature Publishing Group: 106–17.

Kaufman, Randal J, and Jyoti D Malhotra. 2014. "Calcium Trafficking Integrates Endoplasmic Reticulum Function with Mitochondrial Bioenergetics." *Biochimica et Biophysica Acta (BBA)-Molecular Cell Research* 1843 (10). Elsevier: 2233–39.

Kawabe, Yoh-ichi, Yu Xin Wang, Iain W McKinnell, Mark T Bedford, and Michael A Rudnicki. 2012. "Carm1 Regulates Pax7 Transcriptional Activity Through MLL1/2 Recruitment During Asymmetric Satellite Stem Cell Divisions." *Cell Stem Cell* 11 (3): 333–45. doi:10.1016/j.stem.2012.07.001.

Kim, Hyo Jeong, Cécile Jamart, Louise Deldicque, Gang-Li An, Yoon Hee Lee, Chang Keun Kim, Jean-Marc Raymackers, and Marc Francaux. 2011. "Endoplasmic Reticulum Stress Markers and Ubiquitin-Proteasome Pathway Activity in Response to a 200-Km Run." *Med Sci Sports Exerc* 43 (1): 18–25.

Komati, Hiba, Alessandra Minasi, Fabio Naro, Michel Lagarde, Annie-France Prigent, Sergio Adamo, and Georges Némoz. 2004. "Phorbol Ester-induced Differentiation of L6 Myogenic Cells Involves Phospholipase D Activation." *FEBS Letters* 577 (3). Wiley Online Library: 409–14.

Kosugi, Shunichi, Masako Hasebe, Masaru Tomita, and Hiroshi Yanagawa. 2009. "Systematic Identification of Cell Cycle-Dependent Yeast Nucleocytoplasmic Shuttling Proteins by Prediction of Composite Motifs." *Proceedings of the National Academy of Sciences* 106 (25). National Acad Sciences: 10171–76.

Kovac, Cecilia R, Alexander Emelyanov, Mallika Singh, Nasrin Ashouian, and Barbara K Birshtein. 2000. "BSAP (Pax5)-Importin α1 (Rch1) Interaction Identifies a Nuclear Localization Sequence." *Journal of Biological Chemistry* 275 (22).

ASBMB: 16752–57.

Kuang, Shihuan, Sophie B Chargé, Patrick Seale, Michael Huh, and Michael A Rudnicki. 2006. “Distinct Roles for Pax7 and Pax3 in Adult Regenerative Myogenesis.” *The Journal of Cell Biology* 172 (1). The Rockefeller University Press: 103–13. doi:10.1083/jcb.200508001.

Lagha, M, T Sato, L Bajard, P Daubas, M Esner, D Montarras, F Relaix, and M Buckingham. 2008. “Regulation of Skeletal Muscle Stem Cell Behavior by Pax3 and Pax7.” In *Cold Spring Harbor Symposia on Quantitative Biology*, 73:307–15. Cold Spring Harbor Laboratory Press.

Langenbach, K.J., and T.A. Rando. 2002. “Inhibition of Dystroglycan Binding to Laminin Disrupts the PI3K/AKT Pathway and Survival Signaling in Muscle Cells.” *Muscle & Nerve* 26 (5). Wiley Subscription Services, Inc., A Wiley Company: 644–53. doi:10.1002/mus.10258.

Lepper, Christoph, Simon J Conway, and Chen-Ming Fan. 2009. “Adult Satellite Cells and Embryonic Muscle Progenitors Have Distinct Genetic Requirements.” *Nature* 460 (7255): 627–31. doi:10.1038/nature08209.

Lepper, Christoph, Terence A Partridge, and Chen-Ming Fan. 2011. “An Absolute Requirement for Pax7-Positive Satellite Cells in Acute Injury-Induced Skeletal Muscle Regeneration.” *Development (Cambridge, England)* 138 (17). Company of Biologists: 3639–46. doi:10.1242/dev.067595.

Liao, Yong, and Mien Chie Hung. 2010. “Physiological Regulation of Akt Activity and Stability.” *American Journal of Translational Research*. doi:20182580.

Luan, Zhidong, Ying Liu, Timothy J Stuhlmiller, Jonathan Marquez, and Martín I García-Castro. 2013. “SUMOylation of Pax7 Is Essential for Neural Crest and Muscle Development.” *Cellular and Molecular Life Sciences* 70 (10): 1793–1806. doi:10.1007/s00018-012-1220-1.

Mallouk, Nora, Vincent Jacquemond, and Bruno Allard. 2000. “Elevated Subsarcolemmal Ca2+ in Mdx Mouse Skeletal Muscle Fibers Detected with Ca2+-Activated K+ Channels.” *Proceedings of the National Academy of Sciences* 97 (9). National Acad Sciences: 4950–55.

Mammucari, Cristina, Giulia Milan, Vanina Romanello, Eva Masiero, Ruediger Rudolf, Paola Del Piccolo, Steven J. Burden, et al. 2007. “FoxO3 Controls Autophagy in Skeletal Muscle In Vivo.” *Cell Metabolism* 6 (6): 458–71. doi:10.1016/j.cmet.2007.11.001.

Masiero, Eva, Lisa Agatea, Cristina Mammucari, Bert Blaauw, Emanuele Loro, Masaaki Komatsu, Daniel Metzger, Carlo Reggiani, Stefano Schiaffino, and Marco Sandri. 2009. “Autophagy Is Required to Maintain Muscle Mass.” *Cell Metabolism* 10 (6): 507–15. doi:10.1016/j.cmet.2009.10.008.

McCullough, K D, J L Martindale, L O Klotz, T Y Aw, and N J Holbrook. 2001. “Gadd153 Sensitizes Cells to Endoplasmic Reticulum Stress by down-Regulating Bcl2 and Perturbing the Cellular Redox State.” *Molecular and Cellular Biology* 21 (4): 1249–59. doi:10.1128/MCB.21.4.1249-1259.2001.

McGreevy, Joe W, Chady H Hakim, Mark A McIntosh, and Dongsheng Duan. 2015. “Animal Models of Duchenne Muscular Dystrophy: From Basic Mechanisms to Gene Therapy.” *Disease Models & Mechanisms* 8 (3). The Company of Biologists Limited: 195–213. doi:10.1242/dmm.018424.

McKinnell, Iain W., Jeff Ishibashi, Fabien Le Grand, Vincent G. J. Punch, Gregory C. Addicks, Jack F. Greenblatt, F. Jeffrey Dilworth, and Michael A. Rudnicki. 2008. “Pax7 Activates Myogenic Genes by Recruitment of a Histone Methyltransferase Complex.” *Nature Cell Biology* 10 (1): 77–84. doi:10.1038/ncb1671.

McMillan, Elliott M., and Joe Quadrilatero. 2014. “Autophagy Is Required and Protects against Apoptosis during Myoblast Differentiation.” *Biochemical Journal* 462 (2): 267 LP-277. http://www.biochemj.org/content/462/2/267.abstract.

Mekahli, Djalila, Geert Bultynck, Jan B. Parys, Humbert de Smedt, and Ludwig Missiaen. 2011. “Endoplasmic-Reticulum Calcium Depletion and Disease.” *Cold Spring Harbor Perspectives in Biology*. doi:10.1101/cshperspect.a004317.

Merrick, Deborah, Lukas Kurt Josef Stadler, Dean Larner, and Janet Smith. 2009. “Muscular Dystrophy Begins Early in Embryonic Development Deriving from Stem Cell Loss and Disrupted Skeletal Muscle Formation.” *Disease Models & Mechanisms* 2 (7–8): 374–88. doi:10.1242/dmm.001008.

Meryon, Edward. 1852. “On Granular and Fatty Degeneration of the Voluntary Muscles.” *Medico-Chirurgical Transactions* 35. Royal Society of Medicine Press: 73.

———. 1866. “On Granular Degeneration of the Voluntary Muscles.” *Medico-Chirurgical Transactions* 35: 73–84.1. doi:10.1136/bmj.2.497.32.

Messina, Graziella, and Giulio Cossu. 2009. “The Origin of Embryonic and Fetal Myoblasts: A Role of Pax3 and Pax7.” *Genes and Development*. doi:10.1101/gad.1797009.

Millarte, Valentina, and Hesso Farhan. 2012. “The Golgi in Cell Migration: Regulation by Signal Transduction and Its Implications for Cancer Cell Metastasis.” *The Scientific World Journal* 2012: 1–11. doi:10.1100/2012/498278.

Miller, Patrick J, Kevin N Dietz, and Andrew D Hollenbach. 2008. “Identification of Serine 205 as a Site of Phosphorylation on Pax3 in Proliferating but Not Differentiating Primary Myoblasts.” *Protein Science : A Publication of the Protein Society* 17 (11). Cold Spring Harbor Laboratory Press: 1979–86. doi:10.1110/ps.035956.108.

Mizushima, Noboru. 2004. “Methods for Monitoring Autophagy.” *International Journal of Biochemistry and Cell Biology*. doi:10.1016/j.biocel.2004.02.005.

Mizushima, Noboru, and Tamotsu Yoshimori. 2007. “How to Interpret LC3 Immunoblotting.” *Autophagy*. doi:4600 [pii].

Nakanishi, Keiko, Naoshi Dohmae, and Nobuhiro Morishima. 2007. “Endoplasmic Reticulum Stress Increases Myofiber Formation in Vitro.” *The FASEB Journal : Official Publication of the Federation of American Societies for Experimental Biology* 21 (11): 2994–3003. doi:10.1096/fj.06-6408com.

Nakanishi, Keiko, Tatsuhiko Sudo, and Nobuhiro Morishima. 2005. “Endoplasmic Reticulum Stress Signaling Transmitted by ATF6 Mediates Apoptosis during Muscle Development.” *Journal of Cell Biology* 169 (4): 555–60. doi:10.1083/jcb.200412024.

Nardozzi, Jonathan D, Kaylen Lott, and Gino Cingolani. 2010. “Phosphorylation Meets

Nuclear Import: A Review." *Cell Communication and Signaling : CCS* 8 (1): 32. doi:10.1186/1478-811X-8-32.

Neel, Brian A, Yuxi Lin, and Jeffrey E Pessin. 2013. "Skeletal Muscle Autophagy: A New Metabolic Regulator." *Trends in Endocrinology and Metabolism: TEM* 24 (12): 10.1016/j.tem.2013.09.004. doi:10.1016/j.tem.2013.09.004.

Nowak, Kristen J, and Kay E Davies. 2004. "Duchenne Muscular Dystrophy and Dystrophin: Pathogenesis and Opportunities for Treatment." *EMBO Reports* 5 (9): 872–76. doi:10.1038/sj.embor.7400221.

Olguin, Hugo C., Zhihong Yang, Stephen J. Tapscott, and Bradley B. Olwin. 2007. "Reciprocal Inhibition between Pax7 and Muscle Regulatory Factors Modulates Myogenic Cell Fate Determination." *Journal of Cell Biology* 177 (5): 769–79. doi:10.1083/jcb.200608122.

Olguin, Hugo C, and Bradley B Olwin. 2004. "Pax-7 up-Regulation Inhibits Myogenesis and Cell Cycle Progression in Satellite Cells: A Potential Mechanism for Self-Renewal." *Developmental Biology* 275 (2). Elsevier: 375–88.

Olguín, Hugo C, and Addolorata Pisconti. 2011. "Marking the Tempo for Myogenesis: Pax7 and the Regulation of Muscle Stem Cell Fate Decisions." *Journal of Cellular and Molecular Medicine*, 1–14. doi:10.1111/j.1582-4934.2011.01348.x.

Ono, Hiraku, Hideki Katagiri, Makoto Funaki, Motonobu Anai, Kouichi Inukai, Yasushi Fukushima, Hideyuki Sakoda, Takehide Ogihara, Yukiko Onishi, and Midori Fujishiro. 2001. "Regulation of Phosphoinositide Metabolism, Akt Phosphorylation, and Glucose Transport by PTEN (Phosphatase and Tensin Homolog Deleted on Chromosome 10) in 3T3-L1 Adipocytes." *Molecular Endocrinology* 15 (8). Endocrine Society: 1411–22.

Oustanina, S, G Hause, and T Braun. 2004. "Pax7 Directs Postnatal Renewal and Propagation of Myogenic Satellite Cells but Not Their Specification." *Embo J* 23 (16): 3430–39. doi:10.1038/sj.emboj.7600346.

Palma, C De, F Morisi, S Cheli, S Pambianco, V Cappello, M Vezzoli, P Rovere-Querini, et al. 2012. "Autophagy as a New Therapeutic Target in Duchenne Muscular Dystrophy." *Cell Death and Disease* 3 (11): e418.

doi:10.1038/cddis.2012.159.

Palma, Clara De, Cristiana Perrotta, Paolo Pellegrino, Emilio Clementi, and Davide Cervia. 2014. “Skeletal Muscle Homeostasis in Duchenne Muscular Dystrophy: Modulating Autophagy as a Promising Therapeutic Strategy.” *Frontiers in Aging Neuroscience* 6 (JUL). doi:10.3389/fnagi.2014.00188.

Passamano, Luigia, Antonella Taglia, Alberto Palladino, Emanuela Viggiano, Paola D’Ambrosio, Marianna Scutifero, Maria Rosaria Cecio, et al. 2012. “Improvement of Survival in Duchenne Muscular Dystrophy: Retrospective Analysis of 835 Patients.” *Acta Myologica*.

Peter, Angela K., and Rachelle H. Crosbie. 2006. “Hypertrophic Response of Duchenne and Limb-Girdle Muscular Dystrophies Is Associated with Activation of Akt Pathway.” *Experimental Cell Research* 312 (13): 2580–91. doi:10.1016/j.yexcr.2006.04.024.

Ploski, Jonathan E, Monee K Shamsher, and Aurelian Radu. 2004. “Paired-Type Homeodomain Transcription Factors Are Imported into the Nucleus by Karyopherin 13.” *Molecular and Cellular Biology* 24 (11). Am Soc Microbiol: 4824–34.

Pluquet, Olivier, Albin Pourtier, and Corinne Abbadie. 2015. “The Unfolded Protein Response and Cellular Senescence. A Review in the Theme: Cellular Mechanisms of Endoplasmic Reticulum Stress Signaling in Health and Disease.” *American Journal of Physiology-Cell Physiology* 308 (6). Am Physiological Soc: C415–25.

Preisinger, Christian, Benjamin Short, Veerle De Corte, Erik Bruyneel, Alexander Haas, Robert Kopajtich, Jan Gettemans, and Francis A. Barr. 2004. “YSK1 Is Activated by the Golgi Matrix Protein GM130 and Plays a Role in Cell Migration through Its Substrate 14-3-3??” *Journal of Cell Biology* 164 (7): 1009–20. doi:10.1083/jcb.200310061.

Rao, Rammohan V., and Dale E. Bredesen. 2004. “Misfolded Proteins, Endoplasmic Reticulum Stress and Neurodegeneration.” *Current Opinion in Cell Biology*. doi:10.1016/j.ceb.2004.09.012.

Rayavarapu, Sree, William Coley, and Kanneboyina Nagaraju. 2012. “Endoplasmic

Reticulum Stress in Skeletal Muscle Homeostasis and Disease." *Current Rheumatology Reports*. doi:10.1007/s11926-012-0247-5.

Relaix, Frédéric, Didier Montarras, Stéphane Zaffran, Barbara Gayraud-Morel, Didier Rocancourt, Shahragim Tajbakhsh, Ahmed Mansouri, Ana Cumano, and Margaret Buckingham. 2006. "Pax3 and Pax7 Have Distinct and Overlapping Functions in Adult Muscle Progenitor Cells." *Journal of Cell Biology* 172 (1): 91–102. doi:10.1083/jcb.200508044.

Relaix, Frédéric, Didier Rocancourt, Ahmed Mansouri, and Margaret Buckingham. 2004. "Divergent Functions of Murine Pax3 and Pax7 in Limb Muscle Development." *Genes and Development* 18 (9): 1088–1105. doi:10.1101/gad.301004.

Rosner, M., N. Siegel, A. Valli, C. Fuchs, and M. Hengstschläger. 2010. "MTOR Phosphorylated at S2448 Binds to Raptor and Rictor." *Amino Acids* 38 (1): 223–28. doi:10.1007/s00726-008-0230-7.

Sabourin, Jessica, Rania Harisseh, Thomas Harnois, Christophe Magaud, Nicolas Bourmeyster, Nadine Déliot, and Bruno Constantin. 2012. "Dystrophin/α1-Syntrophin Scaffold Regulated PLC/PKC-Dependent Store-Operated Calcium Entry in Myotubes." *Cell Calcium* 52 (6). Elsevier: 445–56.

Sambasivan, R, R Yao, A Kissenpfennig, L Van Wittenberghe, A Paldi, B Gayraud-Morel, H Guenou, B Malissen, S Tajbakhsh, and A Galy. 2011. "Pax7-Expressing Satellite Cells Are Indispensable for Adult Skeletal Muscle Regeneration." *Development* 138: 3647–56. doi:10.1242/dev.067587.

Sandri, Marco, Carlo Minetti, Marina Pedemonte, and Ugo Carraro. 1998. "Apoptotic Myonuclei in Human Duchenne Muscular Dystrophy." *Laboratory Investigation; a Journal of Technical Methods and Pathology* 78 (8): 1005–16.

Sarbassov, Dos D, David A Guertin, Siraj M Ali, and David M Sabatini. 2005. "Phosphorylation and Regulation of Akt/PKB by the Rictor-mTOR Complex." *Science* 307 (5712): 1098 LP-1101. http://science.sciencemag.org/content/307/5712/1098.abstract.

Schiaffino, Stefano, and Cristina Mammucari. 2011. "Regulation of Skeletal Muscle

Growth by the IGF1-Akt/PKB Pathway: Insights from Genetic Models." *Skeletal Muscle* 1 (January). BioMed Central: 4. doi:10.1186/2044-5040-1-4.

Schiaffino, Stefano, and Carlo Reggiani. 2011. "Fiber Types in Mammalian Skeletal Muscles." *Physiological Reviews* 91 (4): 1447–1531. doi:10.1152/physrev.00031.2010.

Schlamp, C L, G L Poulsen, T M Nork, and R W Nickells. 1997. "Nuclear Exclusion of Wild-Type p53 in Immortalized Human Retinoblastoma Cells." *Journal of the National Cancer Institute* 89 (20): 1530–36. doi:10.1093/jnci/89.20.1530.

Schönwasser, Dorothee C, Richard M Marais, Christopher J Marshall, and Peter J Parker. 1998. "Activation of the Mitogen-Activated Protein Kinase/extracellular Signal-Regulated Kinase Pathway by Conventional, Novel, and Atypical Protein Kinase C Isotypes." *Molecular and Cellular Biology* 18 (2). Am Soc Microbiol: 790–98.

Screen, Mark, Olayinka Raheem, Jeanette Holmlund-Hampf, Per Harald Jonson, Sanna Huovinen, Peter Hackman, and Bjarne Udd. 2014. "Gene Expression Profiling in Tibial Muscular Dystrophy Reveals Unfolded Protein Response and Altered Autophagy." *PLoS ONE* 9 (3). doi:10.1371/journal.pone.0090819.

Shu, Lili, and Peter J Houghton. 2009. "The mTORC2 Complex Regulates Terminal Differentiation of C2C12 Myoblasts." *Molecular and Cellular Biology* 29 (17): 4691–4700. doi:10.1128/MCB.00764-09.

Siegel, Ashley L, Paige K Kuhlmann, and D D W Cornelison. 2011. "Muscle Satellite Cell Proliferation and Association: New Insights from Myofiber Time-Lapse Imaging." *Skeletal Muscle* 1 (1): 7. doi:10.1186/2044-5040-1-7.

Smith, J., and P. N. Schofield. 1994. "The Effects of Fibroblast Growth Factors in Long-Term Primary Culture of Dystrophic (Mdx) Mouse Muscle Myoblasts." *Experimental Cell Research* 210 (1): 86–93.

Smith, J, and P N Schofield. 1997. "Stable Integration of an Mdx Skeletal Muscle Cell Line into Dystrophic (Mdx) Skeletal Muscle: Evidence for Stem Cell Status." *Cell Growth Differ* 8 (8): 927–34. http://www.ncbi.nlm.nih.gov/entrez/query.fcgi?cmd=Retrieve&db=PubMed&do

pt=Citation&list_uids=9269902.

Smythe, G M, M J Davies, D Paulin, and M D Grounds. 2001. “Absence of Desmin Slightly Prolongs Myoblast Proliferation and Delays Fusion in Vivo in Regenerating Grafts of Skeletal Muscle.” *Cell and Tissue Research* 304 (2): 287–94. doi:10.1007/s004410100366.

Suzuki, Keiko, Pinaki Bose, Rebecca Y Y Leong-Quong, Donald J Fujita, and Karl Riabowol. 2010. “REAP: A Two Minute Cell Fractionation Method.” *BMC Research Notes* 3 (November). BioMed Central: 294. doi:10.1186/1756-0500-3-294.

Tchevkina, Elena, and Andrey Komelkov. 2012. “Protein Phosphorylation as a Key Mechanism of mTORC1/2 Signaling Pathways.” *Protein Phosphorylation in Human Health (Huang C Ed) InTech, Rijeka, Croatia*.

Tollefsen, S. E., R. Lajara, R. H. McCusker, D. R. Clemmons, and P. Rotwein. 1989. “Insulin-like Growth Factors (IGF) in Muscle Development. Expression of IGF-I, the IGF-I Receptor, and an IGF Binding Protein during Myoblast Differentiation.” *Journal of Biological Chemistry* 264 (23): 13810–17.

Valdés, Juan A., Sylvia Flores, Eduardo N. Fuentes, Cesar Osorio-Fuentealba, Enrique Jaimovich, and Alfredo Molina. 2013. “IGF-1 Induces IP3-Dependent Calcium Signal Involved in the Regulation of Myostatin Gene Expression Mediated by NFAT during Myoblast Differentiation.” *Journal of Cellular Physiology* 228 (7): 1452–63. doi:10.1002/jcp.24298.

Vandewynckel, Yves-paul, Debby Laukens, Anja Geerts, Eliene Bogaerts, Annelies Paridaens, Xavier Verhelst, Sophie Janssens, Femke Heindryckx, Hans V A N Vlierberghe, and Hans Van Vlierberghe. 2013. “The Paradox of the Unfolded Protein Response in Cancer.” *Anticancer Research* 33 (11): 4683–94. http://ar.iiarjournals.org/content/33/11/4683.abstract.

Vazquez, Francisca, Satomi Matsuoka, William R Sellers, Toshio Yanagida, Masahiro Ueda, and Peter N Devreotes. 2006. “Tumor Suppressor PTEN Acts through Dynamic Interaction with the Plasma Membrane.” *Proceedings of the National Academy of Sciences of the United States of America* 103 (10): 3633–38.

doi:10.1073/pnas.0510570103.

Verfaillie, T, N Rubio, Ad Garg, G Bultynck, R Rizzuto, J-P Decuypere, J Piette, et al. 2012. “PERK Is Required at the ER-Mitochondrial Contact Sites to Convey Apoptosis after ROS-Based ER Stress.” *Cell Death and Differentiation* 19 (10): 1880–91. doi:10.1038/cdd.2012.74.

Walton, J N, and F J Nattrass. 1954. “On the Classification, Natural History and Treatment of the Myopathies.” *Brain* 77 (2): 169–231.

Wan, Xiaolin, and Lee J Helman. 2003. “Levels of PTEN Protein Modulate Akt Phosphorylation on Serine 473, but Not on Threonine 308, in IGF-II-Overexpressing Rhabdomyosarcomas Cells.” *Oncogene* 22 (50). Nature Publishing Group: 8205–11. http://dx.doi.org/10.1038/sj.onc.1206878.

Webb, Ashley E., and Anne Brunet. 2014. “FOXO Transcription Factors: Key Regulators of Cellular Quality Control.” *Trends in Biochemical Sciences*. doi:10.1016/j.tibs.2014.02.003.

Wente, Susan R., and Michael P. Rout. 2010. “The Nuclear Pore Complex and Nuclear Transport.” *Cold Spring Harbor Perspectives in Biology*. doi:10.1101/cshperspect.a000562.

Wolpert, L, R Beddington, T Jessell, P Lawrence, E Meyerowitz, and J Smith. 2002. *Principles of Development*. *Journal of Anatomy*. Vol. 74. doi:10.1007/s13398-014-0173-7.2.

Yu, Minli, Huan Wang, Yali Xu, Debing Yu, Dongfeng Li, Xiuhong Liu, and Wenxing Du. 2015. “Insulin-like Growth factor-1 (IGF-1) Promotes Myoblast Proliferation and Skeletal Muscle Growth of Embryonic Chickens via the PI3K/Akt Signalling Pathway.” *Cell Biology International* 39 (8). Wiley Online Library: 910–22.

Zammit, Peter S, and Jonathan R Beauchamp. 2001. “The Skeletal Muscle Satellite Cell: Stem Cell or Son of Stem Cell?” *Differentiation* 68 (4–5). Elsevier: 193–204.

Zammit, Peter S, Jon P Golding, Yosuke Nagata, Valérie Hudon, Terence A Partridge, and Jonathan R Beauchamp. 2004. “Muscle Satellite Cells Adopt Divergent Fates.” *J Cell Biol* 166 (3). Rockefeller University Press: 347–57.

Zhou, Hong Ming, Jian Wang, Rhonda Rogers, and Simon J. Conway. 2008. “Lineage-Specific Responses to Reduced Embryonic Pax3 Expression Levels.” *Developmental Biology* 315 (2): 369–82. doi:10.1016/j.ydbio.2007.12.020.

Zhuang, Lizhe, Julie Ann Hulin, Anastasia Gromova, Thi Diem Tran Nguyen, Ruth T. Yu, Christopher Liddle, Michael Downes, Ronald M. Evans, Helen P. Makarenkova, and Robyn Meech. 2014. “Barx2 and Pax7 Have Antagonistic Functions in Regulation of Wnt Signaling and Satellite Cell Differentiation.” *Stem Cells* 32 (6): 1661–73. doi:10.1002/stem.1674.

Appendices

APPENDIX 1. Publication

Muhammad Dain Yazid, Janet Smith & Neil A. Hotchin. 2017. Activation Of The Unfolded Protein Response And Apoptosis In Dystrophin-Deficient Myoblasts. *ER Stress, Autophagy & Immune System, 26th-27th January 2017, Bruges, Belgium.*

Muhammad Dain Yazid, Janet Smith & Neil A. Hotchin. Perturbation of PTEN-PI3K/Akt Signalling Impaired Autophagy Modulation in Dystrophin-Deficient Myoblasts. *[Manuscript to be submitted to Cell Death & Disease]*.

Muhammad Dain Yazid, Chen Hung-Chih, Janet Smith & Neil A. Hotchin. Minidystrophin$^{\Delta H2\text{-}R19}$ Partly Improved Protein Signalling in Dystrophin-Deficient Myoblasts. *[Manuscript to be submitted to American Society of Gene & Cell Therapy]*.

APPENDIX 2. Material suppliers

Amersham Pharmacia Biotech UK Ltd (Amersham Place, Little Chalfont, Buckinghamshire, HP7 9NA, UK)

- Anti-Rabbit Ig biotinylated species specific F(ab)2 fragment from Donkey (Cat No. RPN1064)
- Biotinylated Anti-mouse IgG (whole antibody from goat) (Cat No. RPN1177)
- Protein A Sepharose CL-4B beads (Cat No. 17078001)

Beckman Coulter (UK) Ltd (Oakley Court, Kingsmead Business Park, London Road, High Wycombe HP11 1JU, UK)

- AvantiTM 30 centrifuge

Becton Dickinson UK Ltd (The Danby Building, Edmund Halley Road, Oxford Science Park, Oxford, Oxfordshire OX4 4DQ)

- Purified mouse anti-Caveolin 3 monoclonal Antibody(Cat No. 610420)
- Rabbit polyclonal anti-Caveolin 1 Antibody (Cat No. 610060)

Becton Dickinson Labware (Becton Dickinson Company, Frankline Lakes, NJ, USA)

- 15 mL falcon tubes BLUEMAXTM Polypropylene Conical tube (Cat No. 35-2096)
- 50 ml falcon tubes BLUEMAXTM Polypropylene Conical tube (Cat No. 35-2070)

Bio-Rad Laboratories Ltd (Bio-Rad House, Maxted Road, Hemel Hempstead, Hertfordshire, HP2 7DX, UK)

- Mini Protean II Electrophoresis Cell (Cat No. 1653301)
- Mini Trans-blot blotting Cell (Cat No. 170-3930)

Carbolite (Parsons Lane, Hope, Hope Valley, S33 6RB, UK)

- Carbolite Incubator

Dako UK Ltd (Dako UK Ltd, Cambridge House, St. Thomas Place, Ely Cambridgeshire CB7 4EX)

- Dakocytomation Fluorescence Mounting Medium (Cat No. S3023; Lot No. 301514EFG 010104)

Developmental Studies Hybridoma Bank (DSHB, Department of Biological Science, University of Iowa, 007 Biology Building East, Iowa City, IA52242, USA)

- Anti-MF20
- Mouse monoclonal anti-Pax7 antibody

Eppendorf (Eppendorf UK Ltd, Endurance House, Vision Park, Chivers Way, Histon, Cambridge CB24 9ZR, UK)

- Thermomixer 5436

Fisher Scientific UK Ltd (Bishop Meadow Road, Loughborough, Leicestershire, LE11 5RG, UK)

- Boric Acid (Cat No. B380053)
- Diaminoethanetetra-acetate acid disodium salt (EDTA) (Cat No. D070053)
- DyLight(TM) 800 Conjugates-Streptavidin Thermo Scientific Pierce (Cat NO. PN21851)
- Ethanol, Class 3, analytical reagent grade (Cat No. E/0650DF/17)
- Glycine (Cat No. G/P460/53)
- Haemocytometer (Cat No. 0630030)
- Methanol (Cat No. M/4000/PK4)
- Nitric acid S.G. 1.42 (70%) (Cat No. N/2300/PB17)
- Sodium Chloride (Cat No. 102415K)
- Tri-Sodium Citrate (Cat No. S332053)
- Sodium dodecyl sulphate (SDS; Cat No. S/5200/53; Batch No.0398855)
- 2-propanol (iosopropanal; Cat No. P/7490/17; Batch No. 0380943)
- TRIS (hydroxylmethyl methylamine; Cat No.T/P630/53) Xylene (Cat No. 1330207)

Geneflow Ltd (Fradley Business Centre, WoodEnd Lane, Fradley, Staffordshire, WS13 8NF, UK)

- Protogel, 30% Acrylaminde, 0.8% (w/V)
- Bis-Acrylaminde Stock Solution (37.5:1)

GMBH & CO. KG (Janke & Kunkel-Str. 10, 79219 Staufen, Germany / Deutschland)

- IKA®KS 130 basic orbital shaker

Grants Instruments (Cambridge) Ltd, UK (29 Station Road, Shepreth, Cambridgeshire, SG8 6GB, UK)

- Water Bath

Invitrogen Ltd (Inchinnan Business Park, 3 Fountain Drive, Paisley, PA4 9RF, UK)

- Alexa Fluor® 488 F(ab')2 fragment of goat antimouse IgG (H+L)(Cat No. A11017)
- Alexa Fluor® 488 F(ab')2 fragment of goat antirabbit IgG (H+L)(Cat No. A11070)
- Dulbecco's Modified Eagle Medium (1×) without Glutamine (Cat No. 21969-035)
- Geneticin (G418 sulphate)(Cat No. 11811-031)
- GIBCO BRL 58 horizontal electrophoresis apparatus Kanamycine sulfate (Cat No. 11815-024)

- LipofectamineTM 2000 (Cat No. 11668-027; Lot No. 867692)
- LipofectamineTM LTX & Plus Reagent (Cat No. A12621)
- Luria Broth Base (Cat No. 12795027; Lot No. 80245231))
- 2-Mercaptoethanol (50MM) (Cat No. 31350010; Lot No. 26F0140)

Jenkons (Scientific) Ltd (Cherrycourt Way, Stanbridge Road, Leighton Buzzard, Bedforshire, LU7 4UA, UK)

- Uvitec, UV light box

Kendro Laboratory Products Plc (Stortford Hall Park, Bishop's Sortford, Hertfordshire, CM23 5GZ, UK)

- Labofuge 300 Heraeus centrifuge Heraeus Incubator (D-6450)

Leica Microsystems Ltd, UK (Davy Avenue, Knowlhill, Milton Keynes, MK5 8LB, UK)

- Inverted microscope-Leica
- DMIRB Reichert-Jung 1150/Autocut microtome

LI-COR Biotechnology - UK Ltd (St. John's Innovation Centre, Cowley Road, Cambridge, CB4 0WS, UK)

- Odyssey® infrared imaging system Odyssey anti-mouse IRDye® 680 (Cat No. 92632220; Lot No. B80908_011)

Marval [Premier International Foods (UK) Ltd, Bridge Road, Long Sutton, Spalding, Lincs PE12 9 EQ, UK]

- Non-fat milk

Molecular Device Ltd (135 Wharfedale Road, Winnersh Triangle, Winersh, Wokingham, RG41 5RB, UK)

- Emax microplate reader

NanoWorld AG (Rue Jaquet-Droz 1, CH-2002 Neuchâtel, Switzerland)

- Rectangular Si cantilevers type CONT-L

New Brunswick Scientific (Eppendorf UK Ltd, Endurance House, Vision Park, Chivers Way, Histon, Cambridge CB24 9ZR, UK)

- INNOVATM 433 refrigerated incubator shaker

New England BioLabs (UK) Ltd (75/77 Knowl Piece, Wilbury Way, Hitchin, Herts. SG4 0TY, UK)

- Prestained Protein Marker, Broad Range (7-175 kDa) (Cat No. P7708S)

Nikon UK Limited (380 Richmond Road, Kingston Upon Thames, Surrey, KT2 5PR, UK)

- Eclipse Ti inverted microscope

Nunc Plasticware (Life Technologies Ltd., 3 Fountain Drive, Ichinnan Business Park, Paisley, PA4 9RF, UK)

- CryoTubeTM vials (Cat No. 375353)
- Large culture flasks (175 cm2) (Cat No. 147589A)
- Medium culture flasks (75 cm2) (Cat No. 156462)
- Small culture flasks (25 cm2) (Cat No. 156367)
- 30 mm polystyrene petri dish (Cat No. 150318)
- 60 mm polystyrene petri dish (Cat No. 150288)
- 10 cm polystyrene petri dish (Cat No. 150350)
- 24-well plates (Cat No. 143982A) 48-well plates (Cat No. 150787)
- 96-well plates (Cat No. 167008A)

PALL Life Sciences (Europa House, Havant Street, Portsmouth, Hampshire, PO1 3PD, UK)

- Sterile Acrodisc® Syringe 32 mm Filters with 0.45 μm Supor® Membrane (Cat No. 4654)

Panasonic (Panasonic House, Willoughby Road, Bracknell, Berkshire RG12 8FP, UK)

- microwave

PerkinElmer (PerkinElmer, Saxon Way Bar Hill, Cambridge, Cambridgeshire, CB23 8SL, UK)

- Streptavidin-Texas Red® (Cat No. NEL721001EA)

Pierce (Perbio Sciences UK Ltd, Century House, High Street, Tattenhall, Cheshire, CH3 9RJ, UK)

- Albumin Standard Samples (Cat No. 23209)
- Coomassie® Protein Assay Reagent (Cat No. 1856209)

Roche Diagnostic Ltd (Bell Lane, Lewes, East Sussex, BN7 1LG, UK)

- Protease Inhibitor Cocktail tablets (Cat No. 1836153)

Sanyo (1-300 Applewood Cres. Concord. Ont, L4K 5C7, UK)

- Soni-pre150 machine (Sonicator)

SARSTEDT (SARSTEDT Ltd, 68 Boston Road, Beaumont Leys, Leicester LE4 1AW, UK)

- Cell scraper (Cat No. 83.1830)

School of Bioscience Stores, Birmingham University, UK (University of Birmingham, Edgbaston, Birmingham, B15 2TT, UK)

- Foil, 450 Caterwrap (Cat No. FOI11CC/WRA1)
- 5 ml bijoux tube

Sigma-Aldrich (Sigma-Aldrich Company Ltd, Fancy Road, Poole, Dorest, BD12 4QH, UK)

- Ammonium Persulfate (APS; Cat No. A3678)
- Ampicillin (Cat No. A9518)
- Bovine Serum Albumin (BSA) Fraction V (Cat No. A3059)
- 4',6-Diamidino-2-phenylindole dihydrochloride (DAPI) (Cat NO. D8417)
- Dimethyl Sulfoxide (DMSO)(Cat No. D2650)
- Dithiothreitol (DTT) (Cat No. D9779)
- Fetal Bovine Serum (FBS)-Heat inactivated (Cat No. F9665)
- Gelatin (Cat No. G1890)
- L-Glutamine 200 mM (Cat No. G7513)
- Glycerol (Cat No. G5516)
- HEPES (Cat No. H4034)
- Horse Serum (HS)-Heat inactivated (Cat No. H1138)
- Hydrogen Peroxide Solution (Cat No. H1009)
- IGEPAL® CA-630 (Octylphenyl-polyethylene glycol) (Cat No. I8896)
- 2-Mercaptoethanol (Cat No. M7522-100ML; Lot No. 01496DK)
- Minimum Essential Medium Eagle (MEM)-Alpha Modification (1×) (Cat No. M4526)
- t-octylpheoxypolyethoxyethanol (Triton X-100) (Cat No.T9284)
- Paraformaldehyde (Cat No. 76240)
- Penicillin/Streptomycin solution (100×), cell culture tested (Cat No. P0781)
- Phalloidin
- Tetramethylrhodamine B isothiocyanate (Cat No. P1951)
- Polyethylene glycol MW 8,000 (Cat No. 81268)
- Polyethylene glycol sorbitan monolaurate (Tween®20) (Cat No. P7949)
- Potassium Chloride KCl (Cat No. P9333)
- Sodium phosphate Dibasic Na2HPO4 (Cat No. S7907)
- Sodium phosphate Monobasic NaH2PO4 (Cat No. S8282)
- N,N,N',N'-Tetramethylethylenediamine (TEMED; Cat No. T9281)
- Trypsin (porcine trypsin in 0.2% EDTA·4Na, 0.9% Sodium Chloride (Cat No. T4174))

Sony (Pipersway, Thatcham, Berkshire RG19 4LZ, UK)

- Gel imaging camera,

Spectronic Camspec Ltd (Tudor House, Barley Hill Road, Garforth, Leeds LS25 1DX, UK)

- Camspec M501 Single Beam Scanning UV/Visible Spectrophotometer

Stuart Scientific Co. Ltd (Holmethorpe Industrial Estate, Redhill, Surrey RH1 2NB, UK) Gyro-Rocker Shaker (STR9)

- Hybridization Oven/Shaker (SI 20H)

Swann-Morton Ltd (Swann-Morton Limited, Owlerton Green, Sheffield, S6 2BJ, UK)

- Sterile Disposable Scalpel (Cat No.0508)

Terumo UK Ltd (3 Unily Grove, Off School Lane, Knowsley Industrials Park, Knowsley, Merseyside, L34 9GI, UK)

- 18 gauge needles (1.2×40 mm) (Cat No. NN-1838R)

VECTOR LABORATORIES LTD. (VECTOR LABORATORIES LTD. 3 Accent Park, Bakewell Road, Orton Southgate, Peterborough, PE2 6XS, United Kingdom)

- ImmEdge Hydrophobic Barrier Pen (Cat No. H4000)

VWR International, Formerly "BDH" (Merk Ltd, Hunter Boulevard, Magna Park, Lutterworth, Leics, LE17 4XN, UK)

- Coverglass- 24 mm × 50 mm (Cat No. 406-0188-82)
- Glass Coverslips-9mm2 (Cat No. 631-0169)
- DePex mounting medium (Cat No. 361252B)
- Magnesium Chloride 6-hydrate (Cat No. 101494V)
- Sodium Azide (Cat No.10369 2K)
- Sodium Hypochlorite (Cat No. 301696S)
- Superfrost Plus Microscope Slides (Cat No. 6310108)

The Wolfson Centre for Inherited Neuromuscular Disease (CIND)

- Mouse anti-dystrophin antibody (MANDRA1 7A10) (Morris et al., 1998; Nguyen et al., 1992)

APPENDIX 3. Recipes

Cell culture medium and buffer preparation:

IN-VITRO CELL CULTURE:

C2C12/dfd13 cell culture medium:

DMEM + 10% FCS + 1% P/S + 1%L-Glutamine

450 ml Dulbecco's Modified Eagles Medium (DMEM; Invitrogen Ltd, UK),

50 ml Fetal Bovine Serum (FCS) Batch tested (Sigma-Aldrich, UK),

5 ml L-Glutamine (Sigma-Aldrich, UK),

5 ml Penicillin/Streptomycin (P/S; Sigma-Aldrich, UK)

C2C12/dfd13 differentiation medium:

DMEM + 2% HS + 1% P/S + 1%L-Glutamine

480 ml Dulbecco's Modified Eagles Medium (DMEM; Invitrogen Ltd, UK),

10 ml Horse Serum (HS) Batch tested (Sigma-Aldrich, UK),

5 ml L-Glutamine (Sigma-Aldrich, UK),

5 ml Penicillin/Streptomycin (P/S; Sigma-Aldrich, UK)

10× PBS (phosphate buffered saline)

8 g NaCl (Fisher Scientific, UK),

0.2 g KCl (Sigma-Aldrich, UK),

1.15 g Na2HPO4 (Sigma-Aldrich, UK),

0.2 g NaH2PO4 (Sigma-Aldrich, UK),

100 ml dH2O (PH7.4)

Trypsin:

Trypsin (porcine trypsin in 0.9% sodium chloride solution; Sigma-Aldrich, UK) in PBS

IMMUNOSTAINING:

Fixation

4 g Paraformaldehyde + 100 ml 1× sterile PBS

Weight 4g Paraformadehyde (Sigma-Aldrich, UK) and add to preheated (60°C) PBS in a fumehood and allow dissolving in 65°C rocking oven, ensuring temperature did not go above 70 °C, as PFA is explosive at high temperatures.

PBST

PBS + 150 mM NaCl + 0.05% Tween20® 500 ml PBS,

1.46 g NaCl, 0.25 ml Tween20® (Sigma-Aldrich, UK)

Running Buffer

3 g Tris (Fisher Scientific Ltd, UK),

14.42 g Glycine (Fisher Scientific Ltd, UK),

1 g SDS (Fisher Scientific Ltd, UK)

Made up to 1 litre with dH2O

1.5 M Tris-HCl

18.17 g Tris Made up to 100 ml with dH2O pH to 8.8 with concentrated HCl (Fisher Scientific Ltd, UK)

1.0 M Tris-HCl

12.1 g Tris Made up to 100 ml with dH2O pH to 6.8 with concentrated HCl (Fisher Scientific Ltd, UK)

10% SDS

10 g SDS made up to 100 ml with dH2O

10X TBS (Tris-buffered saline)

24.2 g Tris,

80 g NaCl

Made up to 100 ml with dH2O pH to 7.6 with concentrated HCl

Blocking Buffer

15 ml 10× TBS (see above) 135 ml dH2O,

0.15 ml Tween®20,

7.5 g non-fat dry milk (Marvel, UK)

Wash Buffer (TBST)

100 ml 10× TBS (see above),

900 ml dH2O, 1 ml Tween®20

Primary Antibody Dilution Buffer

2 ml 10× TBS,

18 ml dH2O,

20 ul Tween®20,

1 g BSA (Sigma-Aldrich, UK)